ICOLD

proceedings

12th International

BENCHMARK WORKSHOP
ON NUMERICAL ANALYSIS OF DAMS, 2nd - 4th October, 2013, Graz – AUSTRIA

Edited by
Gerald Zenz and Markus Goldgruber

PROCEEDINGS OF THE
ICOLD - 12th INTERNATIONAL
BENCHMARK WORKSHOP
ON NUMERICAL ANALYSIS OF DAMS

2nd - 4th OCTOBER, 2013, GRAZ – AUSTRIA

Edited by

Gerald Zenz
Institute of Hydraulic Engineering and Water Resources Management
Graz University of Technology

Markus Goldgruber
Institute of Hydraulic Engineering and Water Resources Management
Graz University of Technology

Published by

ATCOLD – AUSTRIAN NATIONAL COMMITTEE ON LARGE DAMS

Preface

For the International Commission on Large Dams (ICOLD) the "Committee on Computational Aspects of Analysis and Design of Dams" is the general Organizer of Benchmark Workshops. This 12th Benchmark Workshop is held in the city of Graz, situated in the South of the Alps on both sides of the river Mur. Six universities with over 40,000 students are in addition responsible for the young and dynamic charm of our city. Since over 200 years Graz University of Technology is one of them.

Advanced numerical tools with user friendly interfaces are available and widely used for structural analyses. Such numerical analyses require a solid theoretical background of the applicability of methods to be used. On the other hand, the results gained need a careful interpretation with respect to the underlying assumptions and their practical relevance. ICOLD Benchmark examples of generalized engineering problems are devoted to bridge the gap between numerical analyses, the interpretation of results and their theoretical as well as practical relevance. Since 1991 eleven benchmark workshops were organized for different numerical problems in the field of concrete and fill dams under static and dynamic loading conditions. The results of these benchmark workshops are made available to the dam engineering community on the internet and in proceeding. Results are published in ICOLD bulletins:

- Bulletin N 94 Computer Software for Dams
- Bulletin N 122 Computational Procedures for Dam Engineering
- Bulletin N 155 Guidelines for Use of Numerical Models in Dam Engineering

This 12th Benchmark Workshop provides an excellent opportunity for engineers, scientists and operators to present and exchange their experiences and the latest developments related to the design, performance and monitoring of dams. There are three example topics and an open theme formulated and discussed:

Theme A: Fluid Structure Interaction, Arch Dam - Reservoir at Seismic Loading
Formulators: Gerald Zenz, Markus Goldgruber

Theme B: Long Term Behavior of Rockfill Dams
Formulators: Camilo Marulanda, Joan Manuel Larrahondo

Theme C: Computational Challenges in Consequence Estimation for Risk Assessment
Formulators: Yazmin Seda-Sanabria, Enrique E. Matheu, Timothy N. McPherson

The support to this Benchmark Workshop from the Members of the Committee on Computational Aspects of Analysis and Design of Dams and especially from the Formulators is gratefully acknowledged. The contributions from the Core Organizing Team – Markus Goldgruber and Harald Breinhälter – are very much appreciated. Finally, I want to thank the participants for their scientific contributions herein.

Gerald Zenz
Chairman

Table of Content

Table of Content

Conference Organizations

The conference was organized by
Graz University of Technology, Graz, Austria

Conference Chairman
Gerald Zenz (Graz University of Technology, Austria)

Committee on Computational Aspects of Analysis and Design of Dams

Chairman
I. Escuder-Bueno (Spain)

Vize-Chairman
G. Mazza (Italy)

Technical Advisory Team

RESTELLI, F. (Argentina)	MEGHELLA, M. (Italy)
ZENZ, G. (Austria)	UCHITA, Y. (Japan)
CURTIS, D. (Canada)	ANDERSEN, R. (Norway)
CHEN, S. (China)	POPOVICI, A. (Romania)
MARULANDA, C. (Colombia)	GLAGOVSKY, V. (Russia)
VARPASUO, P. (Finland)	MINARIK, M. (Slovakia)
TANCEV, L. (Form. Yug. Rep. of Macedonia)	HASSANZADEH, M. (Sweden)
FROSSARD, E. (France)	GUNN, R. (Switzerland)
BEETZ, U. (Germany)	MATHEU, E. (United States)
DAKOULAS, P. (Greece)	CARRERE, A. (Honorary Member) (France)
NOORZAD, A. (Iran)	FANELLI, M. (Honorary Member) (Italy)

Local Organizing Committee

Graz University of Technology
Institute of Hydraulic Engineering and Water Resources Management

Head
Gerald Zenz

Organizer
Markus Goldgruber

Acknowledgements

THEME A

Theme A
Fluid Structure Interaction
Arch Dam – Reservoir at Seismic loading

Formulators:

Dipl. Ing. Markus Goldgruber

Univ. Prof. Dipl. Ing. Dr. techn. Gerald Zenz

Institute of Hydraulic Engineering and Water Resources Management

Graz University of Technology

Graz University of Technology

Introduction

Advanced numerical tools with user friendly interfaces are available for structural analyses. Such numerical analyses require a solid theoretical background of the applicability of methods to be used. On the other hand, the results gained need a careful interpretation with respect to the underlying assumptions and their practical relevance. ICOLD Benchmark examples of generalized engineering problems are devoted to bridge the gap between numerical analyses, the interpretation of results and their theoretical as well as practical relevance. Challenges of the analyses of concrete dams are always the definition of material parameters, the spatial discretization and the appropriate simulation of loading sequences. Additionally, specific attention is paid on the structural integrity and entire safety under seismic loading conditions. To account for this problem, the interaction of the dam and the reservoir is topic of this theme A.

By means of the Finite Element Method linear and nonlinear analyses under dynamic excitation are carried out. However, for the required and appropriate simulation of the dam reservoir interaction different approaches are used. With respect to future nonlinear dynamic analyses, these simulations herein shall be in the time domain only.

A common approach to take the dynamic water interaction into account is to use an added mass approach. A more sophisticated possibility is the use of Acoustic or Fluid Elements. The simulations of earthquake excitation of arch dams have shown that the analyzed stresses in the structure could vary significantly based on the interaction modeling. The added mass approach is still a widely used technique but tends to overestimate the stresses and therefore it is conservative in contrary to other techniques.

This benchmark now intends to compare different modeling techniques and will show the amount of deviations. All investigations are carried out for an artificially generated symmetric arch dam and simplified loading and boundary conditions.

Universities, engineering companies and regulatory bodies are invited to contribute to the benchmark and take part in the discussion of results gained.

Focus of this benchmark example

The focus of this benchmark is to carry out the Dynamic Fluid Structure Interaction for a large arch dam. Every participant may choose his own order of details in modeling.

The main goal of this example is the application of different approaches like:

- Added mass technique (Westergaard, Zangar,…)
- Acoustic Elements (compressible, incompressible)
- Fluid Elements (compressible, incompressible)

Further on, the usage of different Boundary Conditions is possible for:

- Reservoir - Foundation
    - Reflecting (on the bottom and the sides)
    - Non-reflecting (at the end of the reservoir)

The modeling of the block joint opening – due to tensile stresses and nonlinear effects - is not focus of this benchmark example. However, to carry out this analysis in the time domain will provide the opportunity for further non-linear analyses.

General basic assumptions

The following general basic assumptions and boundary conditions for the investigations should be used:

- Same spatial discretization (Model/Mesh) of the Structure, Foundation and Reservoir
- Same Material Parameters
- Acceleration-Time-History in X-,Y-,Z-Direction
- Reservoir is infinite in length (non-reflecting)
- Rayleigh Damping
- Results to be compared – Visualization

Based on these basic assumptions and results gained the contributors are encouraged to intensify and focus their effort to achieve results with higher profound physical justification and explain the differences. (E.g.: different spatial discretization, more appropriate modeling of the interaction; different length of the reservoir; need for nonlinear effects).

An interpretation of the evaluated results from an engineering point of view should be given.

Model and Geometry

An Arch Dam, Foundation and Reservoir Model layout for the benchmark has been generated and is available for downloading.

Arch Dam Model
- Symmetric Geometry
- Total Height: 220 Meters
- Valley width (crest):   ~ 430 Meters
- Valley width (bottom): ~ 80 Meters

Arch Dam Geometry
The Arch Dam Geometry has been generated with the Program "Arch Dam Design", which was developed as part of the Master-Thesis by DI Manuel Pagitsch.

Arch Dam Model

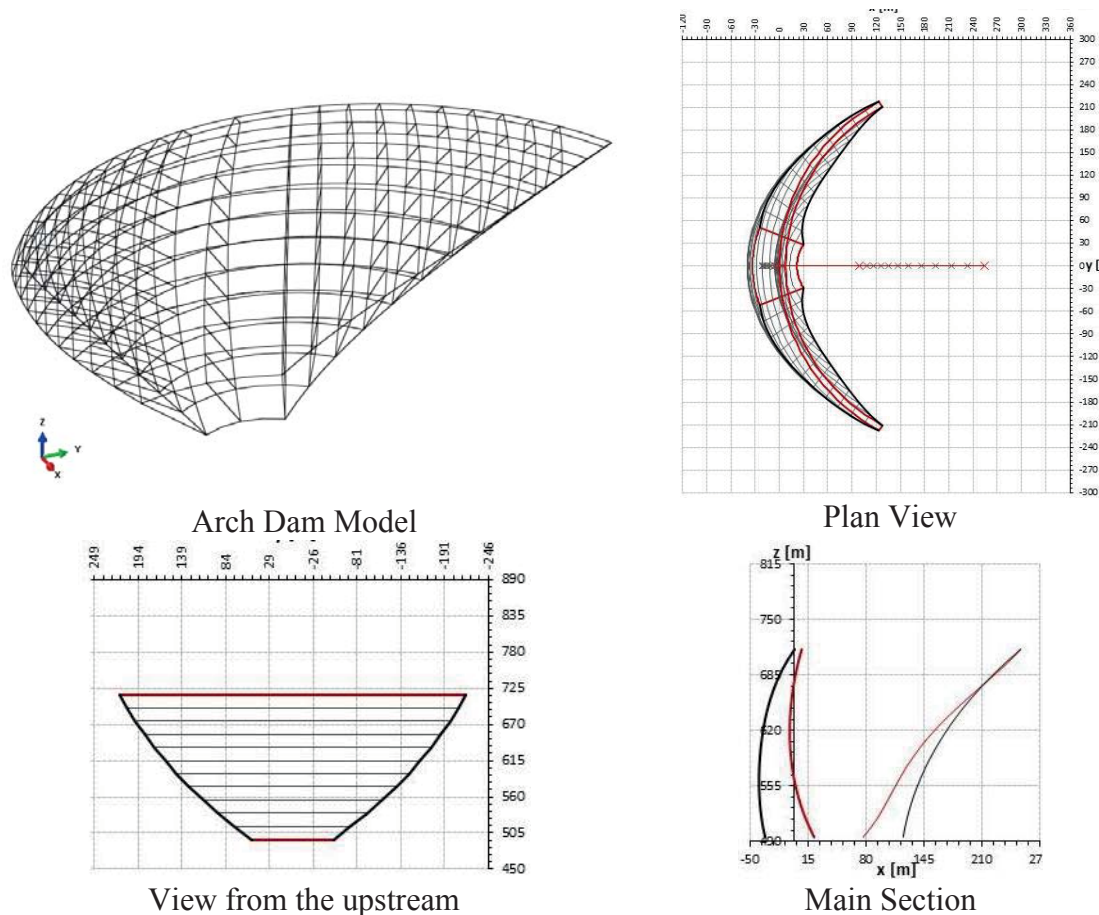Plan View

View from the upstream

Main Section

Figure 1: Arch dam geometry

Foundation Model
Symmetry is used for the foundation too.
- Height: 500 Meters
- Length: 1000 Meters
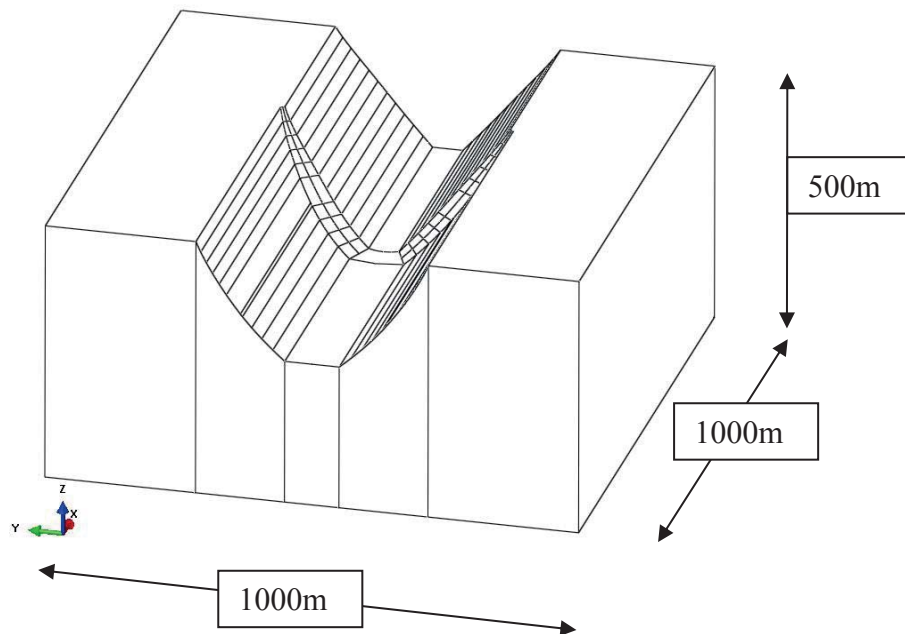- Width   1000 Meters

Figure 2: Foundation geometry

Reservoir Model
- Length: assumed minimum of 460 Meters (> 2x Height of the Dam)
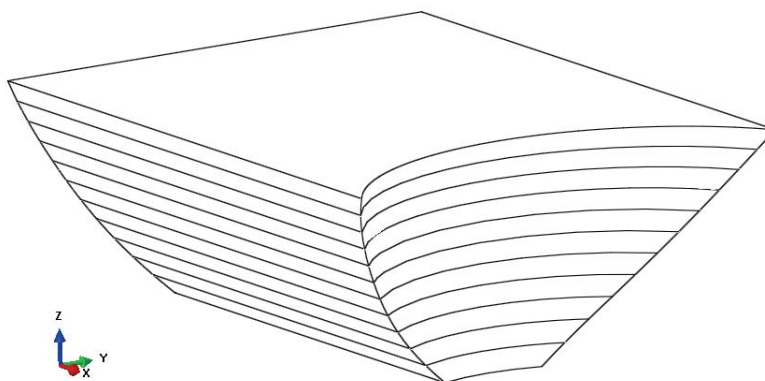- Modeling the interaction with Acoustic- or Fluid Elements

Figure 3: Reservoir geometry

Acceleration Time History
- Transient Acceleration ($a_{max} \approx 0.1g$)
- X-,Y-,Z- Direction
- Artificially generated time history
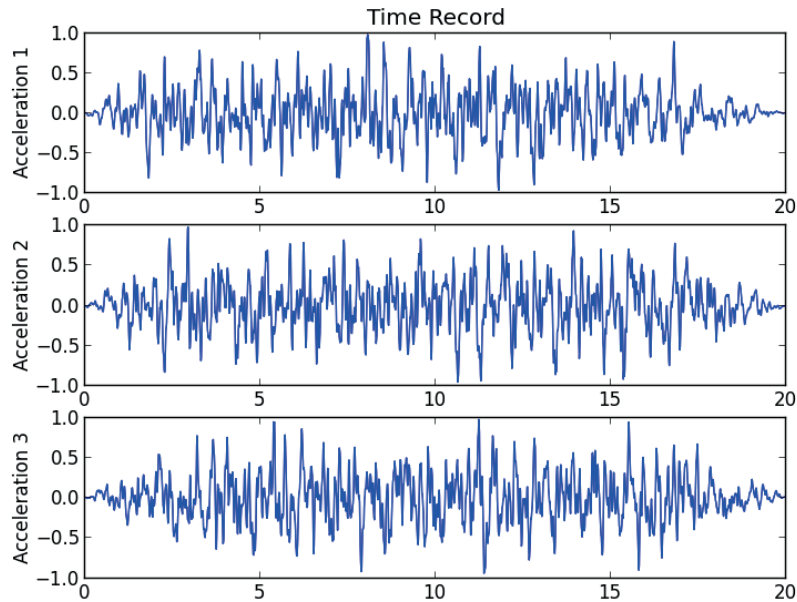

Figure 4: Reservoir geometry

Material Parameters

The Material properties are defined for isotropic and homogenous conditions.

Rock mass
- Density: 0 kg/m^3
- Poisson - ratio: 0,2
- Youngs - modulus: 25000 MPa

Water
- Density: 1000 kg/m^3
- Bulk - modulus: 2200 MPa

Dam
- Density: 2400 kg/m^3
- Poisson - ratio: 0,167
- Youngs - modulus: 27000 MPa

Mesh Properties

Two different Meshes of the entire system are provided for investigations, as these are a coarse and a fine mesh. If desired, the parts can also be provided as ABAQUS/CAE Model File, ACIS- or IGES-Files, if a specific mesh is intended to be discretized.

Coarse Mesh
Arch Dam
- Total number of nodes: 2083
- Total number of elements: 356
- 312 quadratic hexahedral elements of type C3D20R (ABAQUS CAE)
- 44 quadratic wedge elements of type C3D15 (ABAQUS CAE)

Foundation
- Total number of nodes: 11608
- Total number of elements: 2340
- quadratic hexahedral elements of type C3D20R (ABAQUS CAE)

Reservoir
- Total number of nodes: 12493
- Total number of elements: 2640
- quadratic hexahedral elements of type C3D20R (ABAQUS CAE)

Figure 5: Coarse mesh of the dam, foundation and reservoir

Fine Mesh

Arch Dam
- Total number of nodes: 13733
- Total number of elements: 2736
- quadratic hexahedral elements of type C3D20R (ABAQUS CAE)

Foundation
- Total number of nodes: 13298
- Total number of elements: 2700
- quadratic hexahedral elements of type C3D20R (ABAQUS CAE)

Reservoir
- Total number of nodes: 12493
- Total number of elements: 2640
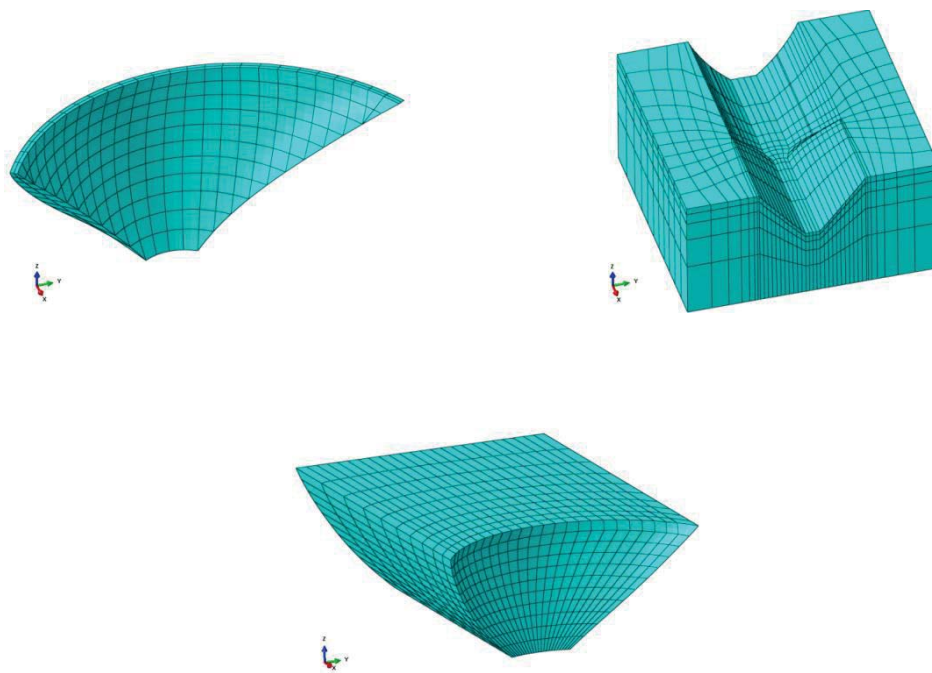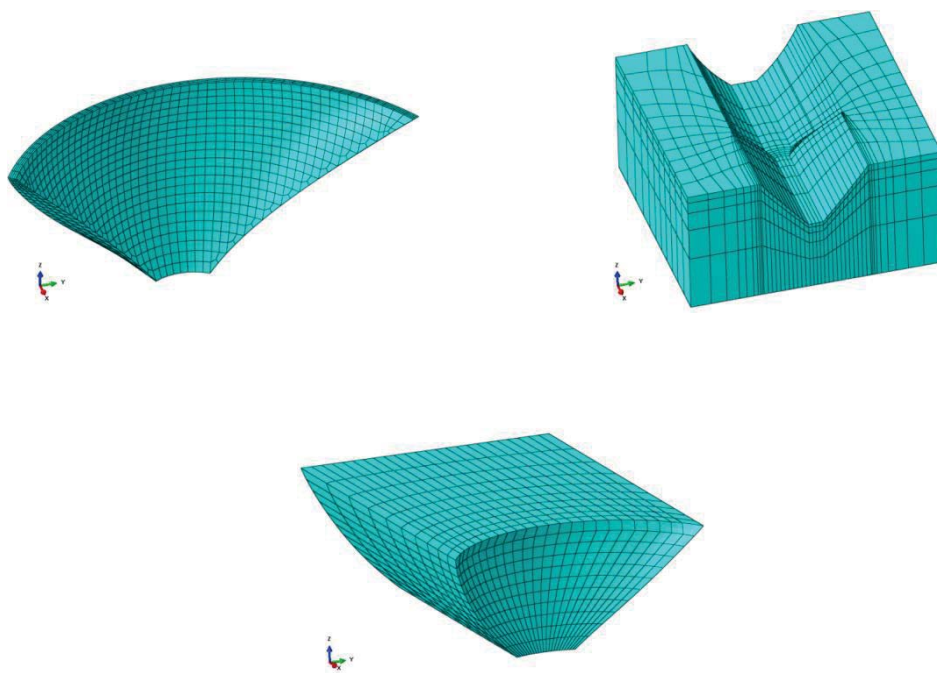- quadratic hexahedral elements of type C3D20R (ABAQUS CAE)

Figure 6: Fine mesh of the dam, foundation and reservoir

Elements and Node Numbering in ABAQUS/CAE

The provided input-files are containing a list of the nodes and elements of the mesh and also predefined "node sets" for the different sections which should be investigated. The Node numbering of ABAQUS/CAE is plotted in the following figures.
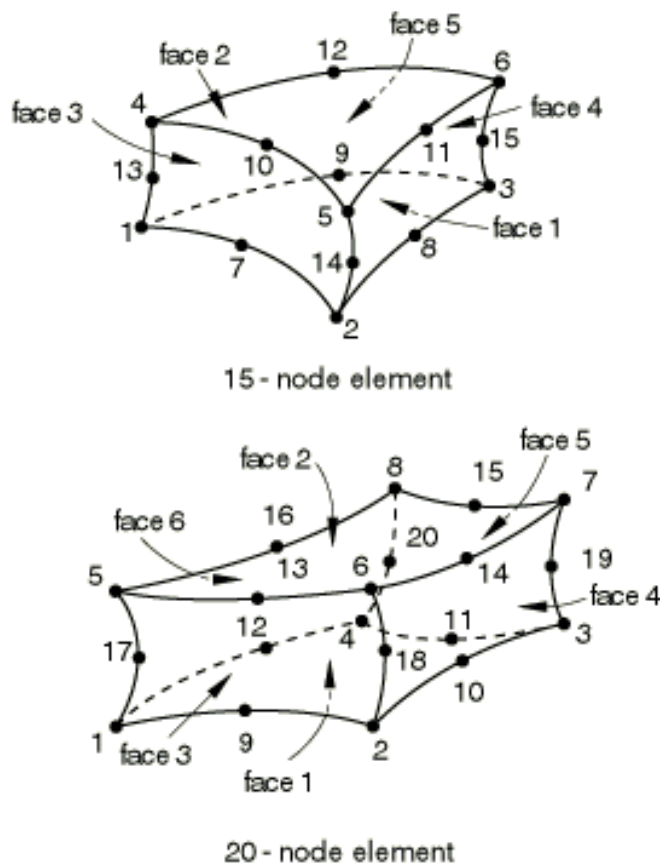
Figure 7: Node numbering of wedge and brick elements in ABAQUS/CAE

These figures are showing the node numbering for the two different element types which are used in the provided input-files.

Loading

The following loading sequence is intended to be used.
- Gravity
- Hydrostatic Water Pressure (full supply water level = Crest Height)
- Seismic Loading
  - Modal Superposition or
  - Direct time integration (Implicit/Explicit)

Results

Following results should be evaluated and plotted.

Eigenfrequencies (1 – 10)
The evaluation of the first 10 Eigenfrequencies of the structure, including the interaction with the reservoir, should be provided.

Mode Shapes (1 – 10)
The evaluation and plotting of the first 10 Mode-Shapes of the structure, including the interaction with the reservoir, should be provided.

Hoop Stresses, Vertical Stresses and Min./Max. Principal Stresses
Evaluation of the different stresses should be done for
- Static Loads
- Seismic Loads (Min., Max.)
- 3 different sections (Main Section and ~45 degrees on the left and right hand side)
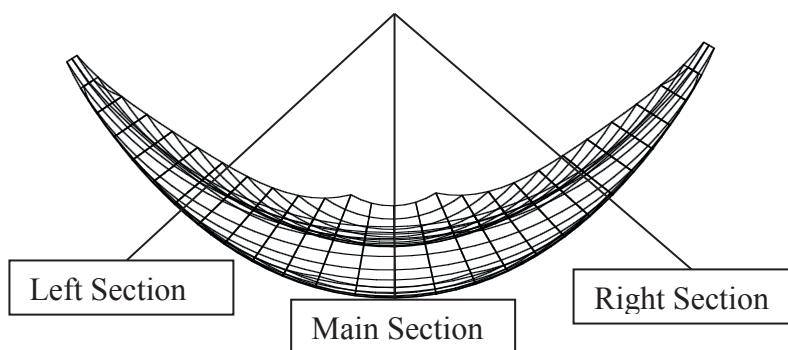

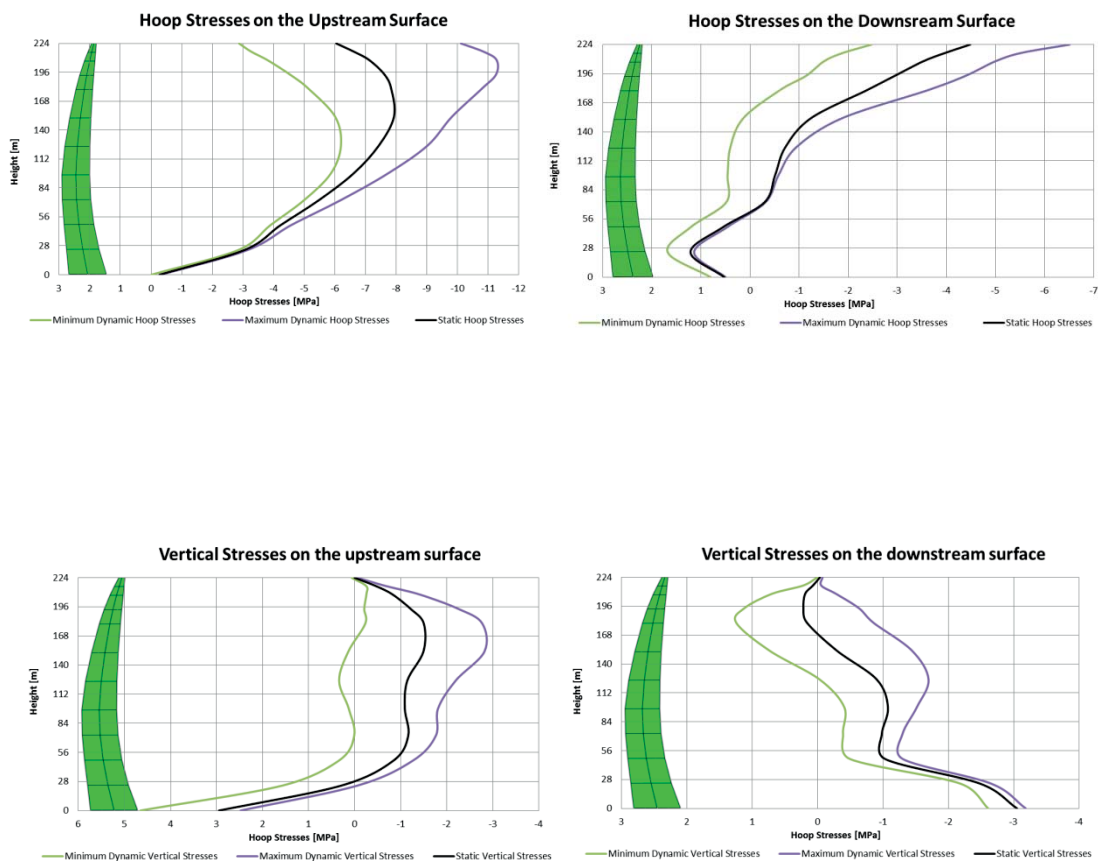Figure 8: Evaluation sections of the arch dam

Figure 9: Evaluation examples for the stresses

Radial Deformation
Evaluation of the Radial Deformation should be done for
- Static Loads
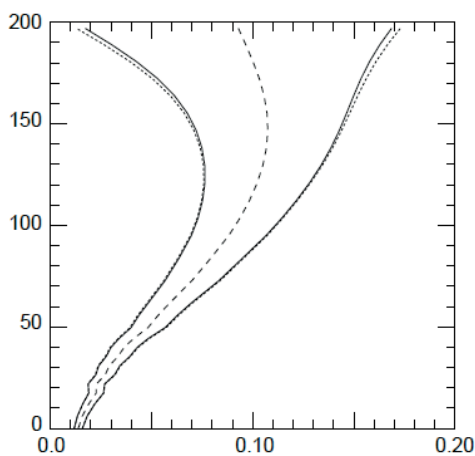- Seismic Loads (Min., Max.)
- Main section

Figure 10: Evaluation examples for the radial deformation

RESULT COMPARISON OF THE PARTICIPANTS

THEME A

Results Comparison

Theme A
Fluid Structure Interaction
Arch Dam – Reservoir at Seismic loading

Participants, Programs and Approaches

Overall there are 11 participants from 9 different countries (Swiss, Netherlands, France, Germany, Sweden, Italy, Iran, Romania and Austria) who were contributing to the workshop and decided to solve the problem. Each participant had the opportunity to choose his preferred numerical program and modelling technique to account for the fluid structure interaction. The prevailing boundary conditions, which are the same for each participant, are defined in the section "Benchmark Problem Description Theme A".

The "Reference Solution" (REF) in the diagrams and tables doesn't claim to be the optimum solution. It shows the results of the simulations done at the Institute of Hydraulic Engineering and Water Resources Management by Markus Goldgruber.

The following table lists the participants and their used programs and approaches. The informations in the last column should point out some specific differences between the participants which may influence the results and are worth mentioning. Some of the participants have provided results of more than just one simulation, but for the comparison just one of these has been used. All the other results of the approaches and models can be found in their papers in the following section (Papers – Theme A)

All participants had to evaluate eigenfrequencies, mode shapes, deformations and stresses. In the case of dynamic simulations one will get minimum and maximum values. Therefore, in the diagrams in the results section every participant has three lines, the minimum (left line) and the maximum line (right line) which indicate the minimum and maximum values out of the time history records and the line for static loading (middle line). This middle line indicates the static value out of the sum of the two load cases, gravity and hydrostatic water load. To retain the overview in the diagrams, the minimum, maximum and static values are not explicitly mentioned in the legend. The diagrams for the deformations and the upstream hoop stresses in the main section were plotted additionally for static and dynamic loading separately.

Table 1: Participants, Programs and Approaches

|		Finite Element Program	Method	Mesh	Some Additional Informations
A	G. Maltidis	ABAQUS	Acoustic Elements	Coarse	7.5% critical damping
B	W.Kikstra, F. Sirumbal, G. Schreppers	DIANA	Acoustic Elements	Coarse	Compressible Fluid, Hybrid Frequency-Time Domain (HFTD) method
C	G. Faggiani, P. Masarati	CANT-SD	Acoustic Elements	Coarse	
D	A. Tzenkov, A. Abiati, G. Gatto	DIANA	Acoustic Elements	Coarse	Same as participant B, Construction steps for loadcase deadweight
E	M. Chambart	DIANA	Added mass (Westergaard)	Fine	$E_{dyn} = E_{sta} * 1.25$
F	A. Popovici, C. Ilinca, R. Vârvorea	ABAQUS	Added mass (Westergaard)	Coarse	
G	R. Malm, C. Pi Rito, C. Hassanzadeh, C. Rydell, T. Gasch	ABAQUS	Acoustic Elements	Fine	Infinite Elements at the boundaries, Acceleration-Time-History applied on the bottom of the model
H	M. Brusin	FENAS ECCON IPP	Added mass (Westergaard)	Fine	Construction steps for loadcase deadweight
I	S. Shahriari	ANSYS	Added mass (Westergaard)	Coarse	Use of the full Westergaard formula (Period/Frequency dependent)
J	A. Frigerio, G. Mazzà	COMSOL	Acoustic Elements	Coarse	
K	A.Diallo, E. Robbe	CODE_ASTER	Incompressible Finite Element added mass	Coarse	Method to calculate the added mass matrices representing the fluid-structure interaction with a potential approach
REF	M. Goldgruber	ABAQUS	Acoustic Elements	Coarse	

Results

Eigenfrequencies
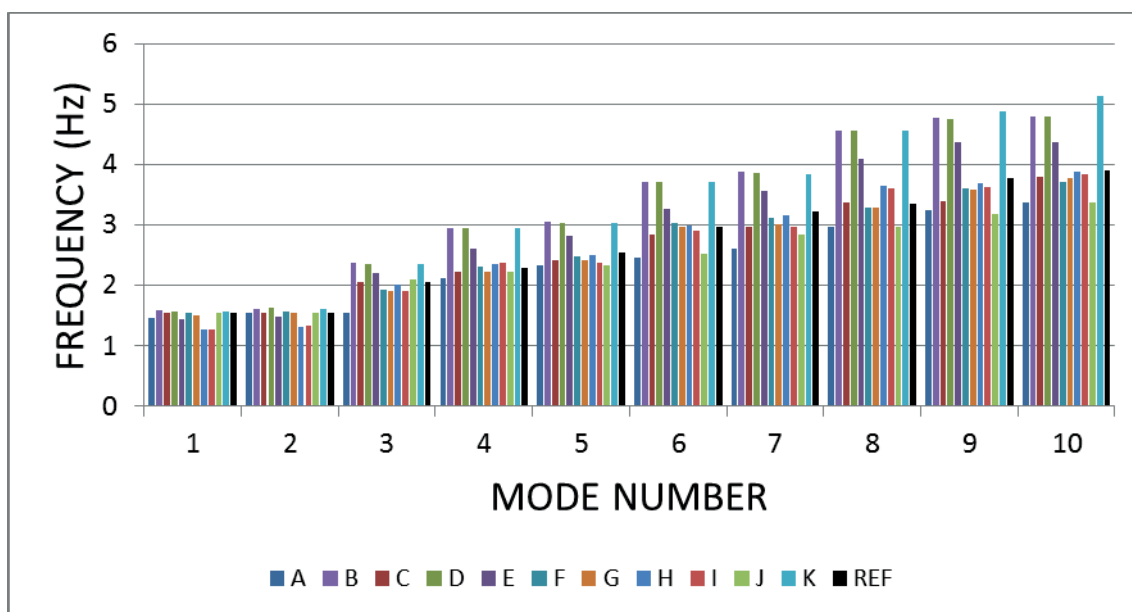
Figure 1: Eigenfrequencies 1 – 10(Column Chart)

Table 2: Eigenfrequencies 1 – 10 (Table)

Participant	Mode									
	1	**2**	**3**	**4**	**5**	**6**	**7**	**8**	**9**	**10**
A	1.47	1.54	1.55	2.11	2.33	2.46	2.61	2.97	3.25	3.37
B	1.57	1.60	2.36	2.94	3.04	3.72	3.88	4.56	4.78	4.80
C	1.54	1.55	2.05	2.22	2.41	2.83	2.98	3.37	3.40	3.79
D	1.57	1.62	2.36	2.94	3.04	3.72	3.87	4.56	4.76	4.80
E	1.43	1.47	2.21	2.61	2.81	3.27	3.56	4.09	4.37	4.37
F	1.54	1.56	1.93	2.30	2.48	3.04	3.12	3.29	3.61	3.71
G	1.51	1.54	1.90	2.22	2.42	2.96	3.01	3.28	3.59	3.76
H	1.26	1.32	2.01	2.36	2.50	3.00	3.17	3.65	3.70	3.88
I	1.28	1.33	1.91	2.37	2.38	2.91	2.98	3.61	3.62	3.85
J	1.54	1.55	2.09	2.22	2.33	2.51	2.83	2.96	3.19	3.37
K	1.57	1.62	2.35	2.95	3.03	3.72	3.85	4.56	4.88	5.13
REF	1.54	1.54	2.05	2.29	2.54	2.96	3.21	3.36	3.76	3.91

Mode Shapes
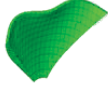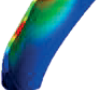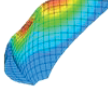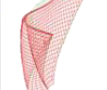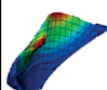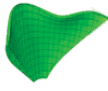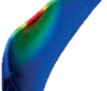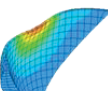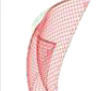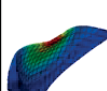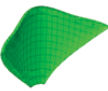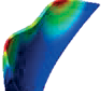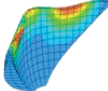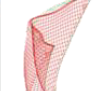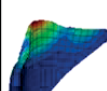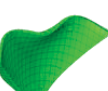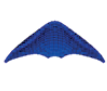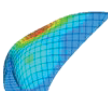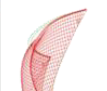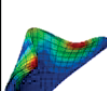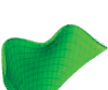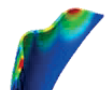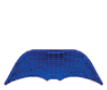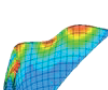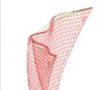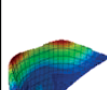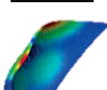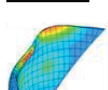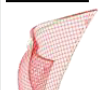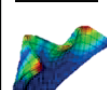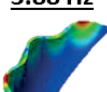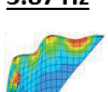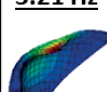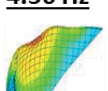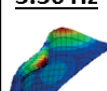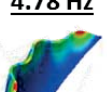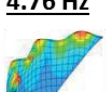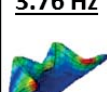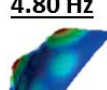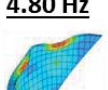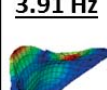
MODE NO.	A	B	C	D	E	REF
1	1.47 Hz	1.57 Hz	1.54 Hz	1.57 Hz	1.43 Hz	1.54 Hz
2	1.54 Hz	1.60 Hz	1.55 Hz	1.62 Hz	1.47 Hz	1.54 Hz
3	1.55 Hz	2.36 Hz	2.05 Hz	2.36 Hz	2.21 Hz	2.05 Hz
4	2.11 Hz	2.94 Hz	2.22 Hz	2.94 Hz	2.61 Hz	2.29 Hz
5	2.33 Hz	3.04 Hz	2.41 Hz	3.04 Hz	2.81 Hz	2.54 Hz
6	2.46 Hz	3.72 Hz	2.83 Hz	3.72 Hz	3.27 Hz	2.96 Hz
7	2.61 Hz	3.88 Hz	2.98 Hz	3.87 Hz	3.56 Hz	3.21 Hz
8	2.97 Hz	4.56 Hz	3.37 Hz	4.56 Hz	4.09 Hz	3.36 Hz
9	3.25 Hz	4.78 Hz	3.40 Hz	4.76 Hz	4.37 Hz	3.76 Hz
10	3.37 Hz	4.80 Hz	3.79 Hz	4.80 Hz	4.37 Hz	3.91 Hz

Figure 2: Mode Shapes 1 – 10; Participants A – E

MODE NO.	F	G	H	I	J	K	REF
1	1.54 Hz	1.51 Hz	1.26 Hz	1.28 Hz	1.54 Hz	1.57 Hz	1.54 Hz
2	1.56 Hz	1.54 Hz	1.32 Hz	1.33 Hz	1.55 Hz	1.62 Hz	1.54 Hz
3	1.93 Hz	1.90 Hz	2.01 Hz	1.91 Hz	2.09 Hz	2.35 Hz	2.05 Hz
4	2.30 Hz	2.22 Hz	2.36 Hz	2.37 Hz	2.22 Hz	2.95 Hz	2.29 Hz
5	2.48 Hz	2.42 Hz	2.50 Hz	2.38 Hz	2.33 Hz	3.03 Hz	2.54 Hz
6	3.04 Hz	2.96 Hz	3.00 Hz	2.91 Hz	2.51 Hz	3.72 Hz	2.96 Hz
7	3.12 Hz	3.01 Hz	3.17 Hz	2.98 Hz	2.83 Hz	3.85 Hz	3.21 Hz
8	3.29 Hz	3.28 Hz	3.65 Hz	3.61 Hz	2.96 Hz	4.56 Hz	3.36 Hz
9	3.61 Hz	3.59 Hz	3.70 Hz	3.62 Hz	3.19 Hz	4.88 Hz	3.76 Hz
10	3.71 Hz	3.77 Hz	3.88 Hz	3.85 Hz	3.37 Hz	5.13 Hz	3.91 Hz

Figure 3: Mode Shapes 1 – 10; Participants F – K

Deformations – Main Section
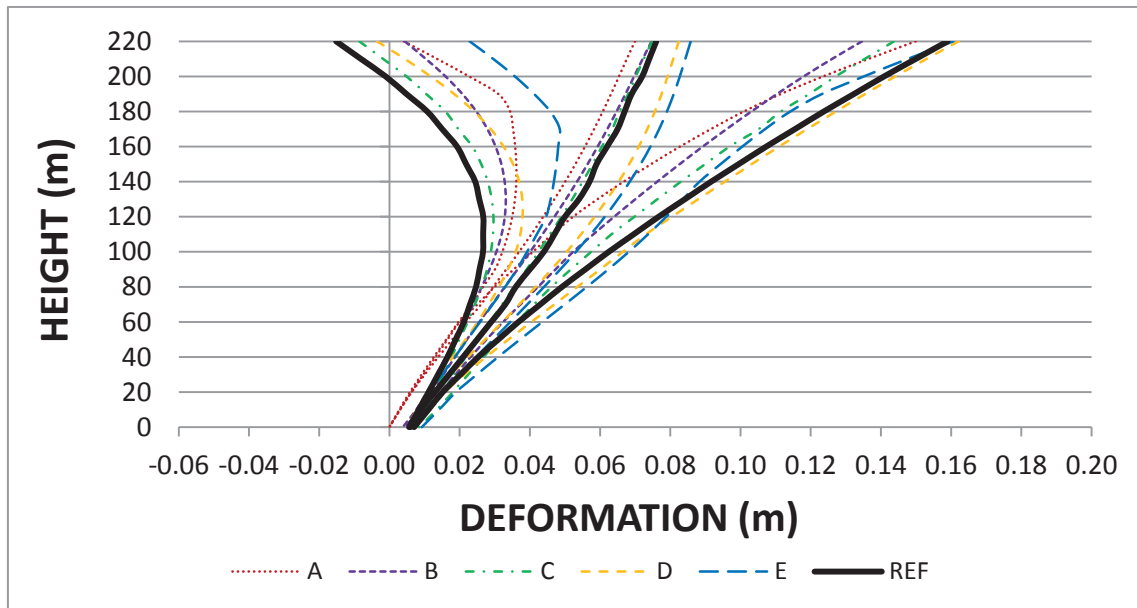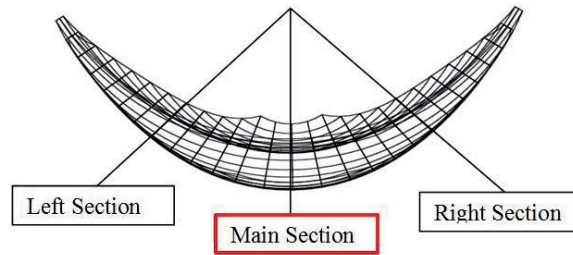
Figure 4: Deformation – Main Section (A – E)
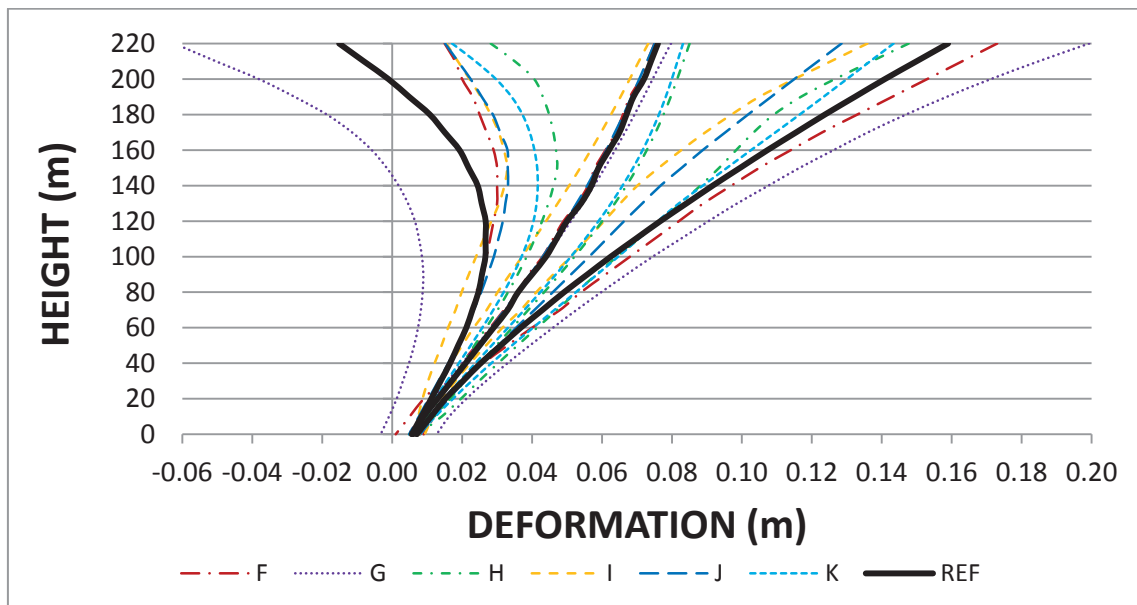
Figure 5: Deformation – Main Section (F – K)

Deformations (Only Static Load) – Main Section
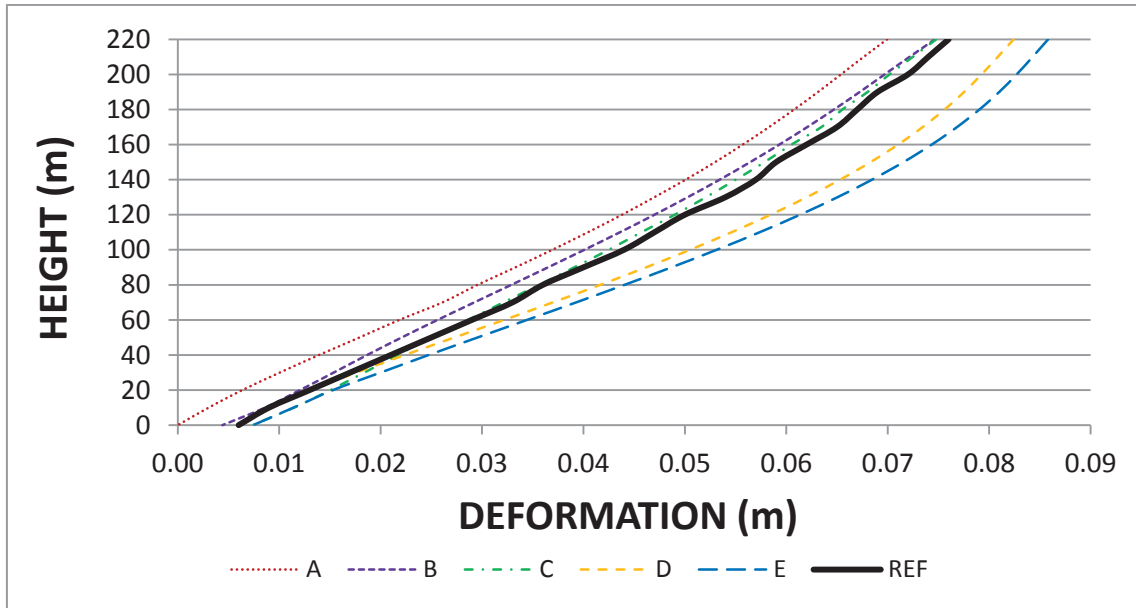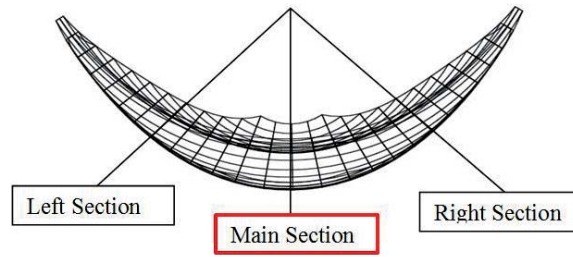
Figure 6: Deformation (Only Static Load) – Main Section (A – E)
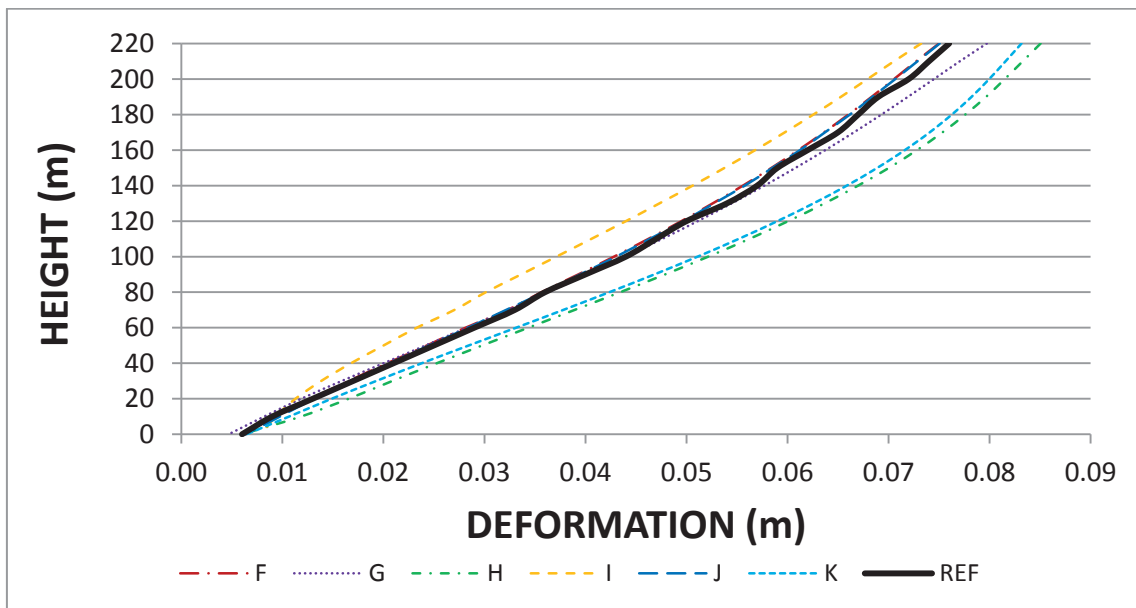
Figure 7: Deformation (Only Static Load) – Main Section (F – K)

Deformations (Only Dynamic Load) – Main Section
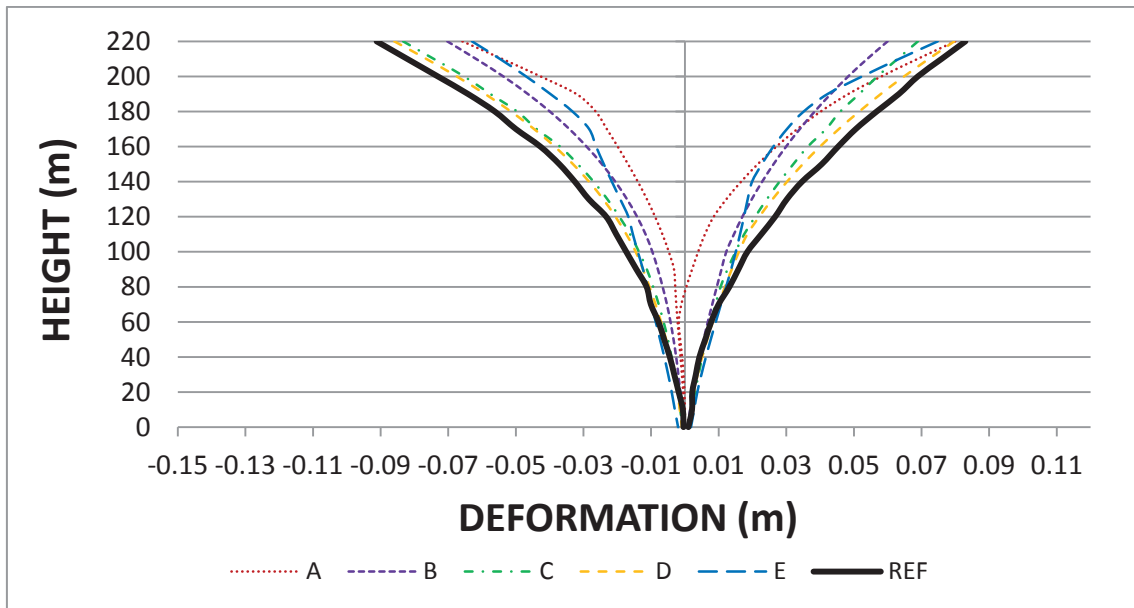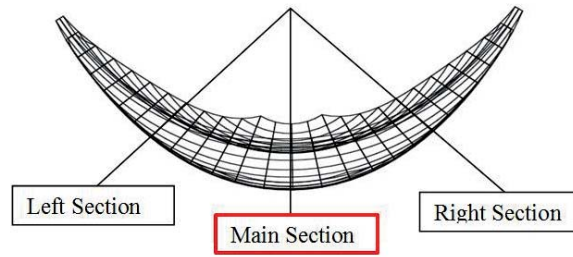
Figure 8: Deformation (Only Dynamic Load) – Main Section (A – E)
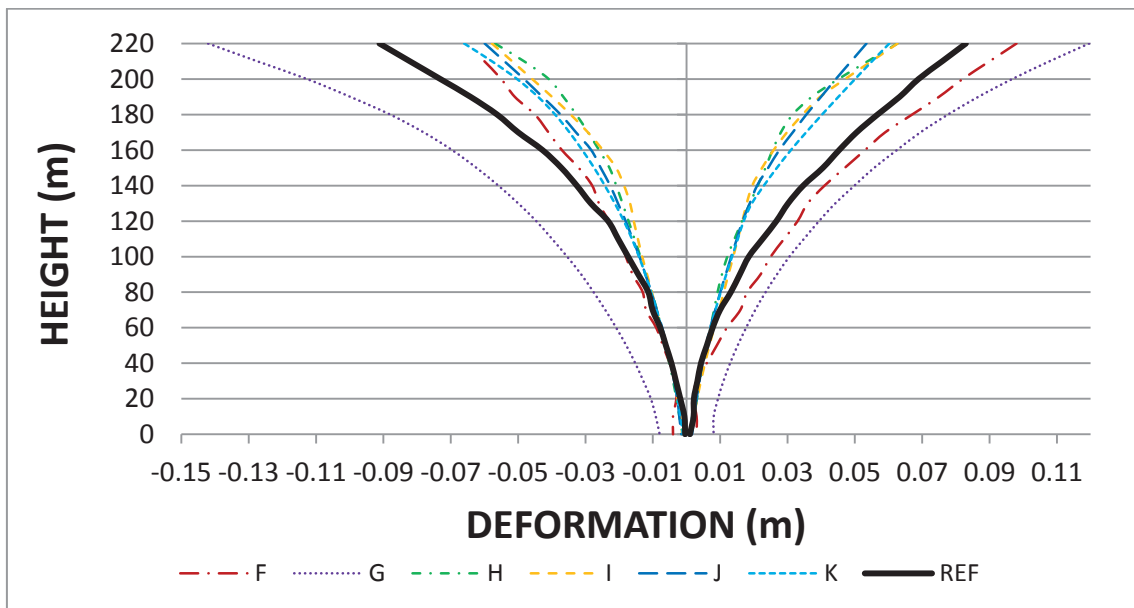
Figure 9: Deformation (Only Dynamic Load) – Main Section (F – K)

Hoop Stresses – Main Section – Upstream
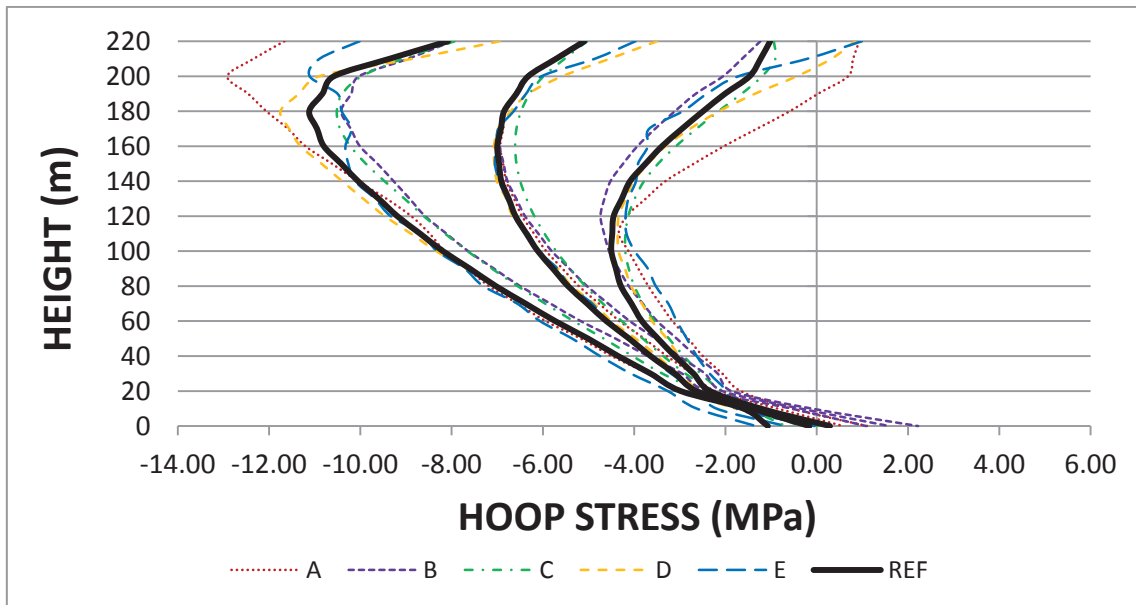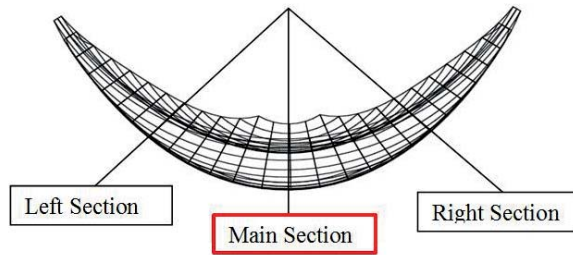
Figure 10: Hoop Stresses – Main Section – Upstream (A – E)
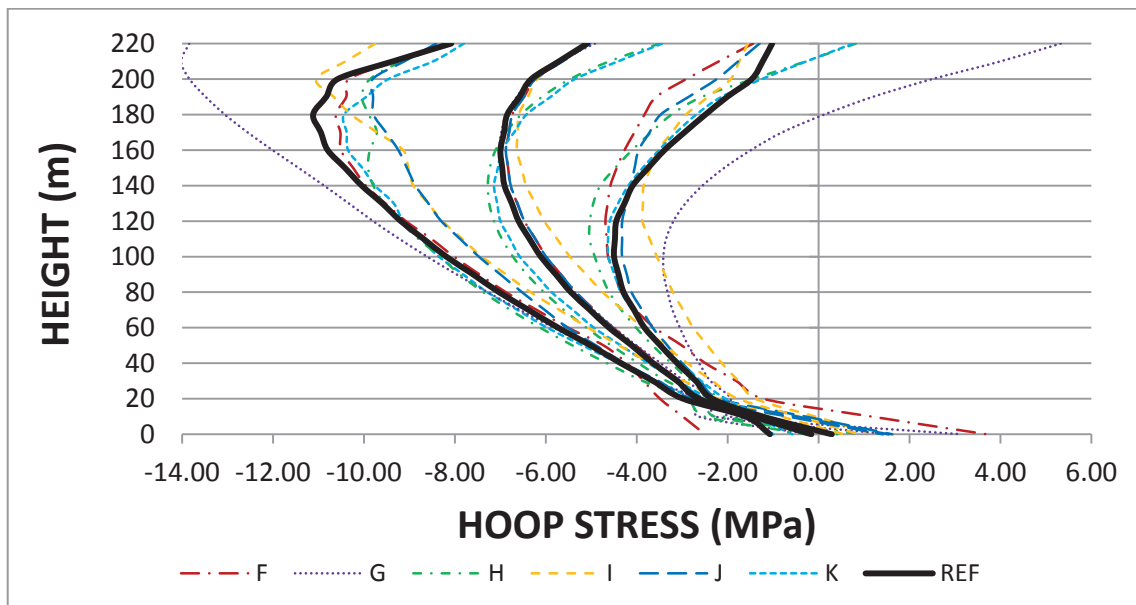
Figure 11: Hoop Stresses – Main Section – Upstream (F – K)

Hoop Stresses (Only Static Load) – Main Section – Upstream
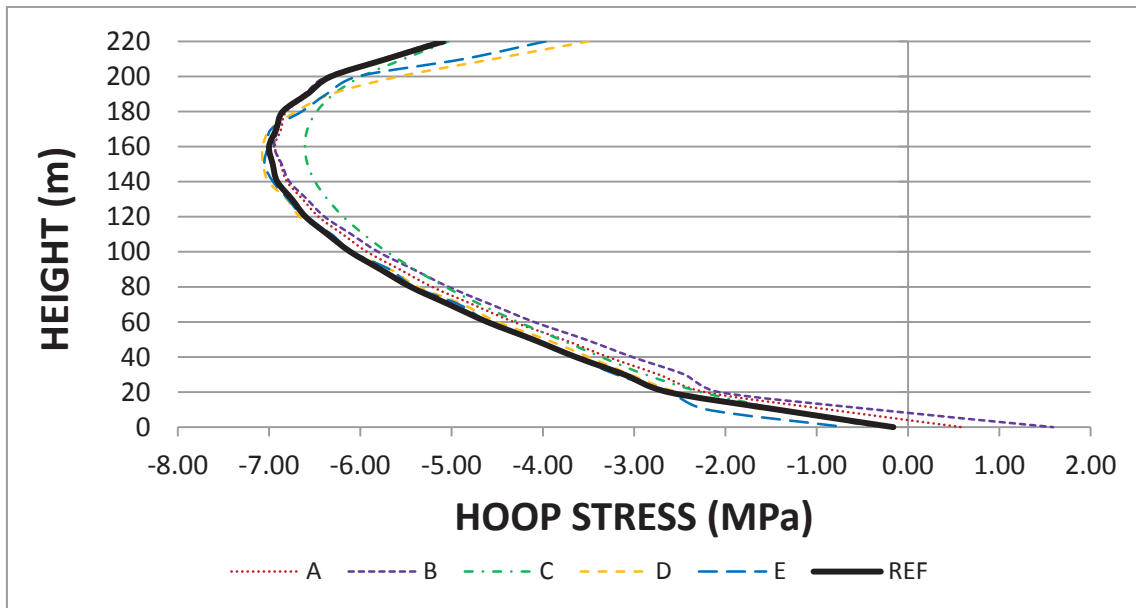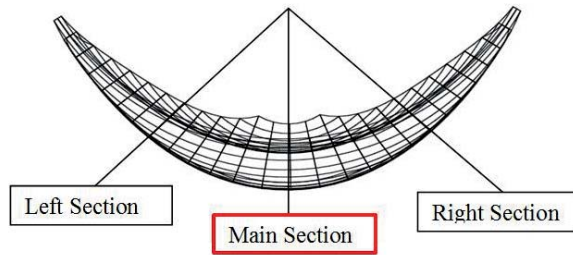
Figure 12: Hoop Stresses (Only Static Load) – Main Section – Upstream (A – E)
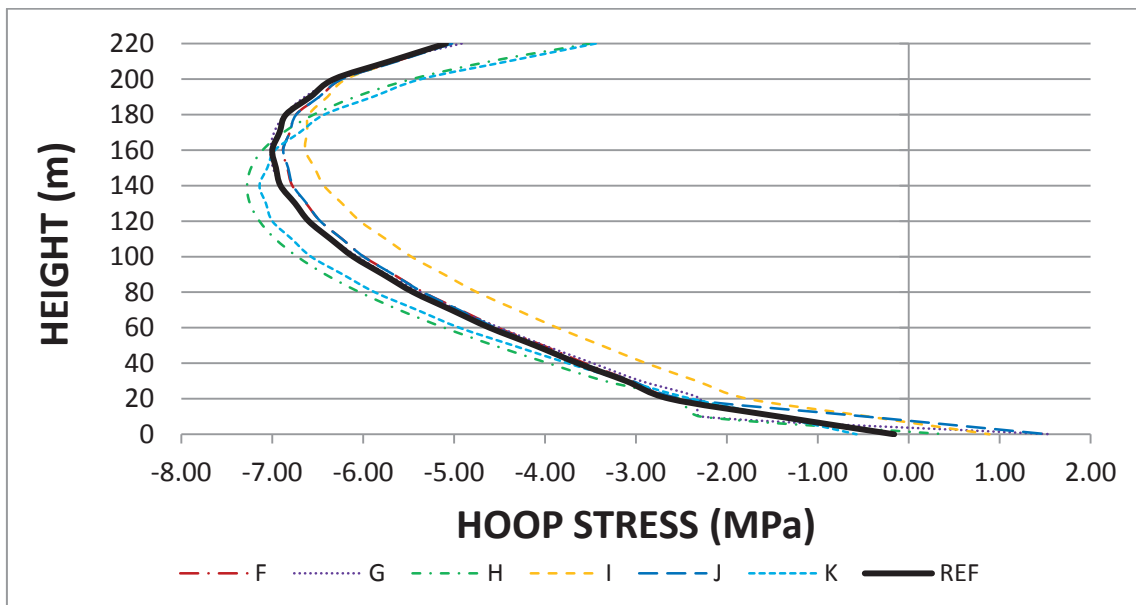
Figure 13: Hoop Stresses (Only Static Load) – Main Section – Upstream (F – K)

Hoop Stresses (Only Dynamic Load) – Main Section – Upstream
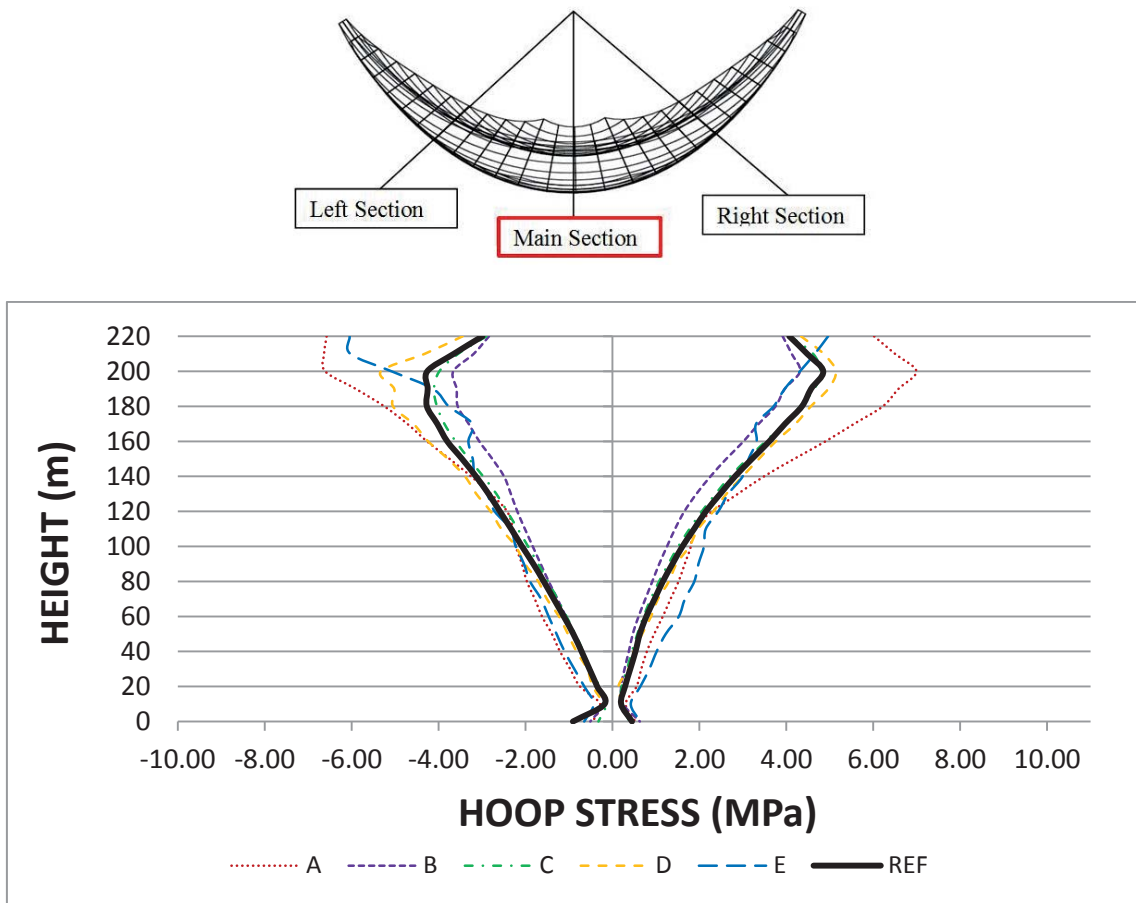
Figure 14: Hoop Stresses (Only Dynamic Load) – Main Section – Upstream (A – E)
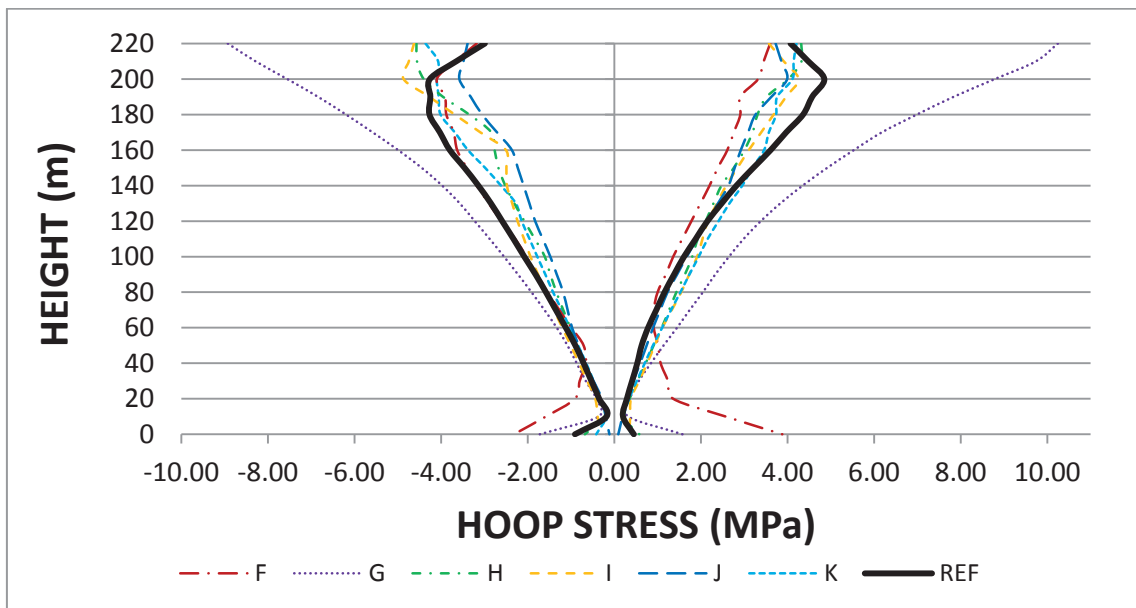
Figure 15: Hoop Stresses (Only Dynamic Load) – Main Section – Upstream (F – K)

Hoop Stresses – Main Section – Downstream
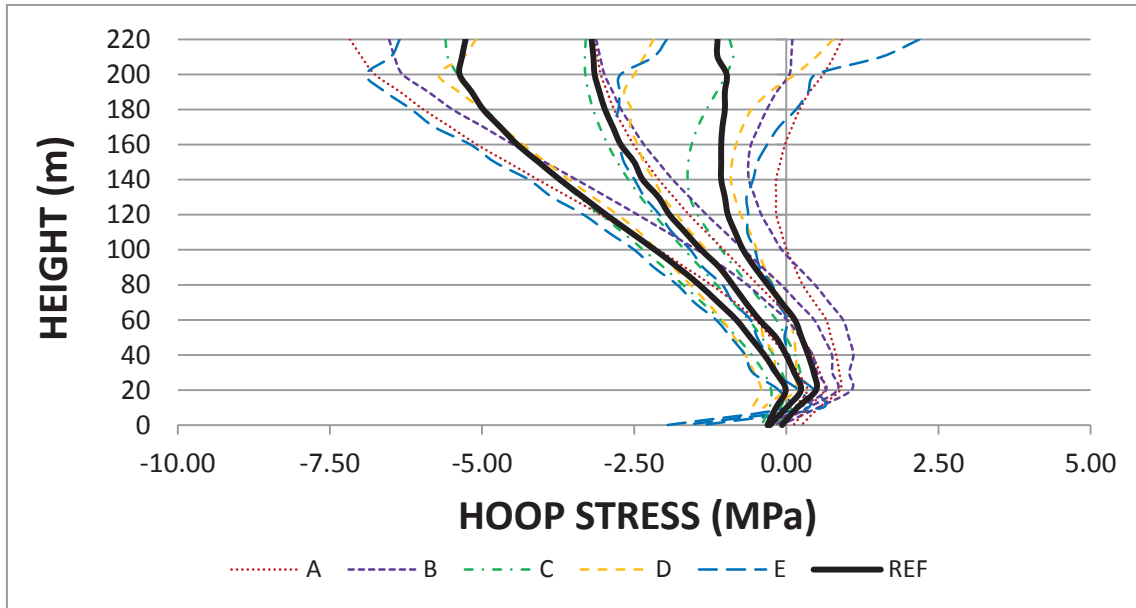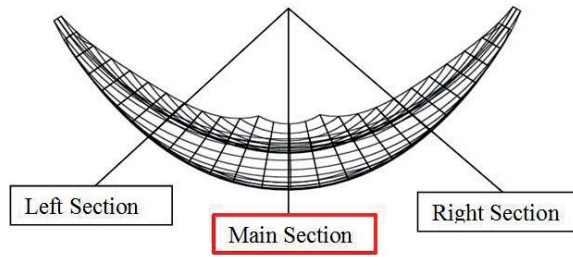
Figure 16: Hoop Stresses – Main Section – Downstream (A – E)
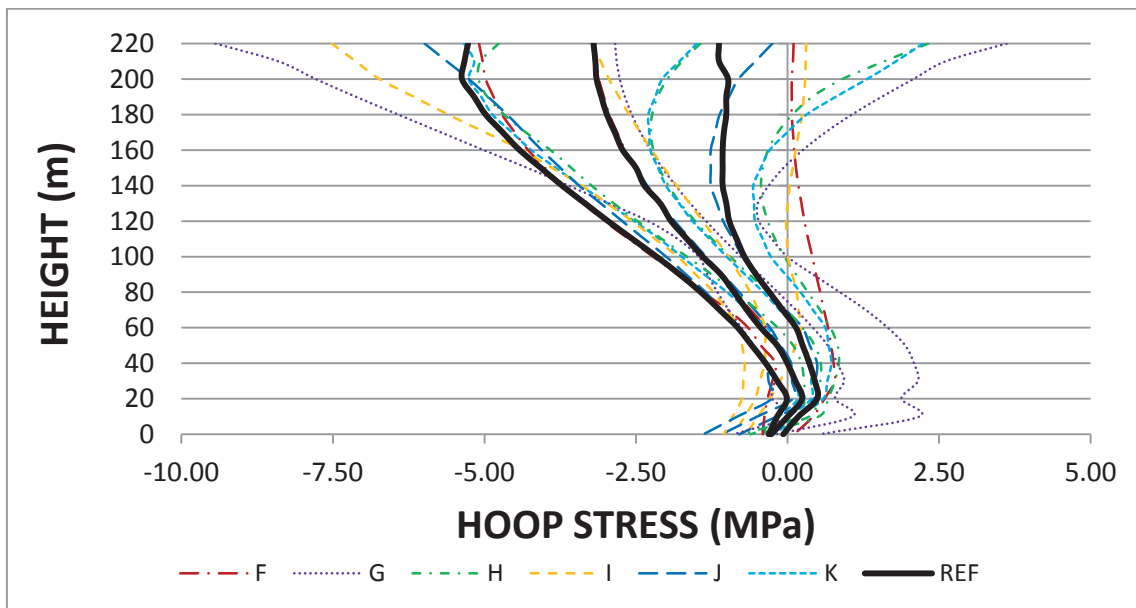
Figure 17: Hoop Stresses – Main Section – Downstream (F – K)

Hoop Stresses – Left Section – Upstream
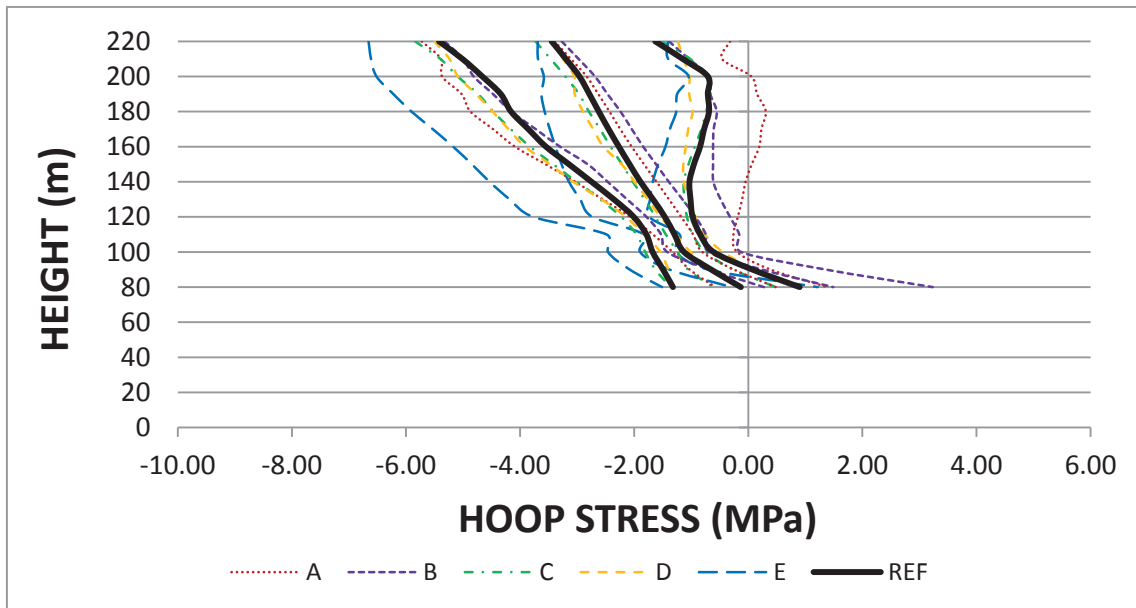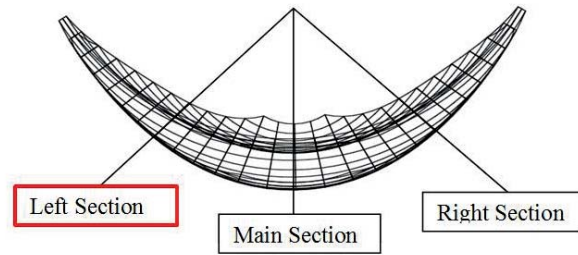
Figure 18: Hoop Stresses – Left Section – Upstream (A – E)
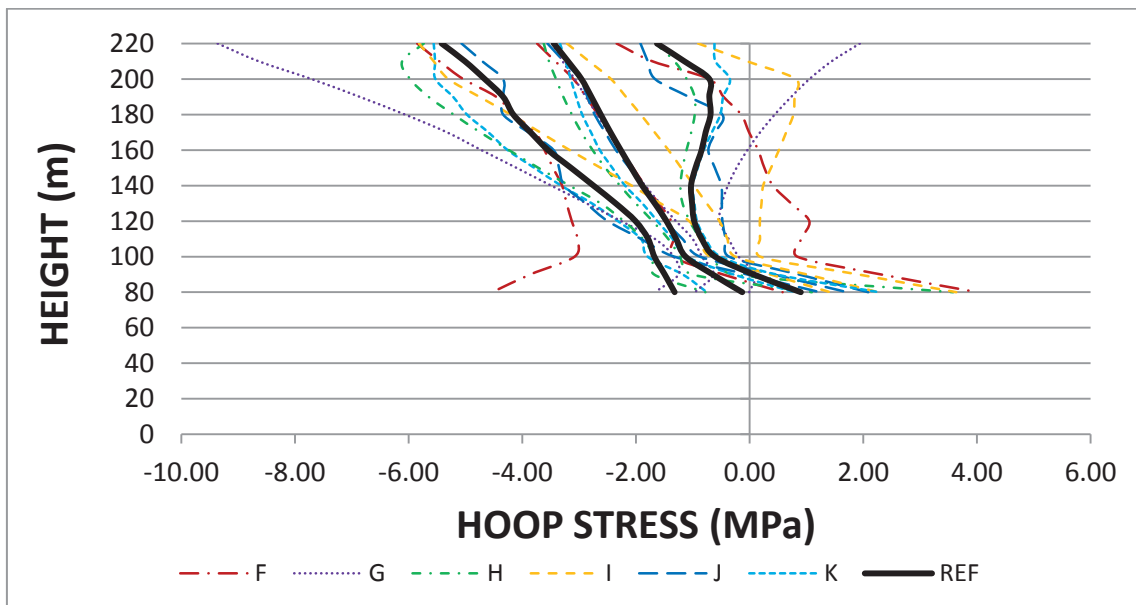
Figure 19: Hoop Stresses – Left Section – Upstream (F – K)

Hoop Stresses – Left Section – Downstream
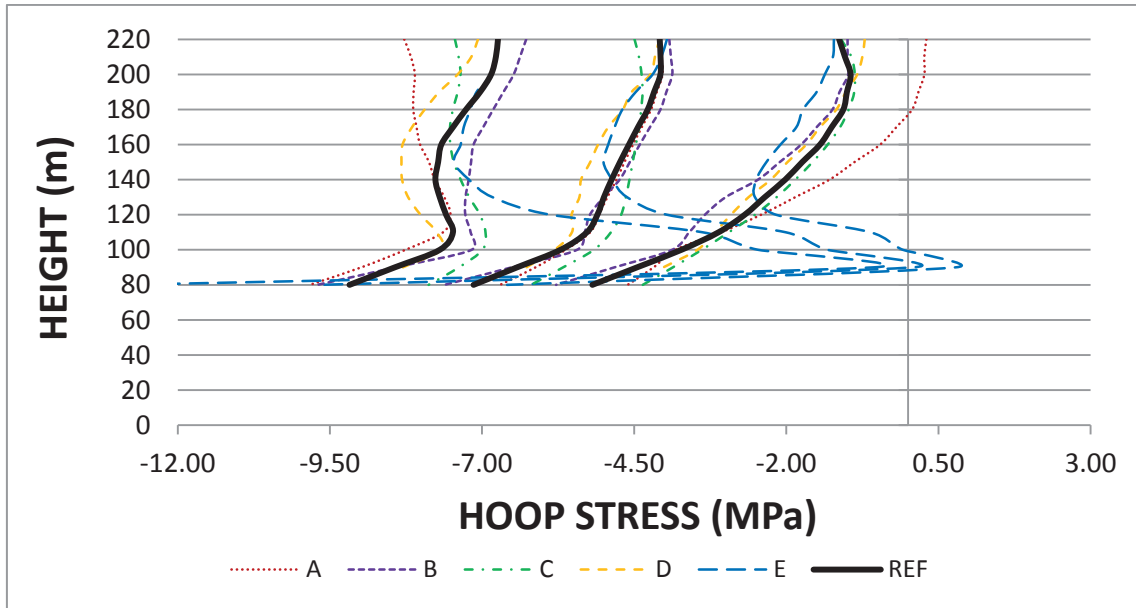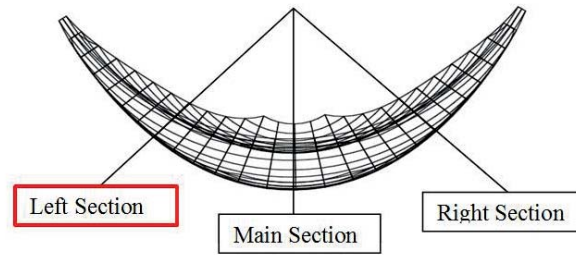
Figure 20: Hoop Stresses – Left Section – Downstream (A – E)
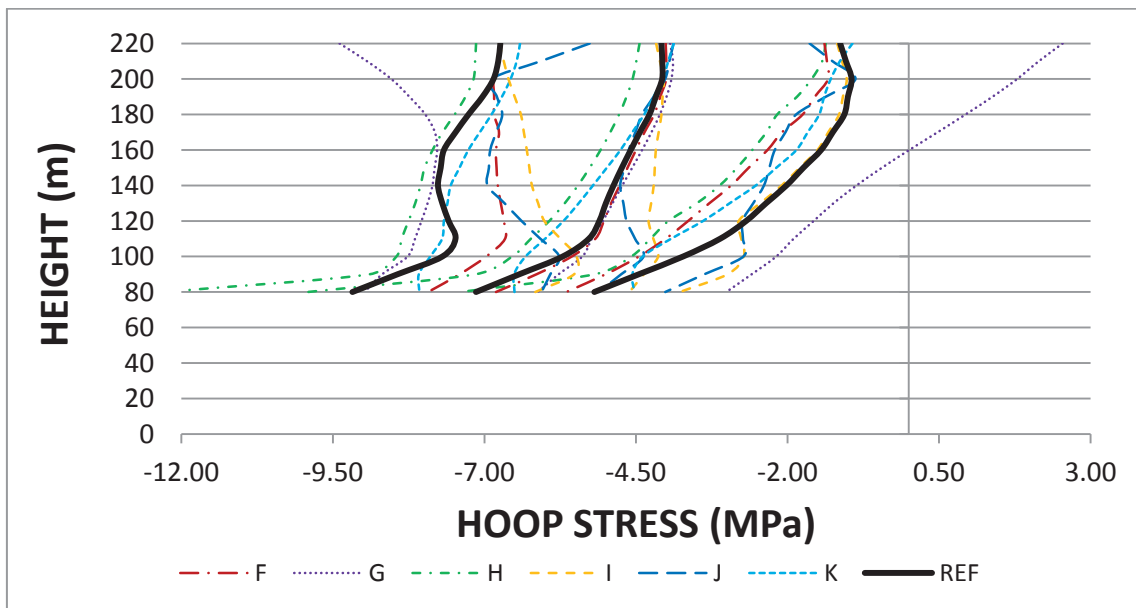
Figure 21: Hoop Stresses – Left Section – Downstream (F – K)

Hoop Stresses – Right Section – Upstream
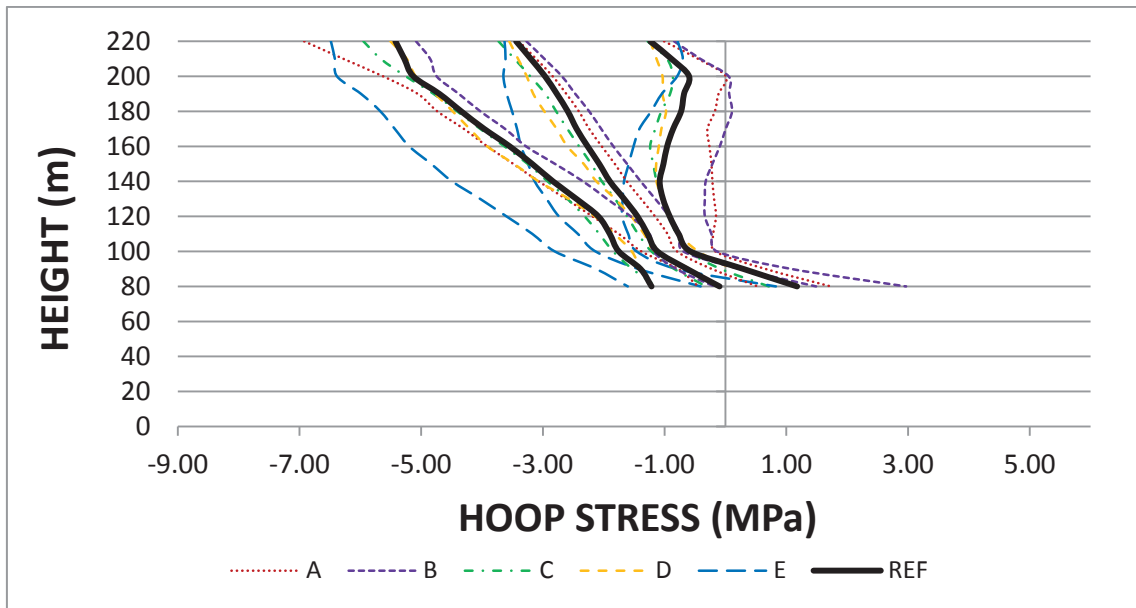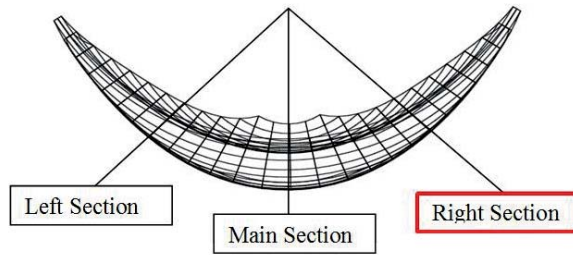
Figure 22: Hoop Stresses – Right Section – Upstream (A – E)
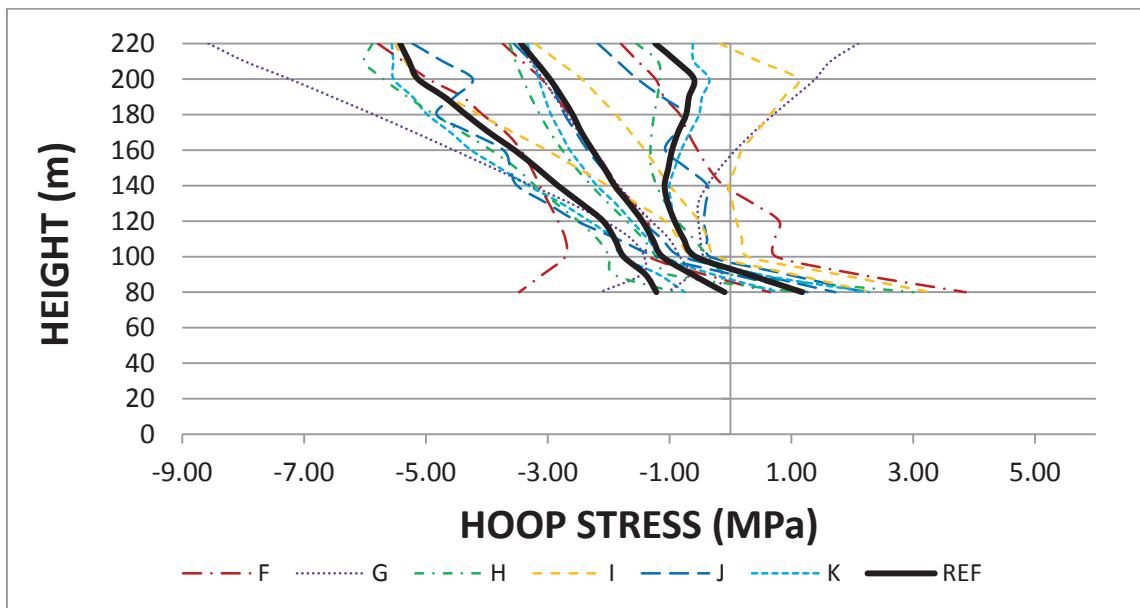
Figure 23: Hoop Stresses – Right Section – Upstream (F – K)

Hoop Stresses – Right Section – Downstream
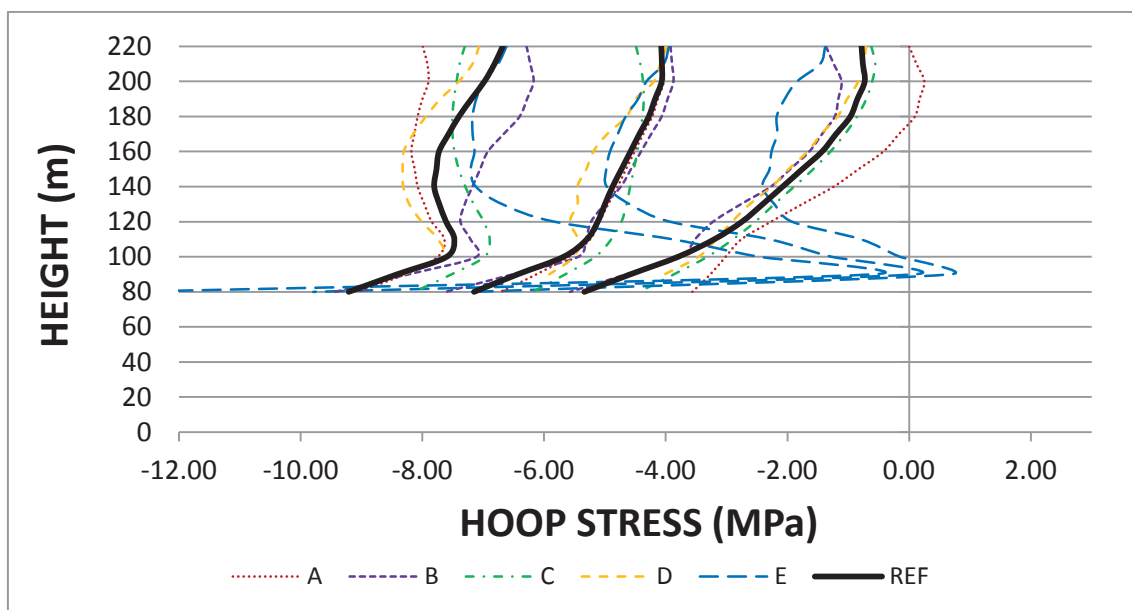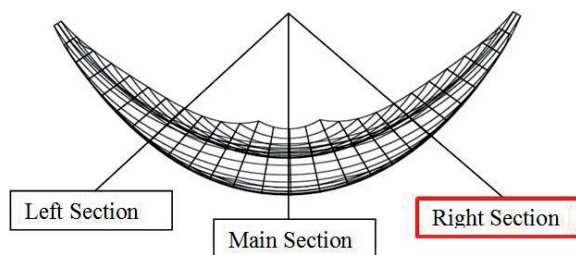
Figure 24: Hoop Stresses – Right Section – Downstream (A – E)
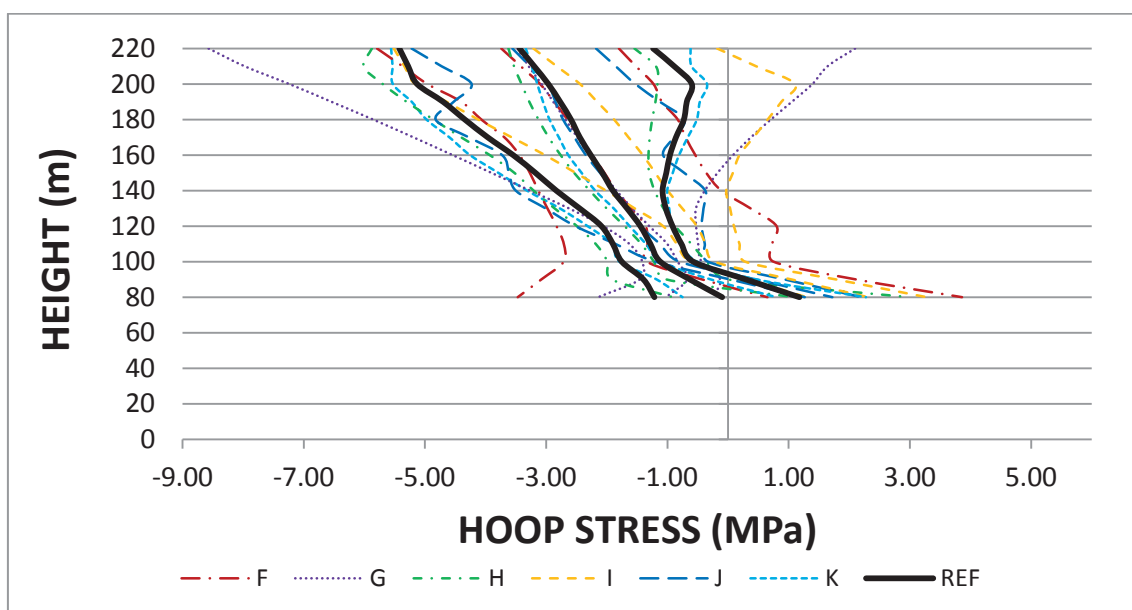
Figure 25: Hoop Stresses – Right Section – Downstream (F – K)

Vertical Stresses – Main Section – Upstream
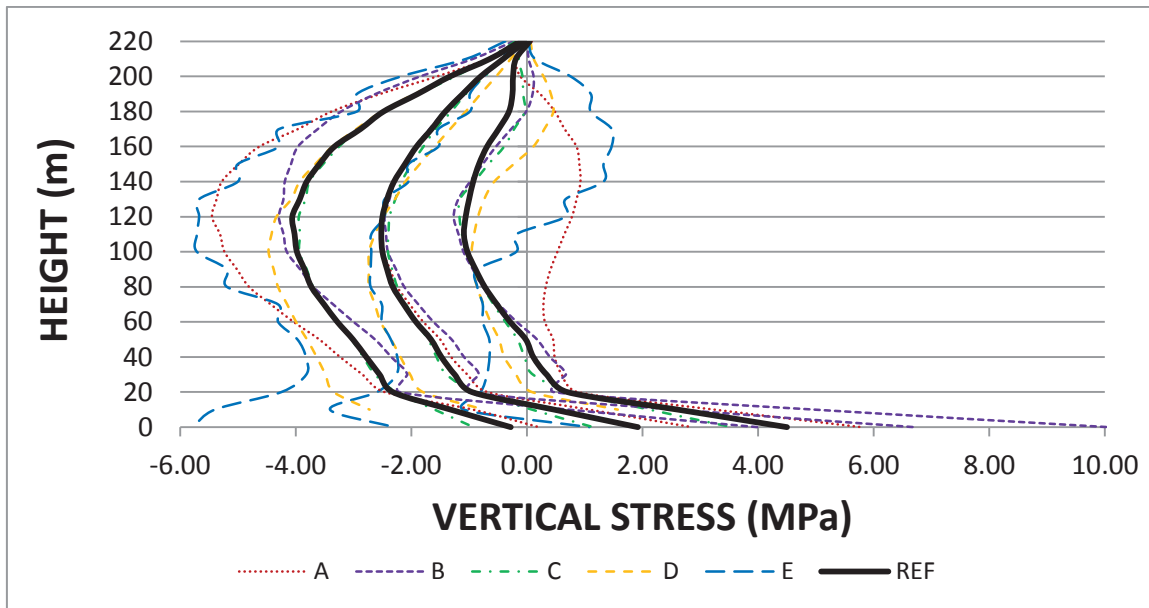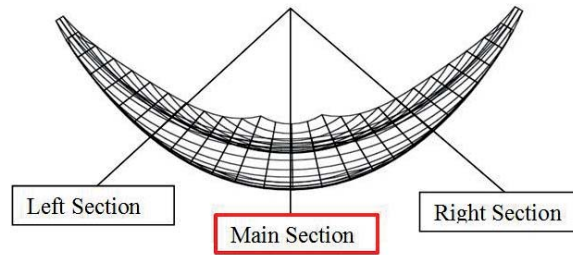
Figure 26: Vertical Stresses – Main Section – Upstream (A – E)
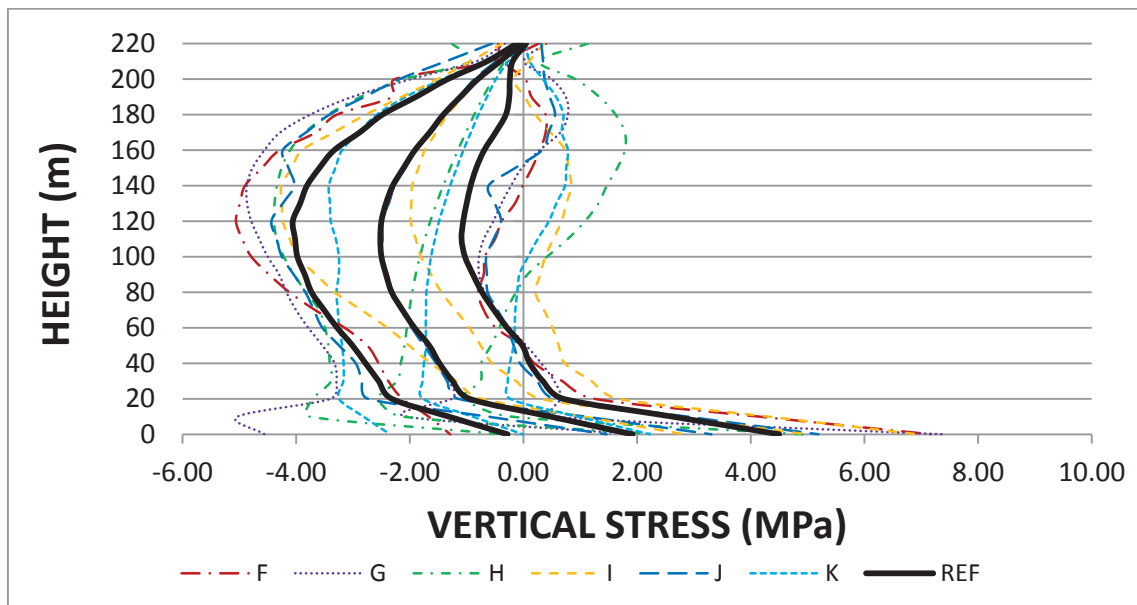
Figure 27: Vertical Stresses – Main Section – Upstream (F – K)

Vertical Stresses – Main Section – Downstream
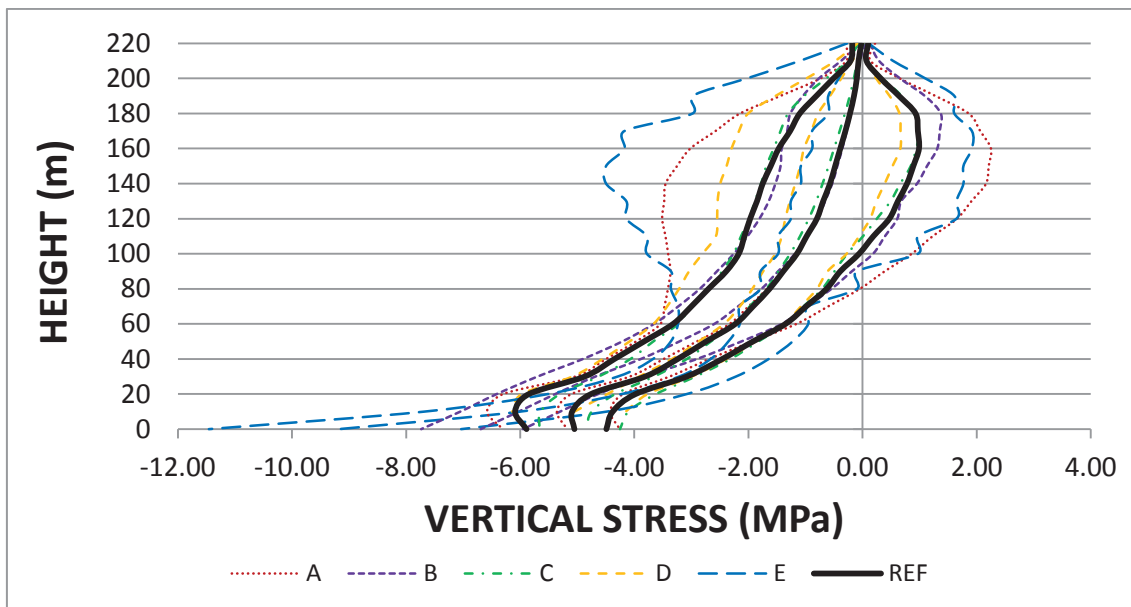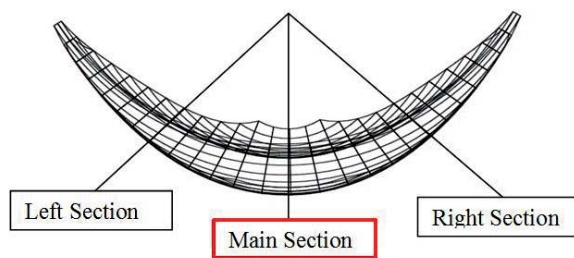
Figure 28: Vertical Stresses – Main Section – Downstream (A – E)
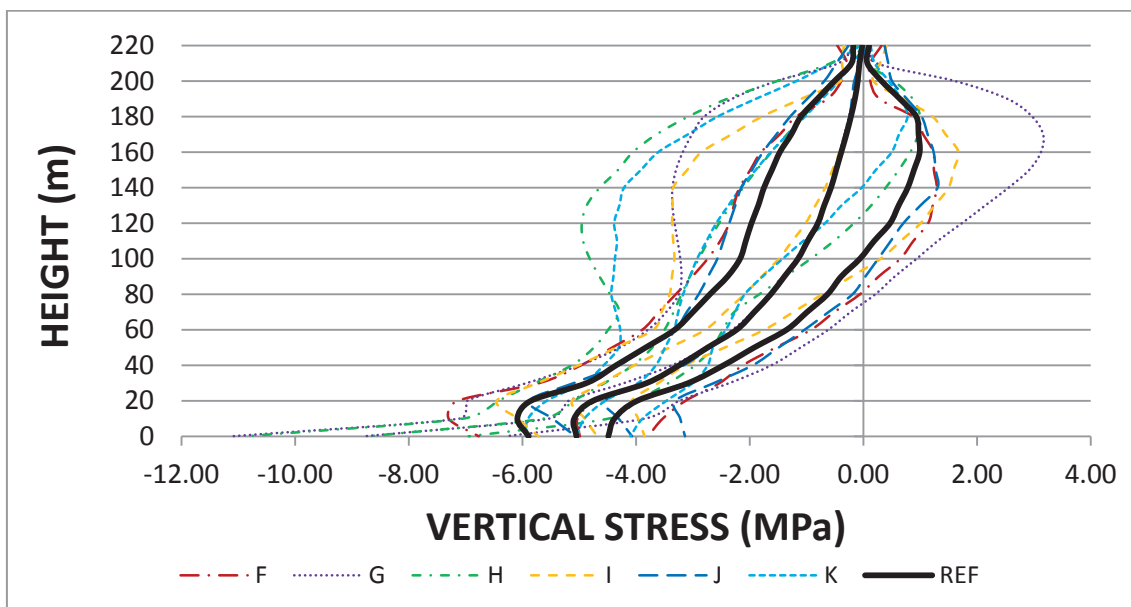
Figure 29: Vertical Stresses – Main Section – Downstream (F – K)

46

Vertical Stresses – Left Section – Upstream
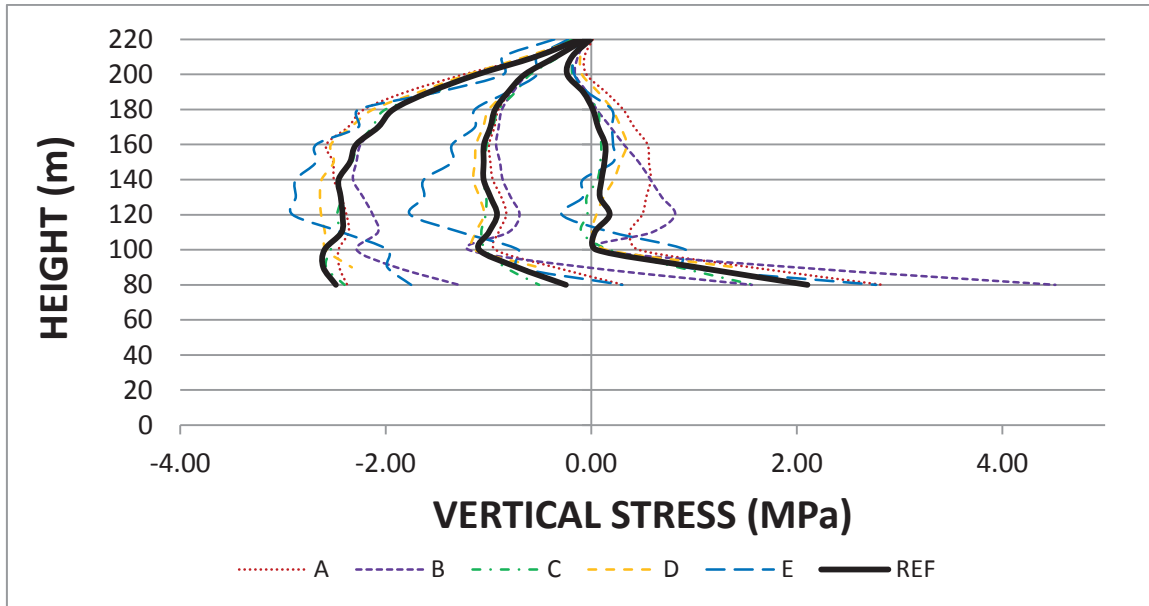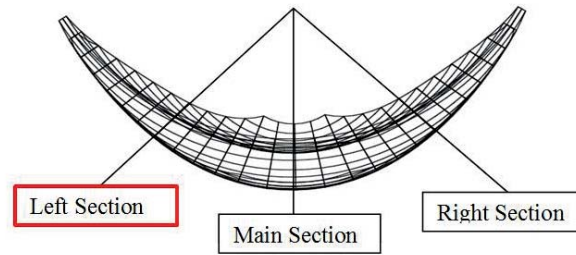
Figure 30: Vertical Stresses – Left Section – Upstream (A – E)
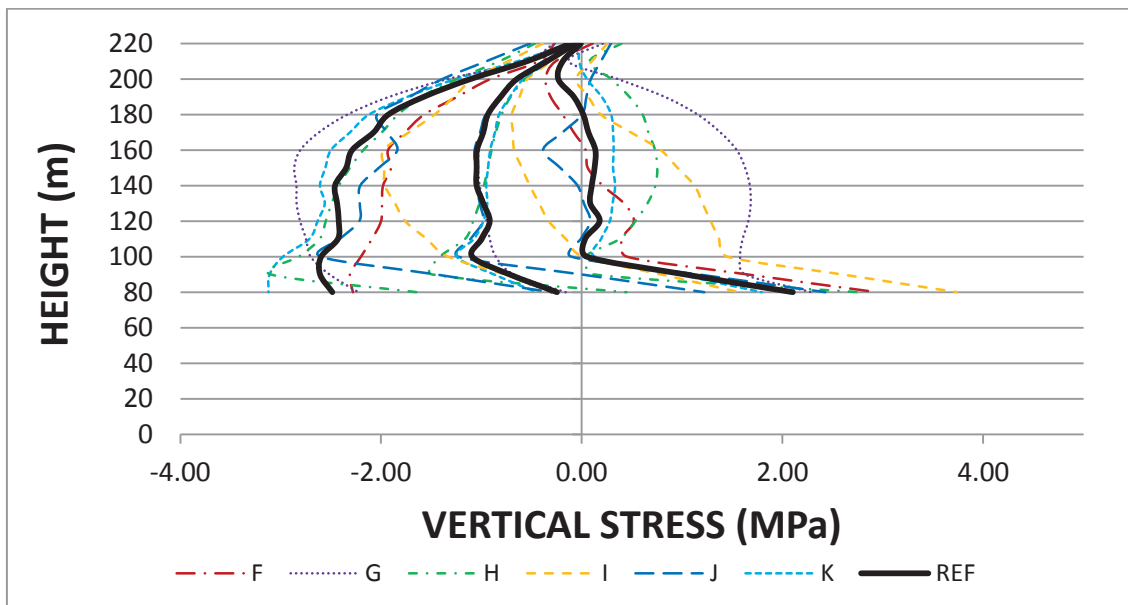
Figure 31: Vertical Stresses – Left Section – Upstream (F – K)

Vertical Stresses – Left Section – Downstream
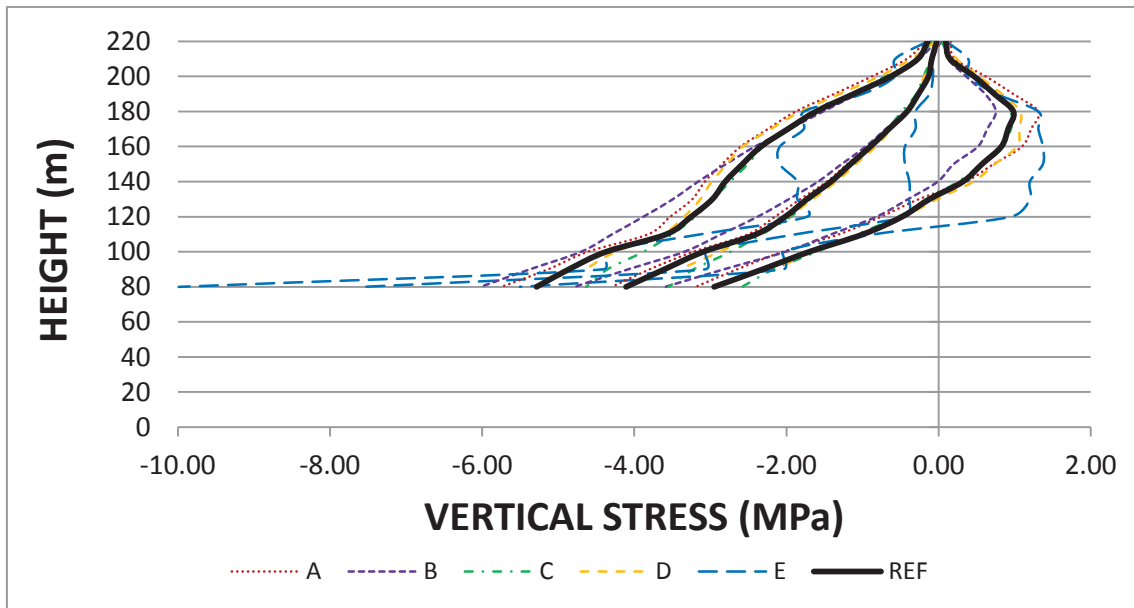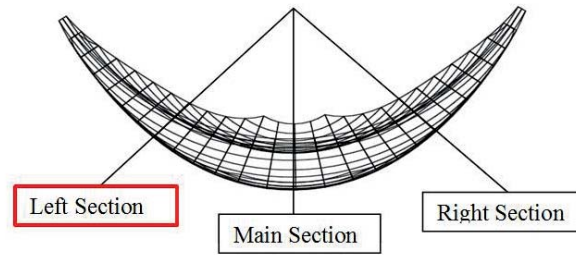
Figure 32: Vertical Stresses – Left Section – Downstream (A – E)
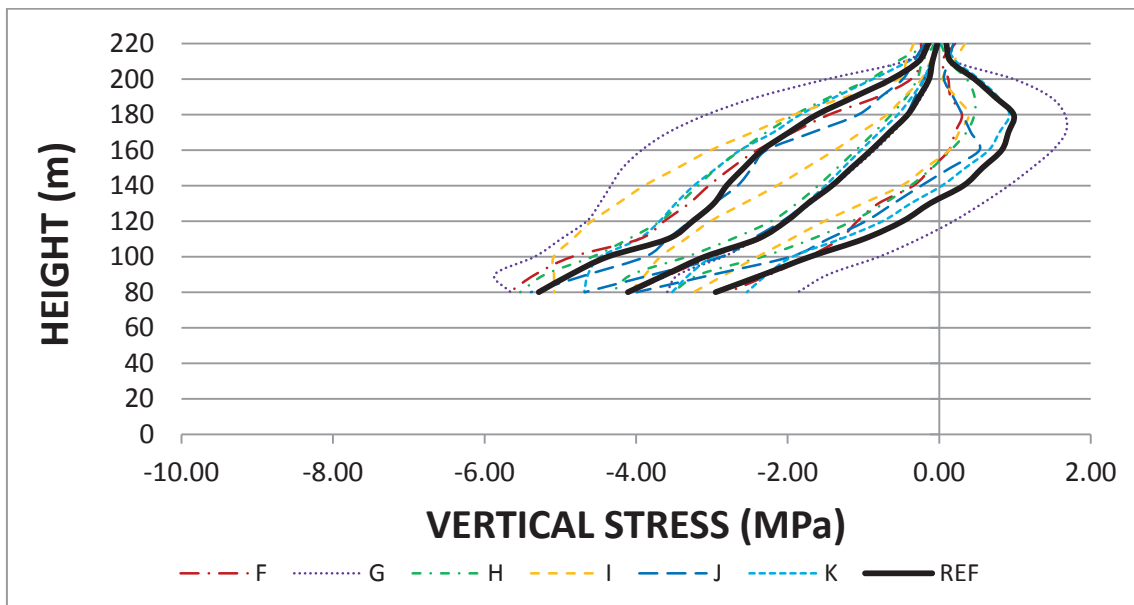
Figure 33: Vertical Stresses – Left Section – Downstream (F – K)

Vertical Stresses – Right Section – Upstream
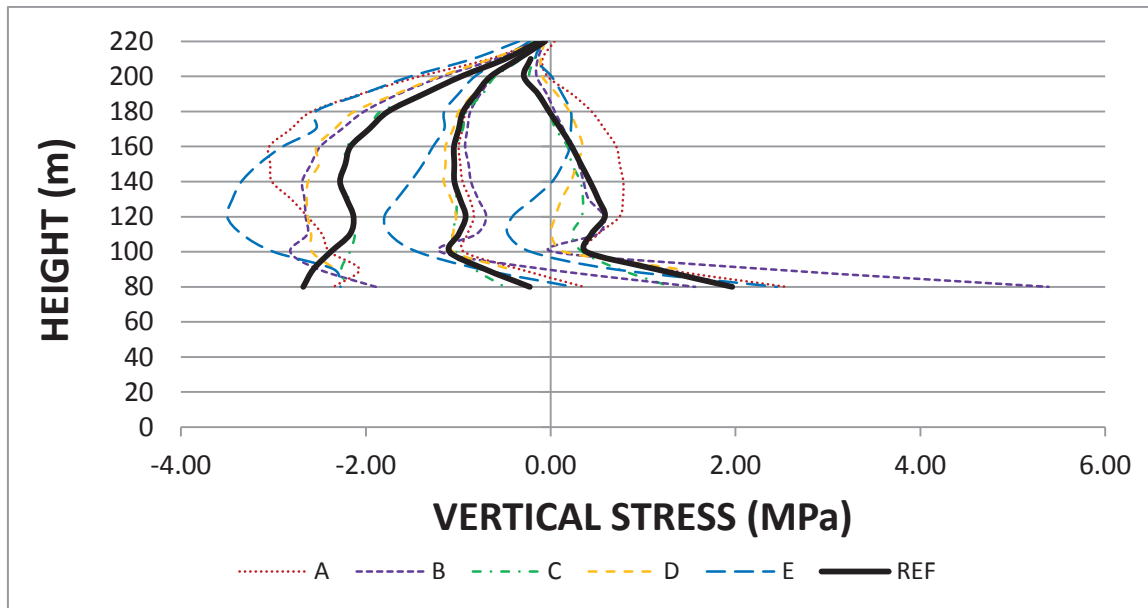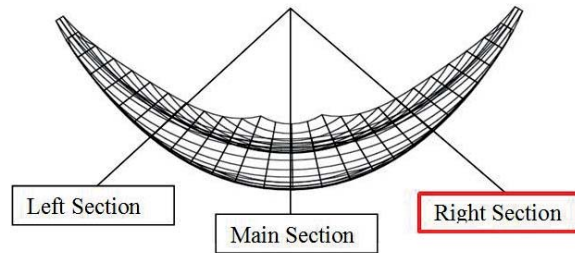
Figure 34: Vertical Stresses – Right Section – Upstream (A – E)
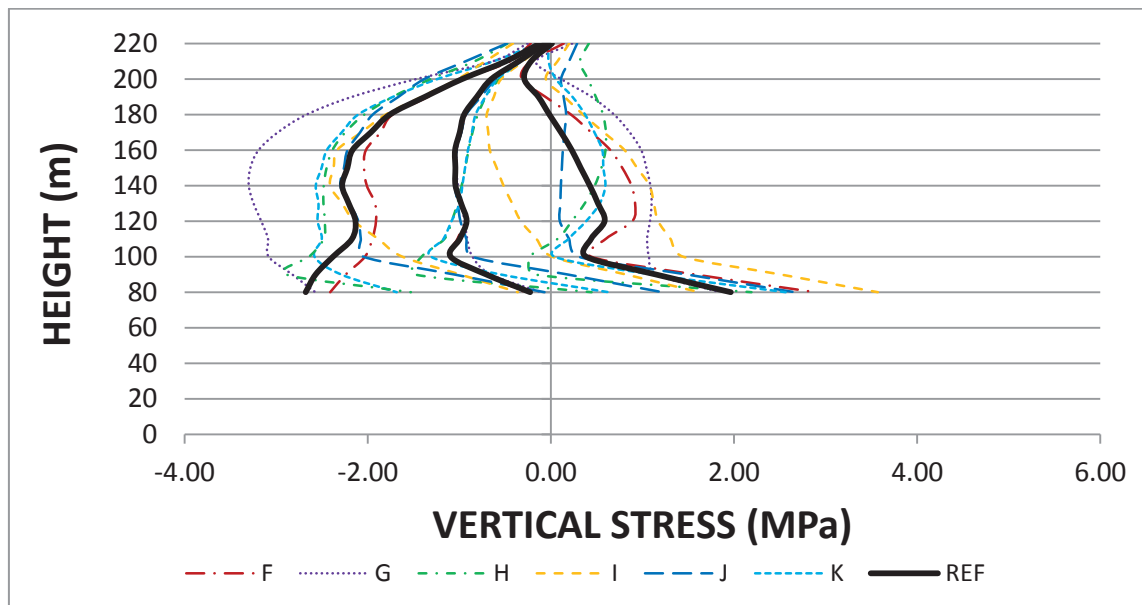
Figure 35: Vertical Stresses – Right Section – Upstream (F – K)

Vertical Stresses – Right Section – Downstream
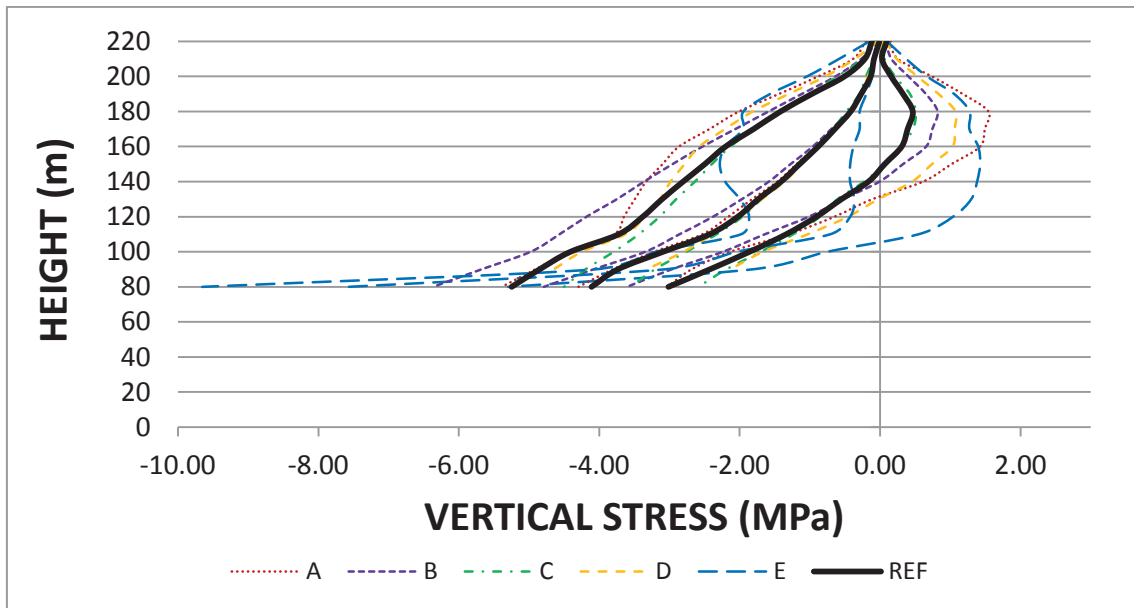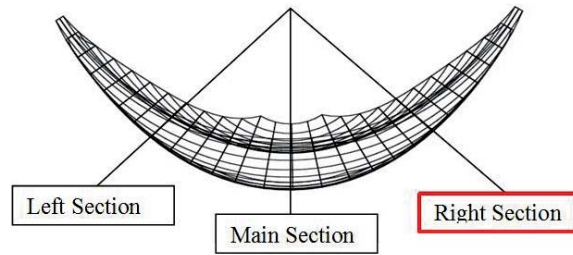
Figure 36: Vertical Stresses – Right Section – Downstream (A – E)
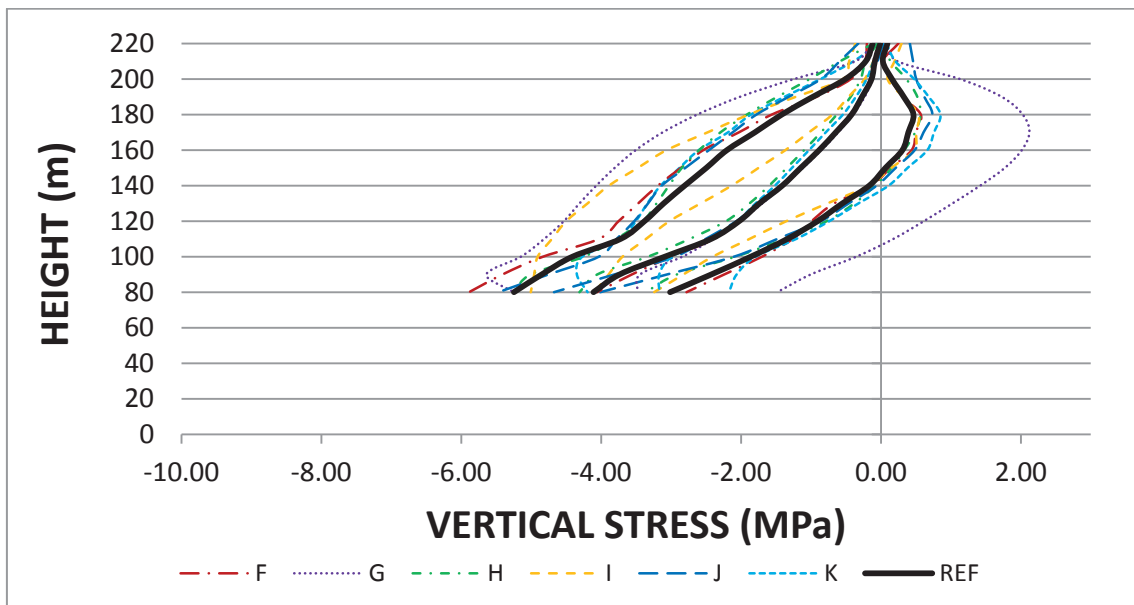
Figure 37: Vertical Stresses – Right Section – Downstream (F – K)

Minimum Principal Stresses – Main Section – Upstream
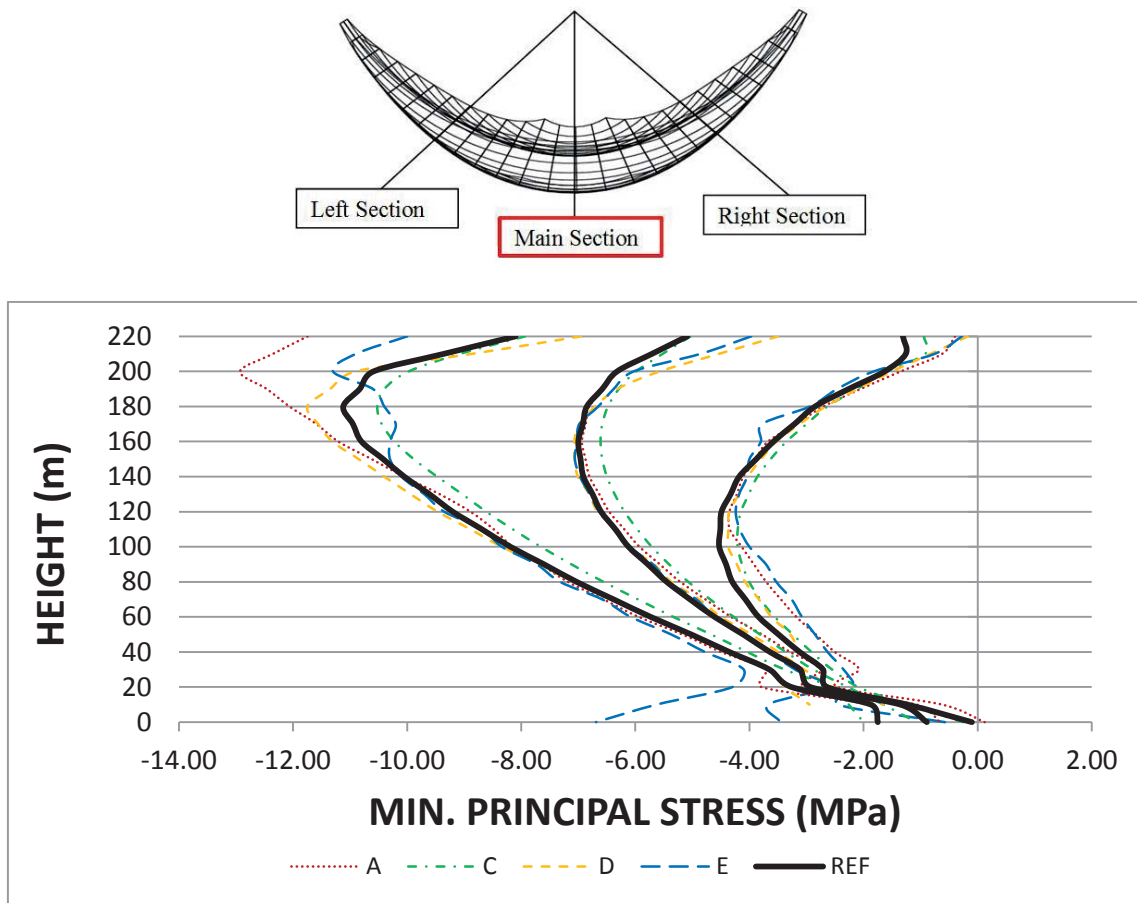
Figure 38: Minimum Principal Stresses – Main Section – Upstream (A – E)
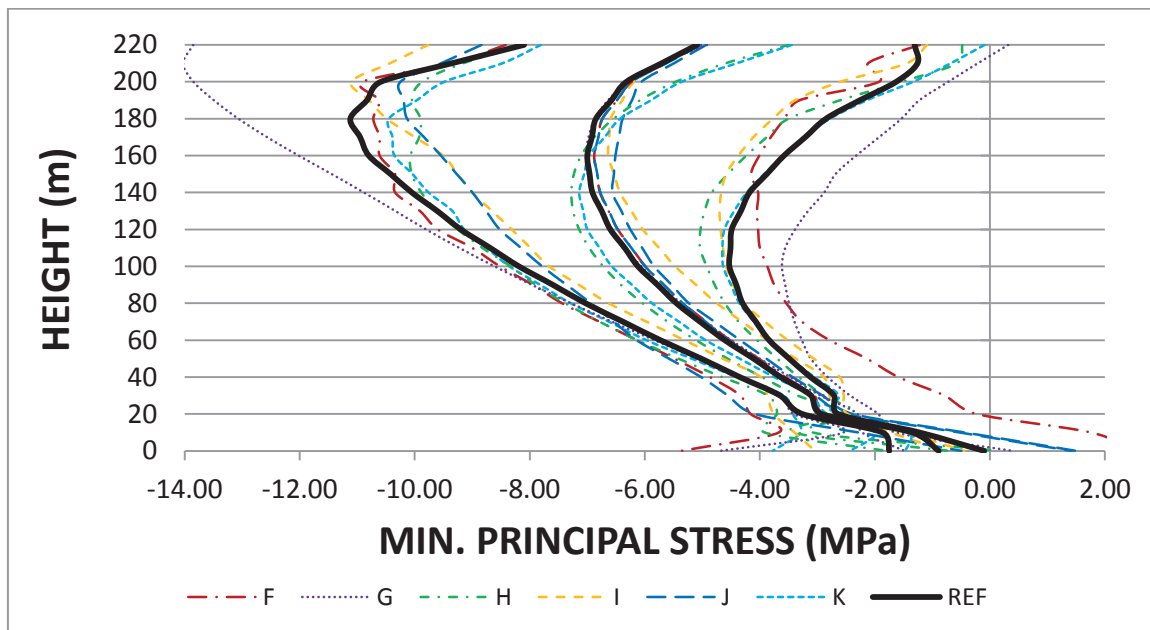
Figure 39: Minimum Principal Stresses – Main Section – Upstream (F – K)

Minimum Principal Stresses – Main Section – Downstream
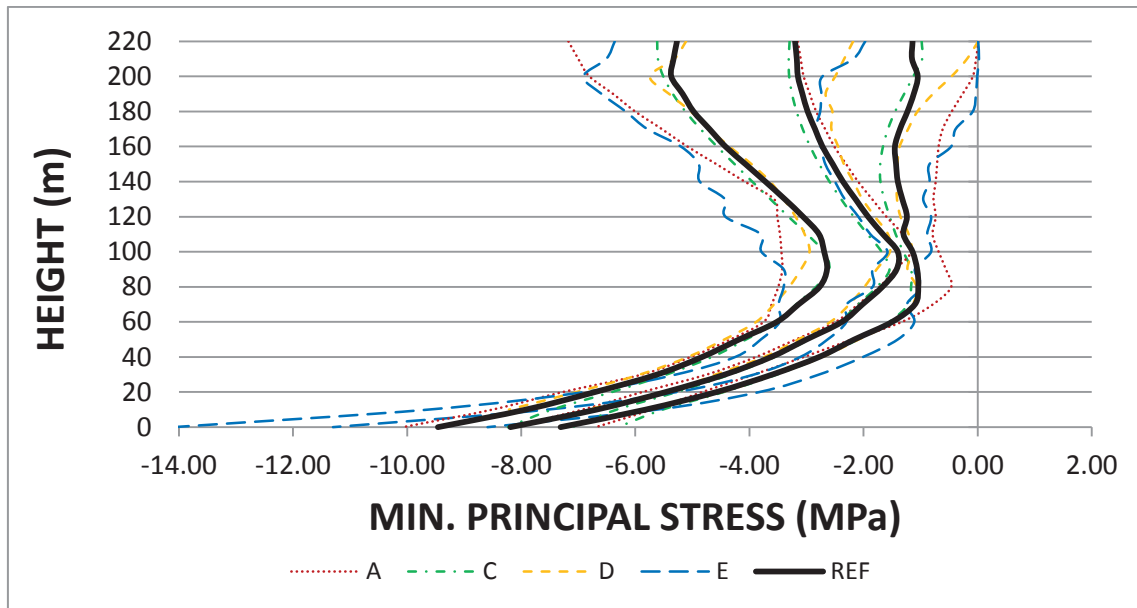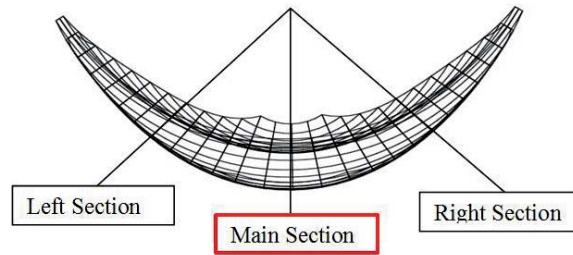
Figure 40: Minimum Principal Stresses – Main Section – Downstream (A – E)
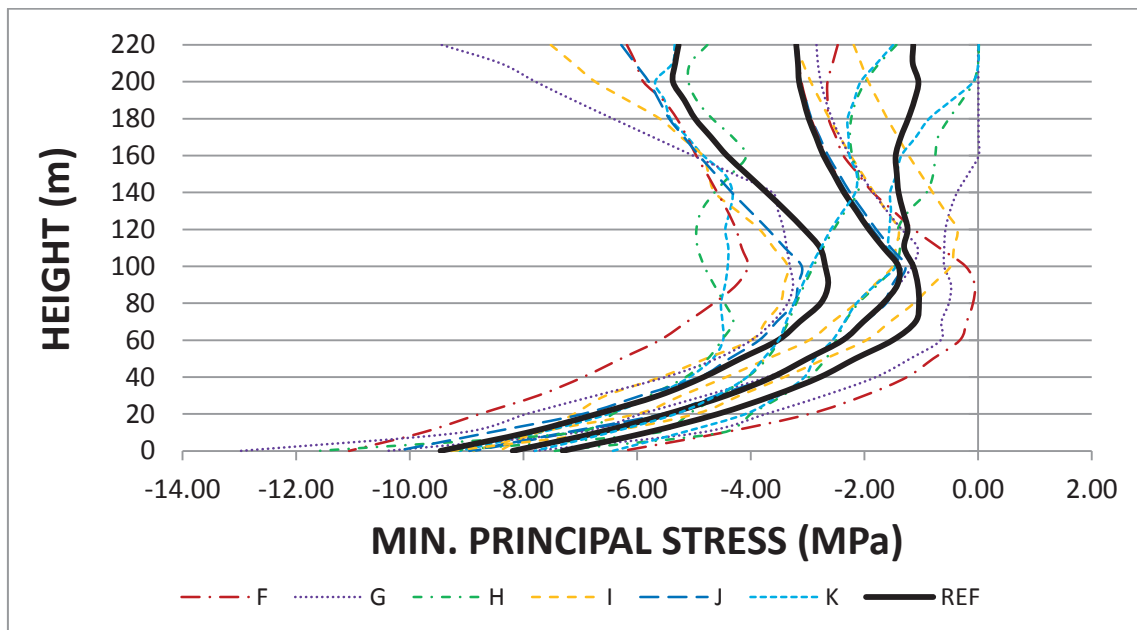
Figure 41: Minimum Principal Stresses – Main Section – Downstream (F – K)

Minimum Principal Stresses – Left Section – Upstream
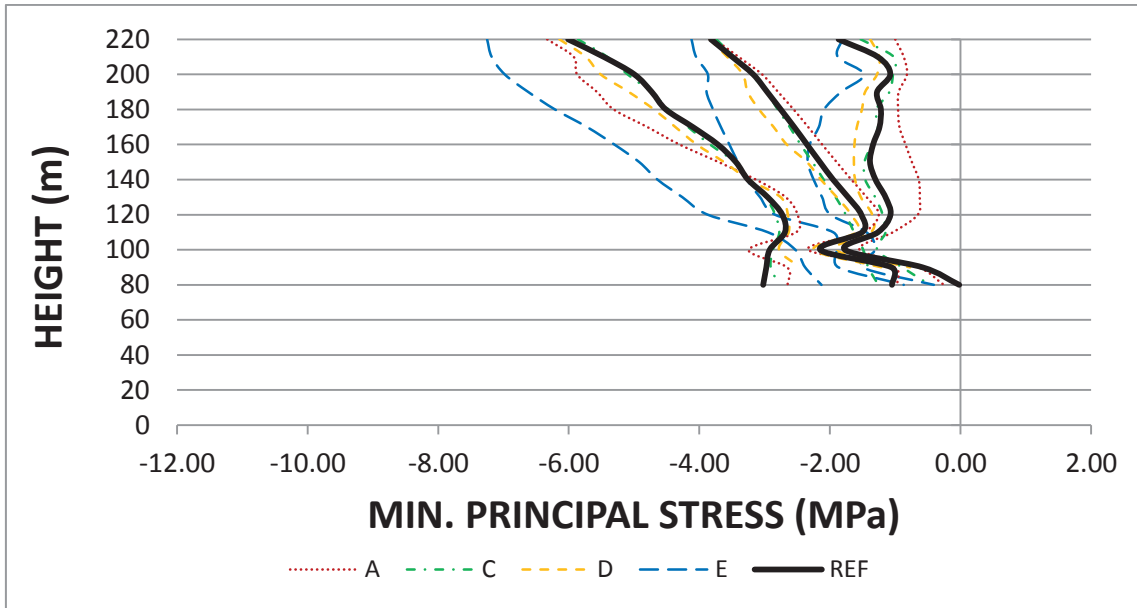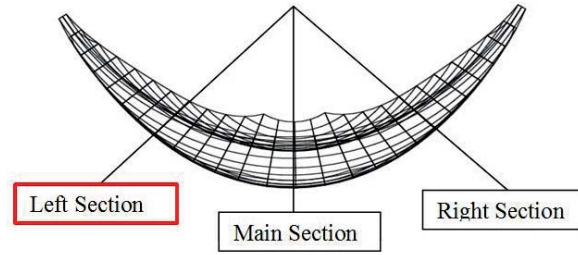
Figure 42: Minimum Principal Stresses – Left Section – Upstream (A – E)
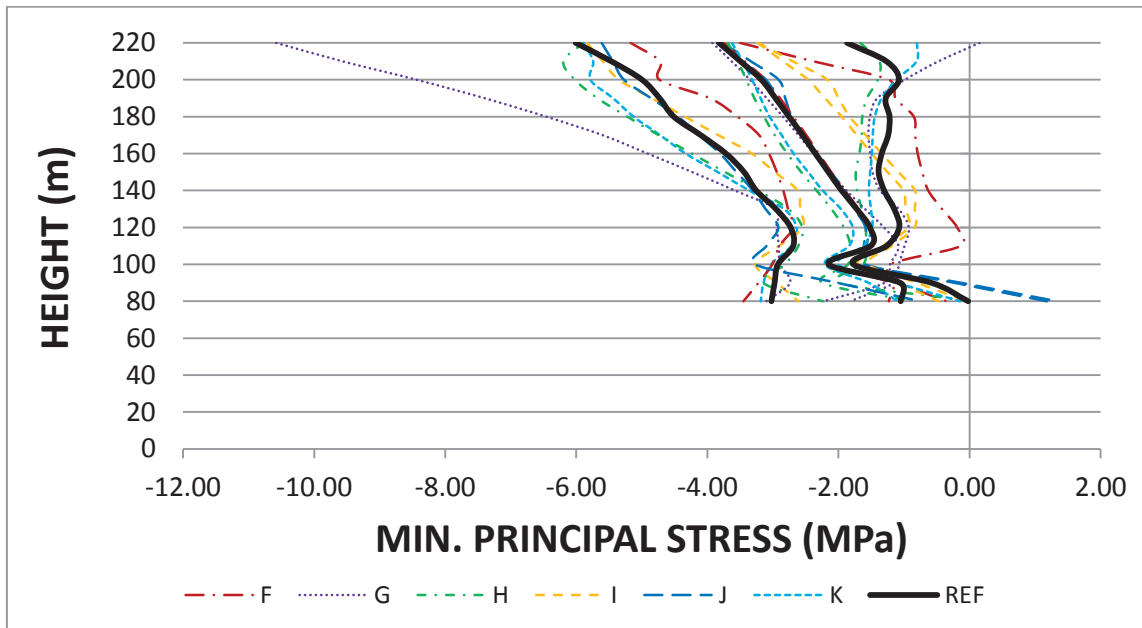
Figure 43: Minimum Principal Stresses – Left Section – Upstream (F – K)

Minimum Principal Stresses – Left Section – Downstream
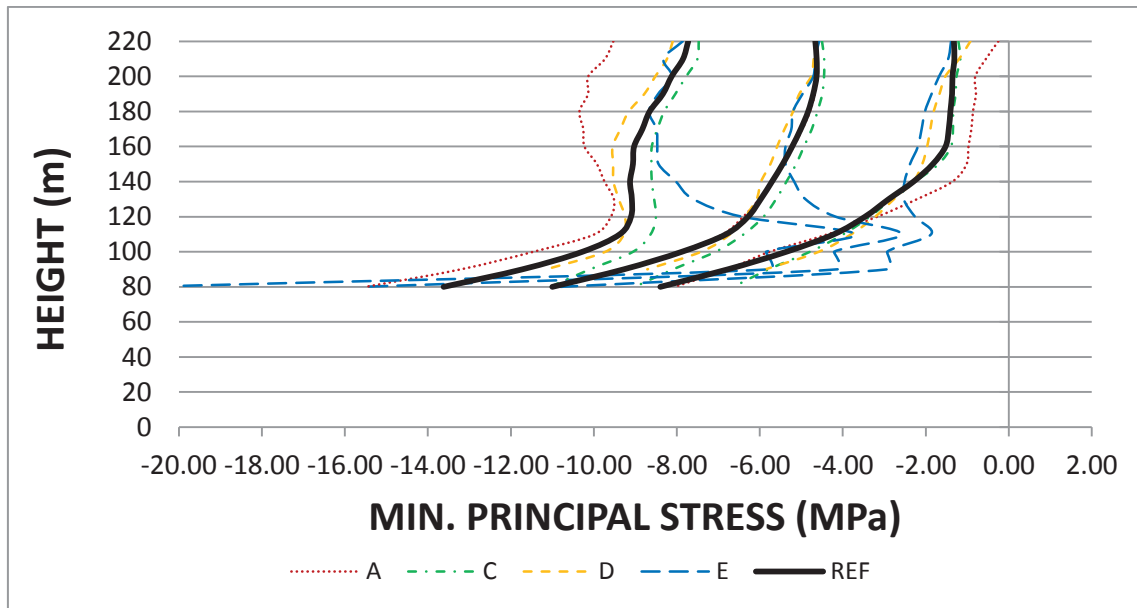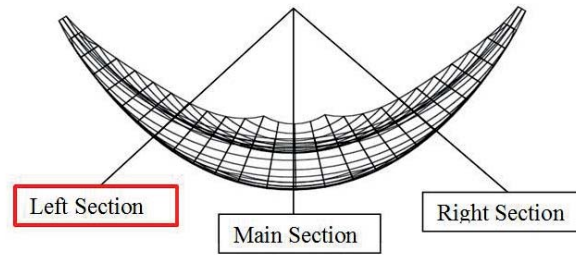
Figure 44: Minimum Principal Stresses – Left Section – Downstream (A – E)
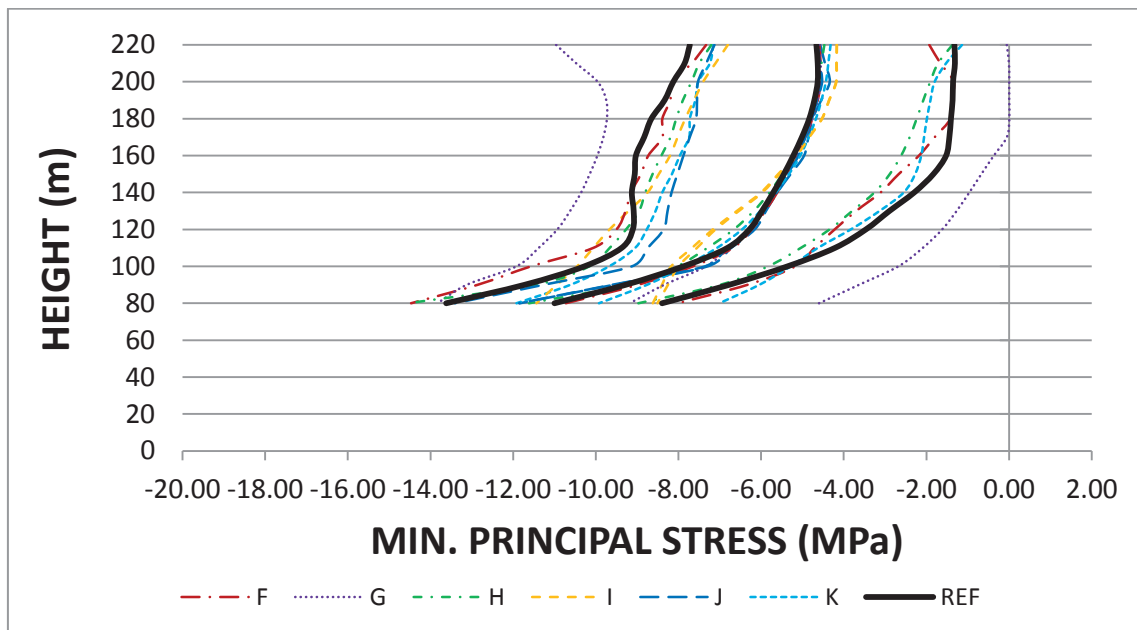
Figure 45: Minimum Principal Stresses – Left Section – Downstream (F – K)

Minimum Principal Stresses – Right Section – Upstream
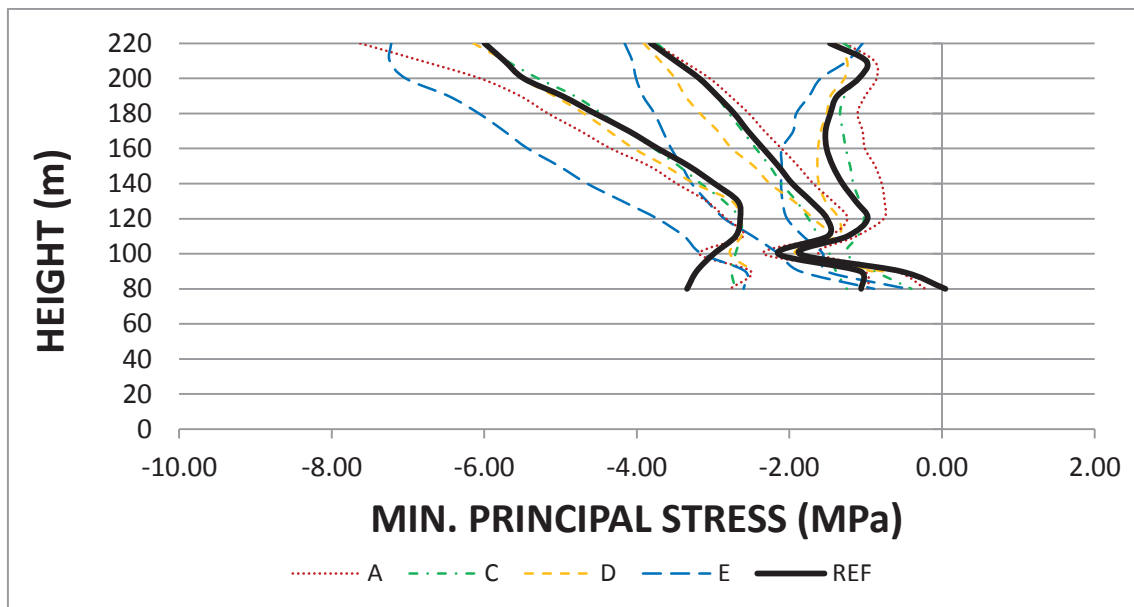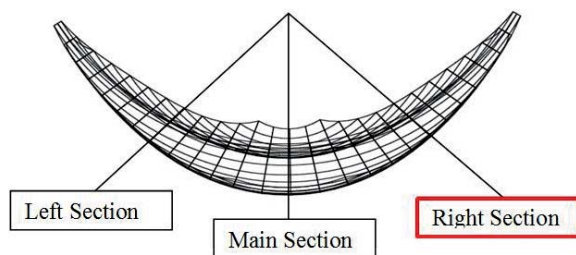
Figure 46: Minimum Principal Stresses – Right Section – Upstream (A – E)
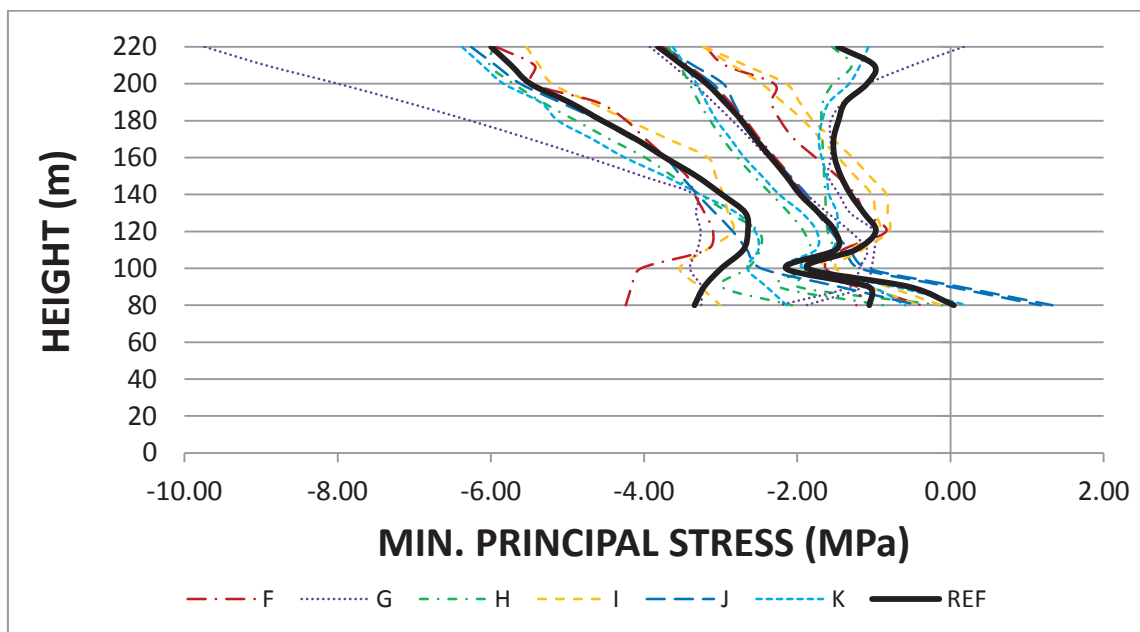
Figure 47: Minimum Principal Stresses – Right Section – Upstream (F – K)

Minimum Principal Stresses – Right Section – Downstream
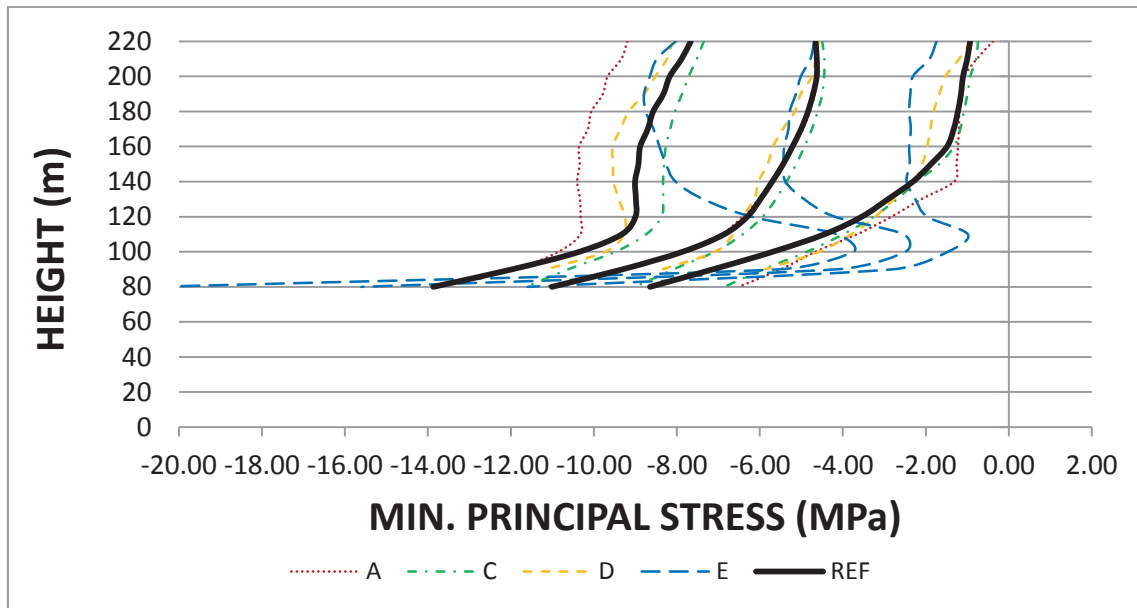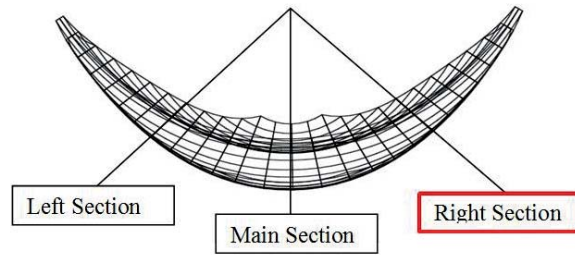
Figure 48: Minimum Principal Stresses – Right Section – Downstream (A – E)
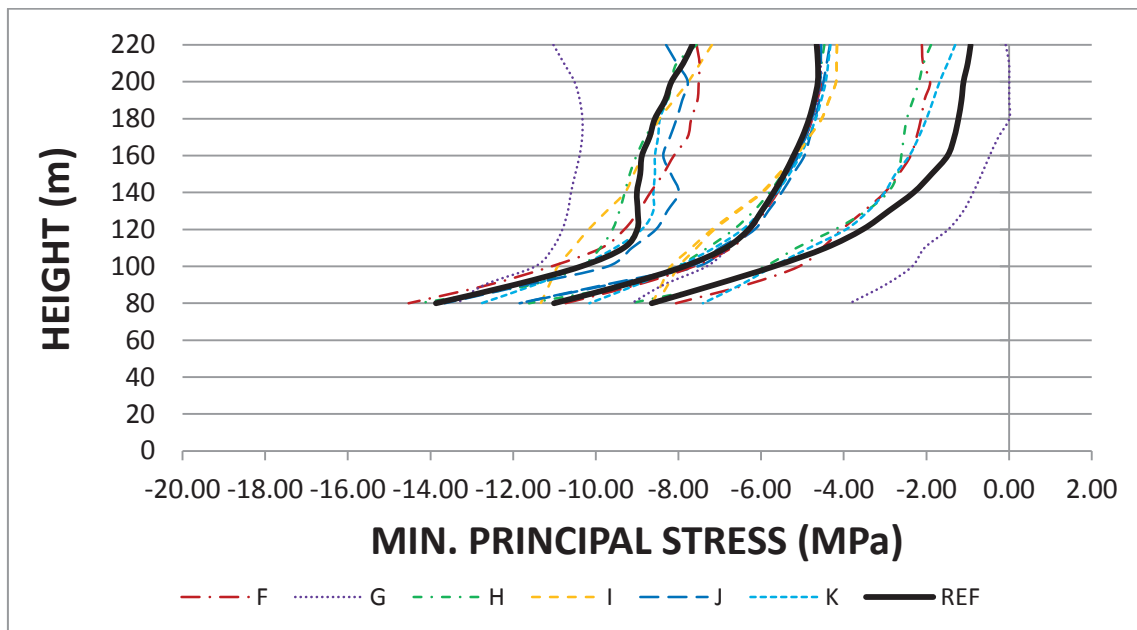
Figure 49: Minimum Principal Stresses – Right Section – Downstream (F – K)

Maximum Principal Stresses – Main Section – Upstream
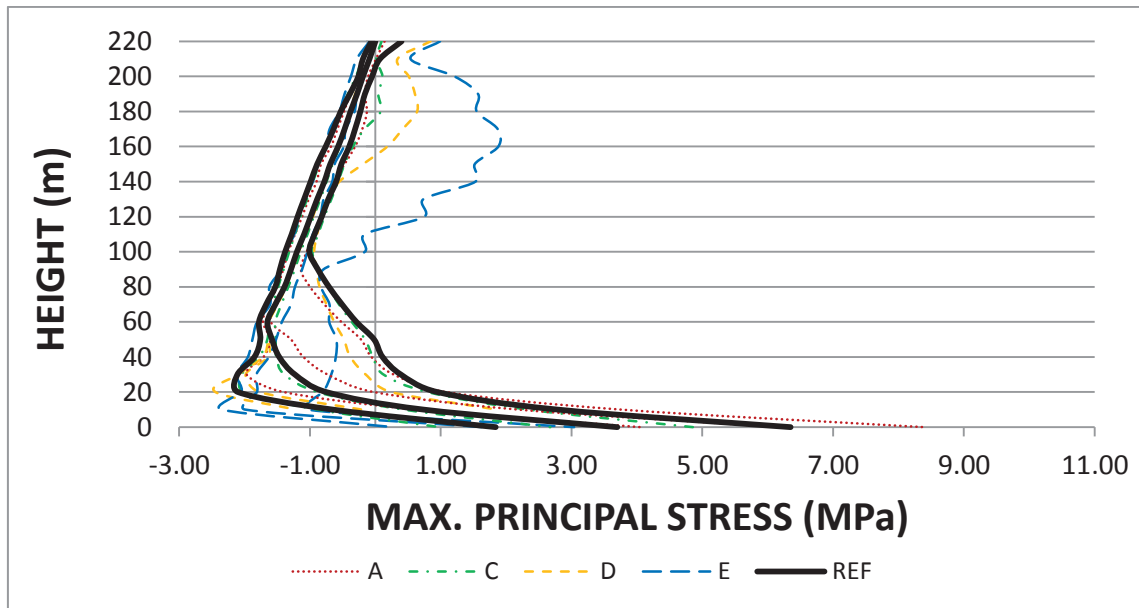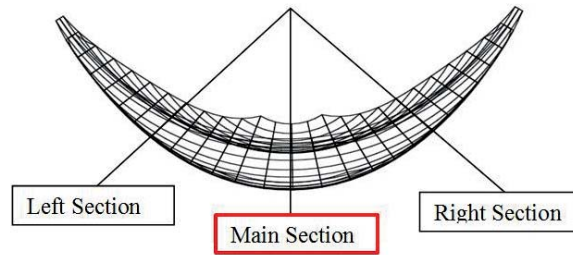
Figure 50: Maximum Principal Stresses – Main Section – Upstream (A – E)
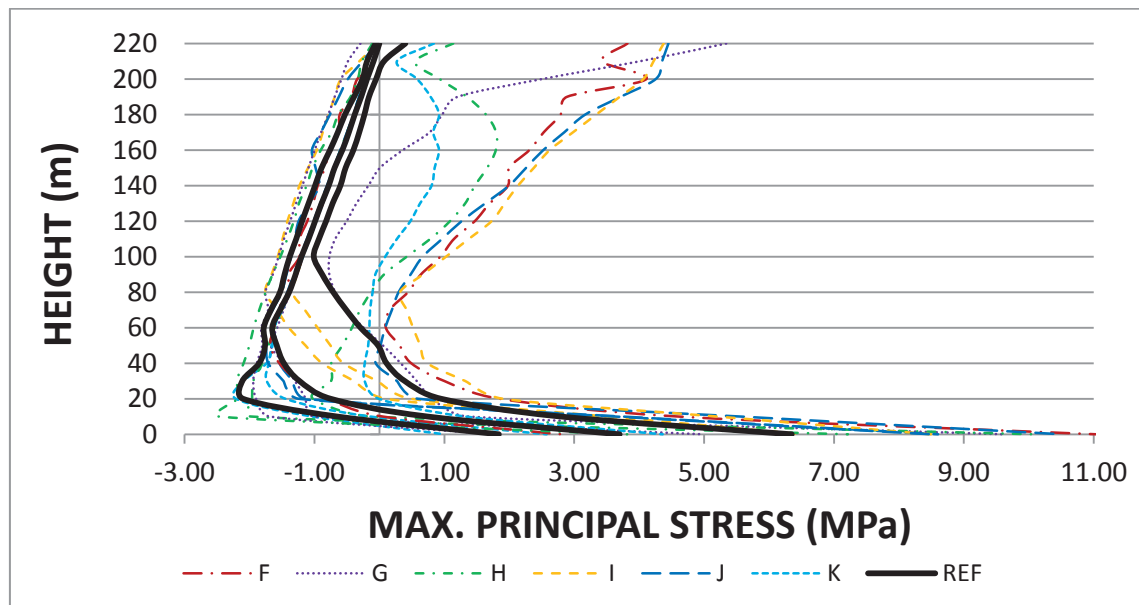
Figure 51: Maximum Principal Stresses – Main Section – Upstream (F – K)

Maximum Principal Stresses – Main Section – Downstream
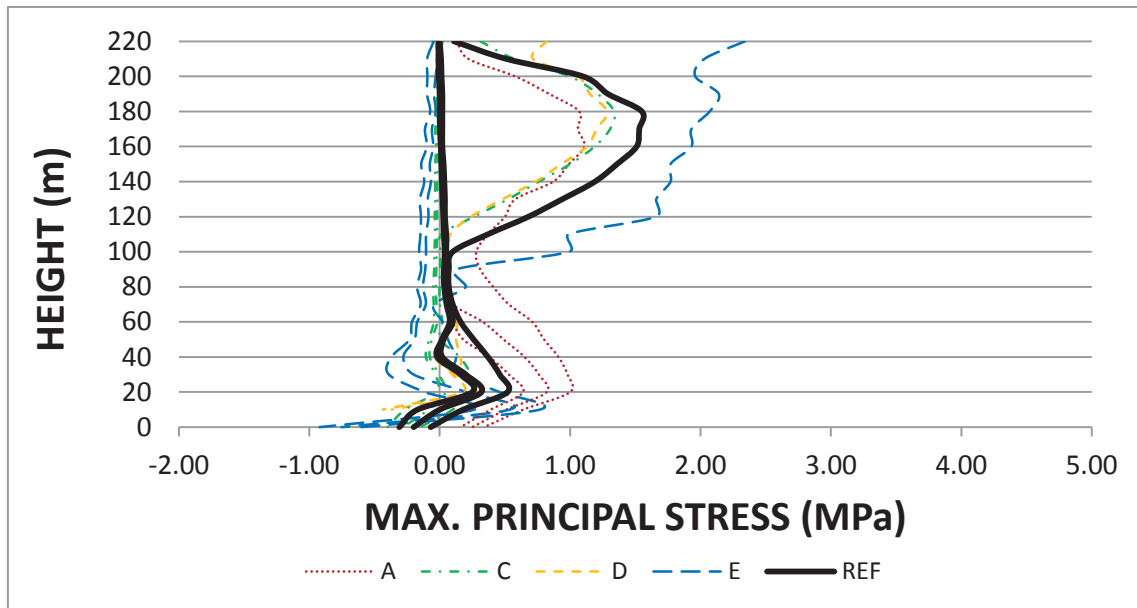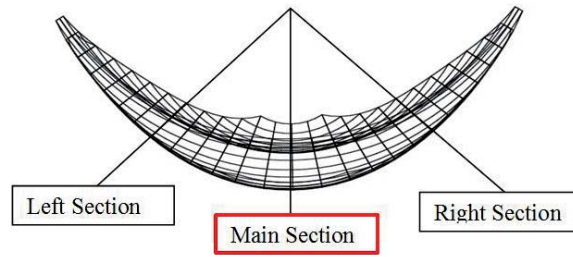
Figure 52: Maximum Principal Stresses – Main Section – Downstream (A – E)
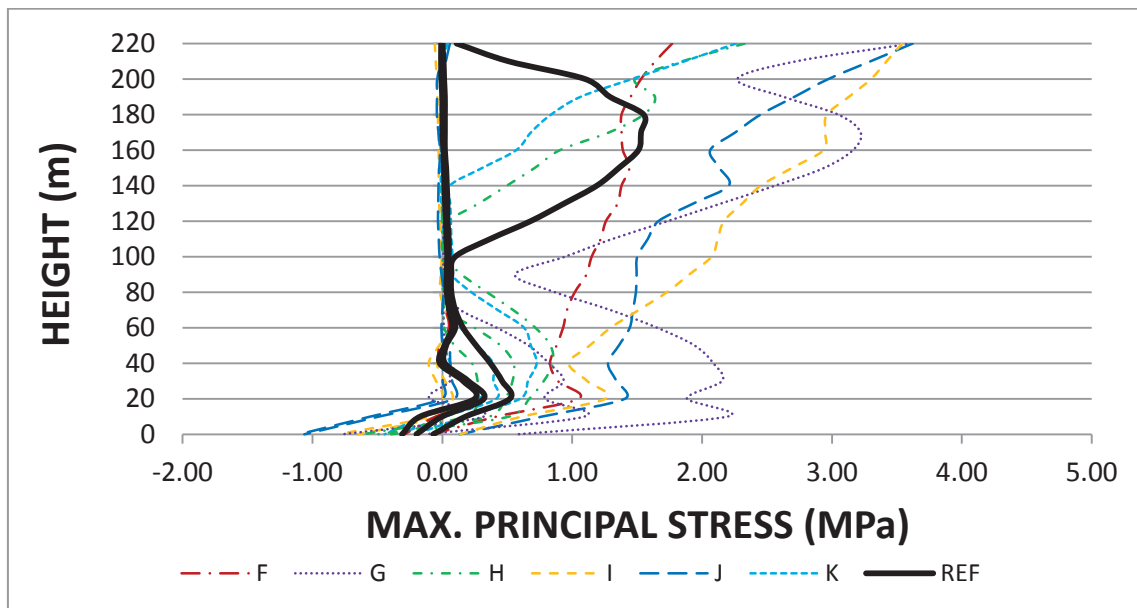
Figure 53: Maximum Principal Stresses – Main Section – Downstream (F – K)

Maximum Principal Stresses – Left Section – Upstream
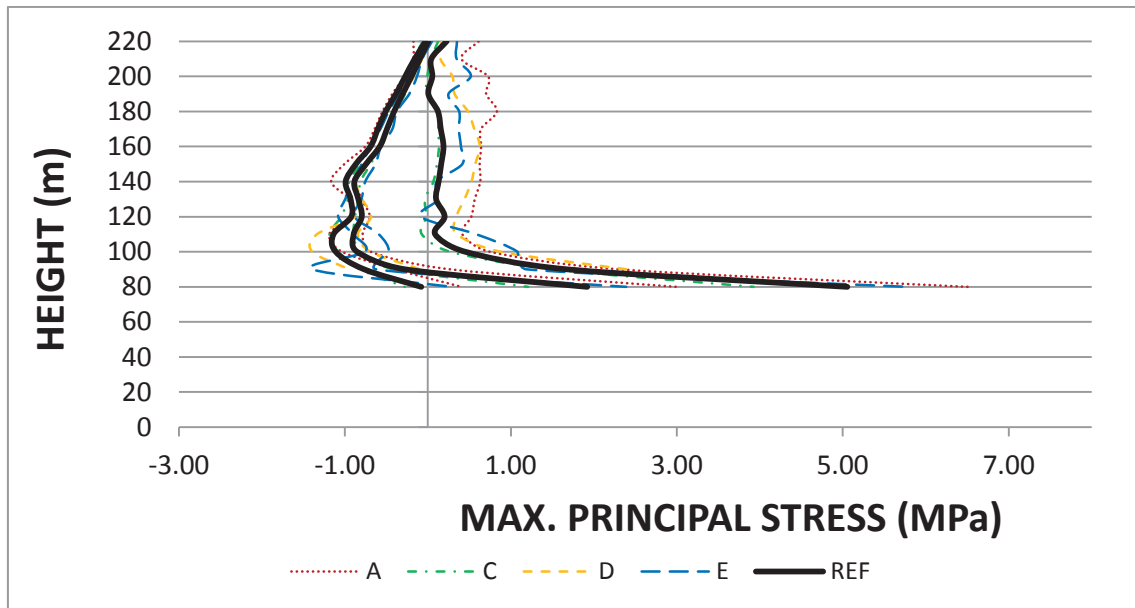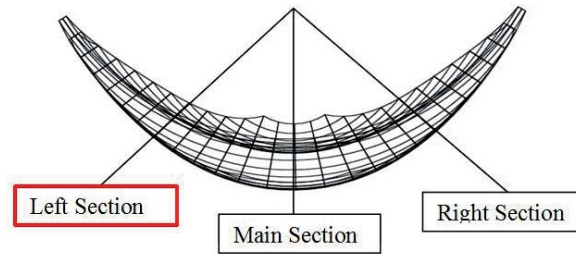
Figure 54: Maximum Principal Stresses – Left Section – Upstream (A – E)
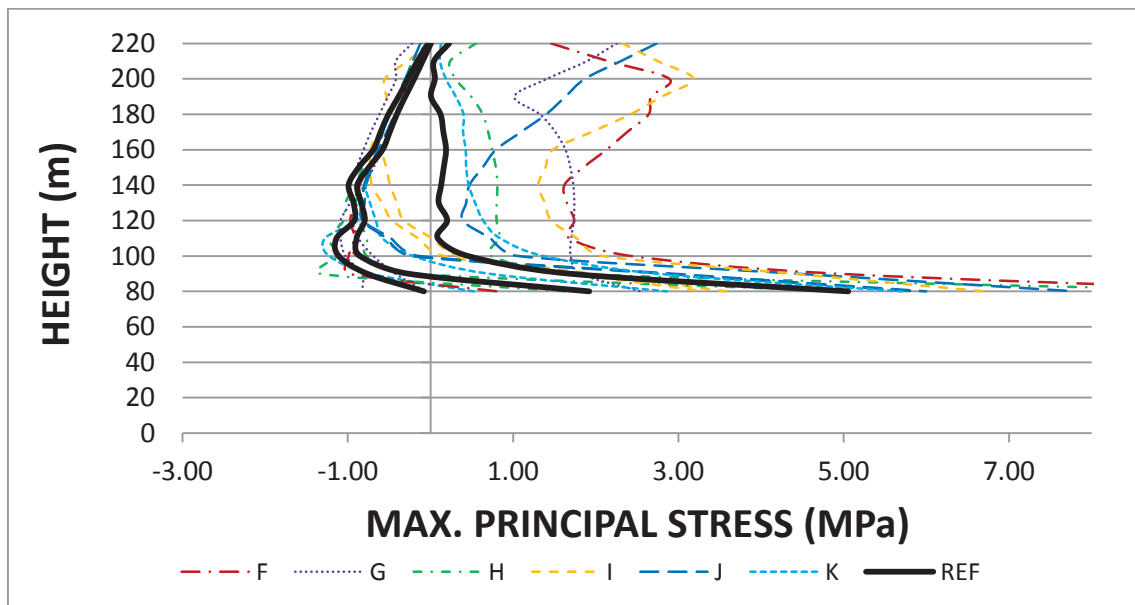
Figure 55: Maximum Principal Stresses – Left Section – Upstream (F – K)

Maximum Principal Stresses – Left Section – Downstream
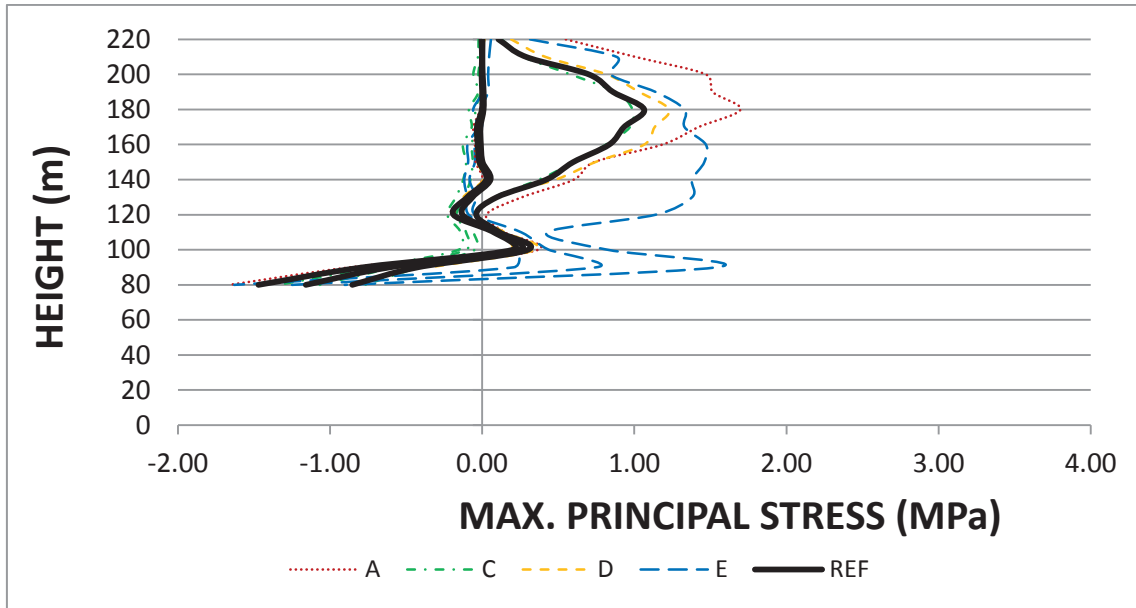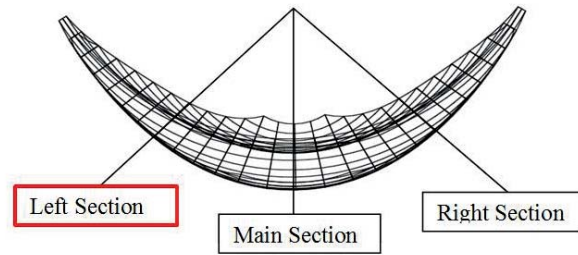
Figure 56: Maximum Principal Stresses – Left Section – Downstream (A – E)
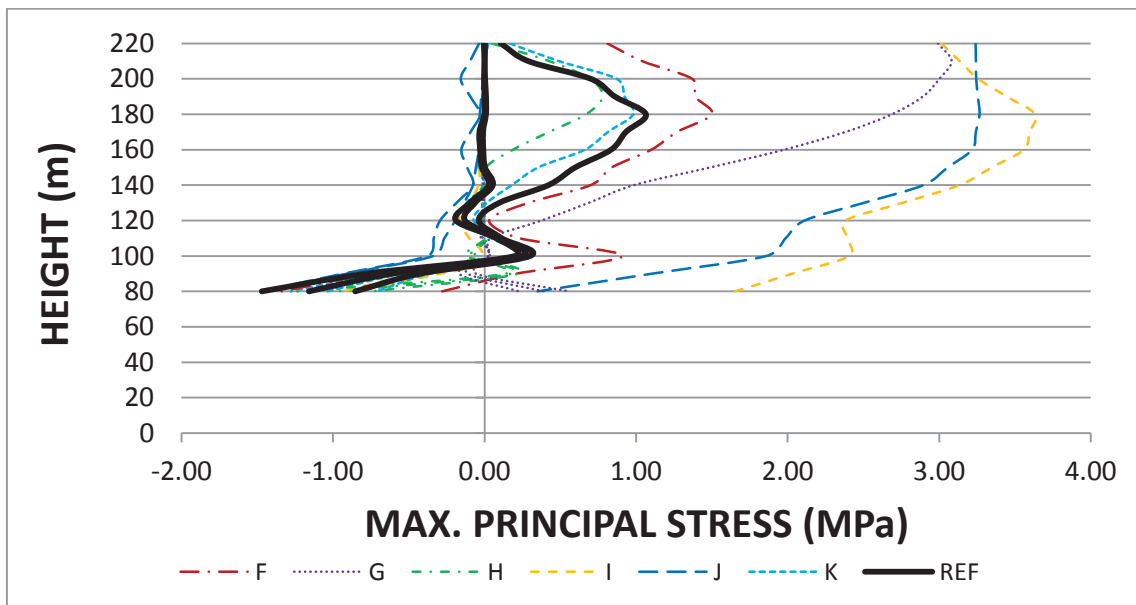
Figure 57: Maximum Principal Stresses – Left Section – Downstream (F – K)

Maximum Principal Stresses – Right Section – Upstream
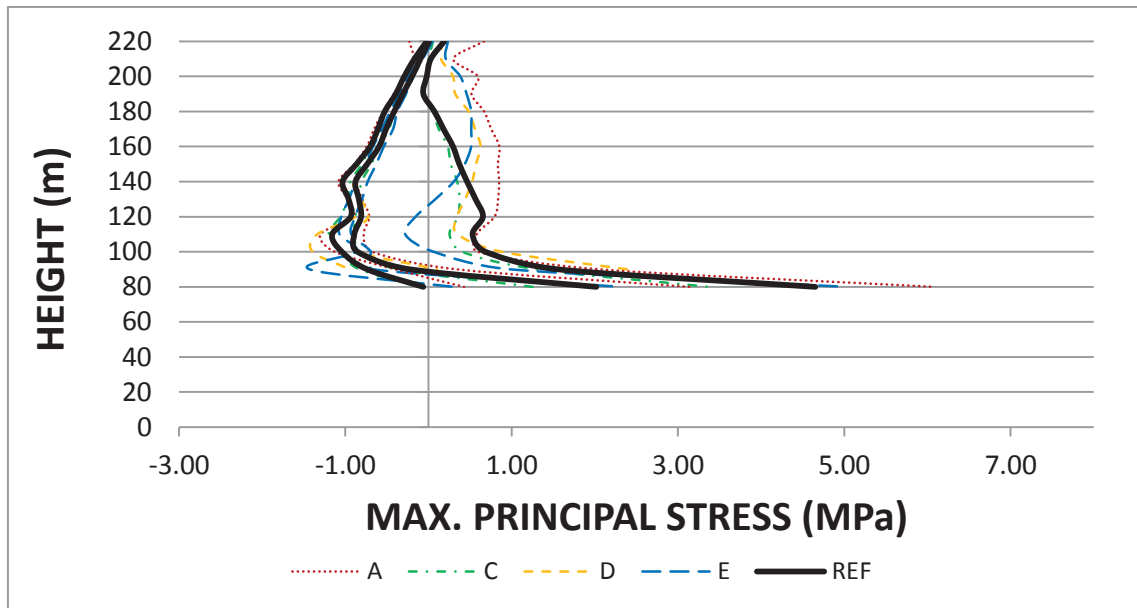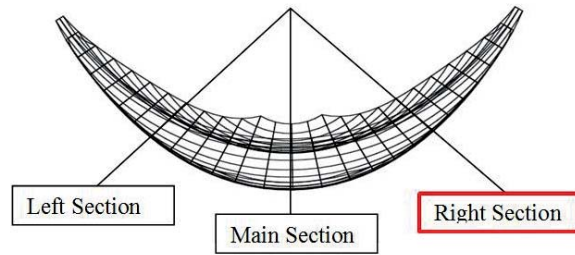
Figure 58: Maximum Principal Stresses – Right Section – Upstream (A – E)
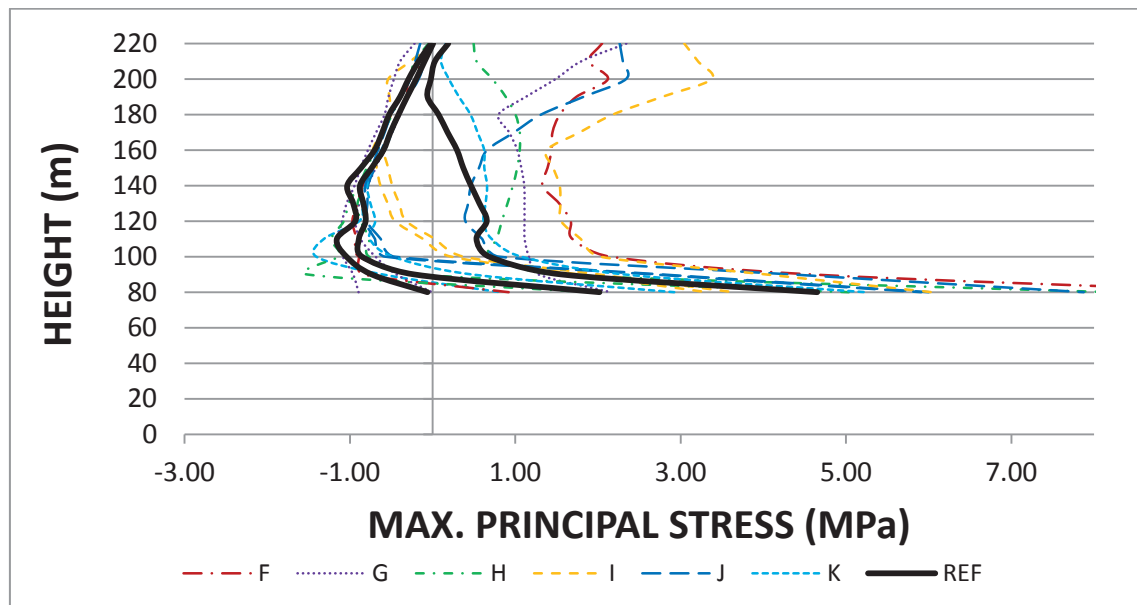
Figure 59: Maximum Principal Stresses – Right Section – Upstream (F – K)

Maximum Principal Stresses – Right Section – Downstream
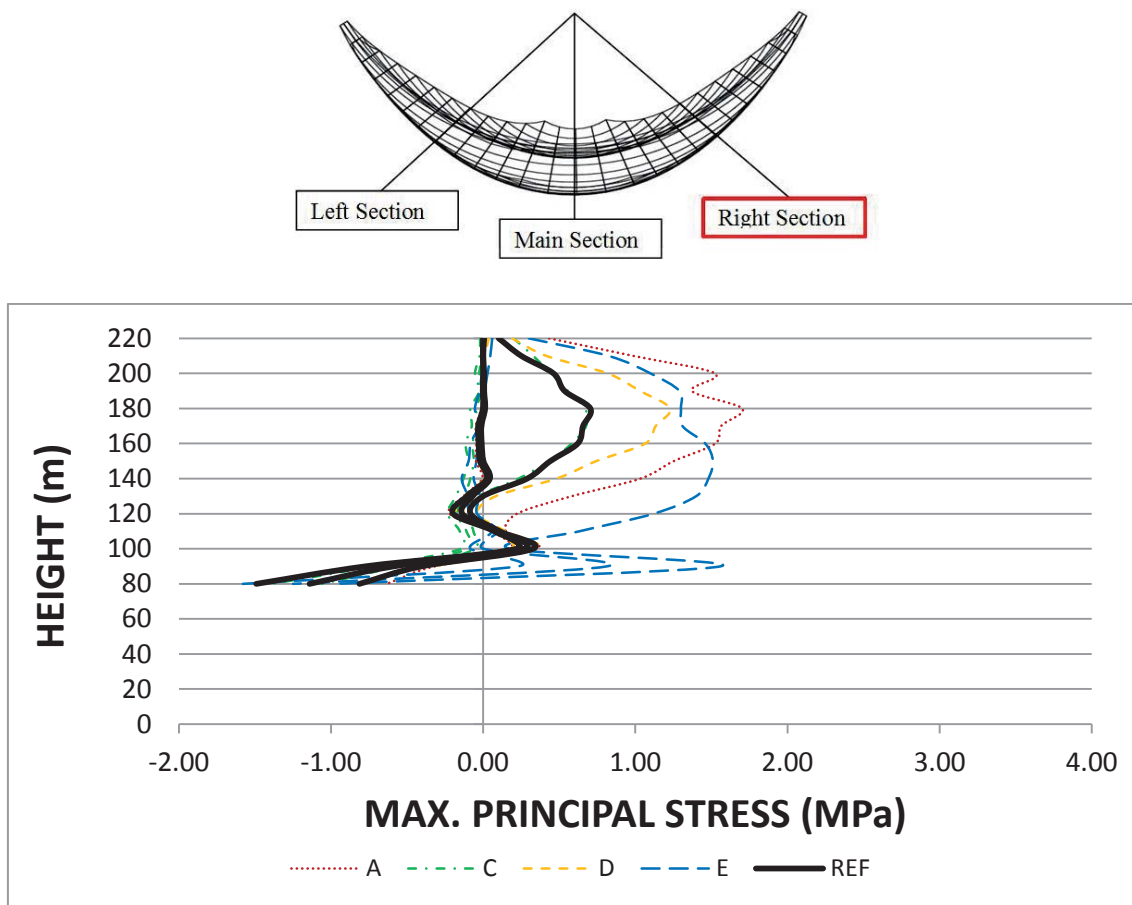
Figure 60: Maximum Principal Stresses – Right Section – Downstream (A – E)
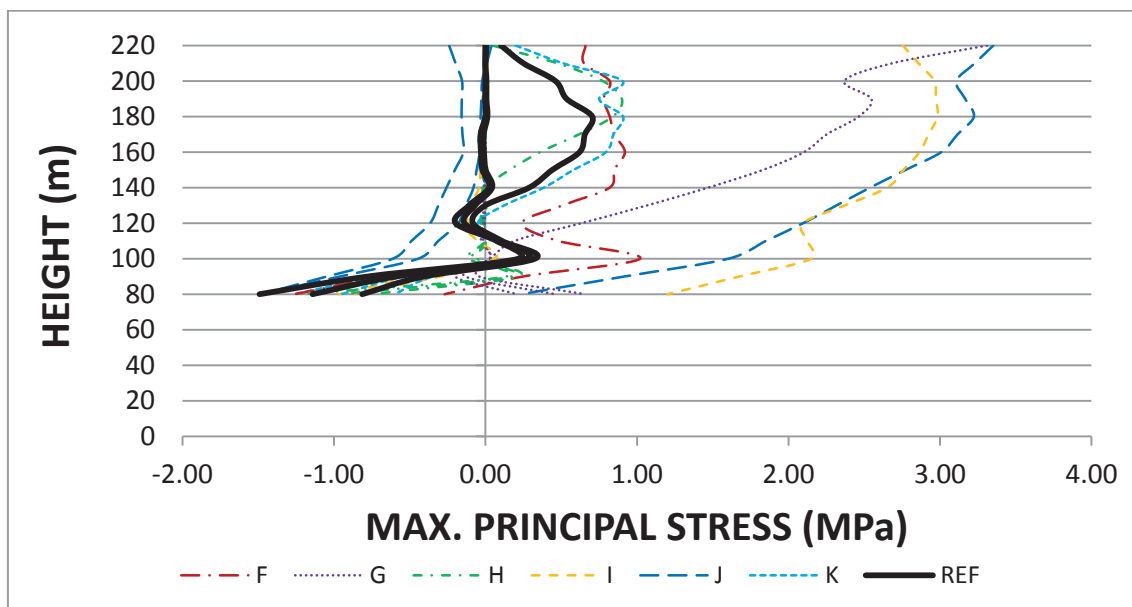
Figure 61: Maximum Principal Stresses – Right Section – Downstream (F – K)

Discussion of Results

Eigenfrequencies

It was to calculate the first 10 Eigenfrequencies of the structural response, including the interaction with the reservoir under full reservoir conditions. The results are summarized in Figure 1 to Figure 3 and Table 2.

The criteria to compare the results are only the Eigenfrequency – no shape deformation, nor mass contribution to the different modes and directions are considered. For commenting in detail, this information would be valuable.

The lower frequencies compared to the others of the first two modes of participants H and I are due to the use of the added mass approach. The overestimation of the additionally excited mass leads to slightly lower Eigenfrequencies, while the remaining are around 1.5 Hz. Noticeable is that the participants who used the program Diana (B, D and E) are getting higher frequencies starting from the third. This counts also for the participant K, who used the Open Source software Code_Aster. All other participants are getting more or less the same Eigenfrequencies for the first 10 modes.

Deformation

The comparison of the deformations is done for the main (middle) section only. The static loading accounts for dead weight and water loading together. No temperature loading is accounted for.

The static deformation reveals, that many results show almost the same behavior, except those from participants D, E, H and K. The higher static deformation of participants D, H and K are due to modelling of the construction stages.

The dynamic deformations are, as expected, varying in a wider range. Especially worth mentioning is also the result by participant G, he, as the only one, used infinite elements on the vertical boundary and applied the acceleration-time-history record on the bottom of the model, which could be the reason for in general higher values. The lower values of radial deformation of participant E are a result of the higher young's modulus used.

Stresses

The comparison of the stresses of each of the participant and each of the diagrams are focused on essential aspects. Therefore, the discussion is kept general and just the quality of some graphs and values is discussed, but not the quantity in detail. Every participant has used his own preferred program, modelling technique and approach, so it's to await that different results are gained.

As it was up to the participant to use immediate or stepped construction sequences, the stress distribution differs. A 0.5[MPa] difference for the static loading, at a stress level of 6[MPa], one might accept, but not larger (Figure 12 and Figure 13).

Worth mentioning are the results by participant G. He used, as already mentioned in the discussion of the deformations, infinite elements and applied the acceleration time history just on the bottom of the model. So the same as for the deformation counts here, the stresses in contrast to the others are far the highest in almost each diagram and beyond awaited results.

Participants B and D used the program Diana with the Hybrid Frequency-Time Domain Method (HFTD-Method), which takes frequency dependent properties, such as compressibility of fluid, reservoir-bottom absorption and far-field reflection, into account. Both of them got similar results compared to the others, which prove the usability of this sophisticated analysis method on the one hand – but shows the applicability of less elaborated models, under these assumptions, too.

Participant K was the only one who used the Open Source software Code_Aster. Such software, which is mostly used at research facilities and universities, is license free, but often more difficult to apply than commercial ones. Nevertheless, the provided results are matching with the results from the other participants.

It is worth mentioning, that the added mass approach (according to Westergaard) is able to provide, comparable results, under the circumstances of this benchmark. All of the three contributors (E, H and I) using this approach are in the range of expected results.

Conclusion

The comparison of all participants' shows, that despite of the same boundary conditions (Model of the Geometry, Finite Element Mesh, Load cases, Material properties, Linear analysis, etc.) still assumptions are taken and required to carry out the analyses. These additional assumptions are starting with the application of the construction sequence, increase of material properties for dynamic loading, abutment boundary properties, application of dynamic loading and some specific assumptions based on the program used.

Best practice examples and recommendations are published in ICOLD Bulletins and are available for engineers. However, for any specific problem to be solved, the assumptions for an analysis applied need to be reconfirmed in the light of the entire problem. In general it is astonishing, to see the large differences between the results of individual.

Everybody had the opportunity to choose his preferred modelling technique to account for the fluid structure interaction, but most of the contributors used either added mass technique or acoustic elements. In practice it is still common to use an added mass approach according to Westergaard. Normally this assumption yields conservative results in contrary to modelling with acoustic elements. The solution of participant e.g. I, who has used Westergaards' formula with its fully, frequency dependent extension, shows very similar results to those analyzed using "higher" constitutive models.

According to results of the participants using either the coarse or fine mesh (described in the former section) had just a marginal influence on the frequencies, deformations and stresses within the structure.

The purpose of choosing this arch dam example (220m in height, totally symmetric) wasn't just for evaluating the influence of different modelling techniques, but also for engineers, scientists and operators to have a kind of reference solution. The diagrams and tables of the results of all participants should help to quantify and compare frequencies, deformations and stresses of such a structure.

Concluding, everybody should be aware of the fact, that results of such simulations should be treated critically, because mistakes in modelling and application cannot be excluded. Usually, reference solutions from former comparable projects for validation should be used to proof the results for plausibility.

PAPERS

THEME A

Fluid Structure Interaction
Arch Dam – Reservoir at Seismic Loading

G. Maltidis[1] and L. Stempniewski[2]

[1] Federal Waterways Engineering and Research Institute, Kußmaulstrasse 17, 76187 Karlsruhe, GERMANY

[2] Karlsruhe Institute for Technology, Institute of Concrete Structures and Building Materials, Department of Concrete Structures, Gotthard-Franz-Str. 3, 76131, Karlsruhe, GERMANY

E-mail: georgios.maltidis@baw.de

Abstract

The fluid structure interaction is an important issue that must be taken into account for the analysis and design of hydraulic structures. Since the first attempts to calculate the hydrodynamic pressures on structures analytically (Westergaard, von Kármán, Mononobe, Housner, Chwang, Zangar) the engineers and researchers have the last years a very useful tool, the finite and boundary element method, in order to analyze complicated structures taking into account different sophisticated phenomena. However, even nowadays, the common praxis is to use the early developed techniques, because of their simplicity and capability of implementation in the most finite element codes.

Introduction

Since 1933, the hydrodynamic pressures on oscillating structures, which are in contact with water, are taken into account with the simplified assumption that the water is incompressible and the structure is star using the added mass approaches, first proposed by Westergaard for vertical star surfaces and later extended by Zangar for inclined surfaces. Although these approaches apply under conditions which hardly are met, they are widely used also nowadays because of their simplicity in incorporating them in finite element codes. However, the result of analysis with the added mass approach may come out to be very conservative leading to wrong decisions. The modeling of the water with finite solid element around the 1980's gave the opportunity for the analyst to take account some phenomena, as the water compressibility but raised other numerical problems as such type of modeling of water is suffering many times of hourglass making the analysis instable. The use of acoustic elements seems to be the more beneficial, as there are hardly numerical problems, and most of the phenomena, which take place for a dynamic fluid structure interaction can be modeled. With acoustic elements the analyst can consider the water compressibility, the wave absorption at the infinite end of the reservoir and the impedance of wave radiation at the reservoir sediments.

Hydrodynamic Pressures

Added mass approaches

The most well-known added mass approach is the one of Westergaard (1933)[1]. Westergaard proposed the following formula for the computation of hydrodynamic pressures as added masses under the restrictions that the reservoir is infinite, the upstream surface of the dam is vertical and the dam is rigid:

$$m = \frac{7}{8} \cdot \sqrt{H \cdot y} \cdot \frac{\gamma_w}{g} \cdot A \tag{1}$$

where m the added mass, H and y the height and the depth of the reservoir respectevily, γ_w the density of the water, g the gravitational acceleration and A the contributing area around the node.
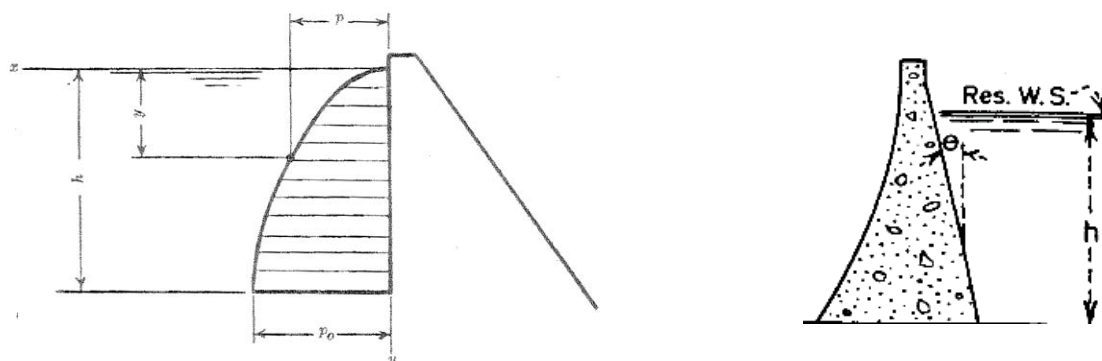
Figure 1: Graphical representation of Westergaard's and Zangar's calculation models.

Zangar (1952)[2], using an electric analogue, extended the added mass approach of Westergaard for inclined upstream surfaces of the dam, introducing reductive factors dependent on the angle of inclination.

$$m = 0,5 \cdot H \cdot C_m \cdot \left[\frac{y}{H} \cdot (2 - \frac{y}{H}) + \sqrt{\frac{y}{H} \cdot (2 - \frac{y}{H})} \right] \cdot \frac{\gamma_w}{g} \cdot A \qquad (2)$$

where C_m a coefficient based on the angle of inclination and the other parameters as Westergaard's formula.

Fluid Elements
The fluid elements are solid elements to which the characteristics of the water are applied. The incompressibility or the water as well as the null shear resistance are introduced with a Poisson number equal with 0,5 or close to this value for the finite element programs. The bulk modulus of the water is K=2,2 GPa. The modeling of the water with solid elements causes numerical instabilities because of the introducing of zero energy modes (hourglass modes). This effect can be mitigated with the use of hourglass control and by applying the free surface boundary condition for the vertical node displacements [9]. Moreover, a nonlinear material behavior with tension cut off or a contact interaction which allows only compression to be transmitted will avoid unrealistic tension stress of the dam caused by the water.

Acoustic Elements
The acoustic elements are used to model the fluid behavior of the air. They have no shear and tension resistance and they transmit only pressures [10]. With assignment of the water bulk modulus they model the water behavior very good. Numerous boundary conditions can be assigned to the acoustic elements, which model natural phenomena such as wave absorption at the far end of the reservoir, sloshing of the free surface, wave impedance at the reservoir's bottom due to sediments etc. For the acoustic elements no special numerical care has to be taken except for assigning the boundary conditions.

Model aspects
For this benchmark two models (one with coarse mesh and one with fine mess) are investigated. The mesh of the reservoir is the same for both cases. The foundation was considered massless, so no further care was taken for wave absorption or deconvolution of the seismic motion. Because of the massless foundation with no radiation absorption of the

seismic waves and due to the lack of further non-linearities of the dam's material and of the contact interfaces, a big enough structural damping is applied. As presented in [6] for a big range of frequencies the total Rayleigh damping is between 8 and 10 %. Due to the linear finite element analysis a 10% viscous damping is used by [6]. Here, because of the small peak ground acceleration of 0,1g a value of 7,5% of structural damping was chosen in order to determine the Rayleigh stiffness damping factor a and the Rayleigh mass factor β.

For the reservoir hydrodynamic pressures, two added mass approaches and one reservoir modeling with acoustic elements were investigated. The generalized Westergaard's [11] and the Zangar's added mass approaches were used. The added masses were given via a user subroutine which defines user elements in Abaqus [5].

The two models with acoustic elements differ only in the wave absorption's method of the far field. The first uses acoustic infinite element whereas the latter impedance boundary condition. The impedance condition can be given either as element based or as surface based condition. Moreover a boundary condition is given at the reservoir free surface constraining the dynamic acoustic pressures to be zero. The surfaces of the rock and the dam are tied with the surfaces of the reservoir.
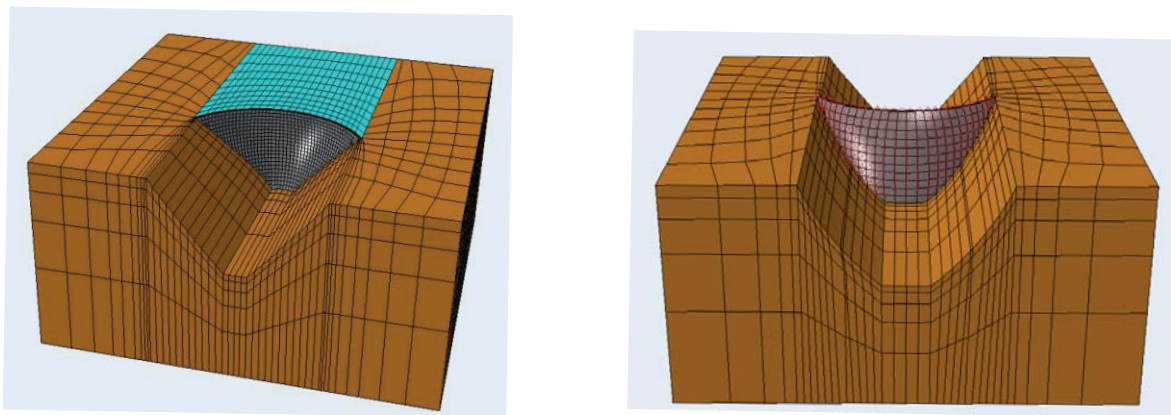
Figure 2: The model with two different meshes and two reservoir modeling approaches: left fine mesh and acoustic elements and right coarse mesh and added mass elements.
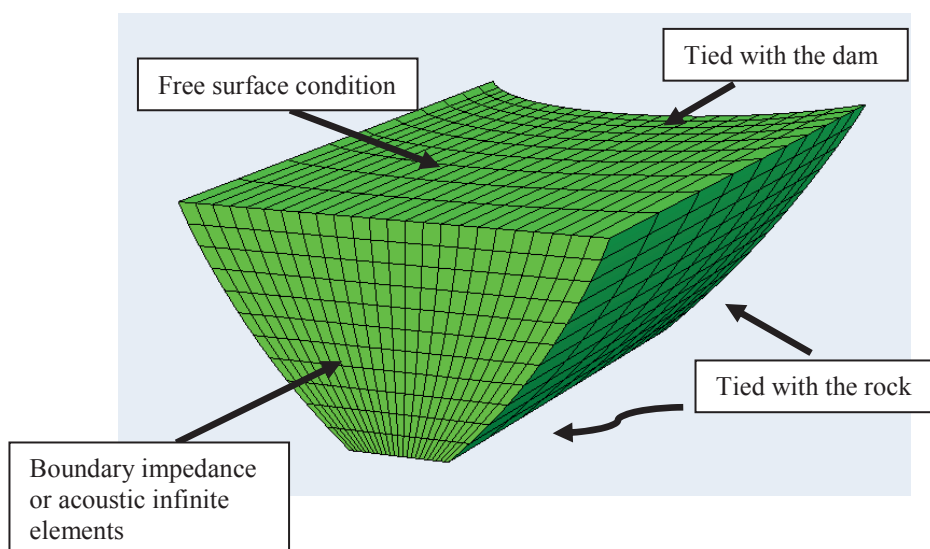
Figure 3: The reservoir with its boundary conditions.

Table 1: Material Parameters

	Rock	Water	Dam
Density (kg)	0	1000	2400
Poisson Ratio	0,2	-	0,167
Young Modulus (MPa)	25000	-	27000
Bulk Modulus (MPa)	-	2200	-

Analysis' methods

The seismic analyses were carried out using the time history with direct integration and the modal time history. From computational time the modal time history is a little bit faster than the time history with direct integration. The time histories were gives as nodal acceleration to the boundaries of the rock. A baseline correction offered by Abaqus was also applied to them.

Results

The results of the analyses are presented at the next tables and diagrams. The first table shows the ten first modes for the dam, with empty and with full reservoir modeled by the different methods described before. The diagrams show due to lack of space only some of the results containing the minimal and maximal vertical, minimum principal and maximum principal stresses of the dam for the different reservoir models and for the different dam mesh. The results are given for the paths along the height of the dam, for the upstream and the downstream sections. For convenience abbreviations were introduced to the diagrams (e.g. *"dti"* refers to direct time integration, *"West"* to Westergaard's added mass, *"ac"* to acoustic element, *"imp"* to impedance boundary condition for the acoustic elements, *"inf"* to acoustic infinite elements, *"modal"* to modal dynamic analysis). The results for the fine mesh model are given with dashpot line in order to differ easier than the ones of the coarse mesh model.

The analysis with the infinite elements had more computational cost than the analysis with the impedance condition. In order to obtain similar results to the impedance boundary condition with the use of infinite acoustic elements, care must be given in the definition of the infinite elements' thickness. There are trivial differences when the analyst uses the improved rather than the planar non-reflecting condition offered by Abaqus.

The results of the fine model with acoustic elements for the reservoir gave too conservative results. The author believes that these results for the given meshes of dam and reservoir are not correct due to violation of the contact condition, according to which the slave surface nodes must be finer than the master surface nodes.

Frequencies - Coarse Model

	1	2	3	4	5	6	7	8	9	10
acoustic	1,47	1,54	1,55	2,11	2,33	2,46	2,61	2,97	3,25	3,37
westergaard	1,29	1,32	1,96	2,3	2,44	2,86	3,08	3,57	3,73	3,77
zangar	1,39	1,44	2,12	2,49	2,65	3,07	3,33	3,82	4,05	4,07
empty	1,92	2,03	2,91	3,59	3,63	4,29	4,5	4,8	5,19	5,52

Frequencies - Fine Model

	1	2	3	4	5	6	7	8	9	10
acoustic	1,47	1,54	1,54	2	2,29	2,46	2,53	2,96	3,13	3,27
westergaard	1,3	1,33	1,98	2,32	2,48	2,91	3,12	3,62	3,81	3,86
zangar	1,41	1,45	2,14	2,5	2,68	3,11	3,37	3,85	4,12	4,13
empty	1,91	2,03	2,9	3,57	3,62	4,27	4,48	4,78	5,17	5,49

Figure 4: The frequencies for the two models (coarse left, fine right) and for the four reservoir models.

Table 2: Ten first modes for the coarse model
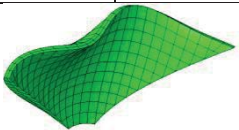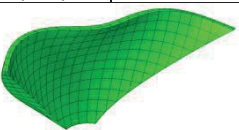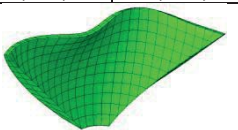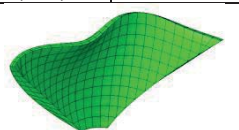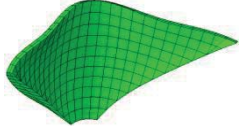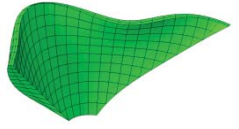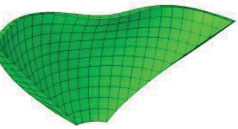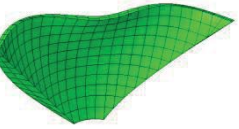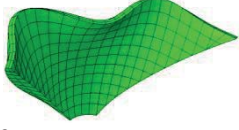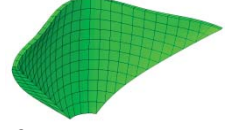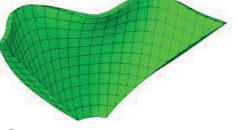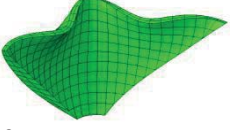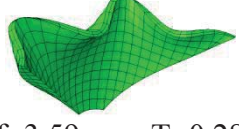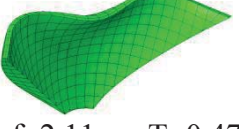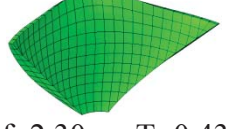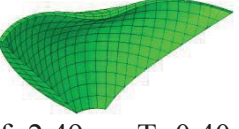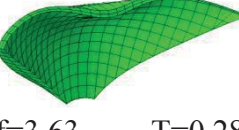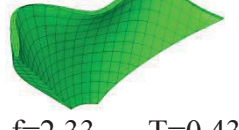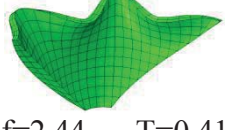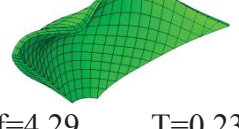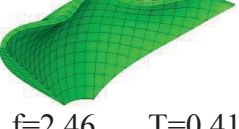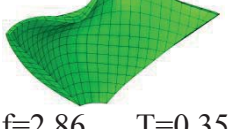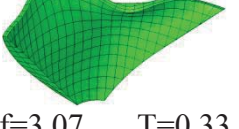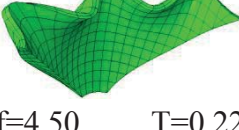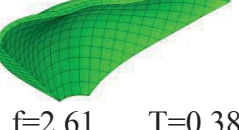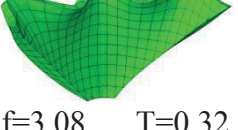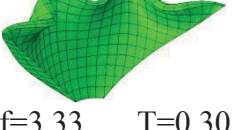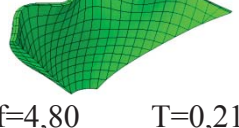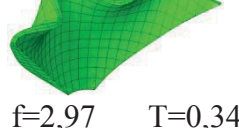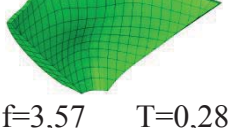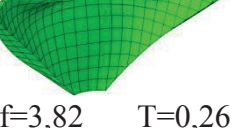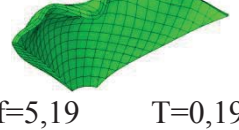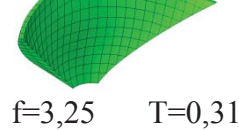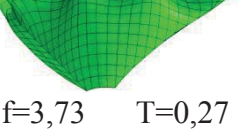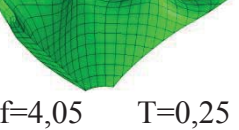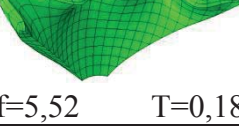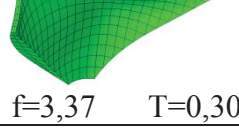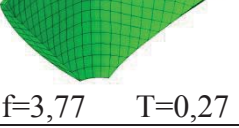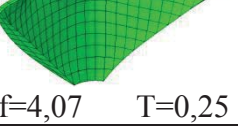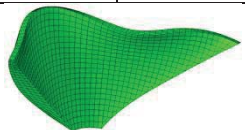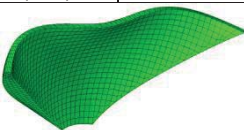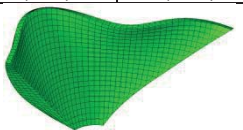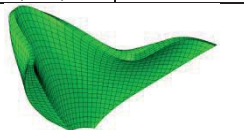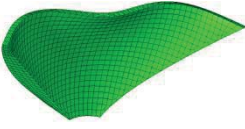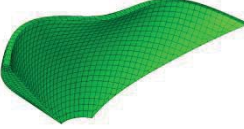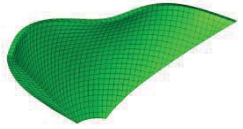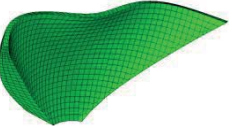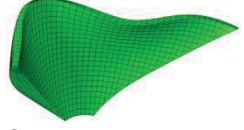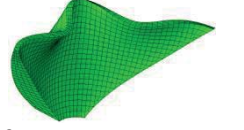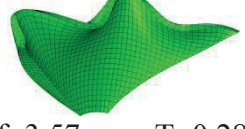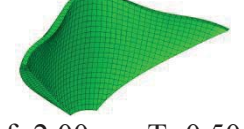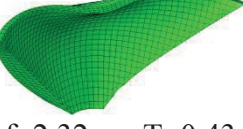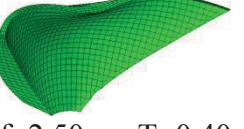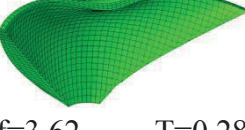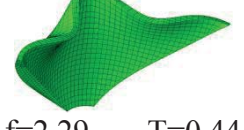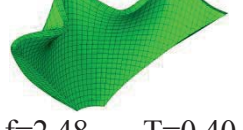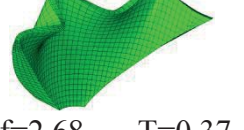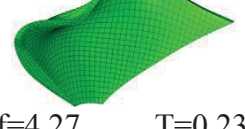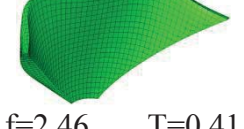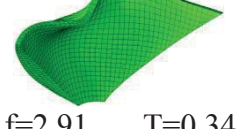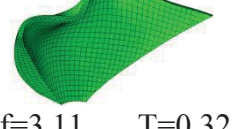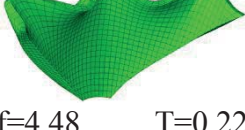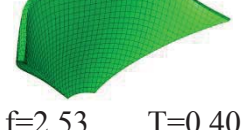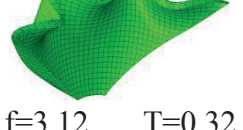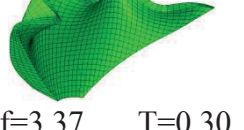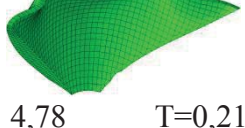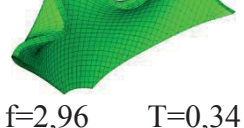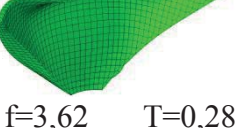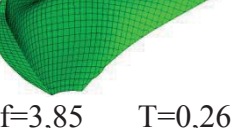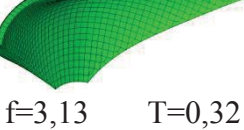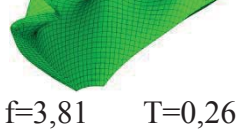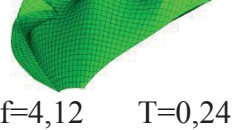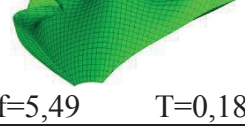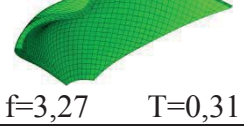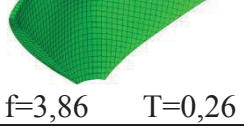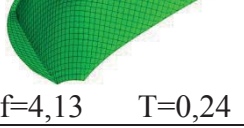
Mode Nr.	Empty		Acoustic		Westergaard		Zangar	
	f (Hz)	T (sec)	f (Hz)	T (sec)	f (Hz)	T (sec)	f (Hz)	T (sec)
1	f=1,92	T=0,52	f=1,47	T=0,68	f=1,29	T=0,78	f=1,39	T=0,72
2	f=2,03	T=0,49	f=1,54	T=0,65	f=1,32	T=0,76	f=1,44	T=0,69
3	f=2,91	T=0,34	f=1,55	T=0,65	f=1,96	T=0,51	f=2,12	T=0,47
4	f=3,59	T=0,28	f=2,11	T=0,47	f=2,30	T=0,43	f=2,49	T=0,40
5	f=3,63	T=0,28	f=2,33	T=0,43	f=2,44	T=0,41	f=2,65	T=0,38
6	f=4,29	T=0,23	f=2,46	T=0,41	f=2,86	T=0,35	f=3,07	T=0,33
7	f=4,50	T=0,22	f=2,61	T=0,38	f=3,08	T=0,32	f=3,33	T=0,30
8	f=4,80	T=0,21	f=2,97	T=0,34	f=3,57	T=0,28	f=3,82	T=0,26
9	f=5,19	T=0,19	f=3,25	T=0,31	f=3,73	T=0,27	f=4,05	T=0,25
10	f=5,52	T=0,18	f=3,37	T=0,30	f=3,77	T=0,27	f=4,07	T=0,25

Table 3: Ten first modes for the fine model

Mode Nr.	Empty		Acoustic		Westergaard		Zangar	
	f (Hz)	T (sec)	f (Hz)	T (sec)	f (Hz)	T (sec)	f (Hz)	T (sec)
1	f=1,91	T=0,52	f=1,47	T=0,68	f=1,30	T=0,77	f=1,41	T=0,71
2	f=2,03	T=0,49	f=1,54	T=0,65	f=1,33	T=0,75	f=1,45	T=0,69
3	f=2,90	T=0,35	f=1,54	T=0,65	f=1,98	T=0,50	f=2,14	T=0,47
4	f=3,57	T=0,28	f=2,00	T=0,50	f=2,32	T=0,43	f=2,50	T=0,40
5	f=3,62	T=0,28	f=2,29	T=0,44	f=2,48	T=0,40	f=2,68	T=0,37
6	f=4,27	T=0,23	f=2,46	T=0,41	f=2,91	T=0,34	f=3,11	T=0,32
7	f=4,48	T=0,22	f=2,53	T=0,40	f=3,12	T=0,32	f=3,37	T=0,30
8	4,78	T=0,21	f=2,96	T=0,34	f=3,62	T=0,28	f=3,85	T=0,26
9	f=5,17	T=0,19	f=3,13	T=0,32	f=3,81	T=0,26	f=4,12	T=0,24
10	f=5,49	T=0,18	f=3,27	T=0,31	f=3,86	T=0,26	f=4,13	T=0,24

The next diagrams give some representative comparisons between results for the different reservoir models and analysis' methods.
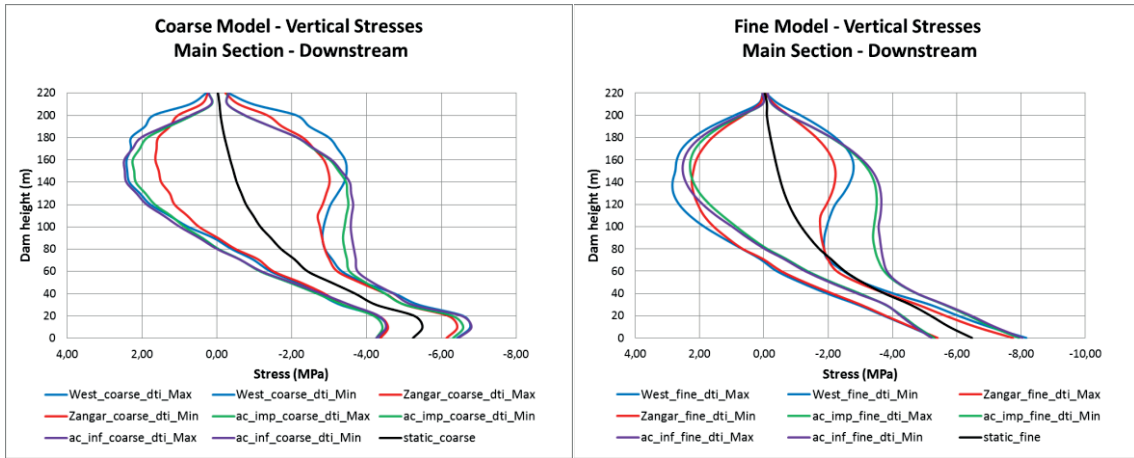
Figure 6: The vertical stresses for the different reservoir models at the downstream main section.
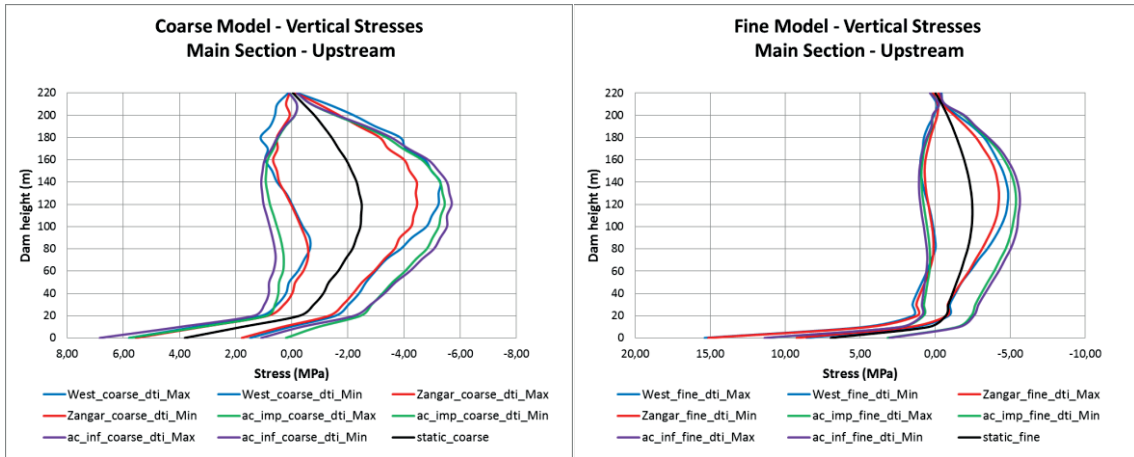
Figure 7: The vertical stresses for the different reservoir models at the upstream main section.
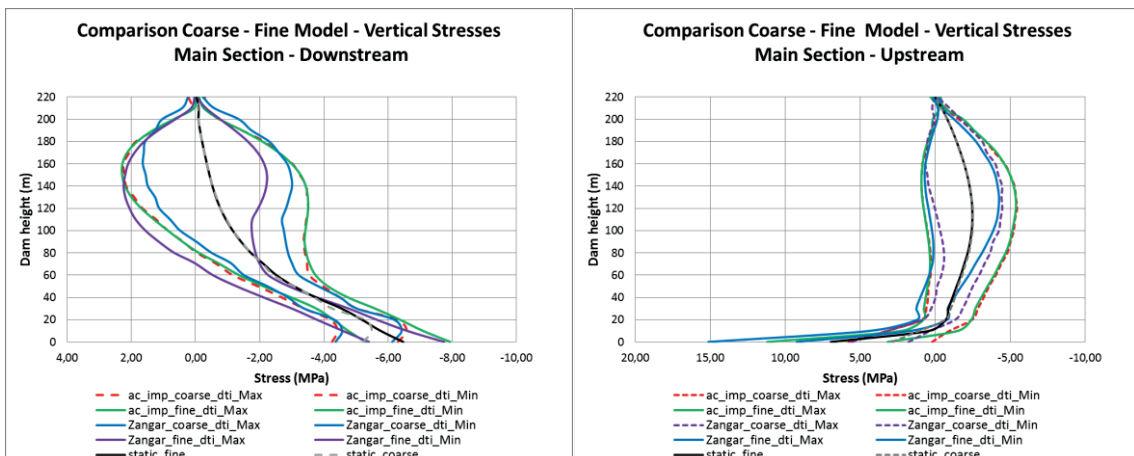
Figure 8: Comparison between the coarse and fine model for the vertical stresses.
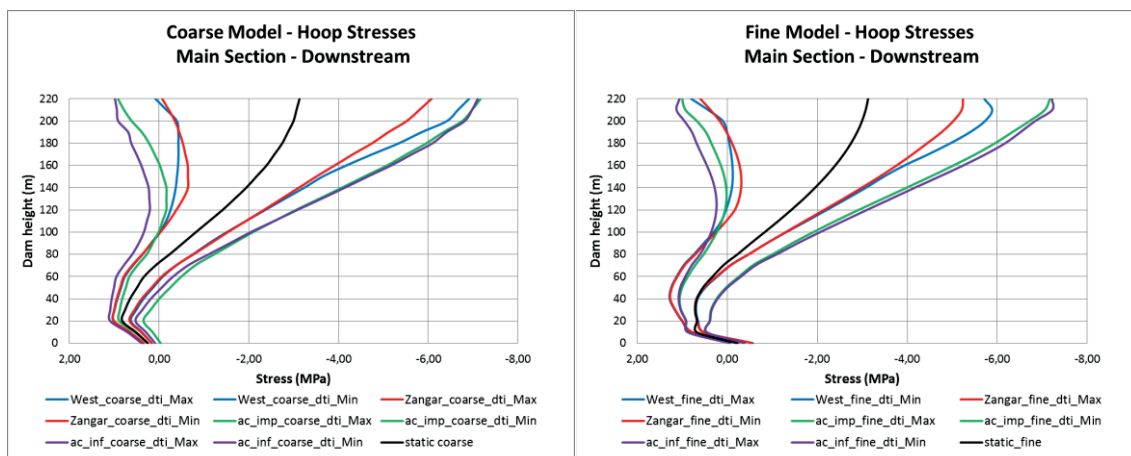
Figure 9: The hoop stresses for the different reservoir models at the downstream main section.
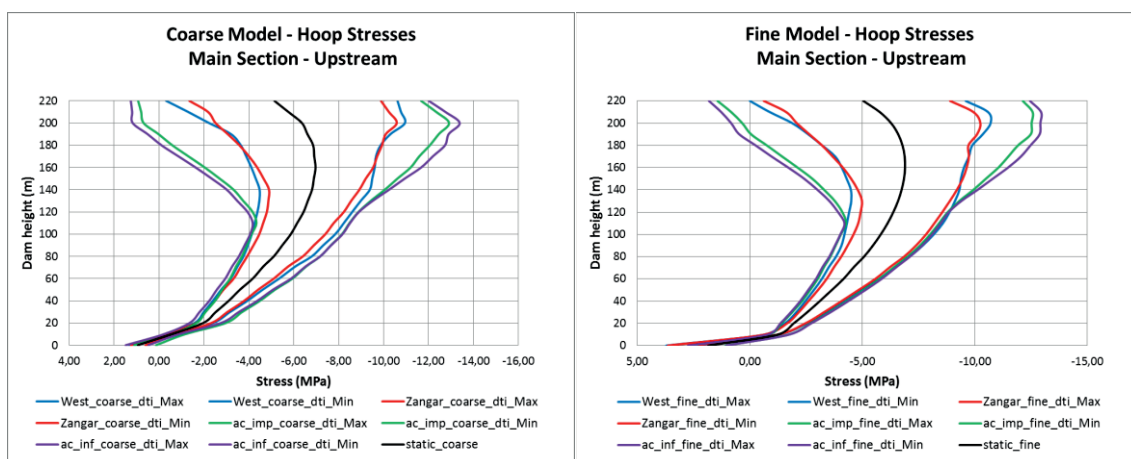
Figure 10: The hoop stresses for the different reservoir models at the upstream main section.
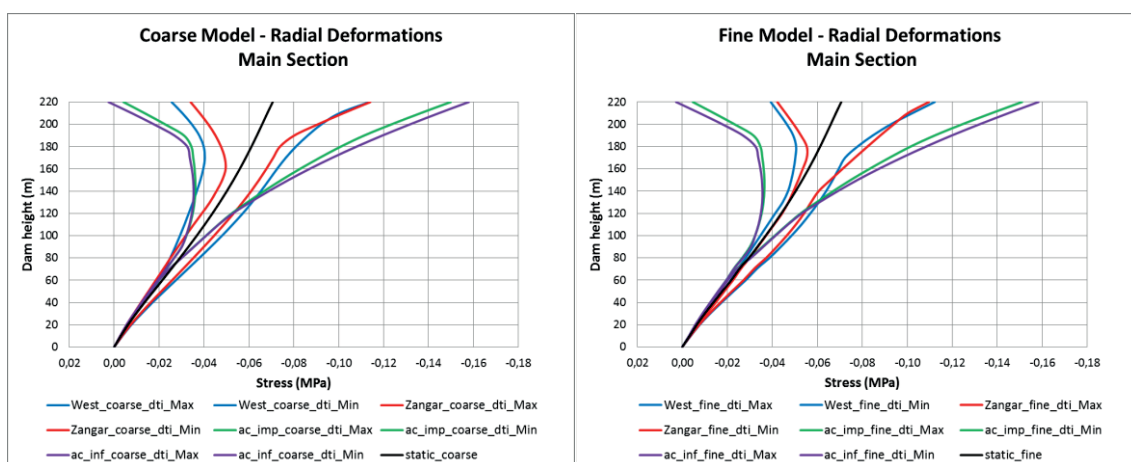
Figure 11: The radial deformations for the different reservoir models at the main section.
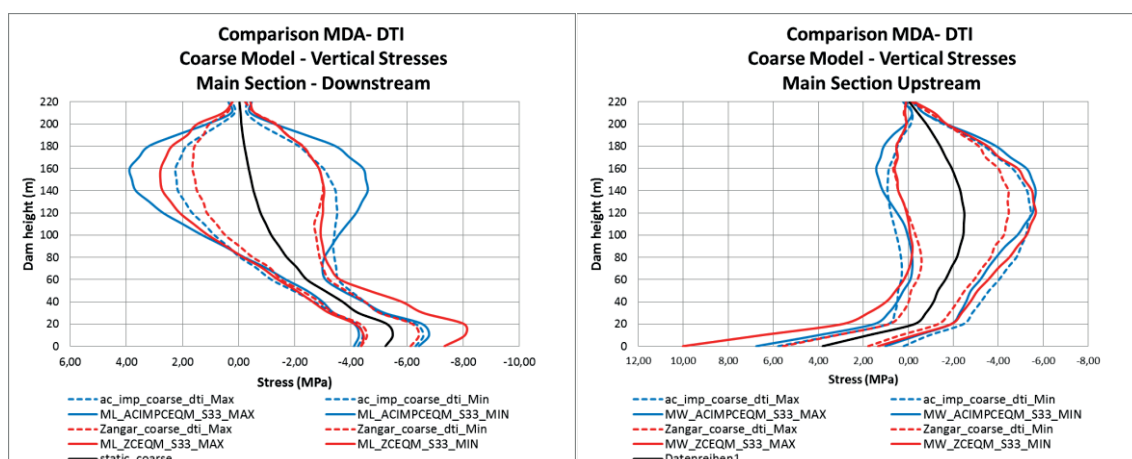
Figure 12: Comparison between the modal dynamic analysis and the direct time integration for the coarse model with the Zangar's approach at the downstream (left) and upstream (right) main section.

Conclusion

The earthquake analysis of an arch dam-reservoir-foundation system was performed with different modeling aspects according to the formulators' directions. The results show very near values for the two added mass approaches, with the one of Zangar to be a little bit more favorable than the one of Westergaard. The acoustic elements models with the two non-reflecting approaches give identical results. The coarse and fine models differ only in the base stresses due to the coarser mess of the coarse model and some deviations are noticed at the added mass models. Although the modal dynamic analysis is much faster than the direct time integration, delivers conservative results.

Acknowledgements

References

[1] Westergaard, H. M. (1933). Water pressures on dams during earthquakes. Transactions of the American Society of Civil Engineers, American Society of Civil Engineers, New York, New York, Paper 1835, 1933.

[2] Zangar, C. N. (1952). Hydrodynamic Pressures on dams due to horizontal earthquake effects. U.S. Departmant of Interior, Bureaus of Reclamation, Engineering Monographs No.11

[3] Chwang, A.T., Housner, G.W. (1978). Hydrodynamic pressures on sloping dams during earthquakes. Part 1. Momentum Method. Journal of Fluid Mechanics, vol. 2, part 2, pp. 335-341

[4] Chwang, A.T. (1978). Hydrodynamic pressures on sloping dams during earthquakes. Part 2. Exact Theory. Journal of Fluid Mechanics, vol. 2, part 2, pp. 343-348

[5] ABAQUS (2011),*User's manual, Version 6.11*. Dassault Systèmes Simulia Corporation, Providence RI, USA.

[6] US Bureau of Reclamation (2006), State-of-Practice for the NonlinearAnalysis of Concrete Dams at the Bureau of Reclamation, USBR Report, Colorado, USA.

[7] United States Society on Dams (2008). Numerical models for seismic evaluation of concrete dams. Review, evaluation and interpretation of results. USSD, Denver, USA.

[8] Zienkiewicz, O. C., Bettess, P. (1978). Fluid-Structure dynamic interaction and wave forces. An introduction to numerical treatment. International Journal For Numerical Methods In Engineering, Vol. 13, 1-16.

[9] Wilson, E.D., Khalvati,M. (1983). Finite elements for the dynamic analysis of fluid-solid systems. International Journal For Numerical Methods In Engineering, Vol. 19, 1657-1668.

[10] Matthew Muto, Nicolas von Gersdorff, Zee Duron, Mike Knarr (2012). *Effective Modeling of Dam-Reservoir Interaction Effects Using Acoustic Finite Elements*, in Proceedings of Innovative Dam and Levee Design and Construction for Sustainable Water Management, 32nd Annual USSD Conference, New Orleans, Louisiana, April 23-27, 2012, Pages 1161-1168.

[11] Kuo, James Shaw-Han, (1982). Fluid-structure interactions: added mass computations for incompressible fluid. UCB/EERC-82/09, Earthquake Engineering Research Center, University of California, Berkeley, 1982-08.

HFTD Analysis of an arched dam at seismic loading

W. Kikstra[1], F. Sirumbal[1] and G. Schreppers[1]

[1] TNO DIANA BV, Delftechpark 19a, 2628 XJ Delft, NETHERLANDS

E-mail: info@tnodiana.com

Abstract

Hybrid Frequency-Time Domain (HFTD) method is applied to analyze the response of a dam-foundation-reservoir system. With this method the effect of frequency dependent properties such as compressibility of fluid, reservoir-bottom absorption and far-field reflection can be considered. HFTD results are compared with transient Newmark-type results and effect of frequency dependent properties is found to reduce amplitudes and stresses in the dam for the chosen bottom absorption in the reservoir.

Introduction and analysis procedure

The benchmark case study of the arch dam-reservoir interaction at seismic loading was modeled with DIANA software. The formulation used by DIANA to couple the Finite Element equations of motion for Fluid-Structure Interaction (FSI) problems is a mixed displacement – scalar potential approach, which defines the solid variables in terms of displacement degrees of freedom (DOF), and the fluid variables in terms of pressure DOF. This definition of the fluid domain using Acoustic Finite Elements is called the Eulerian pressure formulation. One of the advantages of this type of formulation is the simple description of the fluid domain using a single scalar pressure variable (p). This reduces considerably the number of variables of the system since only one DOF per node is required to describe the motion of the fluid domain.

Taking into account that for dam-reservoir interaction problems the fluid motion is not substantial but small, considerable simplifications can be made in its equation of motion formulation. Those simplifications are a consequence of the following hypotheses assumed in DIANA FSI models:

- Small displacement amplitudes
- Small velocities (convective effects are omitted)
- Inviscid (viscous effects are neglected)
- Small compressibility (variation of density is small)
- No body forces in the fluid

Based on these hypotheses, the scalar fluid wave equation of motion is defined by Eq.(1).The wave speed (c), defined in terms of the fluid density (ρ) and bulk modulus (β), is defined by Eq.(2).

$$\nabla^2 p = \frac{1}{c^2}\ddot{p} \tag{1}$$

$$c = \sqrt{\frac{\beta}{\rho}} \tag{2}$$

In the same way, the FSI condition expressed in Eq. (3) relates the fluid gradient pressure in the normal direction ($\frac{\partial p}{\partial n}$) to the interface surface (Γ_I) with the structure acceleration vector ($\ddot{\mathbf{u}}_S$).

$$\frac{\partial p}{\partial n} = -\rho_0(\mathbf{n}^T\ddot{\mathbf{u}}_S) \text{ on } \Gamma_I \tag{3}$$

In addition to the fluid-structure interface (Γ_I) condition defined in Eq. (3), Figure 1 shows three types of boundary conditions which can be defined in DIANA FSI models.
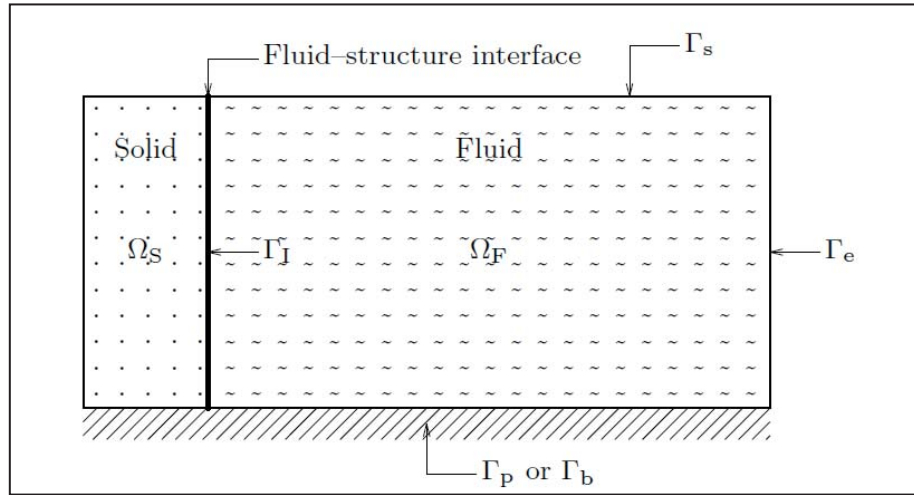
Figure 1: Fluid and solid domains, fluid-structure interface and boundary conditions

It is possible to specify two types of boundary conditions for the free surface of the reservoir (Γ_s). The first and simplest one is a consequence of neglecting the effect of the surface waves, prescribing a pressure equal to zero in the horizontal top free surface, as expressed in Eq. (4). This essential or Dirichlet type of boundary condition is the one used in the benchmark case study. Additionally, in DIANA it is possible to define a second type of boundary condition which takes into account the pressure caused by the free surface gravity waves.

$$p = 0 \quad \text{on } \Gamma_s \tag{4}$$

Two types of infinite extent boundary condition (Γ_e) are considered in the benchmark case study. The first one defined by Eq. (5.a) prescribes the hydrodynamic pressure equal to zero at a distance equal to the reservoir length. The second one defined by Eq. (5.b) is a radiation boundary theoretically located at an infinite distance from the dam, which ensures that no incoming waves enter into the system (only outgoing waves).

$$p = 0 \quad \text{on } \Gamma_e \tag{5.a}$$

$$\frac{\partial p}{\partial x} = -\frac{1}{c}\dot{p} \text{ on } \Gamma_e \tag{5.b}$$

Finally, two types of bottom boundary condition (Γ_b) are considered in the benchmark case study. The first one is setting the gradient of the pressure in the normal direction equal to zero, as expressed in Eq. (6.a). The second one defined by Eq. (6.b) is radiation boundary which takes into account the energy absorption of the bottom materials in terms of the wave

reflection coefficient (α), defined as the ratio between the amplitudes of the incident pressure wave over the reflective pressure wave.

$$\frac{\partial p}{\partial n} = 0 \quad \text{on } \Gamma_b$$

(6.a)

$$\frac{\partial p}{\partial n} = -\frac{1-\alpha}{c(1+\alpha)}\dot{p} \text{ on } \Gamma_b$$

(6.b)

In this paper, the Hybrid Frequency-Time Domain method is applied to solve the fluid equation of motion in the frequency domain. In this way, the hydrodynamic pressure amplitude vector is obtained in terms of the structural displacement amplitude vector.

On the other hand, the structure non-linear equation of motion defined in the time domain is formulated based on relative displacement. In this way, the earthquake ground acceleration vector is introduced as external loading. The non-linear internal force of the structure is defined as the difference between the linear internal force and an unknown pseudo force vector, which is substituted into the non-linear equation to obtain the HFTD pseudo-linear equation of motion of the dam in the time-domain.

Nevertheless, the HFTD method solves the pseudo-linear equation of motion in the frequency domain, and therefore it is required to use the Discrete Fourier Transform (DFT) to pass from one domain to the other. The fluid contribution is defined by additional mass and additional damping which both are defined in the frequency domain, and thus can be defined as frequency dependent properties.

As a consequence the HFTD method can account for the effects of non-linear material behavior, compressibility of fluid, radiation at infinite extend and reservoir-bottom absorption, whereas standard transient analysis with Newmark-type of time-integration schemes cannot consider these effects together.

Model definition

Because in the mesh that has been provided by the benchmark formulators some node connection incompatibilities were found, a new mesh has been defined using the provided geometry specifications as shown in Figure 2.

FOUNDATION	DAM	RESERVOIR
Height = 500 m	Height = 220 m	Length = 500 m
Length = 1000 m	Top width = 430 m	
Width = 1000 m	Bottom width = 80 m	
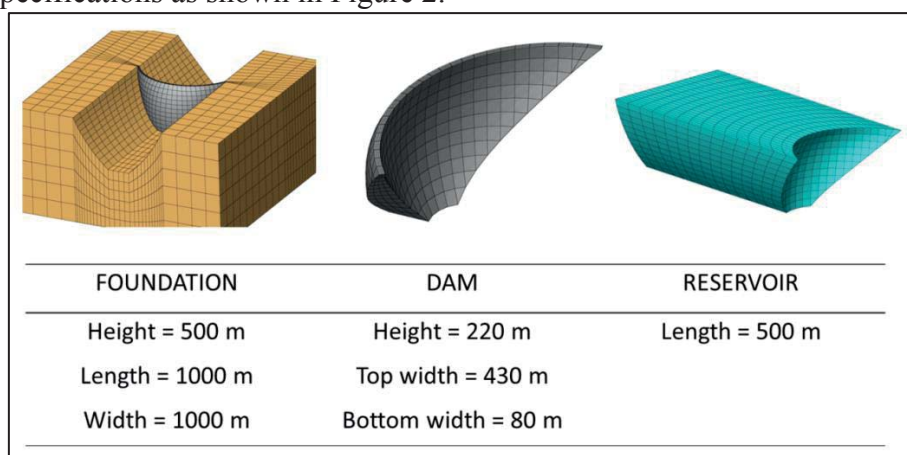
Figure 2: Components and geometrical characteristics of the foundation-dam-reservoir interaction system

Element with second order displacement interpolation were used for foundation and dam and element with linear fluid-pressure interpolation were used for the reservoir. Mesh characterstics are listed in Table 1 and material characteristics are listed in the Tables 2-4.

Table 1: Characteristics of the Finite Element Model Mesh

Component	Type	DIANA element name	Number of Elements	Number of Nodes
Dam	Solid 3D	CHX60	712	3601
		CTP45		
Foundation	Solid 3D	CHX60	4896	23339
		CTP45		
Reservoir	Flow 3D	CTP15H	2670	11950
		CHX20H		

Table 2: Material parameters for the concrete dam

Parameter	DIANA variable name	Value / Type	Units
Modulus of elasticity	YOUNG	2.7×10^{10}	N / m^2
Poison modulus	POISON	1.67×10^{-1}	-
Density	DENSIT	2.4×10^3	kg / m^3
Rayleigh damping	RAYLEI	5.71199×10^{-1}	-
		1.447×10^{-3}	-

Table 3: Material parameters for the reservoir fluid

Parameter	DIANA variable name	Value / Type	Units
Conductivity	CONDUC	1	-
Sonic speed	CSOUND	1.483×10^3	m / s
Density	DENSIT	1.0×10^3	kg / m^3
Wave reflection coefficient for infinite extent boundary	ALPHAB	0	-
Wave reflection coefficient for bottom absorption boundary	ALPHAB	5.0×10^{-1}	-

Table 4: Material parameters for the foundation soil

Parameter	DIANA variable name	Value / Type	Units
Modulus of elasticity	YOUNG	2.5×10^{10}	N / m^2
Poison modulus	POISON	2.0×10^{-1}	-
Density	DENSIT	0	kg / m^3

The transient responses of the two analysis cases shown in Figure 3 are determined and studied. Case I corresponds to the frequency independent system, for which the fluid of the reservoir is assumed to be incompressible ($c \to \infty$) and the infinite extent and bottom boundary conditions of the reservoir are defined by Eqs. (5.a) and (6.a), respectively. This frequency independent analysis case is solved with both HFTD and Newmark methods, with the objective of assessing the accuracy of HFTD method. On the other hand, Case II corresponds to a frequency dependent system in which fluid compressibility and reservoir radiation boundary conditions are included. Reservoir bottom absorption ($\alpha = 0.5$) and radiation boundary of infinite extent, defined by Eqs. (6.b) and (5.b), respectively, are

included in the analysis. As it was previously explained, the transient analysis of this frequency dependent system cannot be solved by the standard Newmark method, only by the HFTD method. Non-linear material behavior of the dam-structure is not considered in these cases.
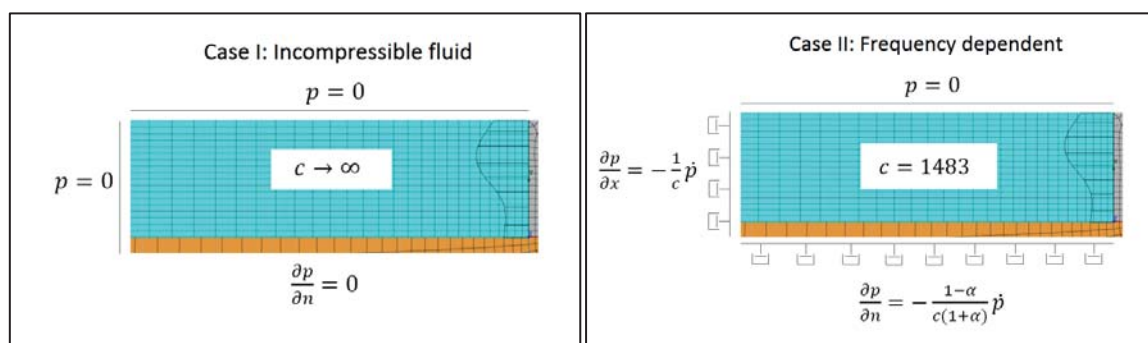
Figure 3: Foundation-dam-reservoir interaction analysis cases

Results

Prior to the time domain analysis, eigenvalues of the dam-foundation system including interaction with the fluid reservoir were determined. The first 10 mode-shapes and corresponding eigenvalues are presented in Figure 4.

Case I was solved using both Newmark time integration and HFTD analysis. Figure 5 shows the amplitude of the displacement of the crest at the main section. Agreement is so close that the vertical stress, hoop stress and radial displacement results for Case I will only be displayed for the Newmark time stepping analysis. The envelopes for hoop stresses, vertical stresses and radial displacements along with their static values are given in figures 6 to 8, respectively.

On the other hand, the frequency dependent properties of the reservoir and reservoir boundaries of Case II introduce more damping in the system which should lead to lower responses to the earthquake loading. Figure 9 shows that the crest amplitude has considerably lower peaks compared to Case I. The same magnitude reduction is observed in the envelopes of hoop stresses, vertical stresses and radial displacements given in Figures 10 to 12, respectively.

A 2D study to discriminate the effects of fluid compressibility, radiation boundary and bottom absorption shows that reservoir fluid compressibility increases the response, that there is minimal influence of the radiation boundary if sufficient reservoir length is modeled and that bottom absorption damps the response of the dam-reservoir system [3].

For all the analysis results presented (Eigen-analysis, Newmark and HFTD), the effect of self-weight gravity and hydrostatic pressure loads were taking into account as initial conditions.
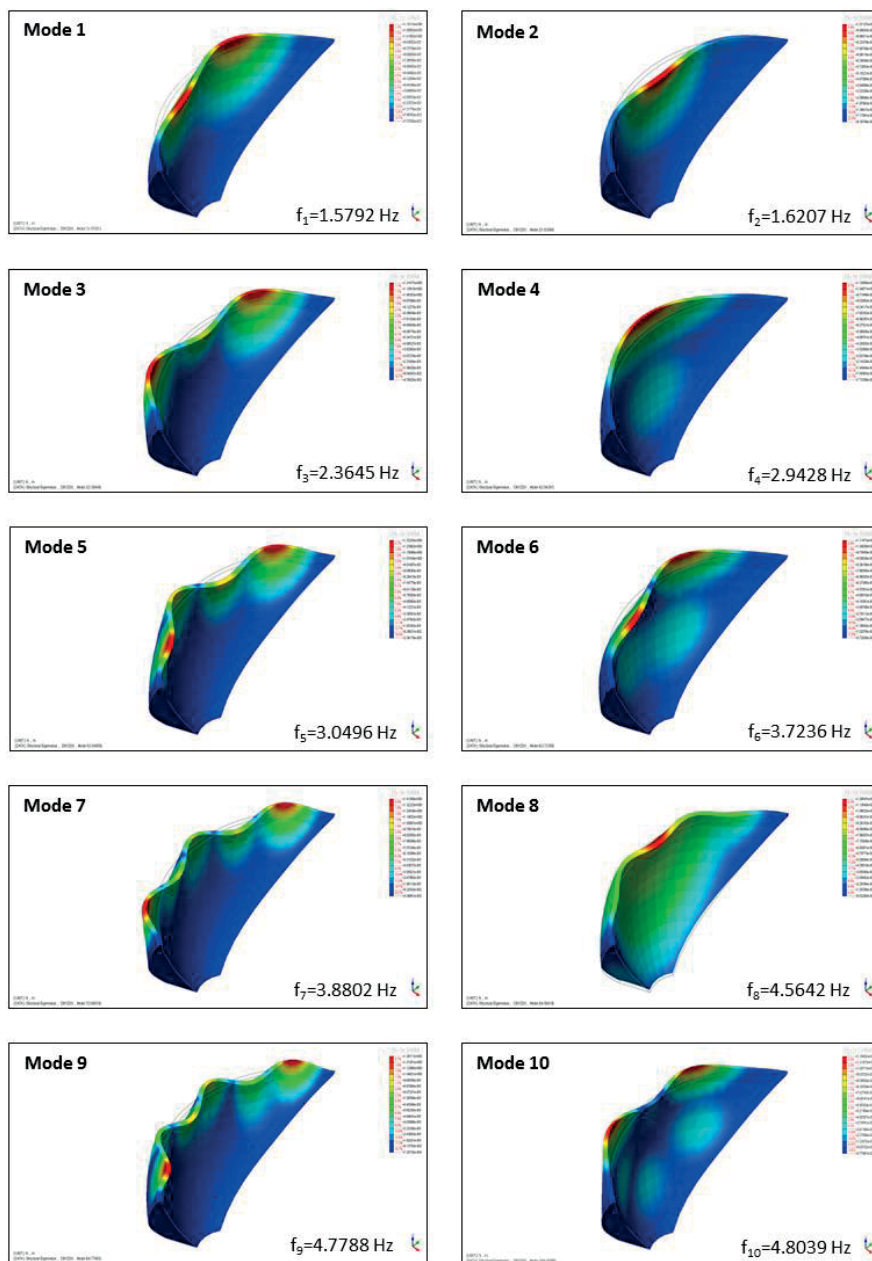
Figure 4: Mode-shapes and eigenvalues of the dam-foundation-reservoir interaction system
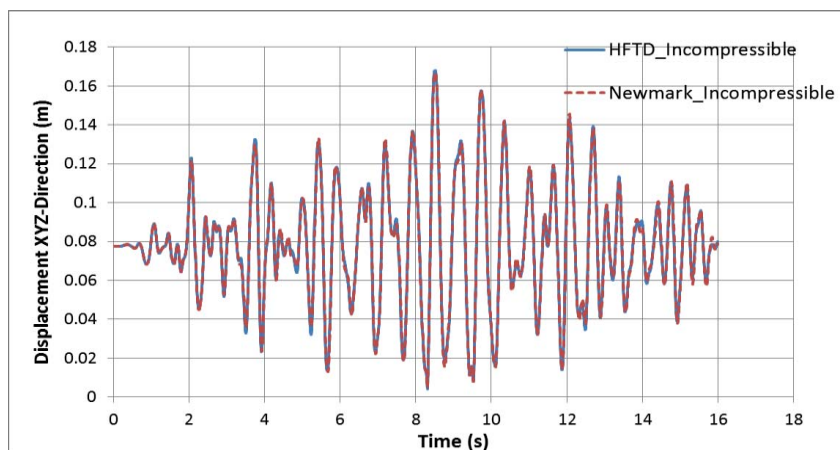
Figure 5: HFTD vs Newmark. Crest amplitude [m] at main section
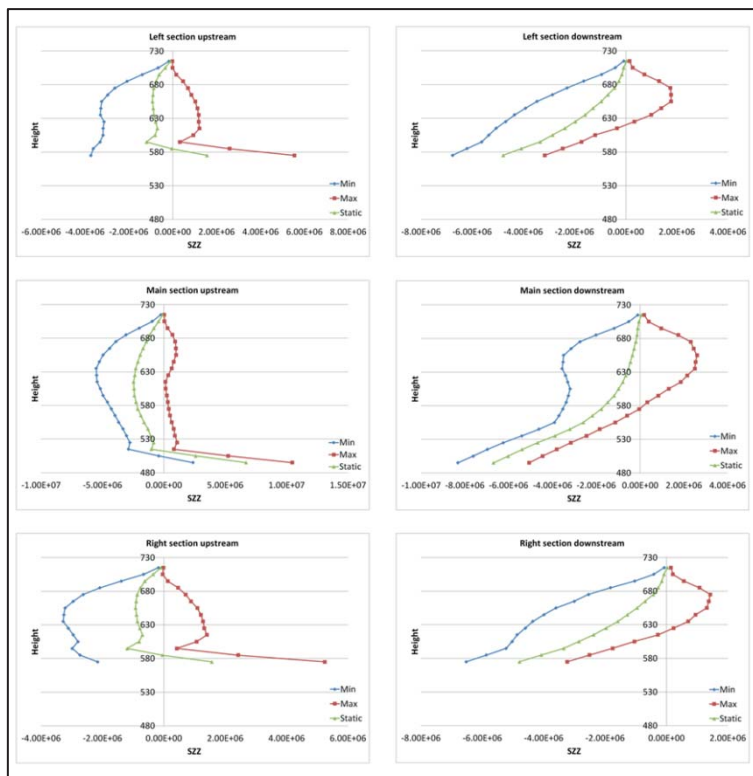
Figure 6: Vertical stress [Pa] against elevation [m] for left, main and right dam sections at upstream and downstream dam face for incompressible reservoir.
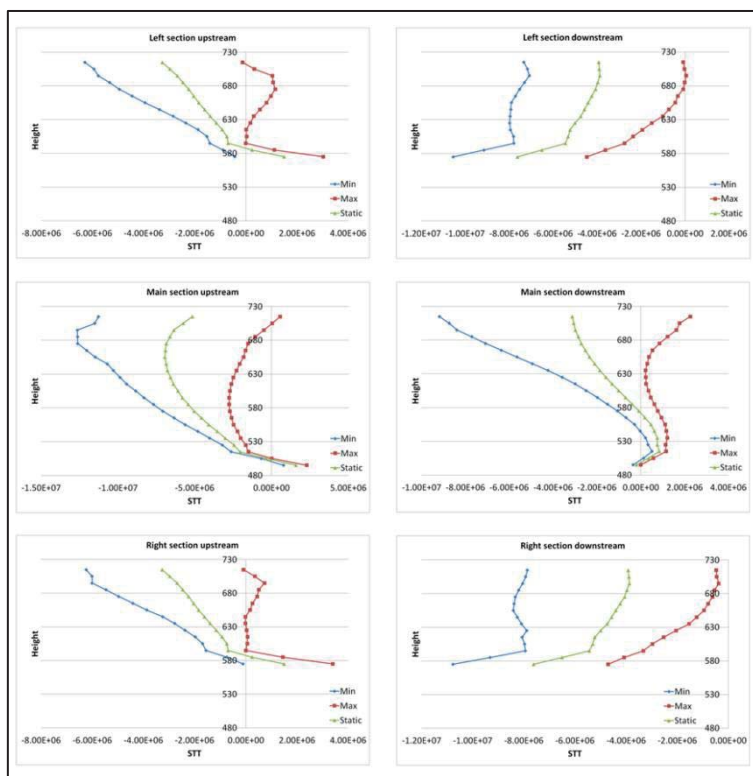
Figure 7: Hoop stress [Pa] against elevation [m] for left, main and right dam sections at upstream and downstream dam face for incompressible reservoir.
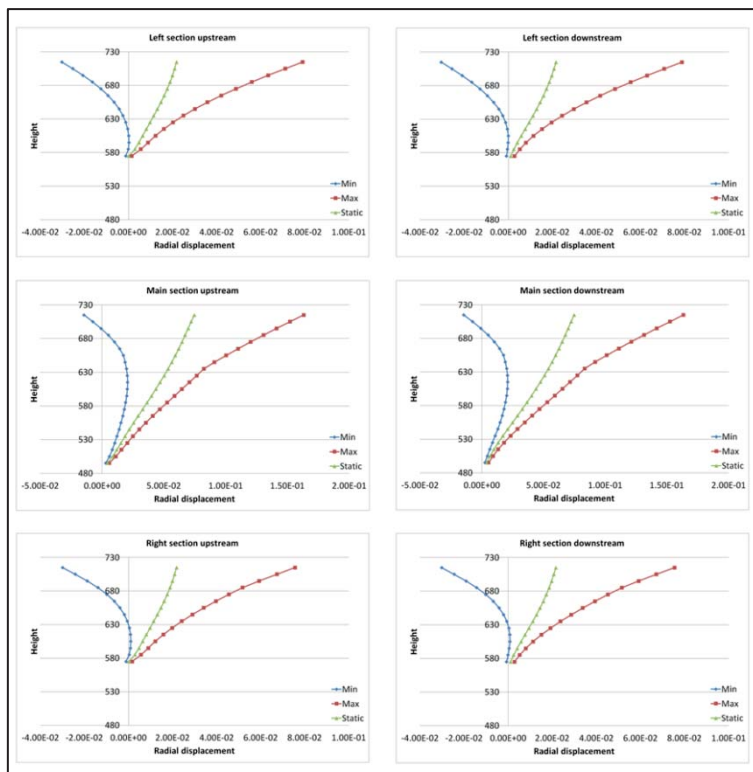
Figure 8: Radial displacement [m] against elevation [m] for left, main and right dam sections at upstream and downstream dam face for incompressible reservoir.
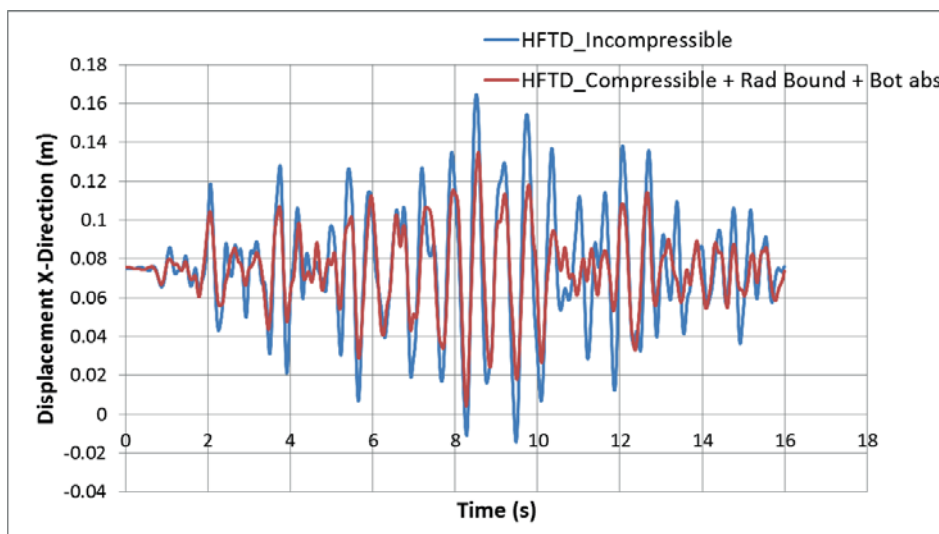
Figure 9: Compressible vs Incompressible. Crest amplitude [m] at main section
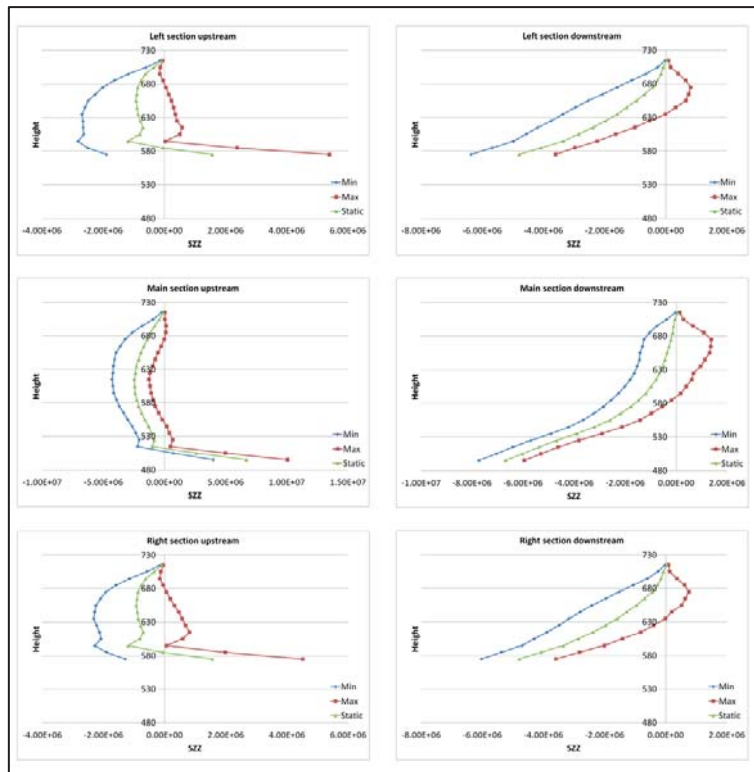
Figure 10: Vertical stress [Pa] against elevation [m] for left, main and right dam sections at upstream and downstream dam face for compressible reservoir.
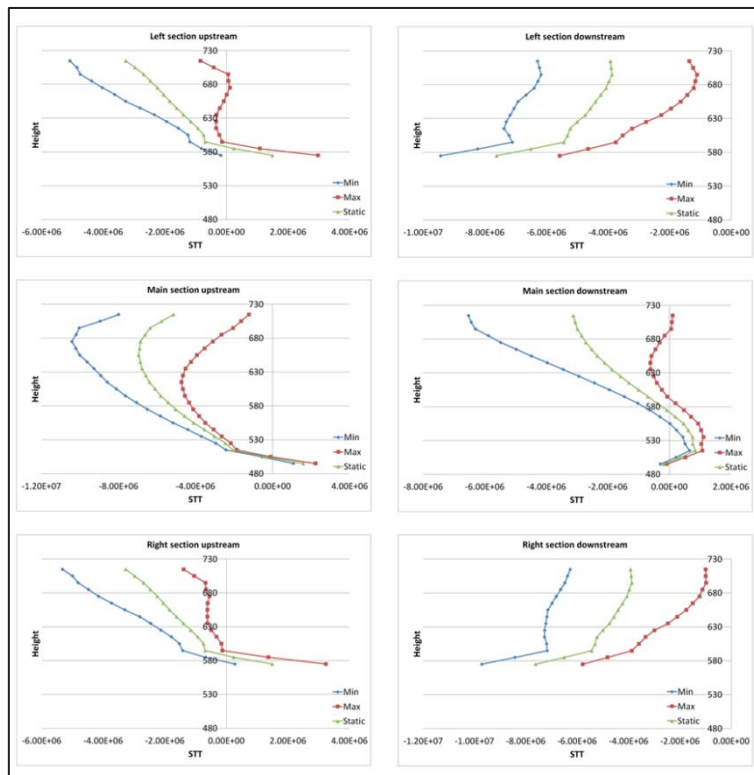
Figure 11: Hoop stress [Pa] against elevation [m] for left, main and right dam sections at upstream and downstream dam face for incompressible reservoir.
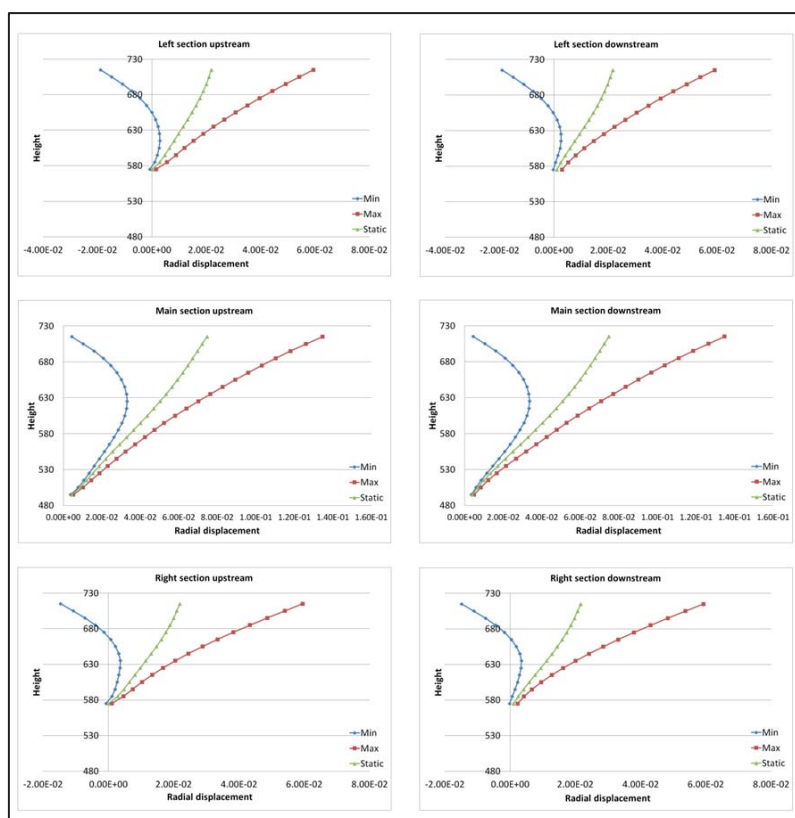
Figure 12: Radial displacement [m] against elevation [m] for left, main and right dam sections at upstream and downstream dam face for compressible reservoir.

Conclusion

The given foundation-dam-reservoir system was analyzed for the full duration of the earthquake. With the HFTD method implemented in the standard version of DIANA for the case of frequency independent properties the same results could be reproduced as with implicit time stepping with Newmark's method. With HFTD the effect of frequency dependent properties such as compressibility of fluid, reservoir bottom absorption and infinite extend reflection have been analyzed and quantified, resulting in an interesting method to be applied specially in the dynamic analysis of dam-reservoir interaction models.

References

[1] Veletsos, A.S., and Ventura, C.E. (1985). *Dynamic analysis of structures by the DFT method.* J. Struct. Eng. ASCE, Vol.111, 2625-2642.

[2] TNO DIANA BV (2011). *DIANA User's Manual – Release 9.4.4*, Delft, The Netherlands.

[3] Sirumbal, F. (2013) *Numerical modeling of dam-reservoir interaction seismic response using the Hybrid Frequency-Time Domain (HFTD) method* Masters thesis, Faculty of Civil Engineering and Geosciences, Delft University of Technology, Delft, The Netherlands.

[4] Darbre, G.R. (1996). *Nonlinear dam-reservoir interaction analysis*. Proc. Eleven World Conf. on Earthquake Engineering, Acapulco, Paper No. 760.

[5] Zienkiewicz, O.C., and Bettes, P. (1978). Fluid-structure dynamic interaction and wave forces. An introduction to numerical treatment. Int J Numer Meth Eng, Vol. 13, 1-16.

Finite Element Modelling of Seismic Fluid-Structure Interaction for a large Arch Dam

G. Faggiani[1] and P. Masarati[1]

[1] Ricerca sul Sistema Energetico - RSE SpA, via R. Rubattino 54, 20134 Milano, ITALY

E-mail: giorgia.faggiani@rse-web.it

Abstract

The linear dynamic fluid-structure interaction at seismic loading for the artificially generated large arch dam provided for the Theme A was modelled using the approach of acoustic compressible elements, with both the coarse and fine meshes provided by the formulators of the 12th ICOLD Benchmark Workshop.

The effects of incompressible fluid (theoretical hypothesis of the added mass models) and of the partial absorption of the hydrodynamic pressure waves at the reservoir boundary (bottom and sides) were also investigated.

Simulations were carried out using the RSE in-house FEM code CANT-SD, specifically designed for dynamic linear and non-linear analyses of dam-reservoir systems.

The coarse and fine meshes showed not dissimilar results, except at dam-foundation interface. The results of the analyses confirmed that incompressible models could result relatively conservative and highlighted the benefits of the approach of acoustic elements, mainly the possibility to take into account the damping effect on the fluid boundary.

Introduction

Seismic safety assessment of large arch dams is actually a very important matter. Both dam-reservoir interaction and non-linear mechanisms due to the contraction joint opening and sliding could greatly affect the mechanical behaviour of the dam: therefore they must be properly considered in order to obtain reliable numerical simulations under strong earthquakes.

Theme A of the 12th ICOLD Benchmark Workshop on Numerical Analysis of Dams [1] is aimed at comparing the different available approaches to model the dynamic fluid-structure interaction: to this purpose the structural response to a seismic loading of an artificially generated large arch dam has to be investigated.

The analyses have been carried out using the RSE in-house FEM code CANT-SD [2], specifically designed for linear and non-linear dynamic (seismic) analyses of dam-reservoir systems. This code is currently used at RSE for safety assessment of concrete dams, and it was adopted to deal with some themes proposed in previous ICOLD Benchmark Workshops [3] [4] [5] [6] [7] [8].

Regarding the main simulation options required to effectively address the present Theme A, CANT-SD models the fluid reservoir by means of acoustic elements and solves the transient dynamic coupled problem using an implicit direct time integration method.

Geometrical and physical model

The two FEM parabolic meshes, Coarse and Fine, considered in the simulations are reported in Figure 1 and 2. Only the dam meshes provided in the Theme A have been adopted unchanged. The fluid domain was obtained by extruding the upstream face of the dam mesh for a length 3 times the total height of the dam (220 m): the resulting mesh was only joined to

the upstream dam face, not to the rock. Foundation meshes were modified in order to obtain coincident meshes at concrete-rock interface as necessary for the proper operation of CANT-SD.
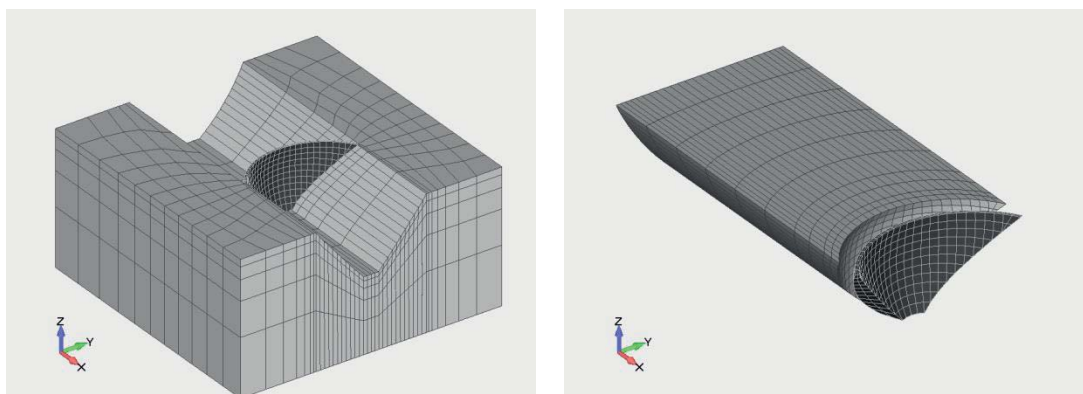
Figure 1: Arch dam FEM model – Coarse mesh
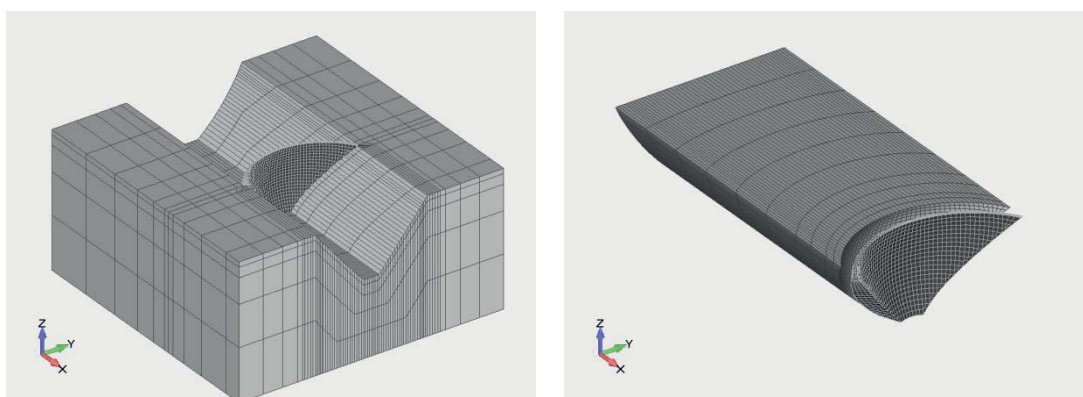
Figure 2: Arch dam FEM model – Fine mesh

A monolithic behaviour of the dam body has been considered, as no construction joints have been modelled. Dam concrete and foundation rock, assumed to behave linear-elastically, were characterized by the physical-mechanical parameters provided by the formulators and reported in Table 1 along with the properties of the fluid.

A 5% structural damping ratio (ξ) was assumed in the analyses: damping matrix is expressed as linear combination of mass and stiffness matrices according to Rayleigh formulation. The calibration of structural damping ratio was based on the frequency range resulting from modal analysis, such that the damping was almost constant in this range (Figure 3).

Table 1: Material properties

Parameter	Rock mass	Water	Dam concrete
Modulus of elasticity (MPa)	25000	-	27000
Bulk modulus (MPa)	-	2200	-
Poisson's ratio (-)	0.2	-	0.167
Density (kg/m^3)	0	1000	2400
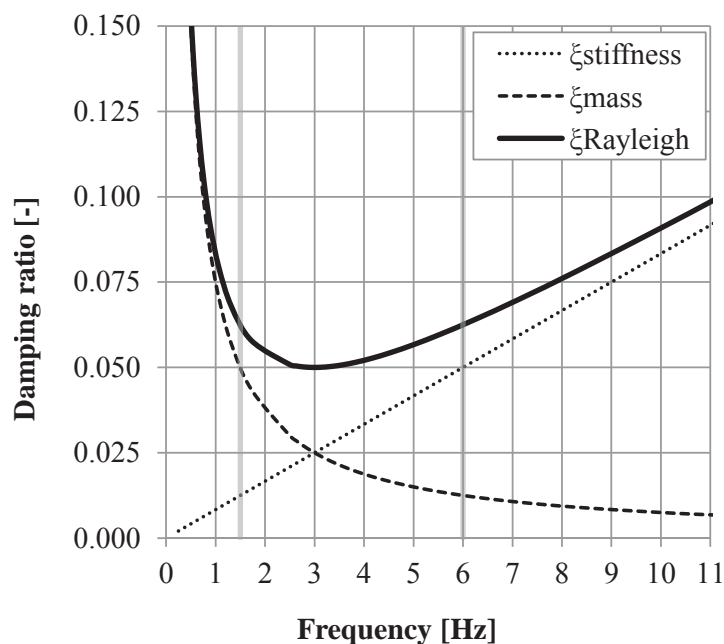
Figure 3: Rayleigh viscous damping

The dynamic fluid-structure interaction, modelled in CANT-SD following the classic acoustic approach [9], is here briefly summarized.

The hydrodynamic pressure in the compressible fluid of the reservoir is governed by the wave equation:

$$\frac{\partial^2 p}{\partial x^2} + \frac{\partial^2 p}{\partial y^2} + \frac{\partial^2 p}{\partial z^2} = \frac{1}{C^2}\frac{\partial^2 p}{\partial t^2} \tag{1}$$

where $C = \sqrt{(k/\rho)}$ is the velocity of sound in the fluid, k the bulk modulus and ρ the density.

The boundary conditions are (Figure 4):

- free surface $\qquad\qquad\qquad\qquad p = 0$
- upstream face of the dam $\qquad \dfrac{\partial p}{\partial n} = -\rho\ddot{u}$
- open boundary $\qquad\qquad\qquad \dfrac{\partial p}{\partial n} = -\dfrac{1}{c}\dot{p}$
- bottom and sides $\qquad\qquad\quad \dfrac{\partial p}{\partial n} = -q\dot{p}$

where $\boldsymbol{n}$ is the outward normal, $\ddot{u}$ the normal acceleration and q the damping coefficient on the bottom and sides.

The upstream face of the dam results the only surface of interaction between structure and fluid: the accelerations at the dam face represent the "actions" of the dam on the reservoir, which in turn "reacts" through the hydrodynamic pressures exerted on the dam face.

The last boundary condition accounts for the partial absorption of hydrodynamic pressure waves [10] [11]: this damping phenomenon is mainly caused by the layer of sedimentary material possibly deposited in the reservoir, but could be significant also in cases of few or no accumulated sediments.
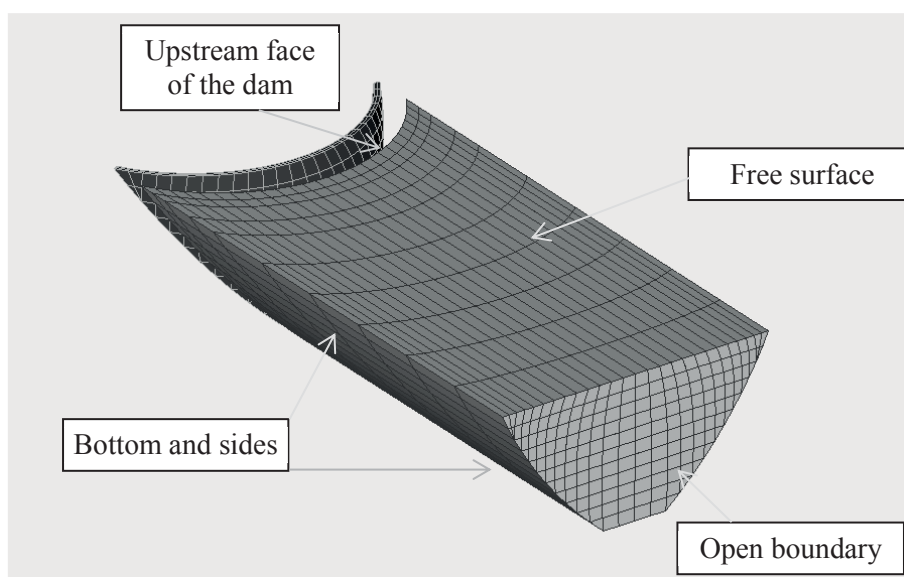
Figure 4: Boundaries of reservoir

Finite element subdivision of the reservoir leads to the discretized form of the outlined acoustic problem, i.e. a system to be coupled with the structural one (that includes the hydrodynamic pressure loads). The fluid-structure coupled problem is governed by the following system:

$$\begin{cases} K\underline{u} + M\underline{\ddot{u}} + C\underline{\dot{u}} = \underline{f} + H^T\underline{p} \\ \quad A\underline{p} + B\underline{\ddot{p}} + D\underline{\dot{p}} = -H\underline{\ddot{u}} \end{cases} \tag{2}$$

The first subsystem governs the mechanical behaviour of the dam and the (unknown) pressure $\underline{p}$ represents an applied load; the second governs the acoustic behaviour of the reservoir and the (unknown) acceleration $\underline{\ddot{u}}$ represents an assigned boundary condition.

The seismic analysis proposed in Theme A was performed for three physical models of the reservoir behaviour, differing in fluid compressibility and/or boundary absorption.

The first physical model (Base Case) fully respects the requirements of the formulators: the provided value of the bulk modulus of water (2200 MPa) was adopted, boundary absorption was neglected ($q=0$ on bottom and sides, i.e. reflecting condition) and the non-reflecting condition was considered at the end of the reservoir.

The other physical models have the aim to examine, for the particular given scenario, the following interesting aspects: the effect of the incompressibility hypothesis and the importance of the boundary absorption. A brief hint of both aspects follows, along with the necessary choices for the two additional simulations.

The assumption of fluid incompressibility is connected with the "added mass models", which assimilate the action of the fluid to that of "some kind of mass" (physical mass or a mass matrix) attached to the upstream face of the dam. It is worth noting that the comparison reported in this paper just concerns the incompressibility hypothesis, and can be therefore only applied to the rigorous "added mass matrix" model, clearly defined in [9] and referred to as "Finite Element Added Hydrodynamic Mass Model" in [12]. No investigation was made about the effects of any possible change on this matrix (i.e. for computational convenience), nor any comparison was made with Westergaard-type techniques, however strongly discouraged in [12] for arch dams.

A key simplified parameter [13] that determines the significance of water compressibility is the ratio $\Omega_r = f_1^r/f_1$ of the fundamental frequency of the reservoir to that of the dam-foundation system without water: the higher this ratio, the less the importance of fluid compressibility. Although the limit $\Omega_r = 2$ is valid only for gravity and not for arch dams, as clearly stated in [13], it has often been used, at least as a broad clue, for arch dams too [12].

The fundamental frequency f_1^r of the reservoir can be roughly evaluated as $C/4H$, where C is the velocity of sound in water and H is the water depth: for the analysed system the value is $f_1^r = 1.7$ Hz. The fundamental frequencies of the dam-foundation system without water were calculated and resulted 1.9 Hz for anti-symmetric mode shape and 2.0 Hz for symmetric mode shape. The value of the ratio Ω_r, about 0.9, indicates that compressibility should probably be important.

The physical model to investigate the effects of compressibility (Incompressible Case) was developed using a value of the bulk modulus one hundred times greater than that of the Base Case ($k = 2200 \times 100$ MPa) and assuming the reflecting boundary condition at the end of the reservoir. Two modal analyses were carried out, the first with $k = 2200 \times 100$ MPa and the second with $k = 2200 \times 10000$ MPa to verify that the value of the bulk modulus assumed in dynamic analysis was great enough to simulate incompressibility: no significant differences were found in the results.

The coupled mechanical-acoustic approach allows taking into account the effect of the partial absorption of hydrodynamic pressure waves on the boundary of the reservoir [10] [11], impossible to simulate using any added mass model. To assign the boundary absorption, the damping coefficient q must be quantified: to this purpose it is convenient to express it by means of the wave reflection coefficient α (the ratio of the amplitude of the reflected hydrodynamic pressure wave to the amplitude of the incident one) [11]:

$$q = \frac{1}{C}\frac{(1-\alpha)}{(1+\alpha)} \tag{3}$$

The wave reflection coefficient α represents a more physically meaningful description of the phenomenon: $\alpha = 1$ corresponds to a reflecting (rigid) boundary, $\alpha = 0$ corresponds to a non-reflecting (transmitting) boundary, $-1 < \alpha < 0$ corresponds to an even major damping behaviour. The value of α can be determined on the basis of field investigations [12] [14] [15]. The results reported in [14] indicate values of α, measured at seven concrete dam sites, varying over a range from -0.55 to 0.66: three of these values were negative, due to thick layers of soft sediments. A value of 0.82 was determined at the dam site investigated in [15]: a rock site with very little or no accumulated sediments.

Making reference to the reported results of field investigation, a value $\alpha = 0.5$ was considered sensible to examine the importance of the boundary absorption in the seismic analysis: the corresponding physical model (Damped Case) was obtained from the Base Case using a damping coefficient $q = 0.000225$.

Table 2 summarizes all the simulations: Base Case (B) was performed both with the coarse and fine meshes, while Incompressible (I) and Damped (D) Cases only with the coarse mesh.

Table 2: Summary of simulations

Case	Coarse mesh	Fine Mesh
Base	B	B
Incompressible	I	-
Damped	D	-

Loadings

The numerical analyses simulated the effects of the following loadings/actions:

1. dead weight
2. hydrostatic pressure with water level at crest height
3. seismic loading

The seismic loading was provided in the Theme by means of artificially generated acceleration time histories in the three coordinate directions X (upstream), Y (cross-stream) and Z (vertical): the elastic response spectra (5% damping ratio) are reported in Figure 5. It's worth noting that the given time histories represent a quite moderate intensity earthquake.

The acceleration time histories were only assigned to the bottom and sides of the foundation, not to the boundary of the reservoir too.

The transient dynamic coupled problem was solved using an implicit direct time integration method (HHT) [16]; an integration step of 0.002 s was chosen, in order to well represent frequencies up to 25 Hz.
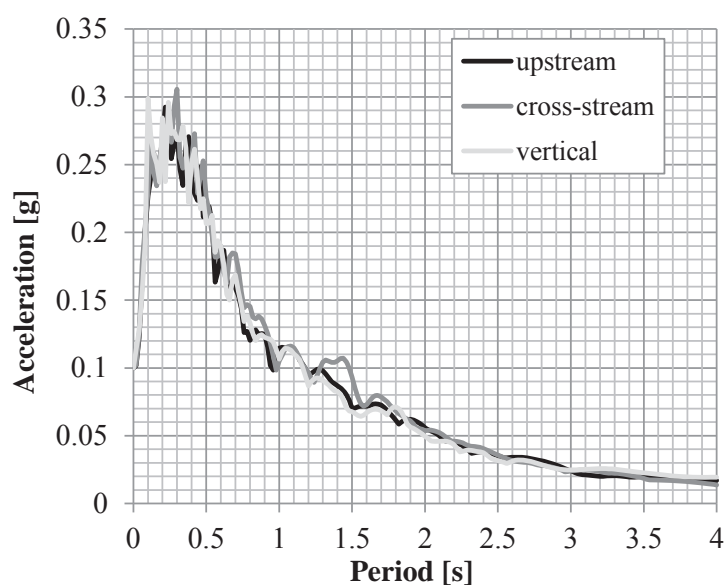
Figure 5: Elastic response spectra

Results

The following sections report and discuss the results of Base Case with both coarse and fine meshes and of Incompressible and Damped Cases.

The stress state is represented either by diagrams showing vertical and hoop static and dynamic (envelope) stresses, or by contour plots showing principal stresses envelopes, expressed in megapascal, positive if tensile.

The displacements of the dam, expressed in metres, are positive if directed downstream.

Eigenfrequencies and mode shapes

The modal analysis allowed the computing of the natural resonant frequencies of the dam-reservoir system and the corresponding mode shapes. Table 3 reports the first four eigenfrequencies for both the coarse and the fine mesh. The values obtained with the two meshes were almost identical: as expected, the refined discretization exhibited a slightly more flexible behaviour than the coarse one. These frequencies corresponded to the first anti-

symmetric and the first three symmetric mode shapes, shown in Figure 6 and 7 for the coarse and fine mesh respectively. The first four eigenfrequencies occurred in a range of periods of about 0.45÷0.65 s, matching the response spectra in their descending branch.

Table 3: Natural frequencies

Mode	Eigenfrequencies [Hz]	
	Coarse Mesh	Fine Mesh
1	1.547	1.540
2	1.551	1.549
3	2.052	2.050
4	2.229	2.222
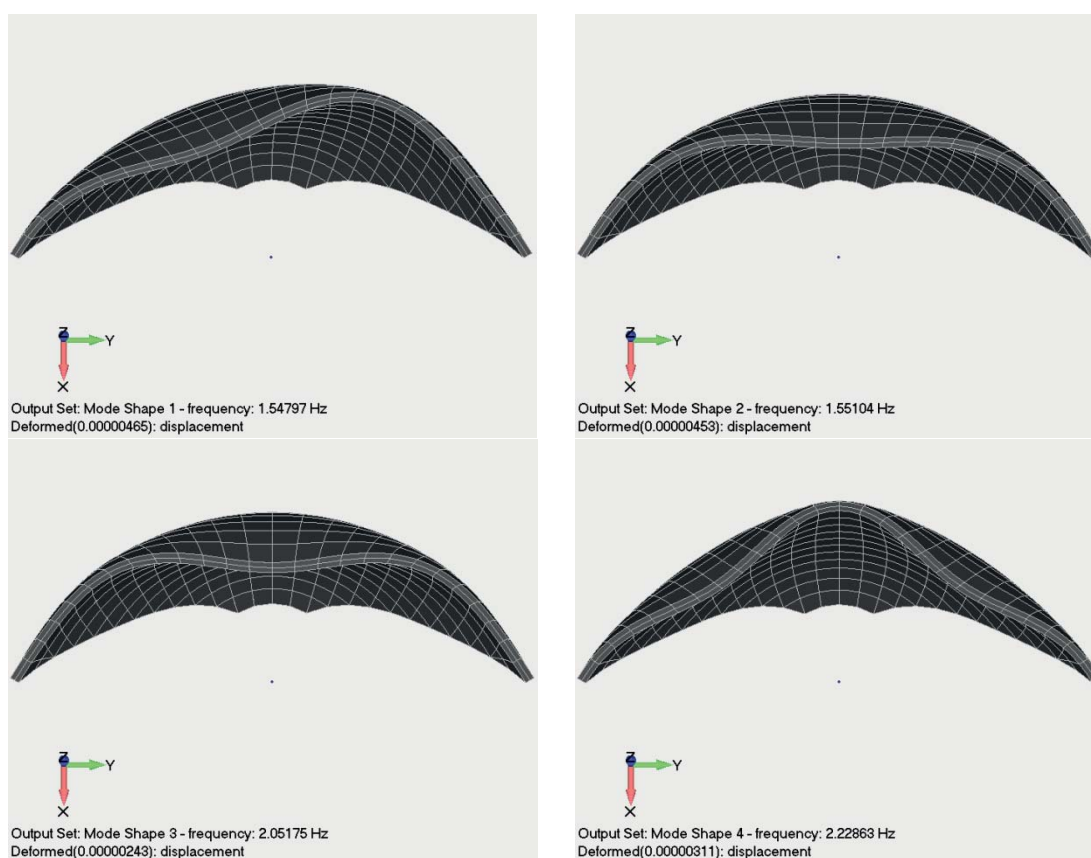
Figure 6: Mode Shapes (Base Case, Coarse Mesh)
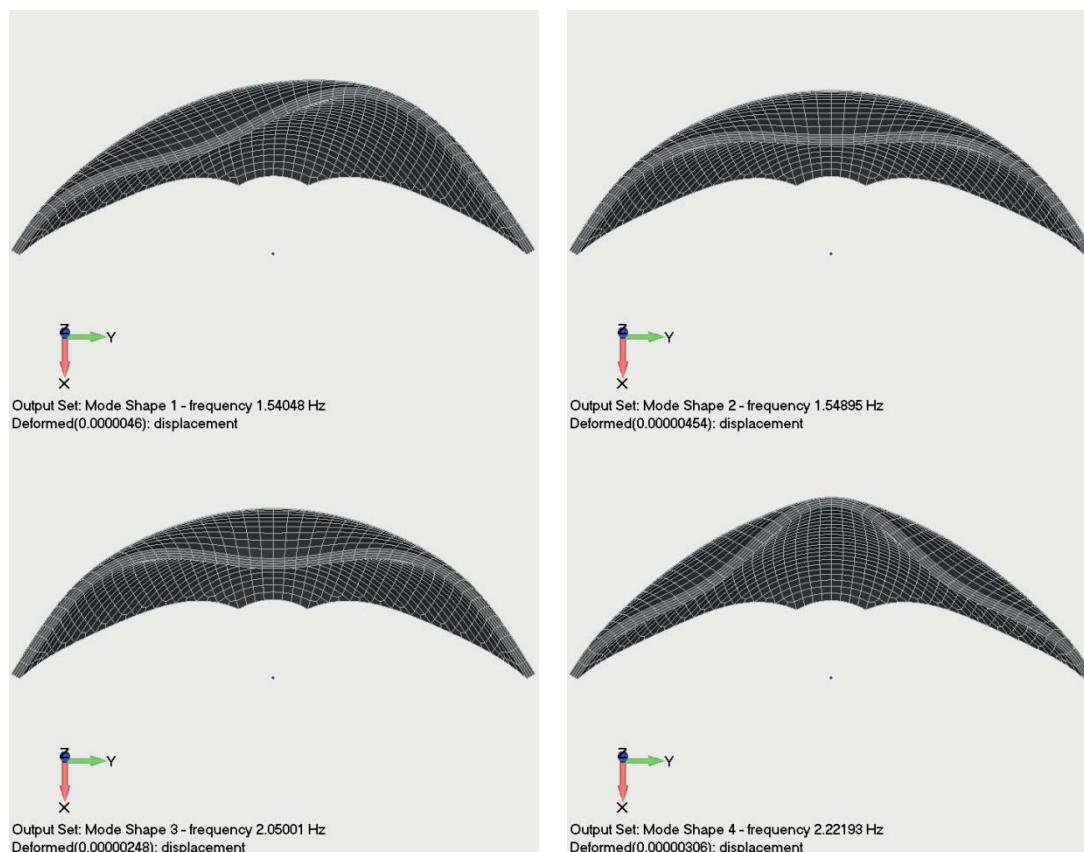
Figure 7: Mode Shapes (Base Case, Fine Mesh)

Seismic simulation with Coarse and Fine Meshes

The transient dynamic analysis supplied the stress-strain state of the system due to the application of the seismic loading.

The simulations developed for the Base Case with Coarse (CB) and Fine (FB) meshes showed how the use of a more refined mesh does not lead to significant differences in the results, though involving quite a higher computational effort (about 5 times).

Vertical and hoop stresses in dam main section are reported in Figure 8 and 9 for upstream and downstream faces respectively, both for fine and coarse meshes: stresses were evaluated for static and seismic loads.

Vertical stresses resulted always compressive upstream, except at dam foundation interface, while downstream tensile vertical stresses, up to 1 MPa, occurred in the upper part of the dam, above 610 m a.s.l., caused by the seismic loading. Due to the seismic loading, a variation of vertical stress of about 1÷1.5 MPa was observed both upstream and downstream. Figure 8 highlights that vertical stresses calculated with the coarse mesh are underestimated near the dam-foundation interface, where tensile stress concentrations are usual in many arch dams.

Hoop stresses both on upstream and downstream faces were compressive, confirming that the arch effect was activated and the dam behaved according to its monolithic scheme. The effect of the seismic loading, greater in the upper part of the dam, involved a stress variation of about 4 MPa upstream (at 675 m a.s.l.) and 2 MPa downstream (at about 695 m a.s.l.).

Figure 10 and Figure 11 report the tensile stress envelope and the dynamic maximum displacement contour plots for the two analysed meshes. Tensile stress on the downstream face was essentially vertically oriented: due to the seismic loading the upper central part of the dam exhibited stresses up to 1.6 MPa. Figure 11 shows a downstream displacement of about

8 cm, due to the seismic loading. A similar upstream displacement was observed for the minimum envelope.

The contour plots allowed the overall comparison between simulations with coarse and fine meshes and confirmed that the spatial trend of the stress-strain state was comparable in the whole dam body.
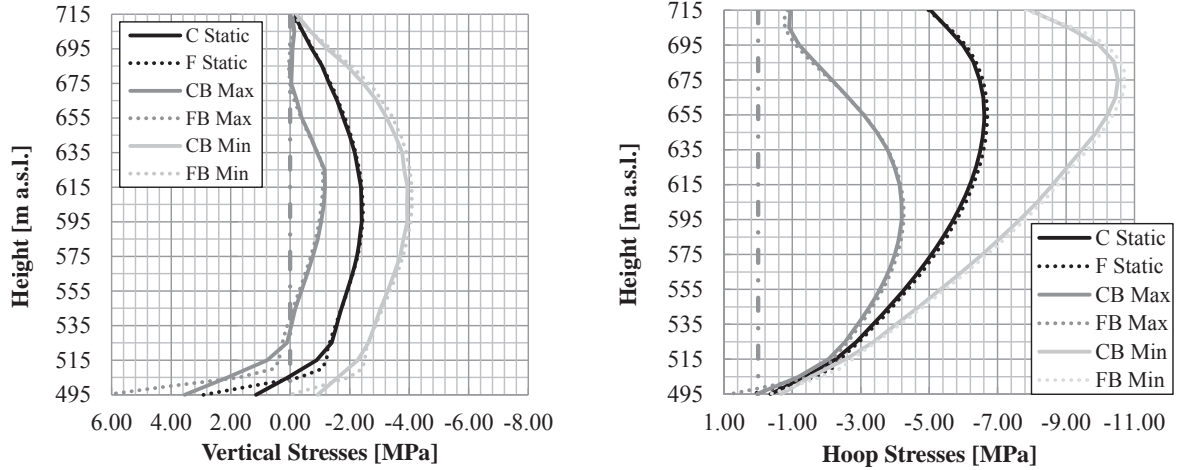
Figure 8: Base Case - Vertical (left) and hoop (right) stresses on the upstream surface
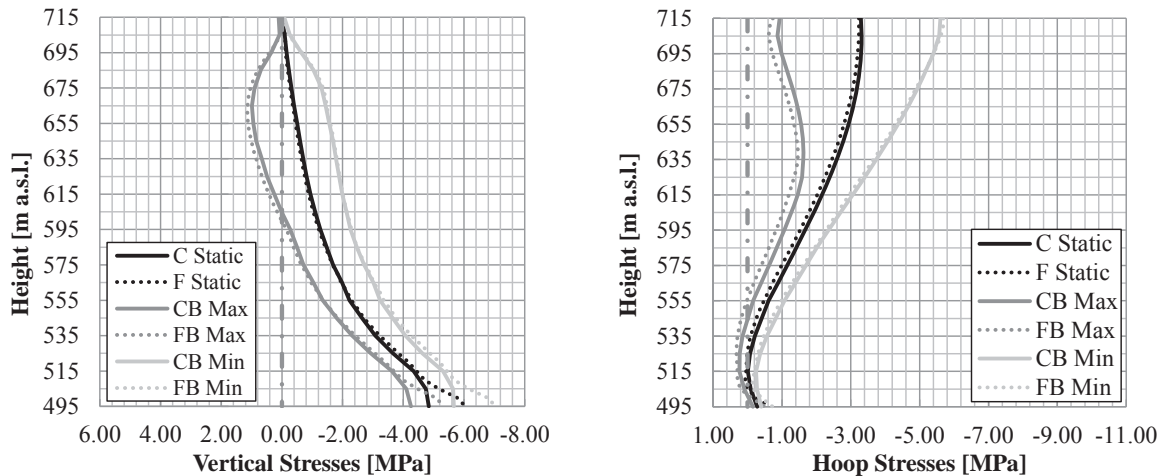
Figure 9: Base Case - Vertical (left) and hoop (right) stresses on the downstream surface
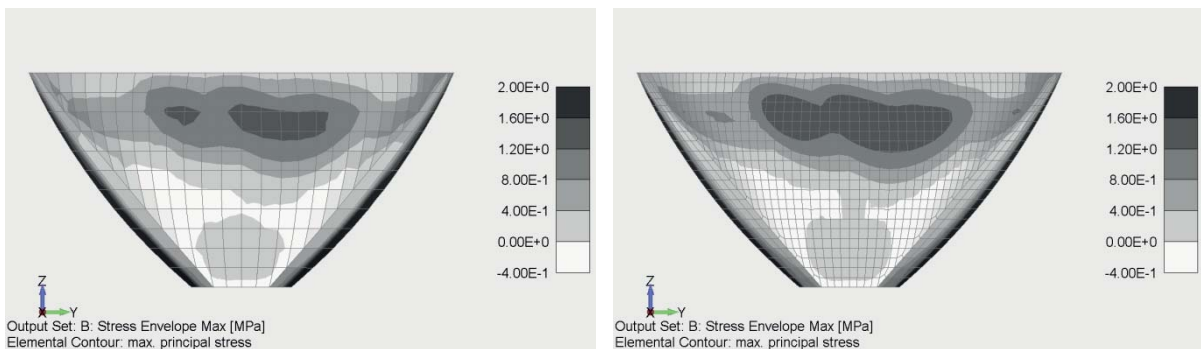
Figure 10: Base Case - Maximum principal stress – Coarse (left) and Fine (right) meshes, downstream view.
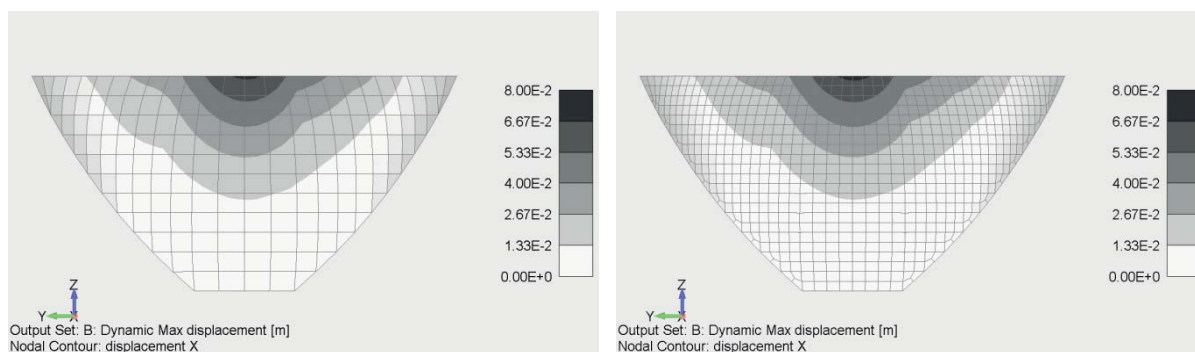
Figure 11: Base Case - Maximum dynamic displacement – Coarse (left) and Fine (right) meshes, upstream view

Incompressible fluid and absorption effects

Based on the comparison discussed in the previous section, the effects of incompressible fluid (Incompressible Case - I) and of the reservoir boundary absorption (Damped Case – D) on the dynamic response of the dam were investigated only with the coarse mesh.

The results of the analyses are summarized and compared with those of the Base Case (B) in Figure 12 and 13, where vertical and hoop stresses in dam main section are reported for upstream and downstream face respectively. The general trend of stresses for the Base Case was already illustrated in the previous section. The curves representing stresses for Incompressible and Damped Case generally laid respectively outside and within those of the Base Case, confirming that the incompressible model could result relatively conservative and that the reservoir boundary absorption could reduce the earthquake response of the dam.

In the analysed situation, relevant to an earthquake of very moderate severity, the difference among the three models could look worthless. However these differences could become highly significant if a greater seismic loading were considered. Referring to the hoop stresses, a 2 times amplified earthquake would result in the occurrence of tensile stresses in the arcs (Figure 14) involving the transition from a monolithic to an independent cantilever separated by vertical joints behaviour, if these stresses act in the dam for a significant height (starting from the crest). Figure 14 illustrates that for incompressible model tensile stresses resulted about 3÷5 times higher than for the damped model, involving the upper 80 m of the dam, a double height if compared with damped model.
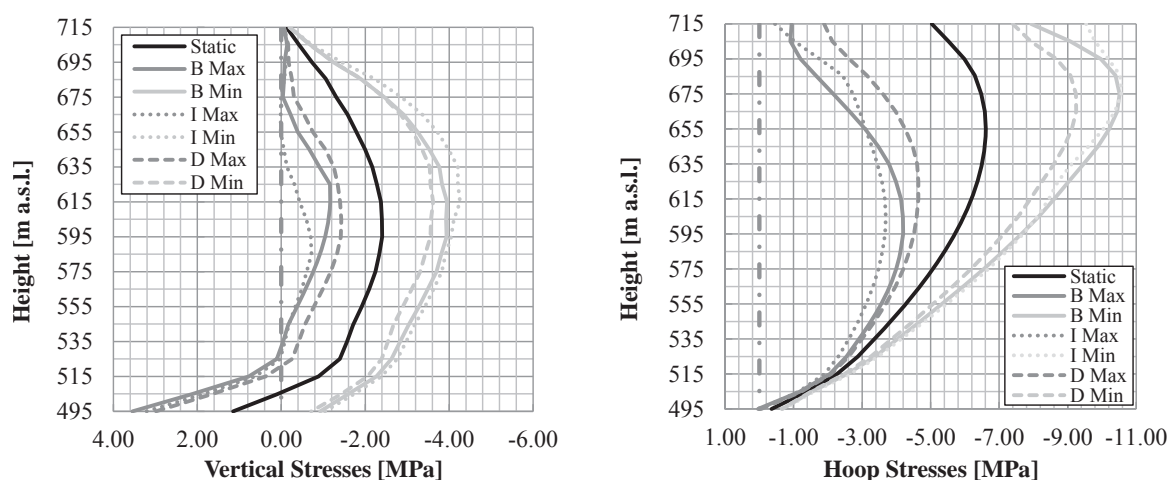
Figure 12: Comparison among Base, Incompressible and Damped Case - Vertical (left) and hoop (right) stresses on the upstream surface
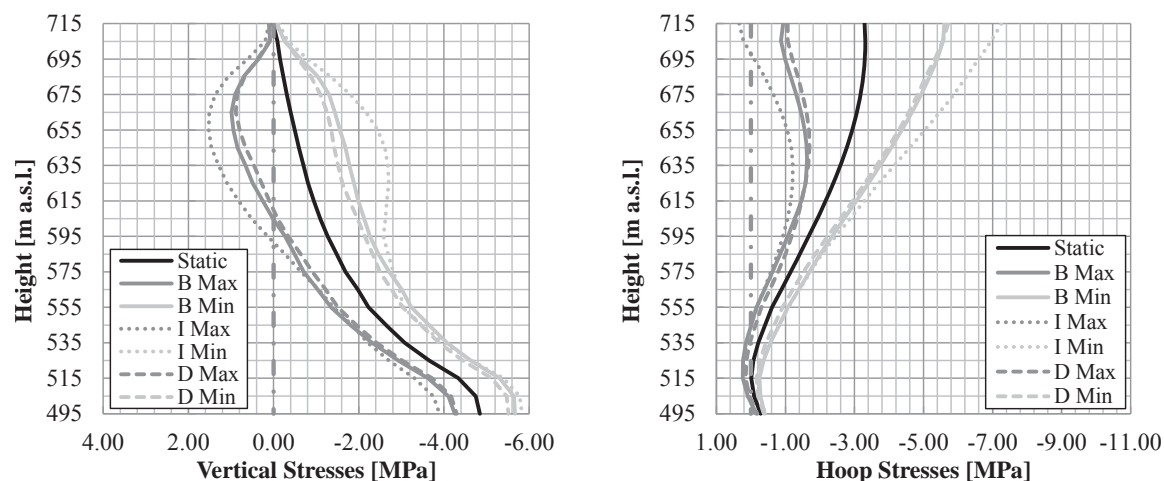
Figure 13: Comparison among Base, Incompressible and Damped Case - Vertical (left) and hoop (right) stresses on the downstream surface
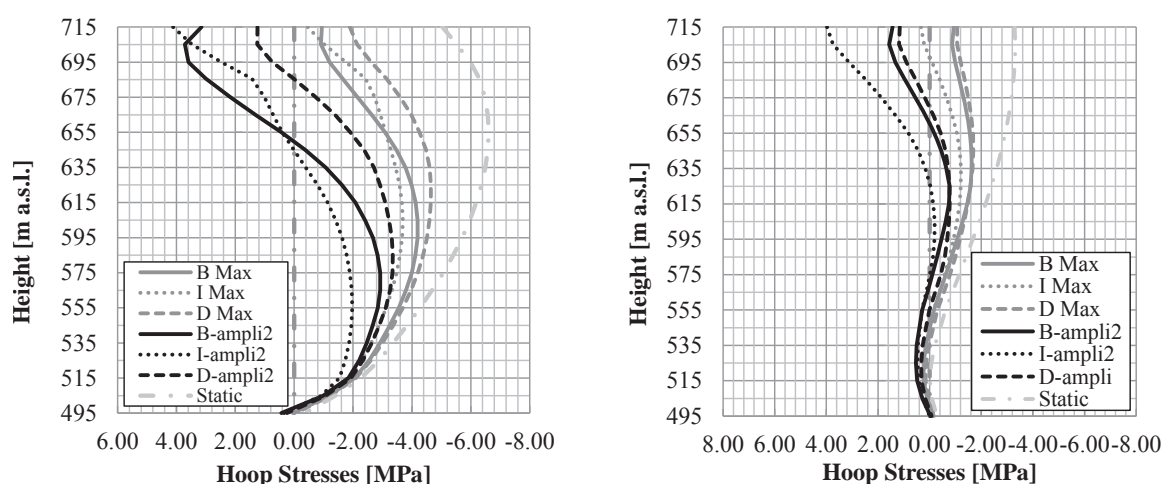
Figure 14: Comparison among Base, Incompressible and Damped Cases for an amplified earthquake- Hoop stresses on upstream (left) and downstream (right) surface

Conclusion

Theme A of the 12th ICOLD Benchmark Workshop on Numerical Analysis of Dams, dealing with the linear dynamic fluid-structure interaction at seismic loading, has been approached by using CANT-SD, a RSE in-house FEM code for dynamic linear and non-linear analyses of dam-reservoir systems. The dynamic fluid-structure interaction was modelled with the approach of compressible acoustic elements.

The analyses with the reflecting boundary condition on the bottom and sides of the fluid domain, performed with both coarse and fine meshes to test the effects of different spatial discretization, showed that the use of a more refined mesh does not lead to significant differences in the results, though involving quite a higher computational effort.

Simulations considering incompressible acoustic elements or reservoir boundary absorption were also performed: the results of these analyses confirmed that the incompressible model could result relatively conservative and that reservoir boundary absorption could significantly reduce the earthquake response of the dam. The use of an incompressible model instead of a compressible one, capable to account for damping effect on the fluid boundary too, speeded up the transition from a monolithic structural scheme to a different one with independent cantilevers and joints.

Acknowledgements

References

[1] Zenz G., Goldgruber M. (2013). Theme A formulation. Fluid Structure Interaction. Arch Dam – Reservoir at Seismic loading. 12th ICOLD Benchmark Workshop on Numerical Analysis of Dams, Graz, Austria.

[2] Masarati P., Meghella M. (2000). The FEM computer code CANT-SD for non-linear static and dynamic analysis of dams. Enel.Hydro rep. n. 6045, Milano, Italy.

[3] Faggiani G., Frigerio A., Masarati P., Meghella M.(2011). Finite element modelling of concrete swelling effects on Kariba dam. 11th ICOLD Benchmark Workshop on Numerical Analysis of Dams, Valencia, Spain.

[4] Meghella M., Masarati P. (2007). FEM analyses for the interpretation of the structural behaviour of La Aceña dam. 9th ICOLD Benchmark Workshop on Numerical Analysis of Dams, St. Petersburg, Russia.

[5] Meghella M., Frigerio A., Masarati P. (2005). Evaluation of AAR on the behaviour of Poglia dam adopting two different approaches. 8th ICOLD Benchmark Workshop on Numerical Analysis of Dams, Wuhan, Hubei, P.R. China.

[6] Meghella M., Mazzà, G. (2003). Safety evaluation against sliding of a gravity dam with curved shape. 7th ICOLD Benchmark Workshop on Numerical Analysis of Dams, Bucharest, Romania.

[7] Bon E., Chillè F., Masarati P., Massaro C. (2001). Analysis of the effects induced by alkali-aggregate reaction (AAR) on the structural behaviour of Pian Telessio dam. 6th ICOLD Benchmark Workshop on Numerical Analysis of Dams, Salzburg, Austria.

[8] Bolognini L., Masarati P., Bettinali F. Galimberti C. (1994). Non-linear analysis of joint behaviour under thermal and hydrostatic loads for an arch dam. 3rd ICOLD Benchmark Workshop on Numerical Analysis of Dams, Paris, France.

[9] Zienkiewicz O. C. (1977). The Finite Element Method, 3rd Edition, McGraw-Hill.

[10] Fok K.L., Chopra A.K. (1986). Earthquake analysis of arch dams including dam-water interaction, reservoir boundary absorption and foundation flexibility. Earthquake Engineering and Structural Dynamics, Vol. 14, pp. 155-184.

[11] Fenves G., Chopra A.K. (1983). Effects of reservoir bottom absorption on earthquake response of concrete gravity dams. Earthquake Engineering and Structural Dynamics, Vol. 11, pp. 809-829.

[12] US Army Corps of Engineers – USACE (2003). Engineering and Design - Time-History Dynamic Analysis of Concrete Hydraulic Structures. EM 1110-2-6051.

[13] Fok K.L., Chopra A.K. (1986). Frequency response functions for arch dams: hydrodynamic and foundation flexibility effects. Earthquake Engineering and Structural Dynamics, Vol. 14, pp. 769-795.

[14] Ghanaat Y., Redpath B.B. (1995). Measurement of reservoir-bottom reflection coefficient at seven concrete dam sites. QUEST Structure Report No. QS95-01.

[15] Ghanaat Y., Hall R.L., Redpath B.B. (2000). Measurement of dynamic response of arch dams including interaction effects. Proc. of 12WCEE2000.

[16] Hilber H.M., Hughes T.J.R., Taylor R.L. (1977). Improved numerical dissipation for time integration algorithms in structural dynamics. Earthquake Engineering and Structural Dynamics, Vol. 5, pp. 283-292.

ICOLD 12-th International Benchmark Workshop on Numerical Analysis of Dams
Theme A: Fluid Structure Interaction Arch Dam - Reservoir at Seismic Loading

A. Tzenkov[1], A. Abati[1] and G. Gatto[1]

[1] STUCKY SA, Rue du Lac 33, PO Box, 1020 Renens, SWITZERLAND

E-mail: a.tzenkov@stucky.ch

Abstract

One of the main concerns regarding the numerical dynamic analysis of arch dams is the proper modelling of the fluid-structure interaction between the dam and the impounded water. There are several approaches to this, which enables accounting for the hydrodynamic pressures on the upstream face of the dam with different precision and, respectively, with different computing effort. This work investigates the impact of the hydrodynamic approach opted for on the computed stresses and displacements of an example 220-m high double-curvature arch dam. It is shown that, for this particular benchmark problem, it is important to consider the compressibility of water.

Introduction

The hydrodynamic phenomena occurring on the interface between a dam and the impounded water may have significant effect on the structural response of the dam. The structure (the dam wall and its foundation) and the fluid (the impounded water) are two different physical systems that interact with each other and thus present a coupled problem. According to the classification given in [1], the latter is a Class I coupled problem in which the coupling occurs on the interfaces between the domains.

A milestone procedure to account for the hydrodynamic effects on dams was established by Westergaard in 1933, [2] by introducing the concept of added mass. Although Westergaard's approach was limited within the assumptions of rigid dams with vertical upstream faces, infinitely long reservoirs, and incompressible fluids, it enabled accounting for the hydrodynamic effects in the everyday engineering practice. Using the electric analog method, Zangar [3] improved Westergaard's approach by establishing a family of parabolas by means of which it is possible to compute the hydrodynamic pressure on rigid dams with sloping upstream face. With the advent of the computer and the increased utilization of the numerical methods, it became possible to account for the effects due to (1) the fluid compressibility, (2) the hydrodynamic pressure waves' partial absorption by deposited sediments, (3) the foundation inertia and damping, as well as for non-linear dam behaviour (4). Frequency domain [4][5], time domain [6], and hybrid frequency-time domain (HFTD) [7] procedures have been developed and used over the past decades. An inherent limitation of the frequency domain approach is that it presupposes linear structural behaviour; on the other hand, it enables readily considering effects (1), (2) and (3). In contrast, in the time-domain, nonlinear structural behaviour can be accounted with reasonable computational effort, but it is more difficult to simulate the other hydrodynamic phenomena.

This work investigates the differences of the stresses and the displacements computed by

means of the FEM in using three different approaches for modelling the hydrodynamic effects. The analyses are performed on the current Benchmark example 220 m high double-curvature arch dam by means of the computer program DIANA [8]. First, two linear seismic analysis are carried out in the time domain by using added masses computed by the Westergaard formula and by means of a fluid-structure interaction analysis in the assumption of incompressible fluid. Next, a linear analysis is performed by means of the HFTD approach and in modelling the fluid's compressibility. In addition, a nonlinear seismic analysis is performed in the time-domain, by means of a fluid-structure interaction analysis for incompressible fluid. Details of the procedures utilized, the results of the computations, and a discussion on the results are presented in the following sections.

Finite Element Model

The finite element model of the example arch dam – foundation – reservoir system is created based on the geometry and the spatial discretization given by the Formulator of the current Theme A [9]. The only difference is that the reservoir model's length is 5 times the dam height. Following the conditions of [9], the investigations have been done on two meshes: a coarse one, and a finer one. The structural system of the coarse mesh is modelled by 2516 hexahedral and wedge isoparametric solid finite elements (356 for the dam and 2160 for the foundation). The reservoir is modelled by 1956 3-D flow elements, while the dam-reservoir interface is represented by 177 fluid-structure interface elements. All the elements are based on quadratic interpolation. The total number of nodes of the coarse mesh is 21547. The fine mesh has 78426 nodes; the dam and the foundation are modelled by 2848 and 10080 elements respectively; however, it yields almost the same result regarding the structural response as the coarse mesh. Translational supports in the three global directions are specified as structural boundary conditions on the bottom and side surfaces of the foundation model. The material parameters of the dam and the foundation are the same as the ones prescribed in [9]. The sonic wave velocity c=1483 m/s is associated with the reservoir fluid elements. Finally, water density of 1000 kg/m^3 is specified for the fluid-structure interface elements.

Westergaard Added Mass (WG)
The added masses computed by means of the Westergaard formula [2] are applied on the nodes of the upstream face of the dam by means of CQ24TM boundary surface elements [8]. 178 such elements are defined for the coarse mesh; they are 712 for the finer model of the system. A distributed translational mass material model is associated to the boundary surface elements, which allows precise automatic calculation of the added masses. The total mass assembled for the coarse mesh finite element model is TM=0.14E+11 kg (for massless rock). Without added mass, TM=0.471E+10 kg.

Fluid - Structure Interaction with Incompressible Fluid (FSI)
As already mentioned, the solution is conducted in the time domain. To render the system frequency independent, the fluid is specified as incompressible by setting c tending to infinity, assigning hydrodynamic pressure $p = 0$ at the far-field and at the free surface of the reservoir, and setting the hydrodynamic pressure gradient equal to zero in the normal direction of the reservoir bottom. In this case, the hydrodynamic effect is represented by a consistent mass matrix that is added to the mass matrix of structural system.

Fluid Structure Interaction with Compressible Fluid (HFTD)
In this case, the system is frequency dependent. Sonic wave velocity c=1483 m/s is associated with the reservoir fluid elements and radiation boundary condition is specified for the fluid far-field, Equation (1):

$$\frac{\partial p}{\partial n} = -\frac{1}{c}\dot{p} \tag{1}$$

Fully reflecting boundary is assumed for the reservoir bottom, Equation (2):

$$\frac{\partial p}{\partial n} = 0 \tag{2}$$

The hydrodynamic pressure is set $p = 0$ at the free surface of the reservoir.

Analysis Performed

The load-cases specified in [9] are the self-weight of the dam, the hydrostatic pressure and the seismic loading. The present study is performed by means of phased analysis, which allows modelling the loading history. Thus, first are computed the stresses due to the self-weight of the dam. The hydrostatic pressure is applied next. Finally, the seismic loading is applied in the three directions of the supports using the base acceleration time-histories given in [9] and multiplied by a factor of $0.1g$, where g is the gravity acceleration.

Static Analysis
The dam construction stages are modelled in an approximate, but realistic way by means of phased activation of the dam elements. It is done in order to obtain correct strain and stress state due to the self-weight of the dam body prior to the application of the hydrostatic loading. In the linear analyses, the hydrostatic pressure is activated in a single phase as an instantaneous loading, whereas in the nonlinear analysis it is applied at ten steps corresponding to ten consecutive levels of filling of the dam reservoir.

Eigenvalue Analysis
The results of the computed eigenfrequencies f for the cases of empty and full reservoir with added masses defined by the Westergaard formula (coarse and fine mesh) and by a FEM incompressible fluid-structure interaction analysis are presented in Table 1. Note that the general coordinate system axes are as follows: X-axis is the stream direction (from u/s to d/s), Y-axis is the cross-stream direction (from right to left), and Z-axis is the vertical direction.

Table 1: Eigenrequencies and Effective Mass Percentage (Empty, WG, WG fine mesh, FSI)

Mode	Empty Reservoir				Full Reservoir, WG				WG FM	FSI
	f, Hz	X, %	Y, %	Z, %	f, Hz	X, %	Y, %	Z, %	f, Hz	f, Hz
1	1.931	0.0	18.4	0.0	1.314	0.0	8.5	0.0	1.305	1.572
2	2.040	30.6	0.0	1.0	1.340	26.4	0.0	0.2	1.336	1.622
3	2.929	15.4	0.0	0.7	2.004	12.4	0.0	0.1	1.992	2.362
4	3.623	0.1	7.5	0.1	2.362	15.7	0.0	1.1	2.352	2.944
5	3.643	13.2	0.0	15.0	2.519	0.0	2.4	0.0	2.498	3.040
6	4.313	0.0	36.2	0.0	2.961	0.0	6.6	0.0	2.944	3.719
7	4.550	3.1	0.0	3.4	3.184	0.8	0.0	0.1	3.153	3.869
8	4.824	4.5	0.0	61.7	3.703	1.4	0.0	0.1	3.680	4.555
9	5.203	0.0	20.8	0.0	3.903	0.0	0.7	0.0	3.860	4.764
10	5.578	0.0	0.1	0.0	3.938	7.1	0.0	1.6	3.914	4.803
	Σ	66.9	83.0	81.8	Σ	63.8	18.1	3.3		
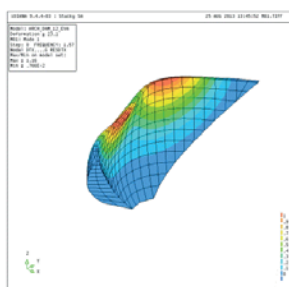
Mode 1, f_1 =1.527 Hz
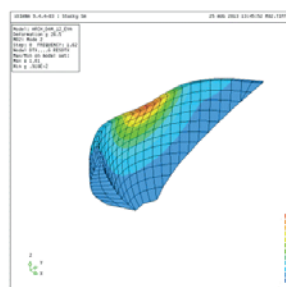
Mode 2, f_2 =1.622 Hz
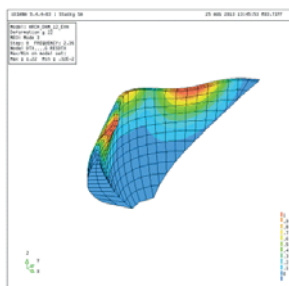
Mode 3, f_3 =2.362 Hz
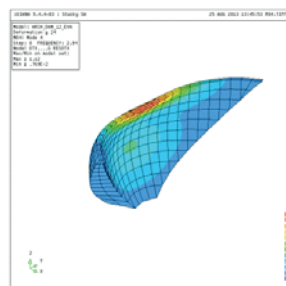
Mode 4, f_4 =2.944 Hz
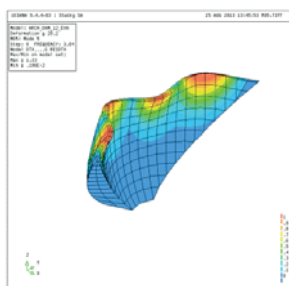
Mode 5, f_5 =3.040 Hz
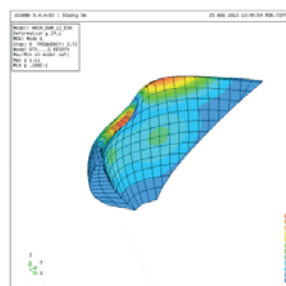
Mode 6, f_6 =3.719 Hz
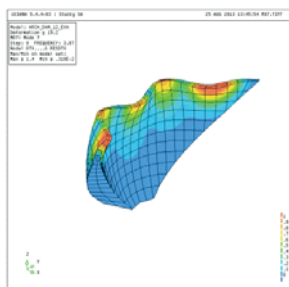
Mode 7, f_7 =3.869 Hz
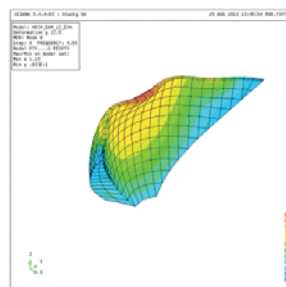
Mode 8, f_8 =4.555 Hz
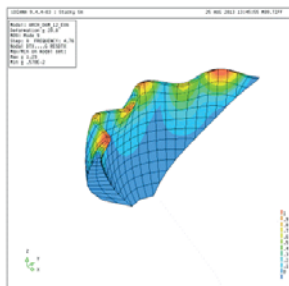
Mode 9, f_9 =4.764 Hz
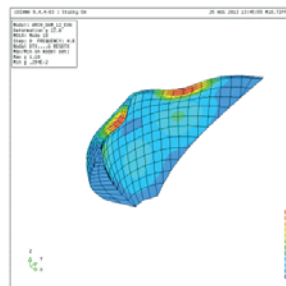
Mode 10, f_{10} =4.803 Hz

Figure 1: Dam Mode Shapes, Incompressible Fluid-Structure Interaction Analysis

Direct Time History Analyses

As already discussed, two linear and a non-linear direct time history analyses are performed. The analyses are carried out by the α −method of Hughes, Hilbert and Taylor with α =-0.3. The Rayleigh proportionality constants are computed so as to give a modal damping ratio of 5% in the first and the twelfth vibration modes. The nonlinear analysis considers only the effects due to opening/closing at the contraction joints (it is assumed that the joints are provided with strong shear keys). The contraction joints are modelled by structural interface elements CQ48I to which is associated a nonlinear elastic interface material model.

Hybrid Frequency Time Domain Analysis

The HFTD analysis is performed assuming linear structural behaviour and for only one time segment comprising the whole duration of the seismic input.

Results

The following line types are used to designate the type of analysis carried out:

——	Static
—△—	WG with Reservoir Damping
—○—	WG w/o Reservoir Damping
—●—	FSI with Incompressible Fluid
—△—	FSI with Compressible Fluid
– –	FSI with Incompressible Fluid and NONLIN Joint
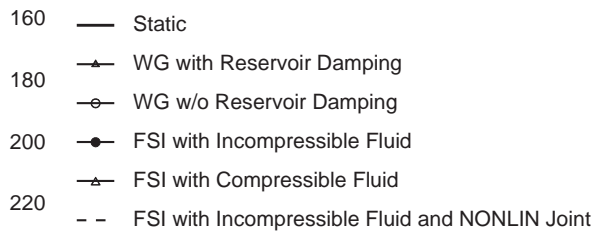
Figure 2: Analysis Type Designation

Hoop Stresses and Cantilever Stresses
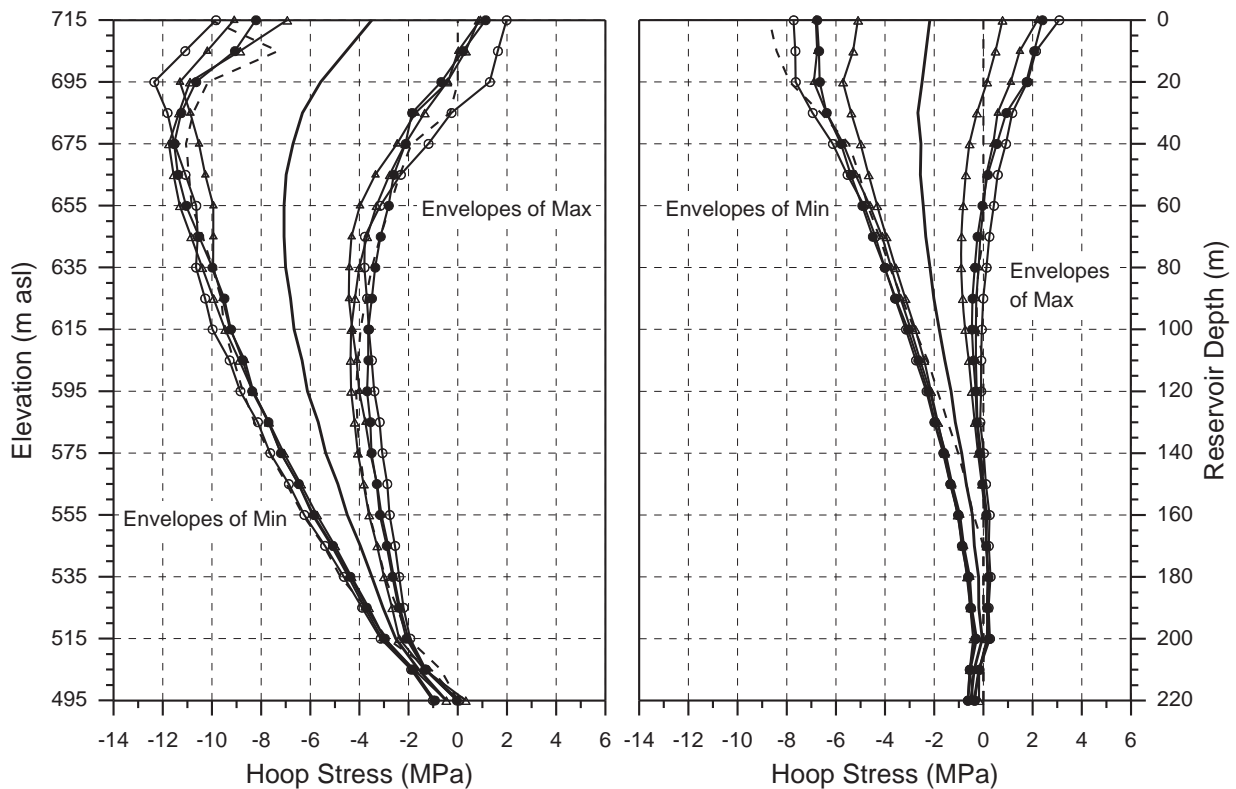
Figure 3: Main Section Hoop Stresses (U/S on left; D/S on right)
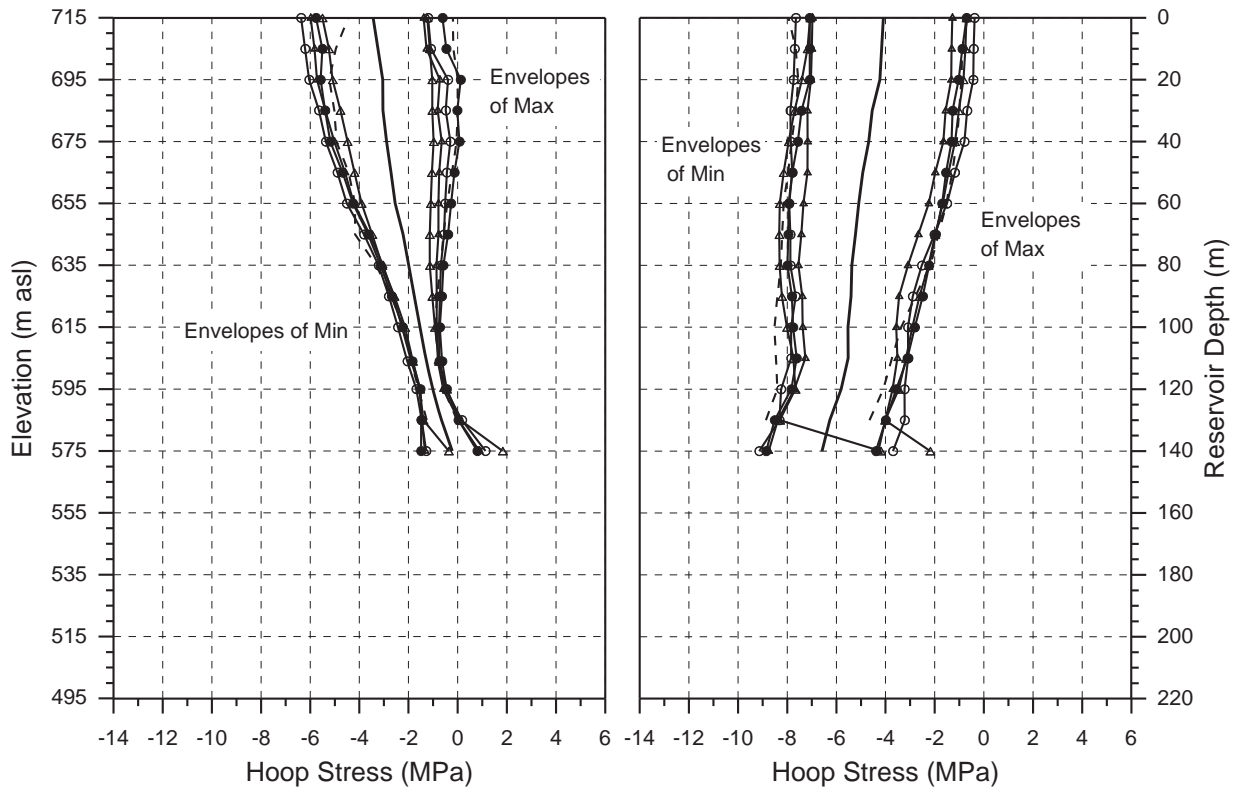
Figure 4: Left Section Hoop Stresses (U/S on left; D/S on right)
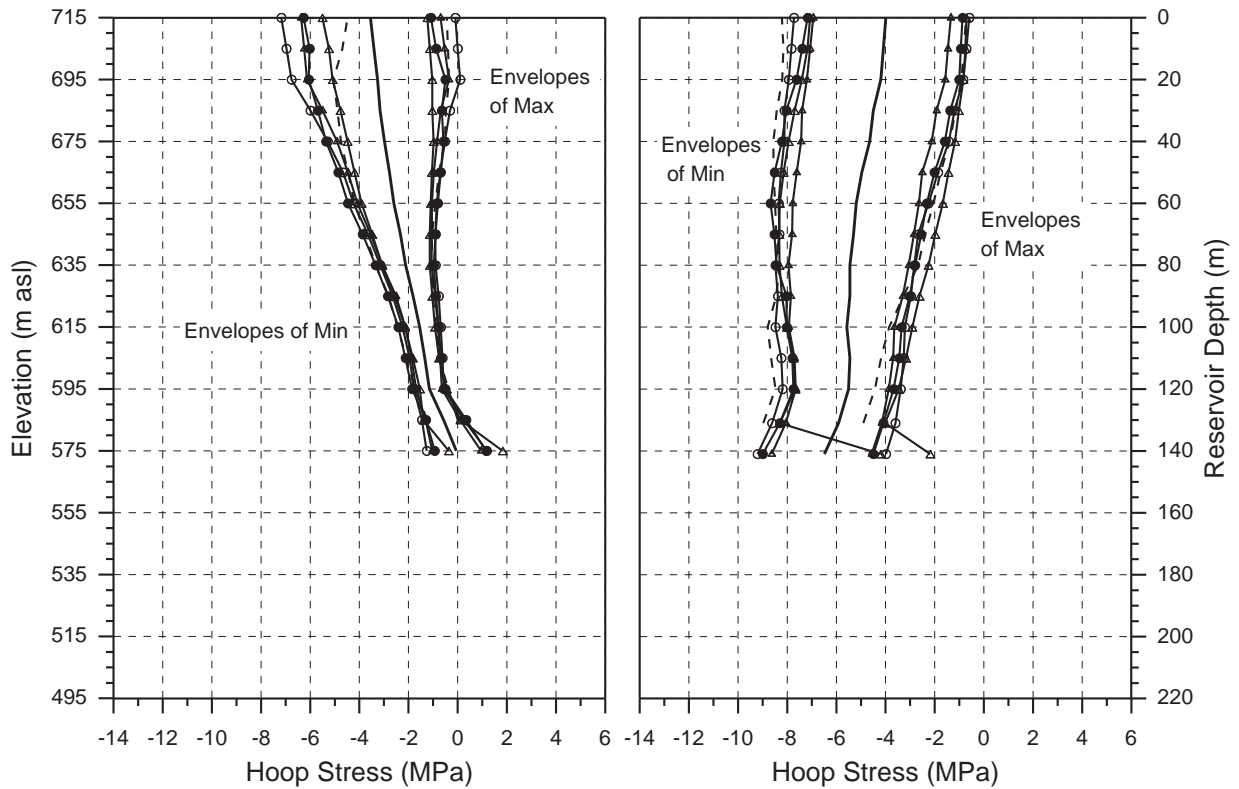
Figure 5: Right Section Hoop Stresses (U/S on left; D/S on right)
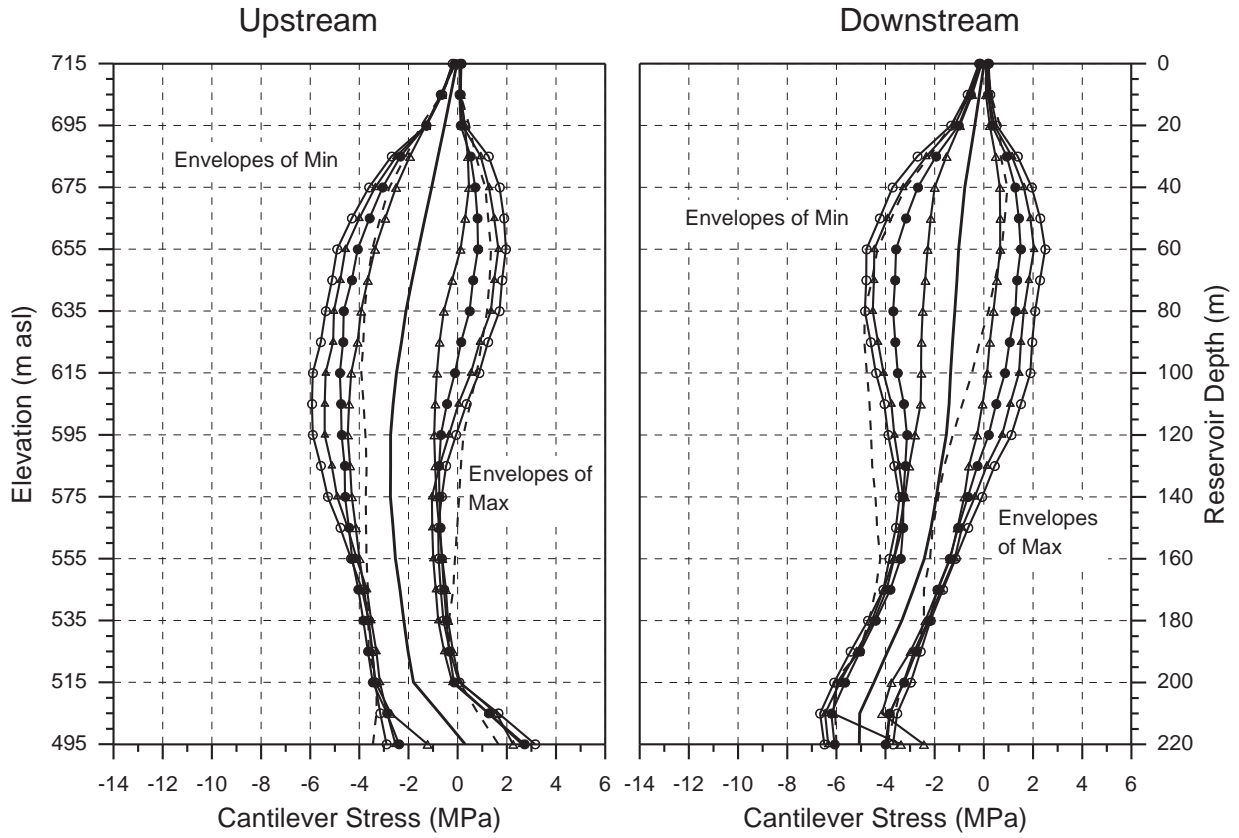
Figure 6: Main Section Cantilever Stresses
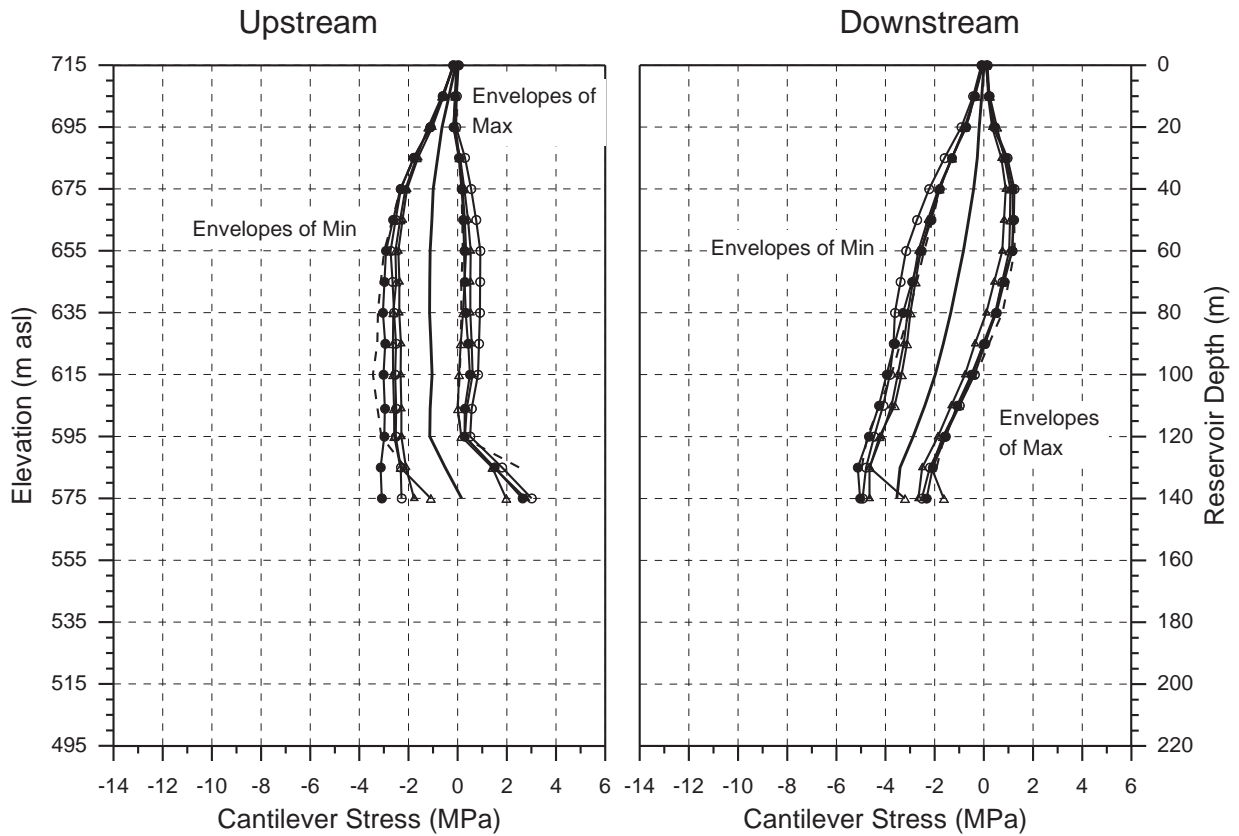
Figure 7: Left Section Cantilever Stresses
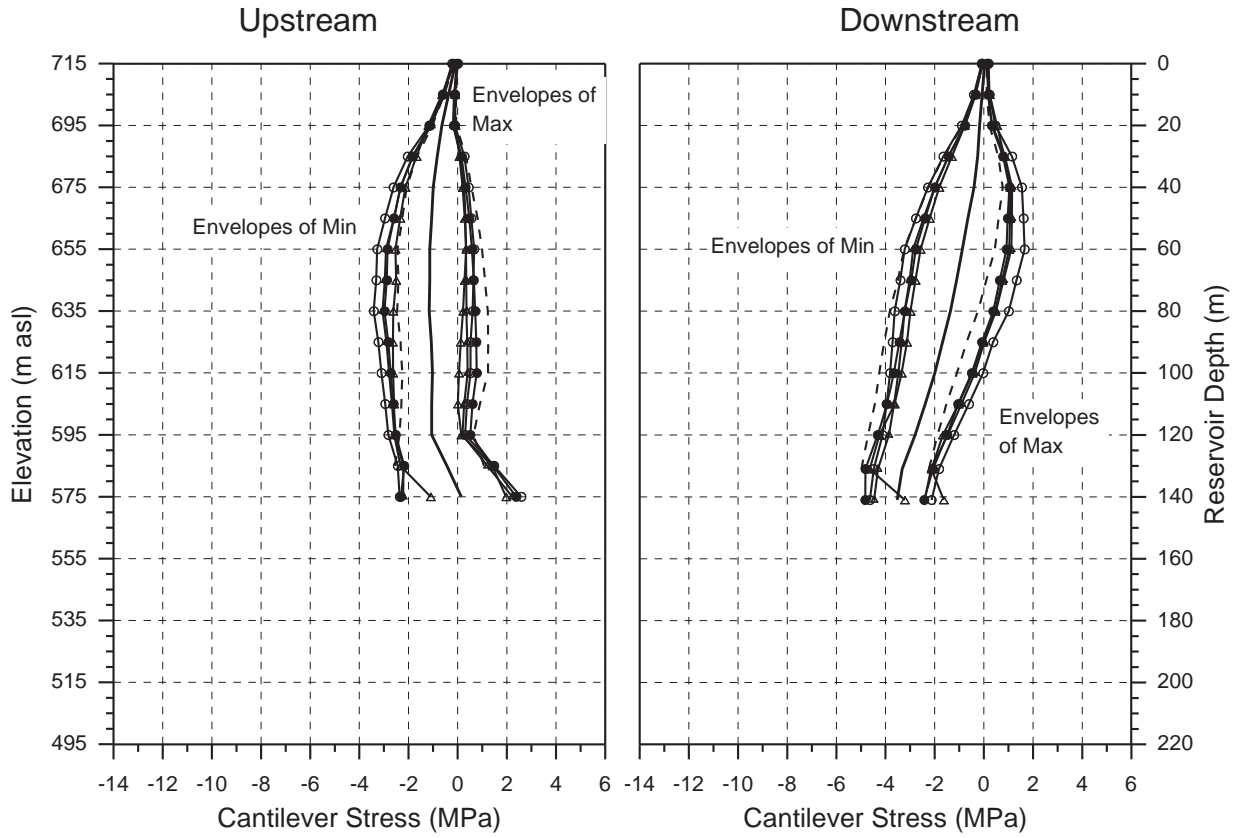
Figure 8: Right Section Cantilever Stresses

Minimum and Maximum Principal Stresses
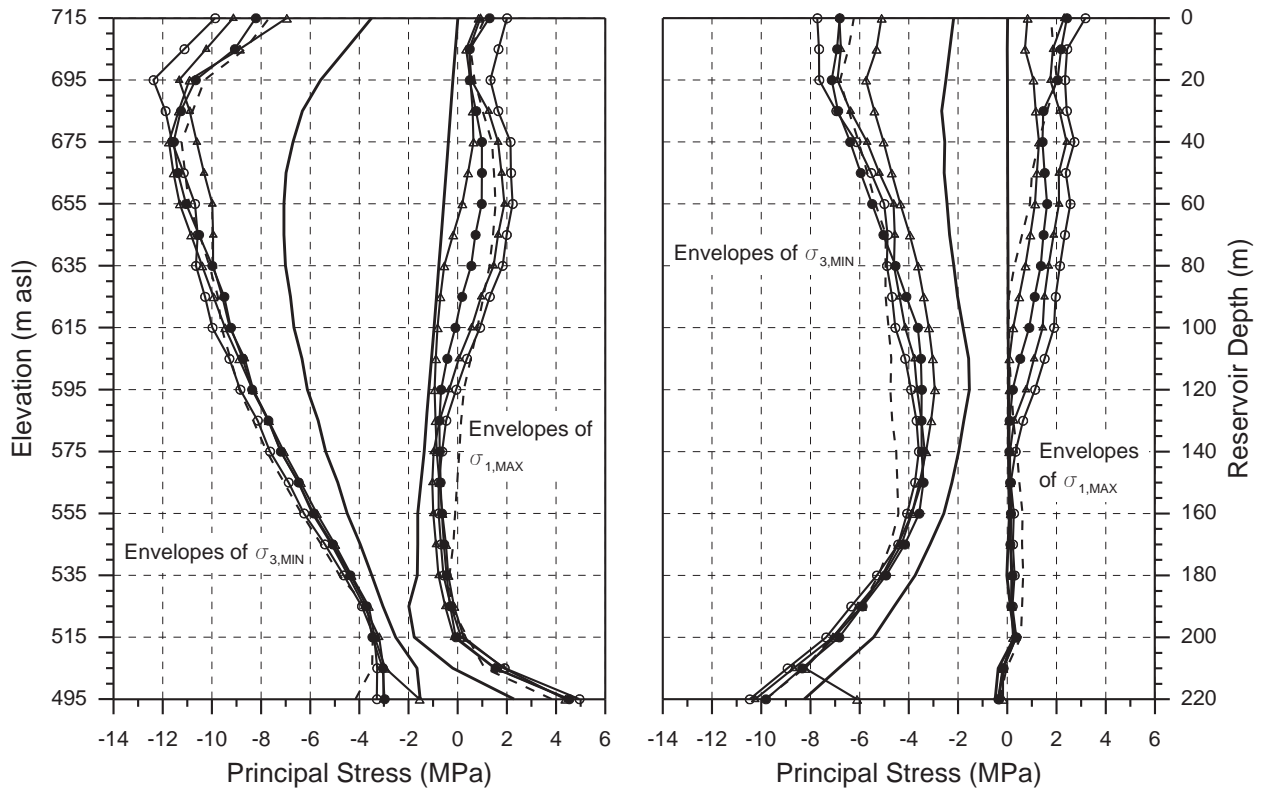
Figure 9: Main Section Minimum and Maximum Principal Stresses (U/S on left; D/S on right)
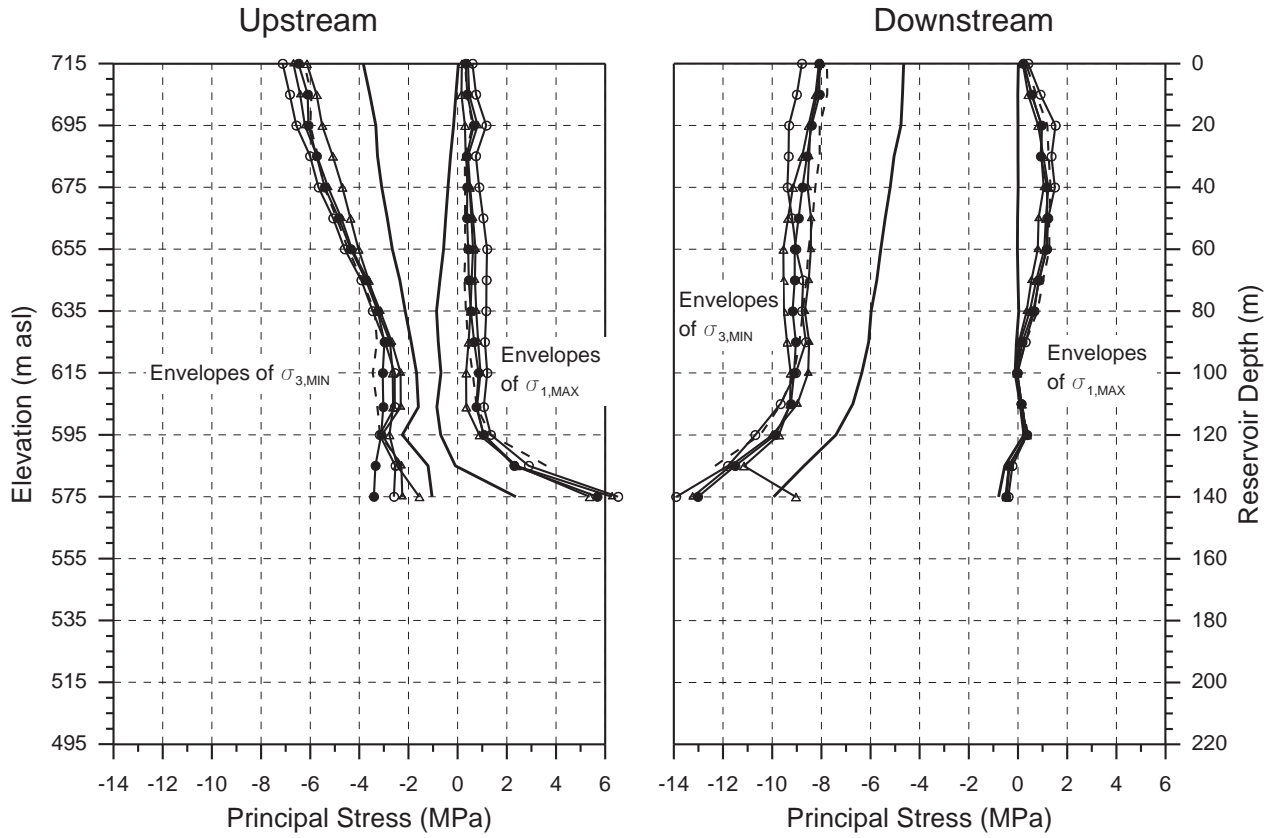
Figure 10: Left Section Minimum and Maximum Principal Stresses
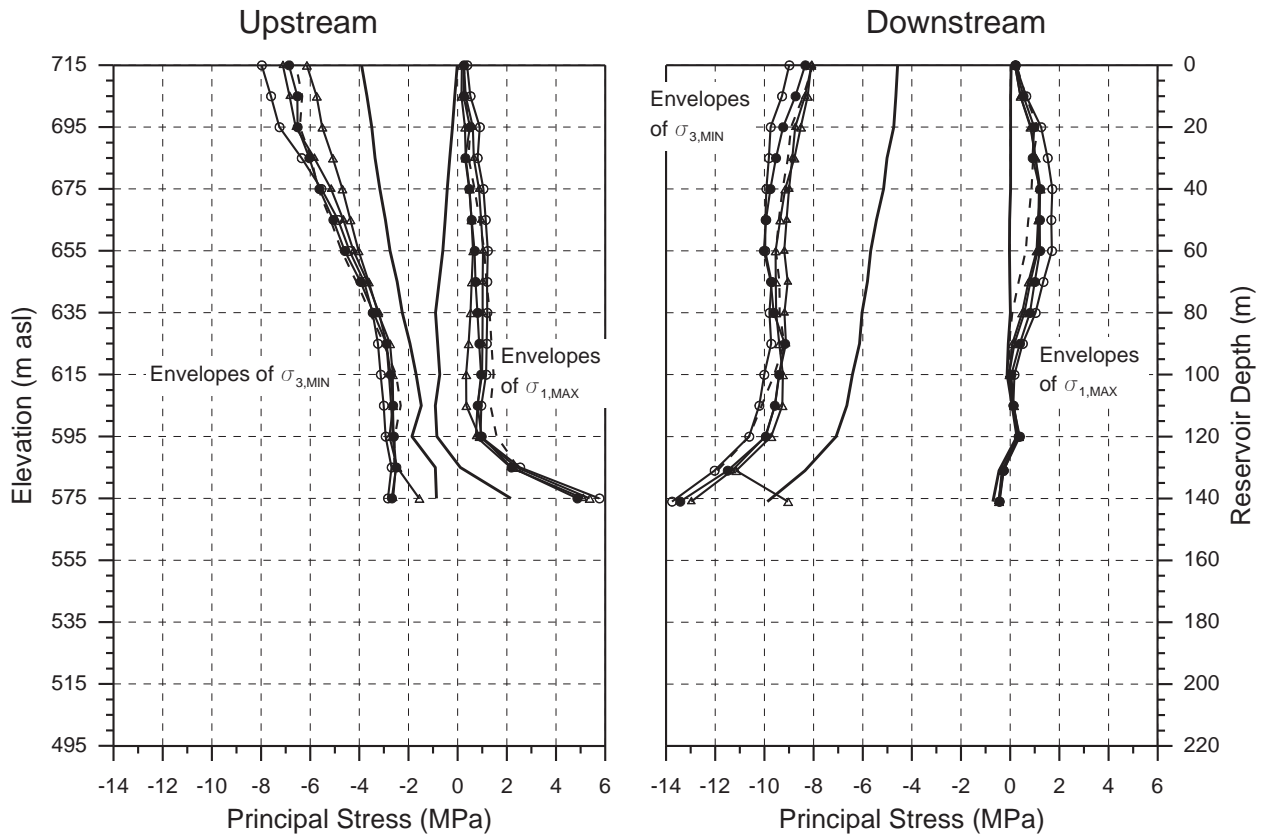
Figure 11: Right Section Minimum and Maximum Principal Stresses

Displacements
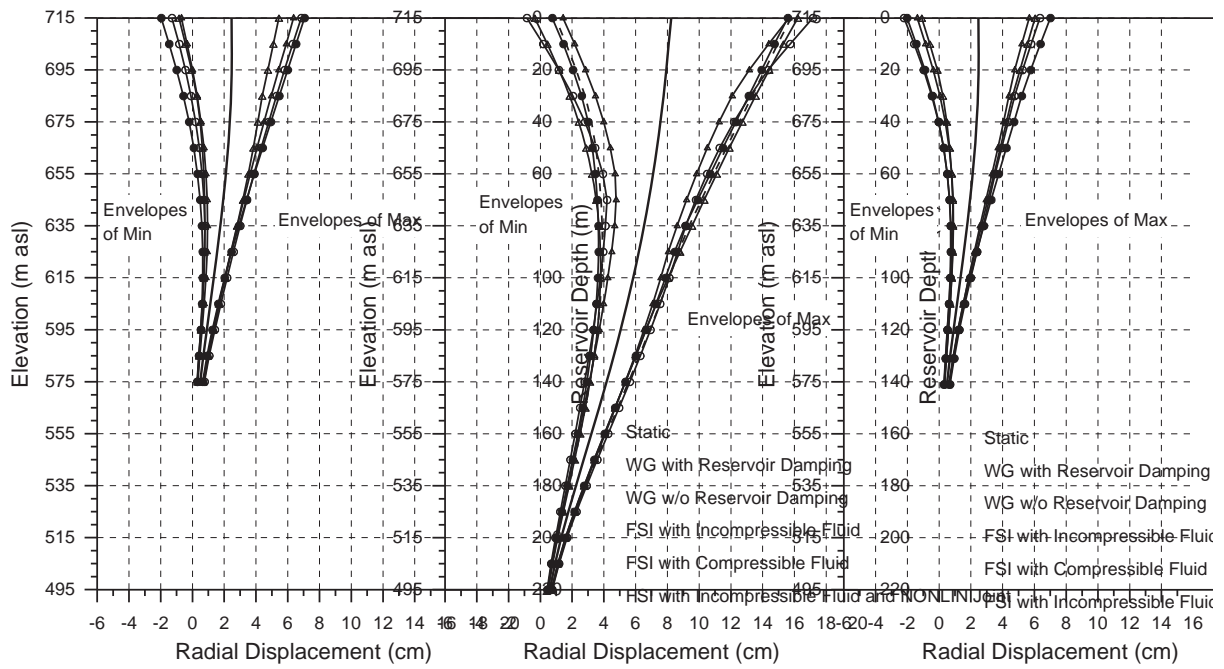
Figure 12: Radial Displacements (Left Section on left; Main Section, Right Section on right)
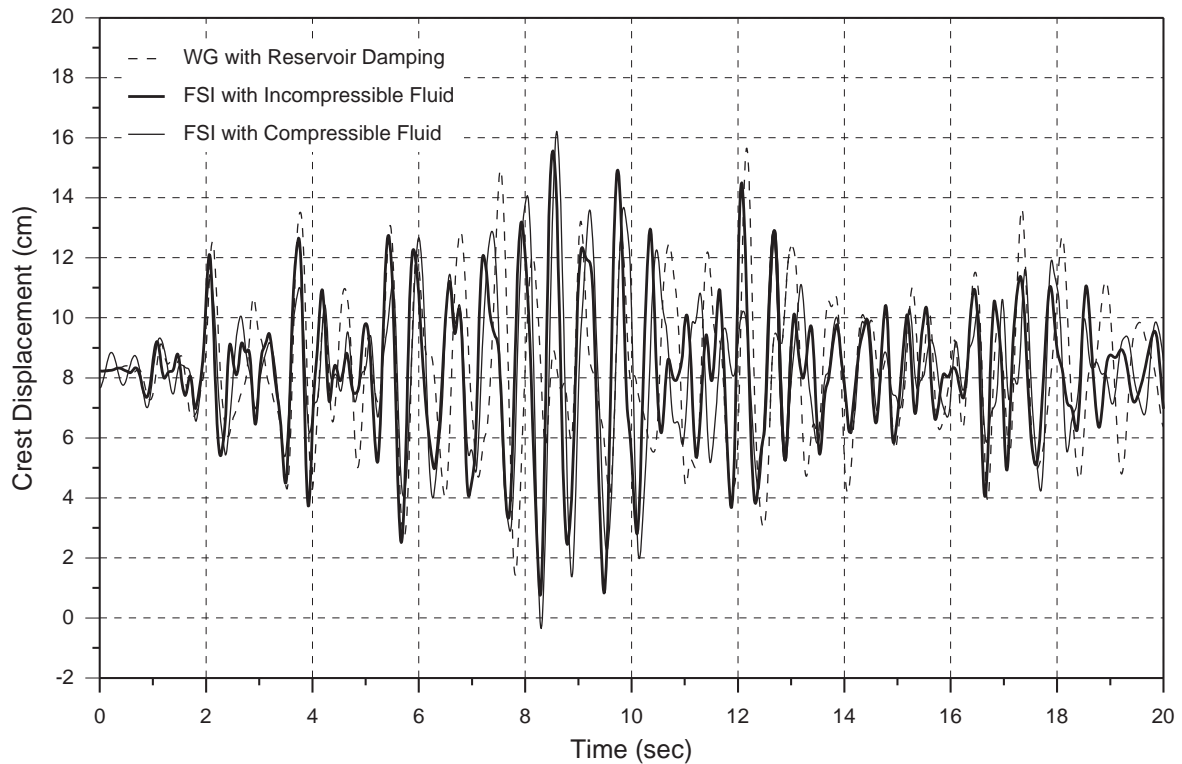
Figure 13: Time History of the Crown Displacement for Different Analyses

Discussion and Conclusion

The maximum static compressive stress is the hoop stress at ¾ the dam height on the u/s face of the main section. It amounts to approximately 7 MPa, which is within the admissible limits regarding the compressive strength of concrete. The maximum static radial displacement reaches 8.2 cm at the top of the central cantilever. The maximum compressive stresses during the ground motion reach approximately 12 MPa in the hoop direction on the u/s face. Seismic tensile hoop stresses varying between 1 MPa and 2 MPa are computed at the top part of u/s face of the main section; they disappear if the contraction joint opening/closing is modelled. The maximum seismic tensile vertical stresses exceed 2 MPA at ¾ the dam height on the upstream face of the main section. The maximum compressive and tensile stresses occurring during the earthquake are below the admissible limits. The maximum amplitude of the dynamic vibrations is about 8 cm with respect to the initial displaced shape of the dam.

The hydrodynamic effect modelling approaches investigated in the present study lead to similar results regarding the structural response of the example arch dam. In general, the Westergaard added masses approach yields higher compressive and tensile stresses, as well as higher radial displacements. The compressible fluid analysis results in lower stresses with respect to the incompressible fluid assumption, which is due to the increased damping of the coupled system. In fact, according to [11], if the natural dam frequencies are significantly lower than this of the dam reservoir, f_r, the behaviour of the latter is similar to the behaviour of incompressible fluid. In our case $f_r =1.98$ Hz; this explains to a certain extent the obtained differences in the results with compressible and incompressible fluid.

References

[1] Zienkiewicz, O.C., Taylor R.L. (2000). The Finite Element Method, Fifth edition, Vol. 1: The Basis, Butterworth-Heinemann, Oxford.

[2] Westergaard, H.W., (1933). Water pressures on dams during earthquakes. American Society of Civil Engineers (ASCE), Proceedings.

[3] Zangar, C.N., (1952). Hydrodynamic pressures on dam due to horizontal earthquake effects. Engineering Monograph No.11, U.S. Bureau of Reclamation.

[4] Tan, H., and Chopra, A.K., (1995). Earthquake analysis of arch dams including dam-water foundation rock interaction. Earthquake Eng. Struct. Dyn., 24(11), 1453–1474.

[5] Wang, J. T., and Chopra, A. K. (2010). Linear analysis of concrete arch dams including dam-water-foundation rock interaction considering spatially varying ground motions. Earthquake Eng. Struct. Dyn., 39(7), 731–750.

[6] Kuo, J. (1982). Added mass computations for incompressible fluid. Report UCB/EERC-82/09, Earthquake Engineering Research Center, University of California at Berkeley.

[7] Chavez, J.W., Fenves, J.L. (1993). Earthquake analysis and response of concrete gravity dams including base sliding. Report UCB/EERC-93/07, Earthquake Engineering Research Center, University of California at Berkeley.

[8] TNO DIANA (2013). DIANA User's Manual, Release 9.4.4. Delft, the Netherlands.

[9] Graz University of Technology, Institute of Hydraulic Engineering and Water Resources Management (2013). 12-th International Benchmark Workshop on Numerical Analysis of Dams, Theme A.

[10] Hughes, T. (1987). The Finite Element Method – Linear Static and Dynamic Finite Element Analysis. Prentice-Hall, Inc.

[11] Sécurité des ouvrages d'accumulation (2003). Documentation de base pour la vérification des ouvrages d'accumulation aux séismes, rapports de l'OFEG, série Eaux, version 1.2.

Dynamic Analysis of an Arch dam with Fluid-Structure Interaction
Use of an Open source code AKANTU

M. Chambart[1], T. Menouillard[1], N. Richart[2], J.-F. Molinari[2] and R. M. Gunn[1]

[1] STUCKY SA, Rue du Lac 33, CH-1020 Renens, SWITZERLAND
[2] EPFL ENAC LSMS, CH-1015 Lausanne, SWITZERLAND

E-mail: mchambart@stucky.ch, tmenouillard@stucky.ch

Abstract

In this contribution, the fluid-structure interaction is modeled using the added mass technique and the incompressible fluid model. Results show that the added mass technique is more conservative. Different meshes are compared with this later method, demonstrating that the problem is not mesh dependent. Finally, the computation times obtained with two different software are compared, showing the efficiency of the new open-source software Akantu

Introduction

One of the exercises proposed by the ICOLD for 12TH INTERNATIONAL BENCHMARK WORKSHOP ON NUMERICAL ANALYSIS OF DAMS consists in the dynamic analysis of an arch dam under a seismic loading. Since the geometry, the material properties and the loading are imposed to the participants, the focus is put on another modelling aspect which is the fluid-structure interaction. The methods proposed to model the fluid-structure interaction starts with the simplest ones, the added mass technique to the most sophisticated ones where the fluid is explicitly modeled as a compressible body. In our practice, as an engineering company, our choice for one method versus another is often governed by the gain in accuracy versus the loss in time. Most of the time in projects, the added mass approach is used because it is the fastest and usually sufficient to fulfill the authorities demands.

This benchmark is an interesting opportunity to compare different methods in terms of results but also in terms of computation time. The comparison is carried out using the finite element software DIANA [1], simply using some of the proposed methods (added mass and incompressible fluid). As a second step, the results obtained with DIANA using the added mass technique are compared with the ones given by a new open-source software AKANTU [2] developed at the Swiss Ecole Polytechnique Fédérale de Lausanne. Akantu is a quite innovative object-oriented program written in C++. The objective using this latter software is to optimize the computation time, in order to get reliable results in shorten time, or run sophisticated computations in an acceptable amount of time. In order to estimate the mesh dependency of the problem, the results with two meshes are compared with the added mass technique. Therefore the need in future for High Performance Computing can be assessed.

Numerical Modelling

Model and Mesh

Figure 1 presents different meshes used with the Westergaard theory for dealing with the hydrodynamic pressure, and also the mesh with the fluid. There are a coarse and a fine mesh, whose numbers of elements are respectively 2874 and 22280.
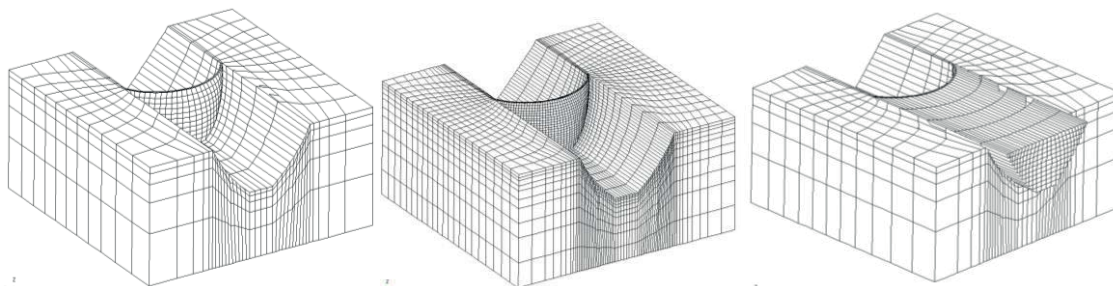
Figure 1: View of the meshes: coarse and fine, and with the fluid.

Materials

In this problem, three different materials are involved: the concrete of the dam, the rock of the foundation, and the water of the reservoir. Their density and stiffness are the valuable data in linear elastic problem. Table 1 presents the materials parameters. The density of the rock is numerically taken to be zero in order to avoid wave propagation at the boundary of the rock foundation. In addition, a dynamic Young's modulus is used, whose value is 125% the static one [4].

Table 1: Materials properties.

Properties	Concrete	Rock	Water
Density	2400 kg/m3	0 kg/m3	1000 kg/m3
Poisson ratio	0.167	0.2	
Young's modulus	27 GPa	25 GPa	

Loadings

Static loadings.

The self-weight of the concrete is given by the density of the concrete and the gravity.

The hydrostatic pressure on the upstream face of the dam is given by the water level, i.e. 715 m asl.

Dynamics loadings.

The acceleration history of the seismic input is given through three accelerograms presented in Figure 2, and these three accelerograms are simultaneously applied at the boundary of the rock foundation. Their corresponding absolute displacement histories are also presented in Figure 2. Depending on the FEM program used, the boundary conditions may have to be given in displacement or in acceleration.
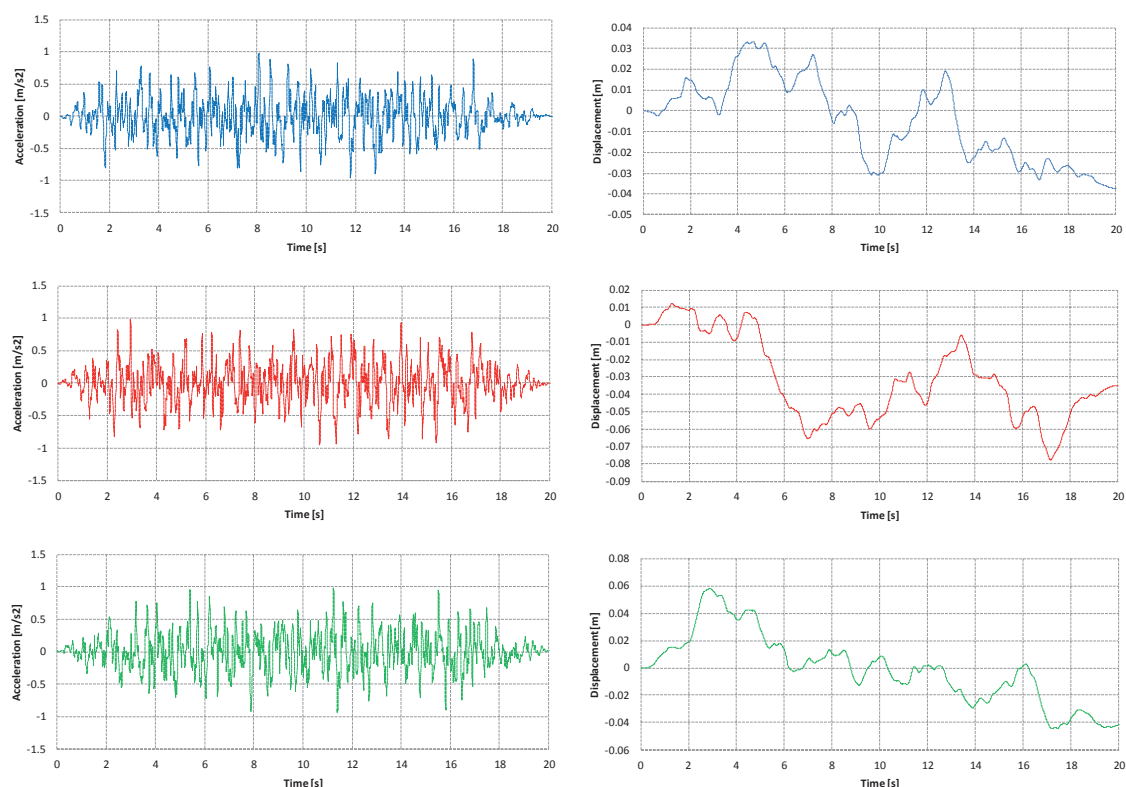
Figure 2: Acceleration and displacement time histories.

Fluid-structure interaction

Two alternatives are explored in this section. First, the most basic development to deal with hydrodynamic pressure on a surface is the method developed by Westergaard [1]; it takes the hydrodynamic effect into account by adding masses on the upstream surface of the structure. There is no need to mesh the fluid, thus the size of the system is restricted to the size of the solids. The added mass is defined according to [1] as:

$$m_w(h) = \frac{7}{8} \rho_w h_w \sqrt{1 - \frac{h}{h_w}}$$

(1)

Where ρ_w is the density of the water, h_w the total height of water and h the distance from the bottom of the reservoir to the current point where m_w is evaluated. Figure 3 illustrates the Westergaard equation.
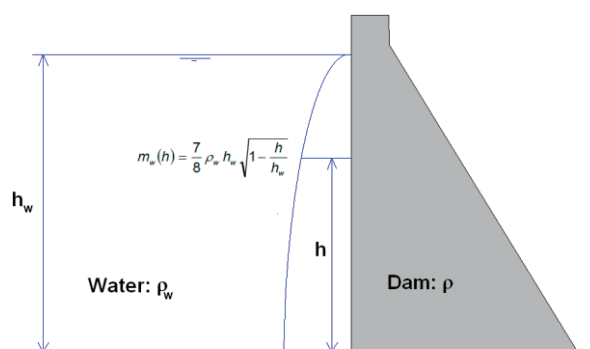
Figure 3: Westergaard theory on the upstream face of a dam.

Second, a method [3] where the fluid, considered incompressible, is explicitly meshed as a 3D part of the system is also considered. Solid elements are quadratic, whereas fluid elements are only linear. Therefore special interface elements are required on the upstream face of the dam

to link the fluid to the solid domains. In addition, special boundary elements are involved to deal with the bottom absorption, the free surface and the far field surface of the reservoir. A method dealing with compressible fluid is not developed in this paper.

Vibration modes

The vibration modes have been evaluated with different meshes and the Westergaard method for describing the hydrodynamic pressure. A very good agreement between the results of the different meshes was observed. The reason is that the linear elastic material model describes similar dynamic behavior of the structure, not depending on the mesh size. Figure 4 presents the deformed shape of the first 10 modes within the coarse mesh.
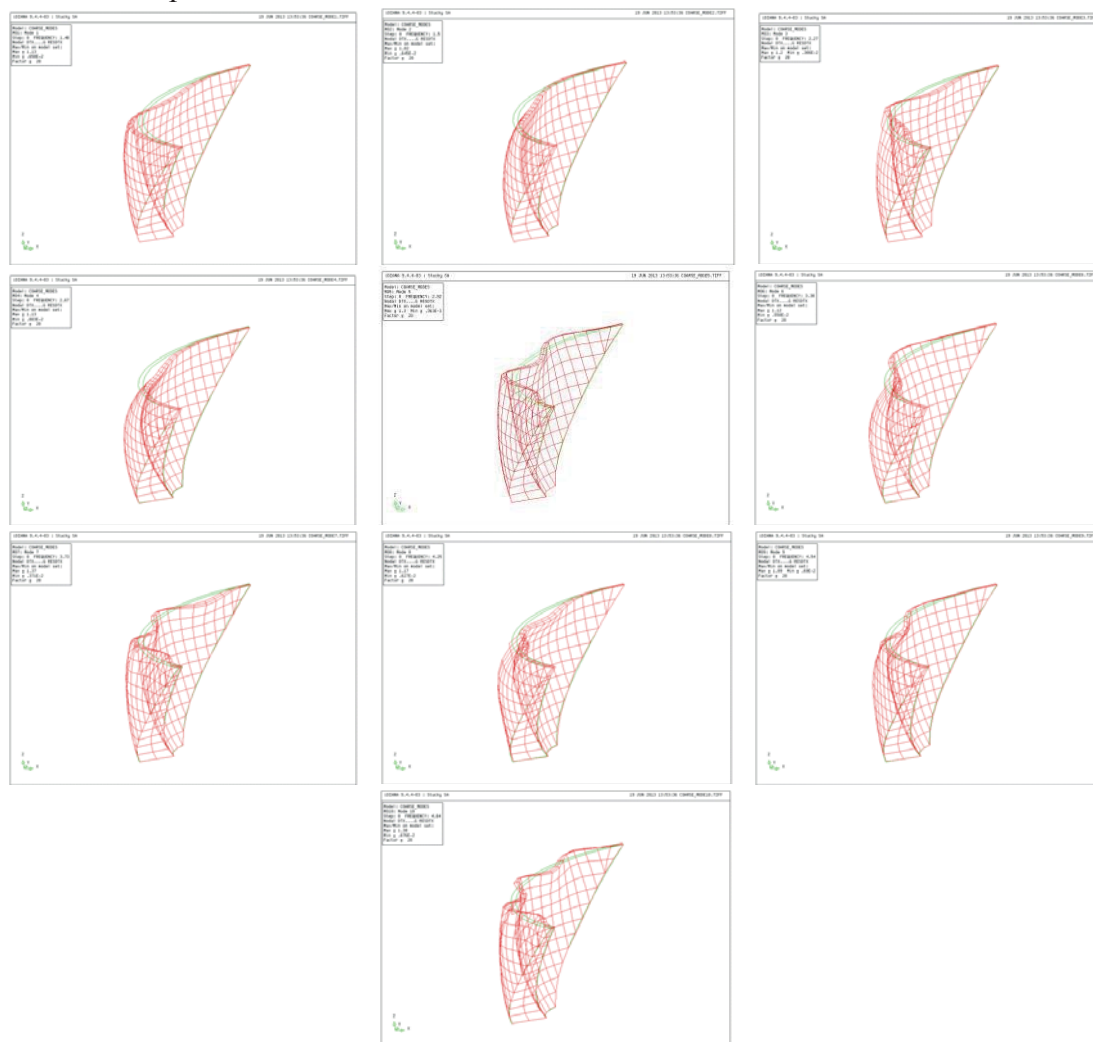
Figure 4: Deformed shapes of the first 10 vibrations modes.

Table 2 presents the vibration frequencies and the mass percentage of the dam in each direction obtained with the coarse mesh and Westergaard theory. Mode 1 is a left-right motion with 20% of the mass of the dam. Mode 2 is the major vibration with 35% of the mass in the upstream-downstream direction.

Table 2: Frequencies and mass percentage for the coarse mesh with Westergaard.

Mode	Frequency [Hz]	Mass percentage US/DS	Mass percentage Vertical	Mass percentage Left-Right
1	1.48	1%	0%	20%

2	1.50	**35%**	1%	0%
3	2.27	**15%**	0%	0%
4	2.67	**20%**	3%	0%
5	2.92	0%	0%	6%
6	3.38	0%	0%	**15%**
7	3.73	1%	0%	0%
8	4.25	2%	1%	0%
9	4.54	9%	6%	0%
10	4.64	0%	0%	3%

A damping effect of 5% is taken through Rayleigh coefficients. They are evaluated from the knowledge of two modes (1 and 13) containing 80% of total mass. The Rayleigh damping matrix C is defined by two parameters α and β as:

$$C = \alpha\, M + \beta\, K \qquad (2)$$

where M is the mass matrix, K the stiffness.

With the selected modes (1 to 13), the coefficients are: α=0.726286 and β=0.002346. Figure 5 shows the damping as a function of the frequency; the crosses on the graphs are the different vibration modes, and the damping of frequencies 1 and 13 are exactly 5%. As it has been selected, 80% of the mass of the dam has a damping between 4 and 5%. The modes with high frequency, i.e. greater than 10 Hz, are minor modes in terms of mass percentage.
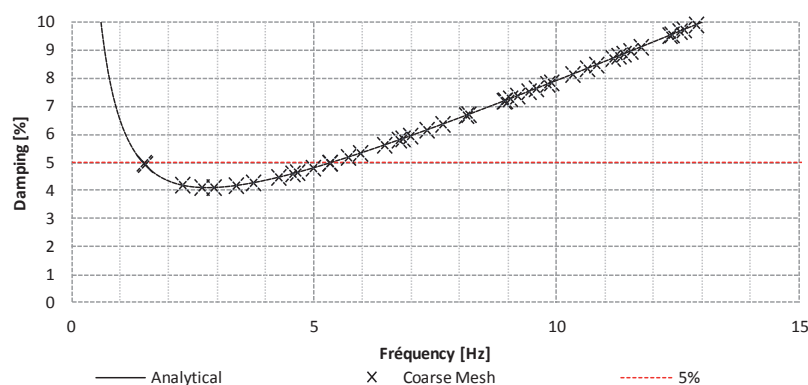
Figure 5: Rayleigh Damping as a function of the frequency, with the Westergaard theory.

Results

Table 3 presents the different computations run and the corresponding mesh size. With DIANA, two simulations with Westergaard and one with the fluid were run, whereas only two simulations were run with AKANTU. All simulation had 2000 steps for the dynamics.

Table 3: Table of the different computations run with the two codes.

	DIANA			**AKANTU**	
	Westergaard		With Fluid	Westergaard	
Mesh	Coarse	Fine	Coarse	Coarse	Fine
Nodes	3614	25057	14478	3614	25057
Elements	2874	22280	3632	2874	22280
Elapsed time	1h10	7h00	4h00	0h13	5h40
CPU time [s]	13'291 s	40'752 s	34'841 s	2'819 s	74'000 s

The computations are run for both codes in parallel with the same number of processors available. However for Akantu the computation is performed on a powerful laptop while for Diana a workstation optimized to numerical simulations is used. The results show that Akantu

is more efficient since the computation time is divided by 5 for the coarse mesh and by 1.25 with the fine mesh.

The evaluation of the hoop, vertical stresses and radial displacement are performed on the three following sections denoted by Left, Mid and Right sections as shown in Figure 6.
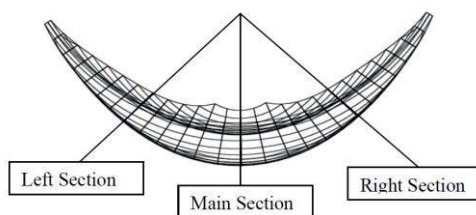
Figure 6: View of the different sections for post-processing the results.

Vertical stresses

The vertical stress is a relevant result within the dam. Thus Figure 7 presents the vertical stress on the upstream and downstream faces of the Left section of the dam: static, maximum and minimum results are presented with the coarse and fine mesh and the Westergaard theory, with Diana and Akantu. Both meshes give similar results too for static, maximum and minimum vertical stresses. The vertical stress is always negative in static, but its maximum reaches positive value in some parts during the earthquake.

All four results obtained with the Westergaard theory agree well. However the stress envelops obtained with the most sophisticated computation, i.e. incompressible meshed fluid, is quite smaller. The Westergaard theory seems conservative.
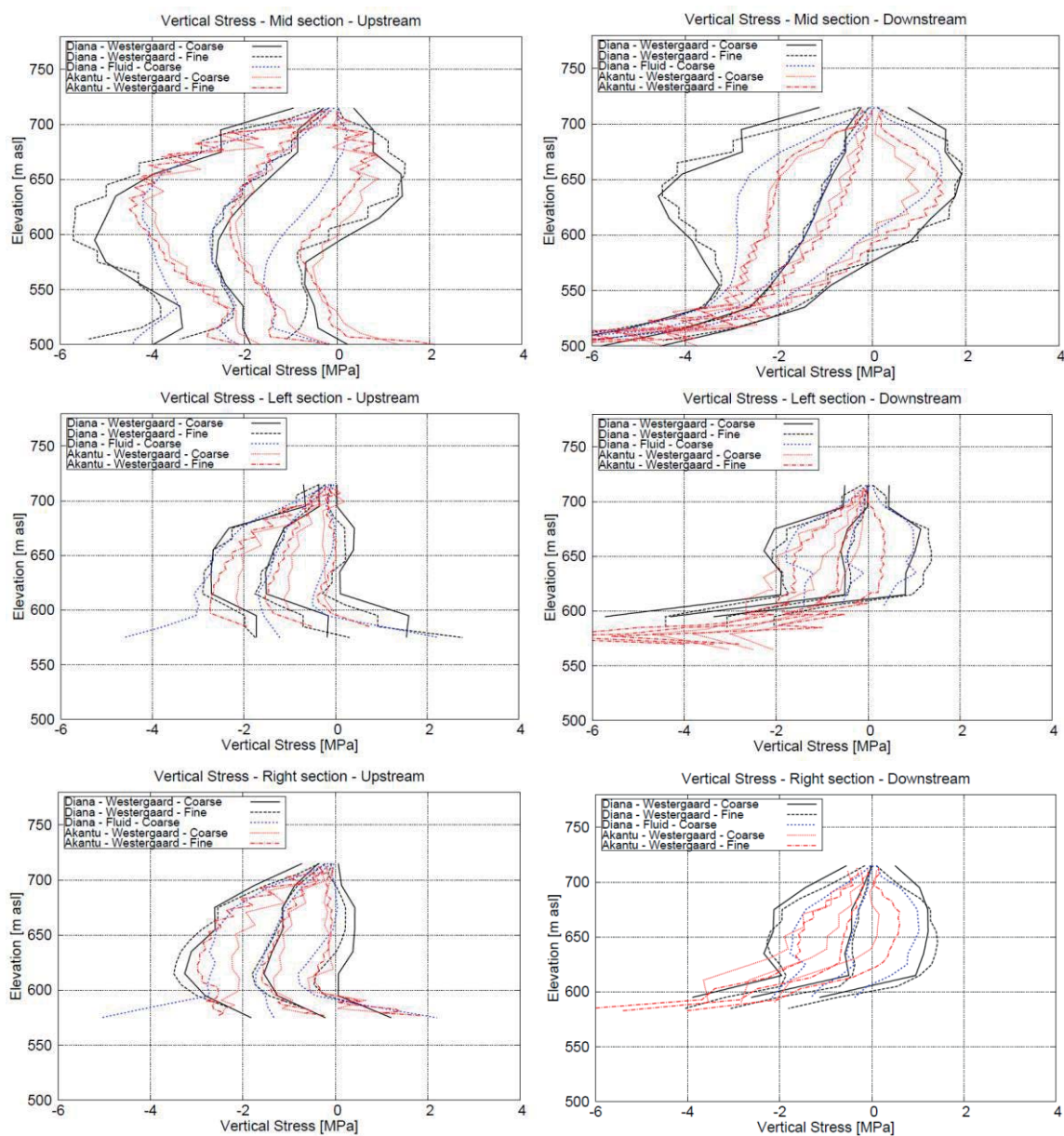
Figure 7: Vertical stresses in the different sections.

Hoop stresses

The hoop stress is the other relevant results in terms of stress in an arch dam. Figure 8 presents the hoop stress at the different sections on the upstream and downstream faces of the dam: static, minimum and maximum stresses are presented for the different computations. There is a good agreement between the results obtained by both meshes and the Westergaard theory. One observes that the hoop during the earthquake is mainly negative, so the arch dam is in compressive stress state in static and also during the earthquake.
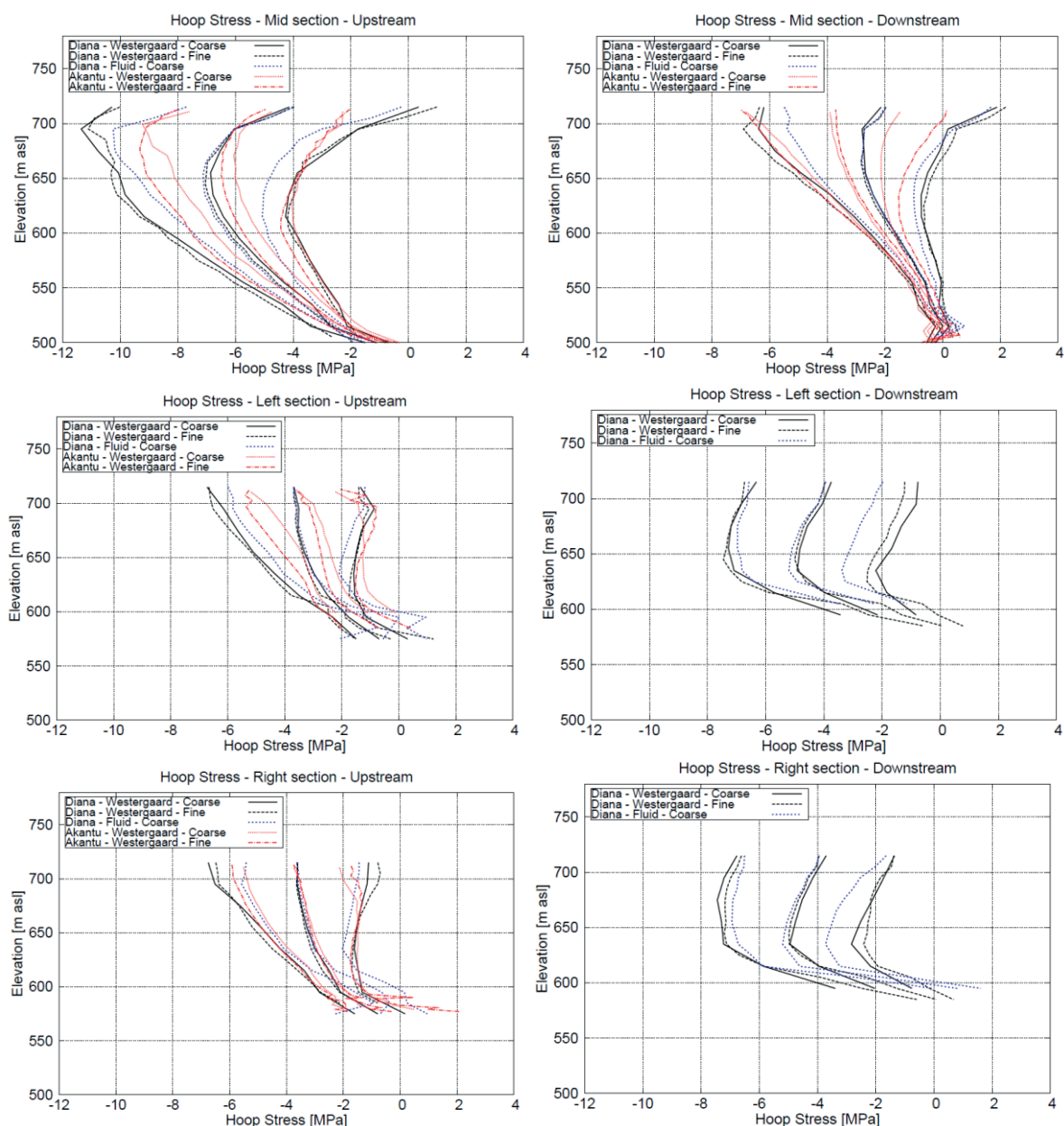
Figure 8: Hoop stresses in the different sections.

Principal maximum stresses

Figure 9 presents the maximum principal stress at the different sections on the upstream and downstream faces of the dam: static, minimum and maximum stresses are presented for the different computations. There is a good agreement between the results obtained by both meshes and the Westergaard theory. One observes that the minimum of the maximum principal stress during the earthquake is close to the static maximum principal stress. Indeed the maximum principal stress can only increase due to the dynamic loading from the static case. This maximum principal stress behaves like the vertical stress in the arch dam during dynamics.
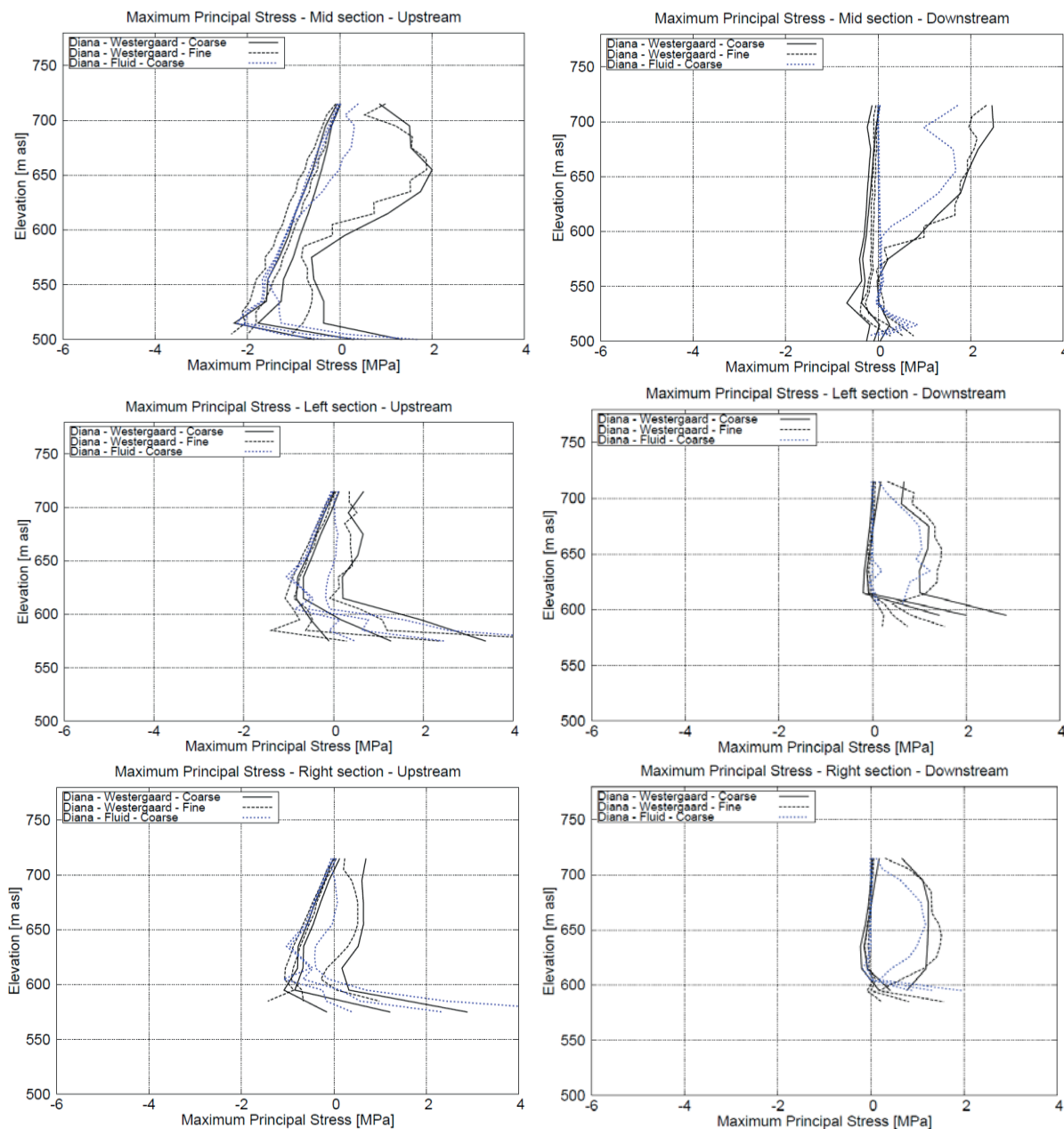
Figure 9: Principal maximum stresses in the different sections.

Principal minimum stresses

Figure 10 presents the minimum principal stress at the different sections on the upstream and downstream faces of the dam: static, minimum and maximum stresses are presented for the different computations. There is a good agreement between the results obtained by both meshes and the Westergaard theory. This minimum principal stress behaves like the hoop stress in the arch dam during dynamics.
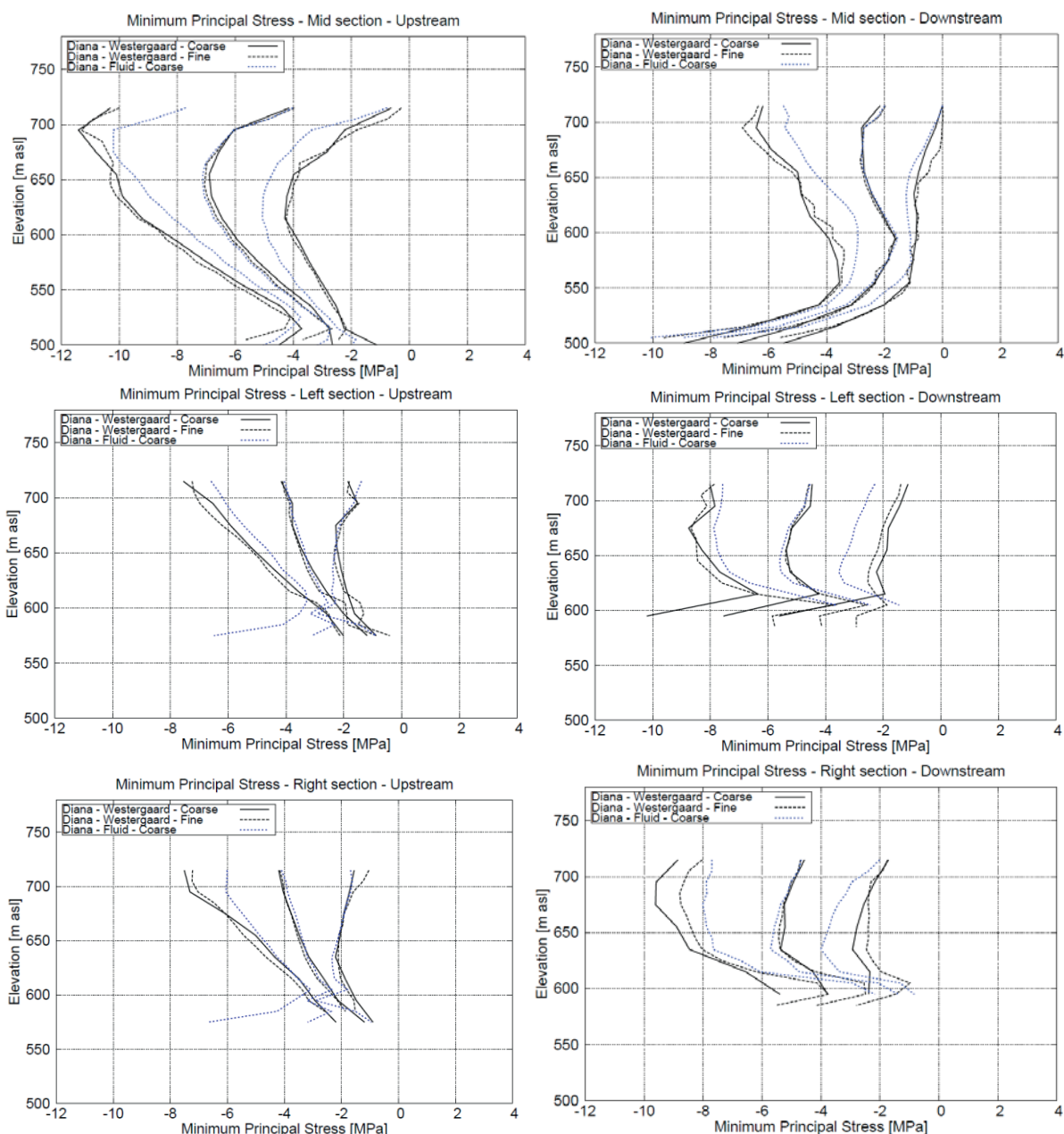
Figure 10: Principal minimum stresses in the different sections.

Radial displacements

The radial displacement quantifies the motion of the dam, in static and during the Earthquake. Figure 11 presents the radial displacement of the different sections: static, minimum and maximum obtained with the coarse and fine mesh and the Westergaard theory with both software and also the displacement obtained with the incompressible fluid. There is a good agreement between these two results in static and in dynamic. The static radial displacement at the top of the Mid section is about 8 cm, whereas the maximum during the Earthquake is about 16 cm, and the minimum about 3 cm.
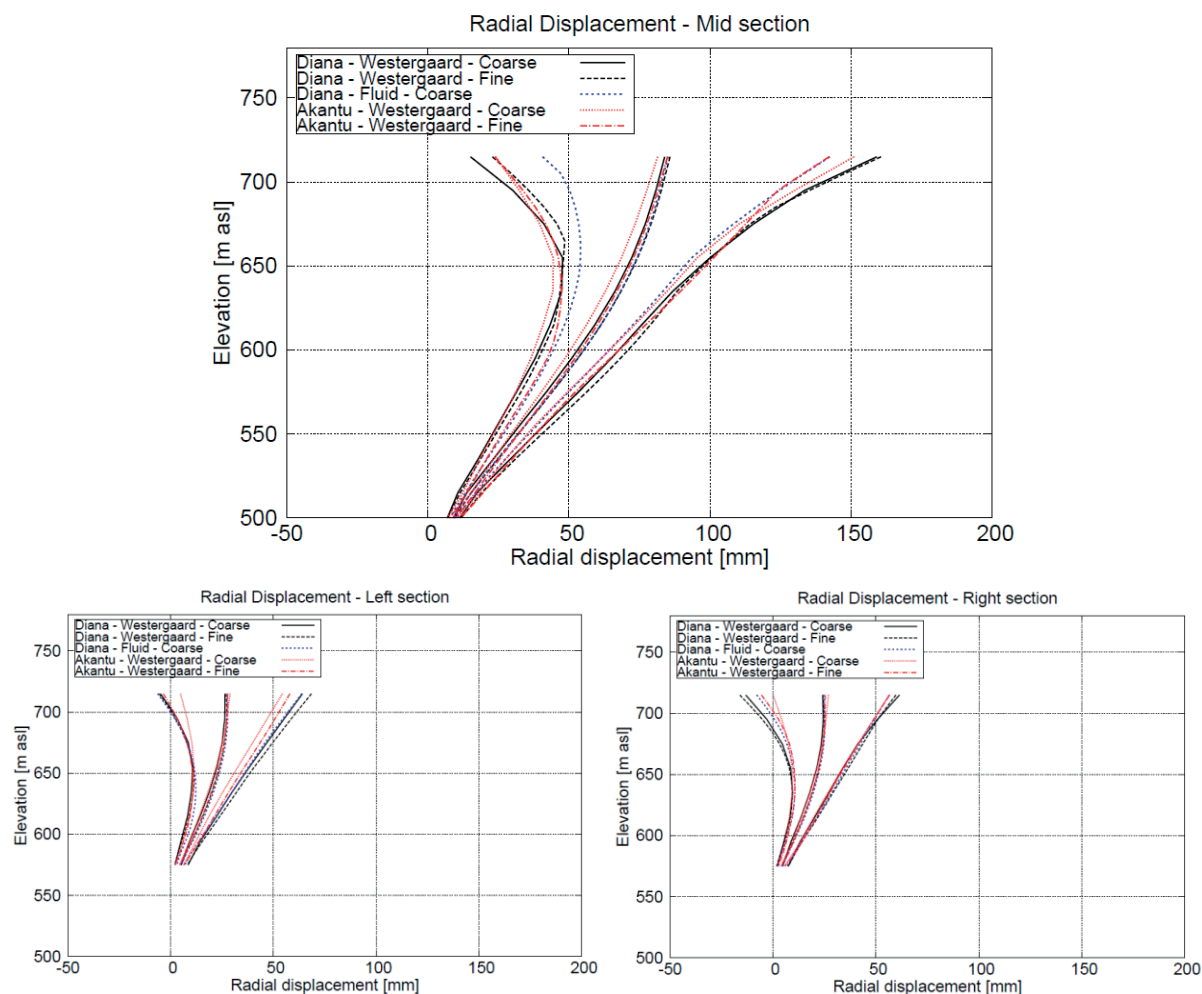
Figure 11: Radial displacements.

Conclusion

This benchmark allowed to investigate the field of how, in term of numerical method, to deal with the hydrodynamic pressure on the upstream face of an arch dam. This has then shown that the Westergaard theory, which consists in simply adding mass on nodes of the upstream face of the dam, is clearly not mesh dependent. Second, the method dealing with the mesh of the incompressible fluid, gives smaller envelops in terms of maximum and minimum of displacement and stresses of the arch dam. In addition, the development of the Westergaard theory in an open source code did not show any relevant difficulties and the computation time can be significantly decreased.

References

[1] Water pressures on Dams during Earthquakes, H.M. Westergaard, Transactions, ASCE 98:418-472, 1933.
[2] Fluid-Structure Interactions: added mass computations for incompressible fluid, James Shaw-Haw Kuo, University of California, Berkeley, August 1982.
[3] Hybrid Frequency Time Domain – Validation, TNO DIANA Report, 2008-DIANA-R003, 2010.
[4] Sécurité des ouvrages d'accumulation – Documentation de base pour la verification des ouvrages d'accumulation aux séismes, rapports de l'OFEG, série Eaux, version 1.2, mars 2003.

Study on Arch Dam– Reservoir Seismic Interaction

A. Popovici[1], C. Ilinca[1] and R. Vârvorea[1]

[1] Technical University of Civil Engineering, 124 Lacul Tei Bd. 020396-Bucharest, ROMANIA

E-mail: popovici@utcb.ro

Abstract

The arch dam – reservoir seismic interaction is investigated using ABAQUS 6.11 and DESARC 3.1 software. DESARC computer code offers the advantage of simplicity and computation speed due to the degrees of freedom based on the stresses (Ritter modified method) being very recommended for arch dams preliminary structural analysis.

The coarse mesh given by formulator was used for investigation in ABAQUS and 12 arches equally spaced on dam height were used in DESARC. The water effect was considered according to added mass procedure as well as acoustic elements. All analyses were performed in the linear elastic field.

The results are presented in compliance with formulator requests: eigenfrequencies and mode shapes, hoop stresses, vertical stresses, min./max. principal stresses and radial displacements in three different sections for static and seismic loads. A special attention is paid to compare the results concerning arch dam – reservoir seismic interaction in different hypotheses applying two software.

Introduction

The effects of different hypotheses on arch dam - reservoir seismic interaction are investigated in this paper based on data provided in Theme A by formulator, Graz University of Technology – Institute of Hydraulic Engineering and Water Resources Management [1].

The arch dam is a symmetrical structure with the followings main characteristics:

- maximum height   220 m
- chord length at dam's crest   430 m
- valley width at bottom   80 m

The analyses are carried out using ABAQUS 6.11 [2] and DESARC 3.1 [3],[4] software.

The finite element mesh of the arch dam structure-foundation-reservoir system used in ABAQUS corresponds with alternative coarse mesh given by formulator (Figure 1). The main features of the coarse mesh are as follows:

- arch dam – total number of nodes   2083
- total number of elements   356 (312 C3D20R and 44 C3D15)
- foundation – total number of nodes   11608
- total number of elements   2340 C3D20R
- reservoir – total number of nodes   12493
- total number of elements   2640 C3D20R
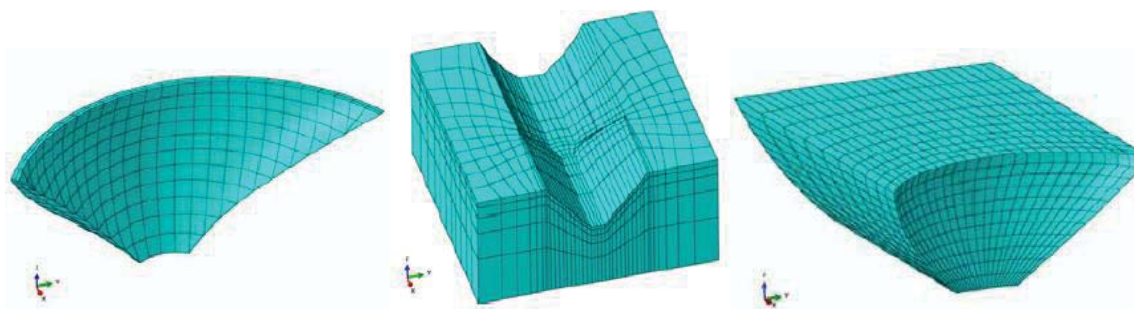
Figure 1: Finite element mesh of the arch dam structure-foundation-reservoir system used in ABAQUS code

Other hypotheses used in analyses performed with ABAQUS were the followings:
- the dead weight were applied on monolithic structure
- the reservoir influence on dam seismic response was considered by added mass procedure excepting the free vibration analysis for full reservoir using acoustic elements C3D20A for reservoir mesh;
- the water was considered as incompressible with shear modulus tends to zero;
- the seismic response was evaluated for empty and full reservoir by modal superposition and direct time integration;
- all analyses were based on assumption of linear elastic behavior of materials;
- three accelerograms in direct time integration were applied on the faces of foundation, respectively x, y and z directions;
- the fraction of critical damping in direct time integration was 5%, α and β coefficients in linear Rayleigh model were computed for ω_1 and ω_2 , resulting α=0.3900 and β=0.0064.

DESARC is an interactive, fast and reliable computer code very recommended for preliminary fast static and dynamic structural analysis of arch dams. The simplicity and computation speed of DESARC is due to the degrees of freedom based on the stresses (Ritter modified method and not on displacements. The program can handle symmetric arch dams both with circular and parabolic midline, rotationally symmetric structure with liquid inside or outside, cooling towers etc.

All the geometrical parameters (thickness, radii, half lengths and cantilever shape) are expressed under assumption of parabolic variation with elevation. Accordingly the real arch dam shape provided by formulator was equated as assumptions presented above (Figure 2)
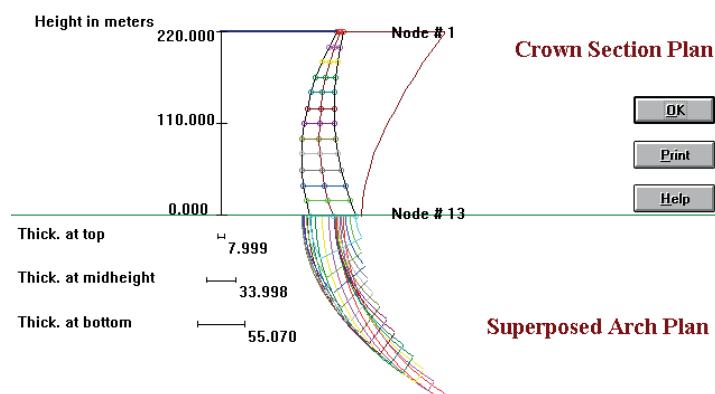
Figure 2: Equating real dam shape under assumptions of DESARC

A number of 12 arches of the dam was considered under analysis (Figure 3). In may be remark from figures 2 and 3, resulting structure under DESARC assumptions has the shape very close to the actual dam.

Height				Number of Arches		
H	(meters)	220.000		n	(non dim.)	12

Thickness				Radii		
$\lambda\,0$	(non dim.)	0.03636		R 0	(non dim.)	1.141
$\lambda\,1$	(non dim.)	0.29496		R 1	(non dim.)	-0.707
$\lambda\,2$	(non dim.)	-0.081		R 2	(non dim.)	-0.0529

Midline				Halflength		
$\eta\,0$	(non dim.)	0.256		S 0	(meters)	258.620
$\eta\,1$	(non dim.)	-0.415		S 1	(meters)	-173.580
$\eta\,2$	(non dim.)	0.374		S 2	(meters)	-43.940

Figure 3: Geometrical features of the arch dam equated under DESARC assumptions

Other hypotheses used in analyses performed with DESARC were the followings:
- the dam-foundation interaction was considered by Vogt coefficients (Er/ Ec=0.90, Er=25000 MPa and Ec=27000 Mpa);
- the reservoir influence on dam seismic response was considered by added mass procedure; the hydrodynamic pressures collinear with the direction of horizontal upstream – downstream earthquake (Phd,0) were evaluated with Westergaard relationship. For other directions (Phd,α) was applied the following relation:

$$P_{hd,\alpha} = P_{hd,0} \cdot \cos \alpha \tag{1}$$

α being the angle between earthquake direction and the normal to the surface at the point considered;
- the dead weight were applied on isolated cantilevers and monolithic structure, too.

Some aspects concerning mathematical models

The effect of the water in the reservoir, under the assumption of an incompressible ideal fluid, is usually calculated by use of the added mass procedure. This is a mathematical artifice used in order to simplify the analysis of the structure-liquid seismic interaction. The added mass is determined from the hydrodynamic forces $\{P_h(t)\}$ and is attached to the mass of the structure. Unlike the dead mass of a structure, the added mass acts only on hydrodynamic force direction, namely the direction of the normal to the surface it is applied. Assuming that the directions of hydrodynamic forces, of earthquake and of degrees of freedom of the structure are similar (Figure 4a), the added mass matrix $[M_h]$ is determined with relation:

$$\{P_h(t)\} = -[M_h] \cdot \{\ddot{u} + \ddot{\delta}_r\}_n \tag{2}$$

where $\{\ddot{u} + \ddot{\delta}_r\}_n$ is total acceleration response to normal direction at surface in the considered point.

In this case the analysis of the structure-liquid seismic interaction is performed as for usual structure according to formula:

$$[M + M_h] \cdot \{\ddot{\delta}_r\} + [C] \cdot \{\dot{\delta}_r\} + [K] \cdot \{\delta_r\} = [M + M_h] \cdot \{^1/_0\} \cdot \ddot{u} \tag{3}$$

In the general case when the directions of the normal to surface, of the earthquake and of the structure degrees of freedom are different, the added masses computed according to *(2)* relationship must be projected successively on the normal to surface direction and on the degrees of freedom of the structure (Figure 4b).

$$e_1 = \cos(n,c)\cos(n,x)$$
$$e_2 = \cos(n,c)\cos(n,y)$$
$$e_3 = \cos(n,c)\cos(n,z)$$
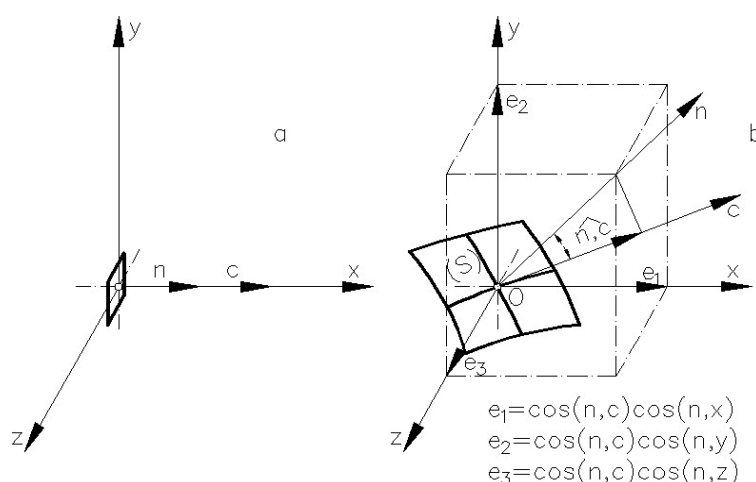
Figure 4: Assessment of added masses

The dynamic equilibrium equations which include the structure-liquid seismic interaction are written in this general case as follows:

$$[M + M_h] \cdot [r_{c,n}] \cdot [r_{n,x,y,z}] \cdot \{\ddot{\delta}_r\} + [C] \cdot \{\dot{\delta}_r\} + [K] \cdot \{\delta_r\} =$$
$$-[M + M_h] \cdot [r_{c,n}] \cdot [r_{n,x,y,z}] \cdot \{r\} \cdot \ddot{u} \tag{4}$$

where *[r_{c,n}]* has dimensions equal with the number of the degrees of freedom of the system and contains on diagonal the cosine directors between the normal to surface in the nodes of the system mesh and earthquake direction

and *[r_{n,x,y,z}]* has dimensions corresponding to the number of the degrees of freedom of the system and contains on diagonal the cosine directors between the normal to surface in the nodes of the system mesh and directions of the dynamic degrees of freedom of the system.

Results of analyses

The results are provided as requested by the formulator.

In the Table 1 are presented the natural circular frequencies (ω, rad/s) and respectively natural frequencies (f, cycles/s) values of the first 10 mode shapes including interaction with the reservoir modeled with acoustic elements C3D20A and added mass procedure computed with ABAQUS and the value of the frequency of the fundamental mode shape including interaction with the reservoir by added masses computed with DESARC. It may remark that natural frequencies computed with ABAQUS by added mass procedure are smaller with about 2…21 % relative to their counterparts having reservoir interaction modeled with acoustic elements. In figure 5 is illustrated the fundamental mode shape of the arch dam in hypothesis of the full reservoir with water elevation at the dam crest.

Table 1: Eigenfrequencies

ABAQUS					DESARC	
Eigenfrequency-acoustic elements			Eigenfrequency-added mass			
Mode no.	(Rad/s)	(Hz)	(Rad/s)	(Hz)	(Rad/s)	(Hz)
1	9.726	1.548	7.756	1.235	10.557	1.681
2	9.843	1.567	7.837	1.248		
3	12.160	1.935	12.139	1.933		
4	14.458	2.301	14.865	2.367		
5	15.584	2.480	15.047	2.396		
6	19.109	3.041	16.460	2.621		
7	19.573	3.115	17.942	2.857		
8	20.695	3.294	19.430	3.094		
9	22.687	3.611	19.594	3.120		
10	23.280	3.705	22.935	3.652		
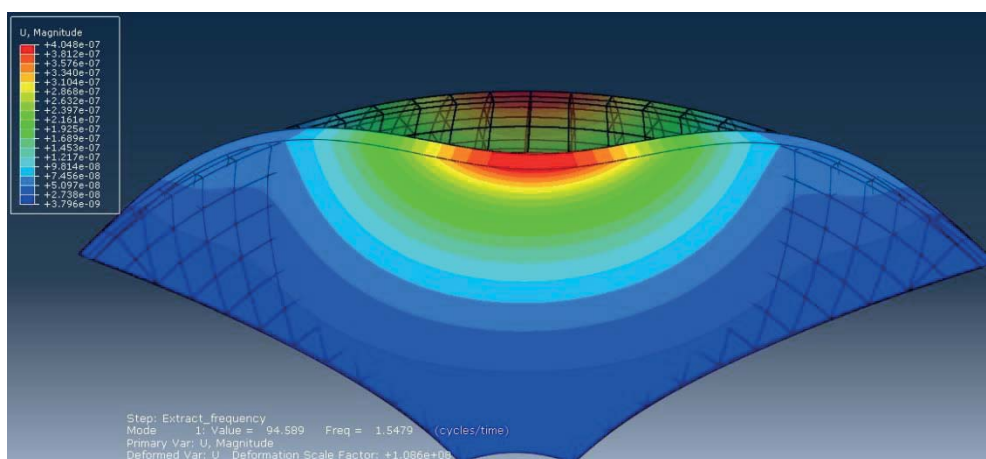
Figure 5: Fundamental mode shape view from downstream

Figure 6 illustrates three accelerograms provided by formulator for earthquake analyses (maximum acceleration 0.1g) and respectively figure 7 response spectra corresponding to accelerograms used for modal superposition analyses (spectral analyses).
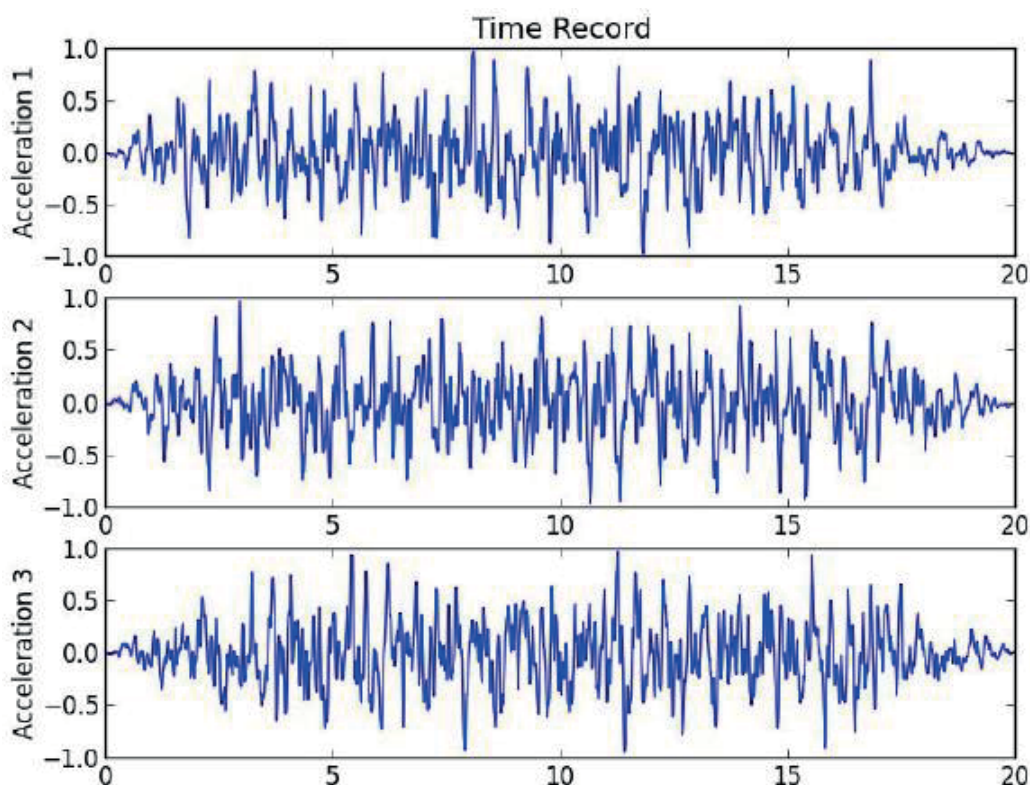
Figure 6: Accelerograms provided by formulator for earthquake analyses
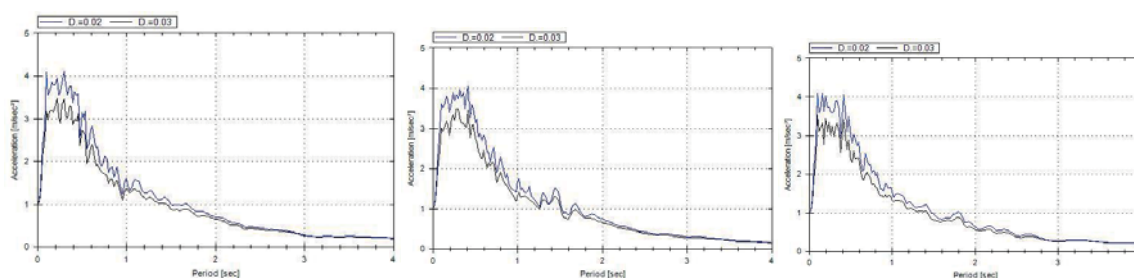
Figure 7: Response spectra (x,y,z) computed from the accelerograms provided by formulator and used in spectral analyses

Radial displacements on x, y and z directions in dam central sections at crest and base levels computed with ABAQUS in direct time integration method are illustrated in figure 8.

Hoop stresses, vertical stresses and radial displacements in the dam central section downstream/upstream faces generated by combined dead weight + hydrostatic pressures are illustrated in figures 9a,b. The results in spectral analysis and direct time integration, in the dam central section, downstream/upstream faces, full reservoir case are comparatively presented in figures 10a,b. The min./max stresses in the dam central section, downstream/upstream faces resulted during direct time integration under combined actions of dead weight + hydrostatic pressures + three-dimensional earthquake 0.1g are illustrated in figures 11a,b
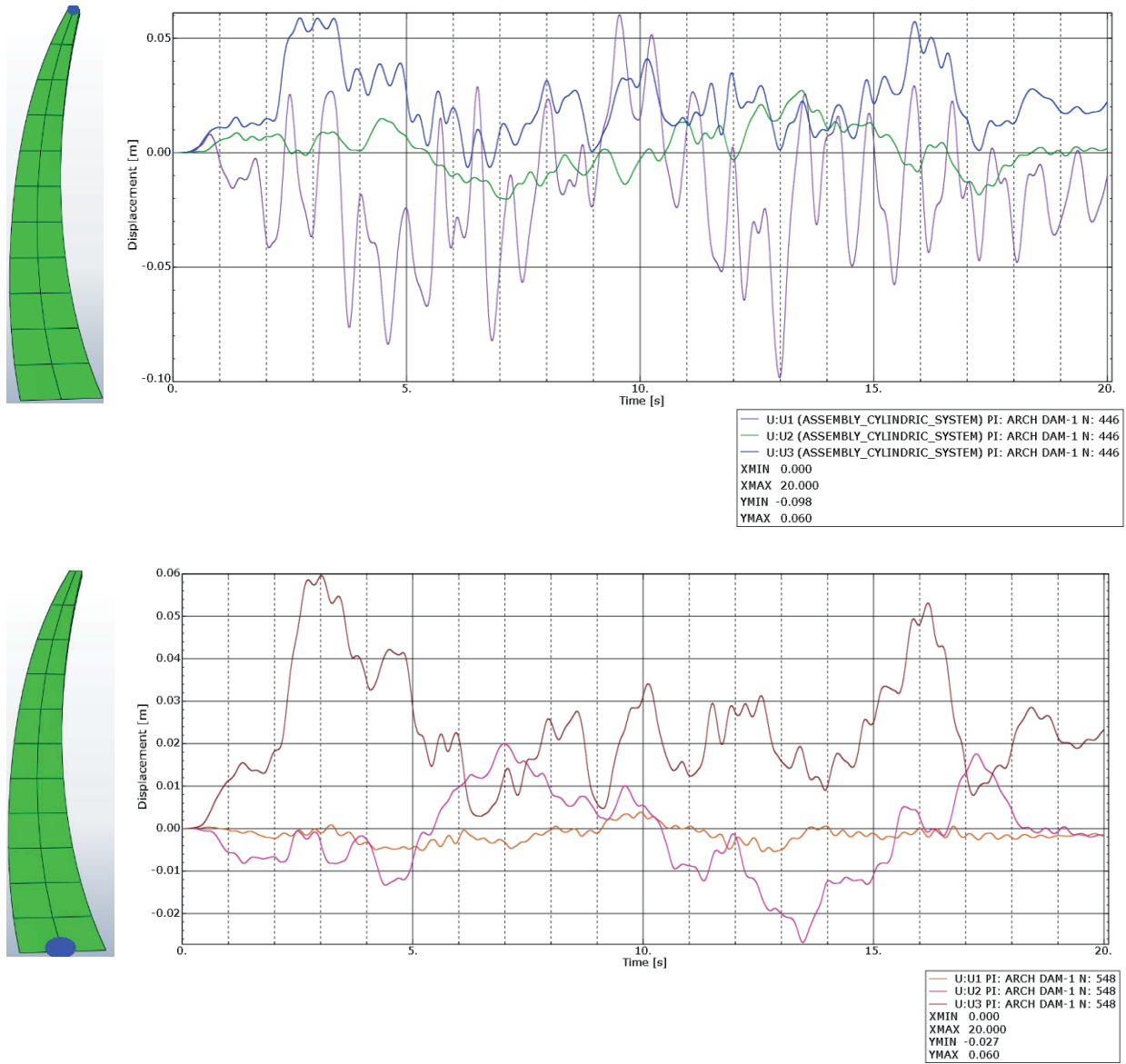
Figure 8: Radial displacements in dam central section at crest (top) and base (bottom) computed with ABAQUS
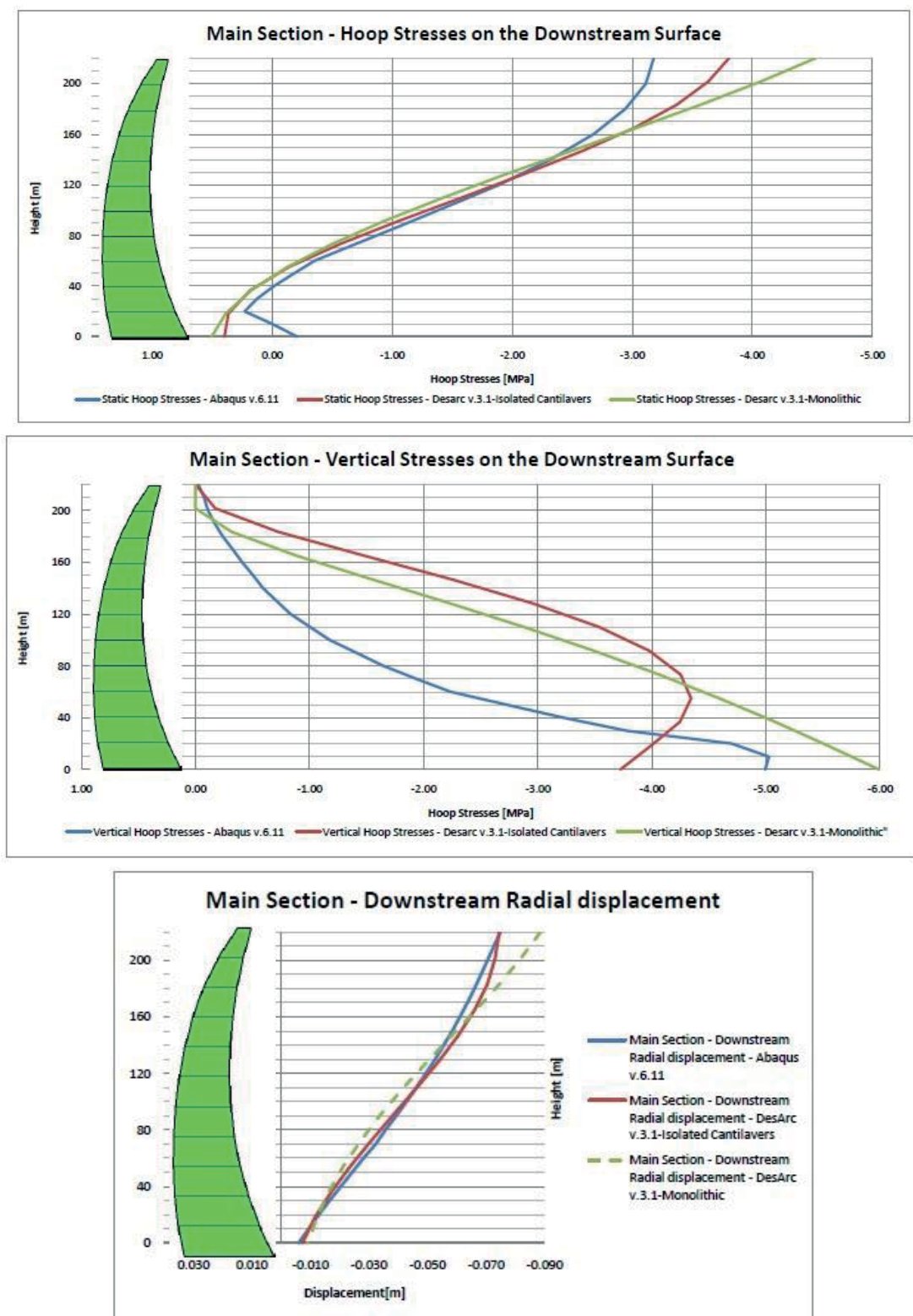
Figure 9a: Combined dead weight + hydrostatic pressures – Hoop and vertical stresses, radial displacements on downstream face, central section
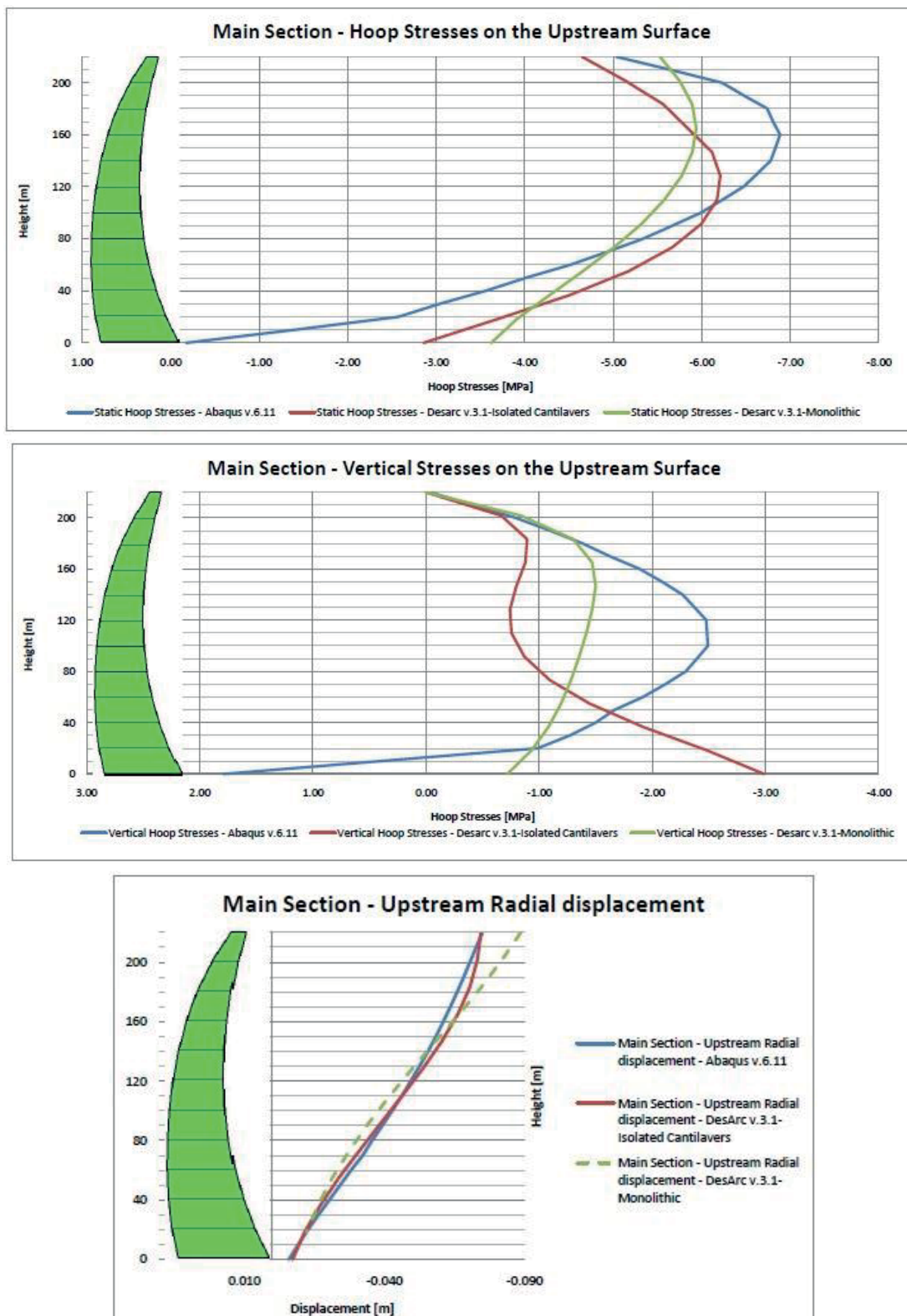
Figure 9b: Combined dead weight + hydrostatic pressures – Hoop and vertical stresses, radial displacements on upstream face, central section
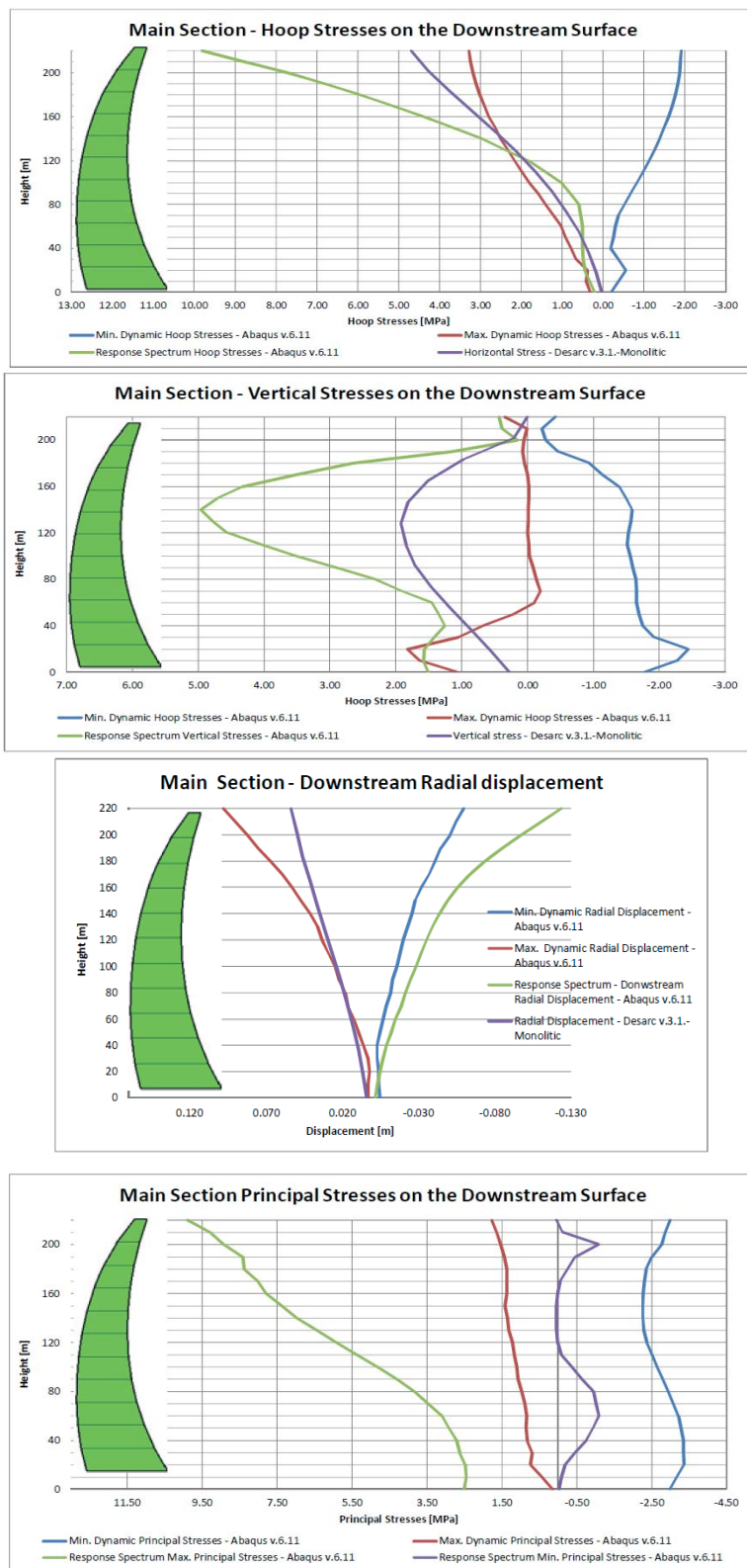
Figure 10a: Spectral analysis and direct time integration, central section, downstream face, full reservoir
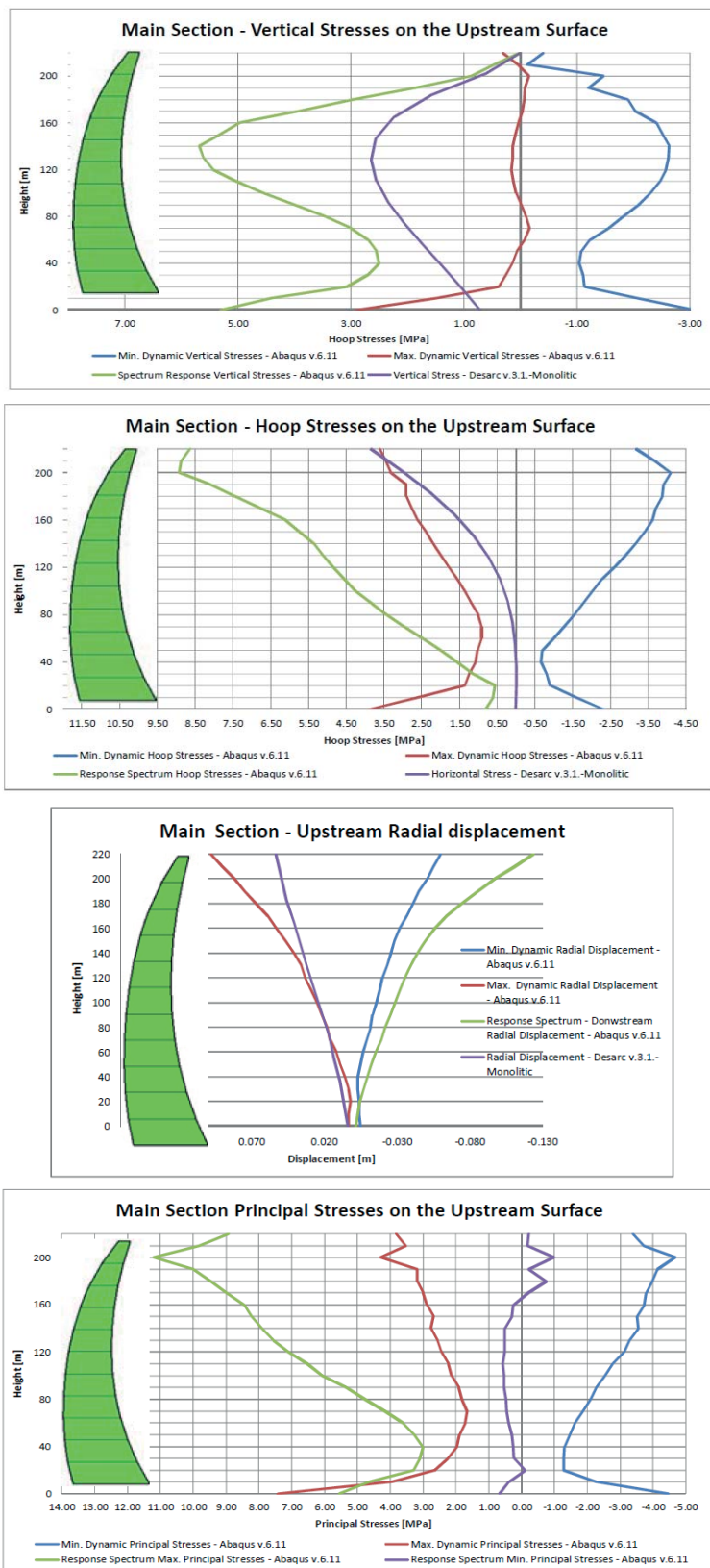
Figure 10b: Spectral analysis and direct time integration, central section, upstream face, full reservoir.
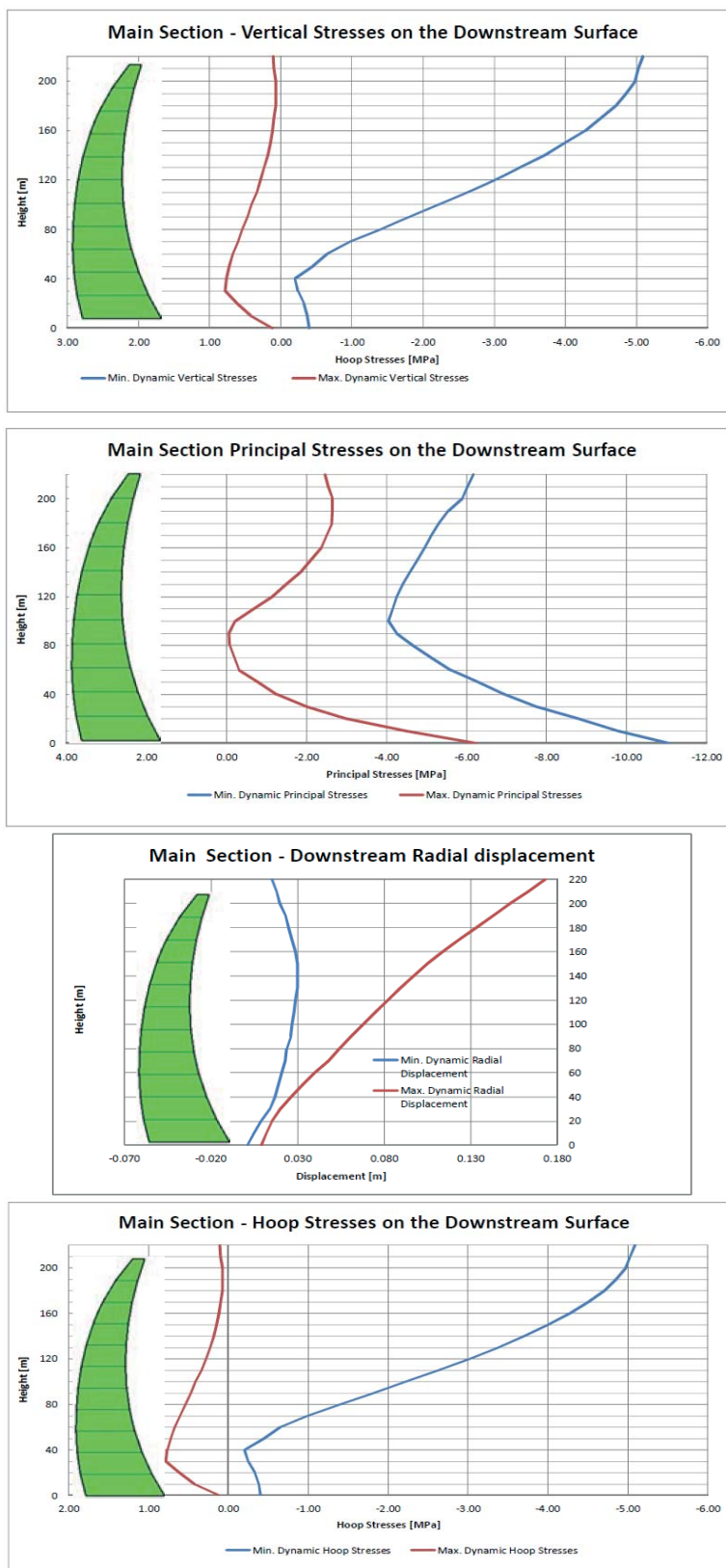
Figure 11a: Min./max stresses, direct time integration, dead weight+ hydrostatic pressure + three-dimensional earthquake 0.1g
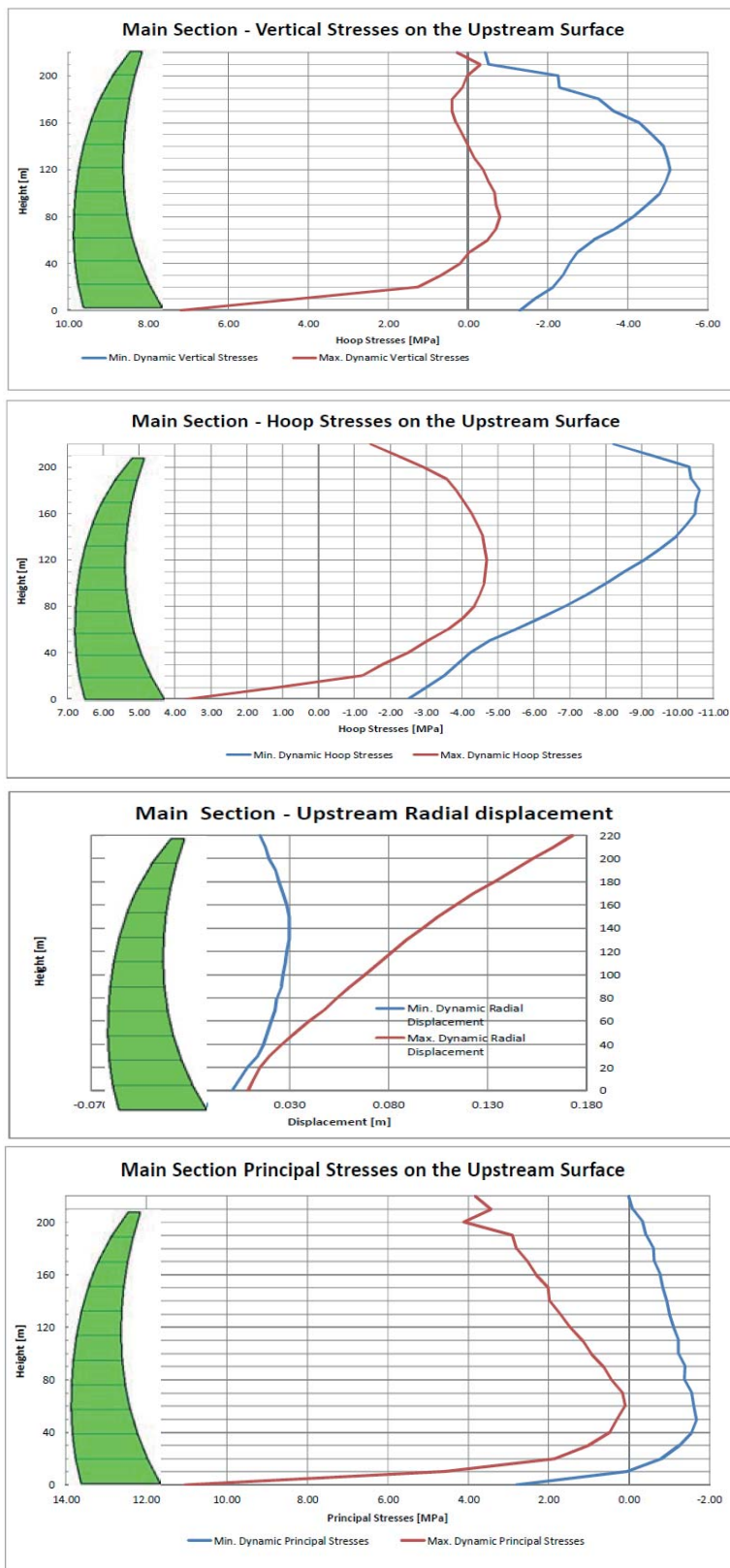
Figure 11b: Min./max., direct time integration, dead weight+ hydrostatic pressure + three-dimensional earthquake 0.1g

Comments on results of analyses

In compliance with some results illustrated in the above captions and other ones resulted from the analyses carried out the followings comments may be pointed out:

DESARC3.1 a very simply, friendly and fast computer code in all applications led to results close to those provided by much more sophisticated ABAQUS6.11 computer code. As a result DESARC computer code is very recommended for arch dams preliminary structural analysis.

Usually, in engineering practice dead loads are applied on arch dam isolated cantilevers, taking into account that during dam construction the contraction joints are not grouted. However, even under these conditions, some of the dead weight of cantilevers is transferred to arches, this quota depending of the dam shape and valley opening. Coming back to the arch dam provided by formulator it may remark from stresses and displacements to dead loads and hydrostatic pressures computed with DESARC in both hypotheses of isolated cantilevers and monolithic structure (fig.8a,b). that the effects of isolated cantilever hypothesis in relation with monolithic structure are not important. Accordingly, the analyses with ABAQUS, for simplicity, were carried out only in case of monolithic structure.

The dam displacements due to dead weight reach about 1 cm to upstream at the crest level. Dead weight is mainly transferred on cantilever. At the bottom of the central section the vertical stresses reach -7 MPa compression at upstream toe and -1.5 MPa compression at downstream heel. The hypothesis with isolated cantilever is a conservative one. On arches, the maximum stress reaches -2 MPa compression at the crest level.

Hydrostatic pressure as independent load generates maximum radial displacement of 7.5 cm in central section, dam crest elevation. The vertical stresses vary between 1 MPa tension and -4 MPa compression at downstream face and, respectively between 8 MPa tension at the dam upstream toe and -2 MPa compression at upstream face. The hoop stresses vary between 0.5 MPa tension, -3.7 MPa compression at downstream face, respectively between 0.5 MPa tension, -7 MPa compression at upstream face. The big vertical tensile stress generated by hydrostatic pressure at the dam upstream toe is reduced to 1.5 MPa by vertical compressive stress in the same point due to dead weight.

Based on results concerning natural periods values computed in full reservoir hypothesis (Table 1) (fundamental period 0.809 s ABAQUS, added mass, 0.645 ABAQUS, acoustic elements)it may conclude the hydrodynamic forces computed with Westergaard formula to generate added masses are higher than hydrodynamic forces developed by acoustic elements.

A comparison between seismic responses computed in the full reservoir hypothesis by spectral analysis and direct time integration with ABAQUS points out a good correlation between correspondent displacements response their maximum reaching about 13 cm but generally significant differences between correspondent stresses. For instance in the dam central section at downstream face the principal stresses vary between 1.50 MPa (tension) and -4 MPa (compression) in direct time integration and respectively 0,9 MPa and -9.50 MPa in spectral analysis.

Maximum displacement obtained in direct time integration at combination static loads (dead weight + hydrostatic pressures) + earthquake (full reservoir) reaches 18 cm to downstream at the crest level in central section. Max/min vertical stresses on downstream face varies between 0.8 MPa and -6.0 MPa . On upstream face at the dam upstream toe the vertical stress reaches tension of 7 MPa. It is a vulnerable point for cracking. On horizontal direction in the same point the hoop stresses vary between 3.5 MPa tension and -2.5 MPa compression. It may conclude that excepting dam upstream toe where exists cracking risk, the dam withstand earthquake action without notable incident.

As a general conclusion based on data presented above, the seismic response parameters of arch dams, especially seismic stress state differ significantly function of method of analysis.

Unfortunately, the scarcity of recordings concerning arch dams behavior during strong earthquakes make difficult to validate a method of analysis using field recordings from.

References

[1] Graz University of Technology THEME A Fluid Structure Interaction Arch Dam – Reservoir at Seismic Loading. 12-th International Benchmark Workshop on Numerical Analysis of Dams, Graz – Austria, 2013.

[2] ABAQUS 6.11. Abaqus / CAE User's Manual. United States of America: Abaqus Inc, 2009.

[3] Fanelli M., Giuseppetti G., Rabagliati U. Il metodo di Ritter Modificato. L'Energia Eletrica, No.3, 1978.

[4] Fanelli M., Fanelli A. Designer's Guide DESARC 3.1 for Windows ISMES S.p.A., Bergamo, 1995.

[5] Popovici A., Popescu C. Dams for water storage (in Romanian) Editura Tehnica, Bucharest, 1992.

[6] Priscu R., Popovici A., Stematiu D., Stere C. Earthquake Engineering for Large Dams Editura Academiei (Romania) and John Willey & Sons Ltd. (U.K.), Chichester, 1985.

[7] Popovici A., Abdulamit A., Toma I. Moldoveanu T. .Assessment of the seismic safety of dams based on „in site" measurements and back analyses. Proceedings XXI-st International Congress on Large Dams, Montreal, 2003.

Concrete arch dam at seismic loading with fluid structure interaction

R. Malm[1,2], C. Pi Rito[2], M. Hassanzadeh[3,4], C. Rydell[1,3] and T. Gasch[1,3]

[1] KTH Royal Institute of Technology, Concrete Structures, Stockholm, Sweden.
[2] SWECO Infrastructure, Hydropower and Dams, Stockholm, Sweden
[3] Vattenfall Engineering, Stockholm, Sweden.
[4] Lund University, Building Materials, Lund, Sweden.

E-mail: richard.malm@byv.kth.se

Abstract

A concrete arch dam have been analyzed during seismic loading with a model based on acoustic elements to describe the water and infinite elements as quiet boundaries to prevent wave reflection. The results have also been compared with a simplified model based on Westergaards added mass approach. The simplified model is only used, in this study, for comparison with the more advanced model with acoustic elements. Therefore the results from this simplified model are just used as a rough estimate of the induced stresses and displacements. Despite this, the simplified Westergaard model gives similar results compared to the more advanced model with acoustic elements for the water and infinite elements for the boundaries. The largest difference between the models often occurs at the nodes in the base of the arch dam, which may be due to poor discretization. Generally, the Westergaard added mass gives higher maximum principal stresses at the base on the upstream side than the acoustic model, while often underestimating the min principal stresses at the base on the downstream side. Both models show high tensile stresses near the base of the arch dam that would result in cracks.

Finite element models

The studied geometry was given by [1], and in this paper, the mesh denoted as fine mesh in [1] has been used. All numerical analyses in this paper have been performed with the commercial software Abaqus ver.6.12. The model consists of a foundation with dimensions 1000 x 1000 x 500 m built up of 2700 second order brick elements with reduced integration. In one of the models presented in this paper, infinite elements have been used for the outer surfaces of the foundation in order to remove reflecting waves on the model edges, see Figure 1 a). The arch dam is 220 m high, with a width of 430 m at the crest and 80 m at the base. The arch dam consists of 2736 second order brick elements with reduced integration (8 integration points). The geometry of the reservoir is 460 m long (i.e. two times the dam height). In the following analyses, two different models to account for the water will be presented. In a simplified model, the reservoir has been replaced with nodal masses corresponding to the Westergaard added mass approach [2]. In the more advanced model, the reservoir has been included by means of acoustic elements and infinite acoustic elements to account for an infinite long reservoir.

Loads and boundary conditions

All analyses have been performed in two steps; static analysis of response due to gravity and hydrostatic water pressure, and dynamic implicit analysis (transient dynamic analysis) to calculate the response from induced ground accelerations due to the seismic load.

In all analyses, the gravity load has only been assigned to the elements that constitute the arch dam. The rock is according to the instructions, [1], defined with zero density. In the simplified model, based on the Westergaard added mass approach, additional nodal masses are introduced on the upstream surface of the arch dam. However, it is important that the nodal masses are not assigned a gravity load since that would affect the static behavior of the dam. The hydrostatic water pressure has been assigned to the upstream surface of the arch dam, and to all rock surfaces subjected to the water pressure, as seen in Figure 1 b). The maximum hydrostatic pressure is defined as 2.1582 MPa (220 m x 9.81 m/s^2 x 1000 kg/m^3). In the more advanced model, with acoustic elements, an additional boundary condition with zero acoustic pressure on the free surface of the water has been defined.

a)   b)
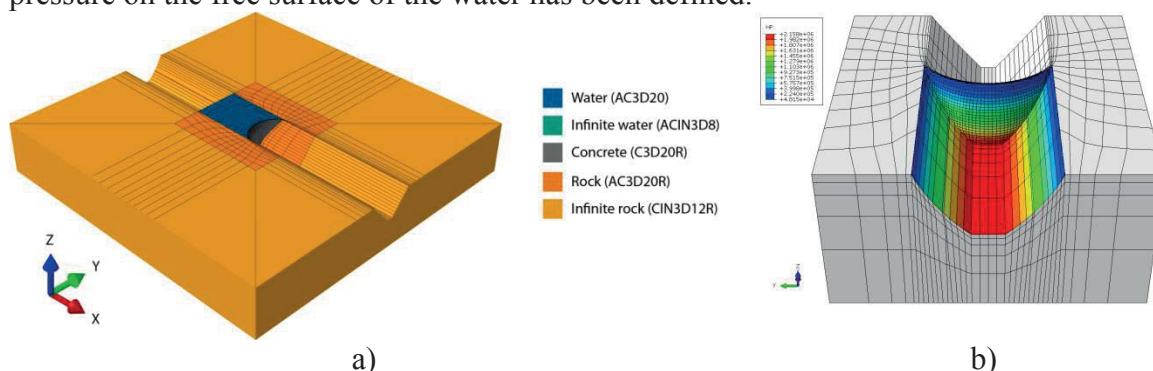
Figure 1: a) Geometry and element types of the model, b) applied hydrostatic water pressure.

The ground accelerations are illustrated in Figure 2. In the dynamic analysis, a constant time step of Δt = 0.01 s have been used. The upper frequency that can be captured in the analysis, i.e. the Nyquist frequency, is thereby 50 Hz. According to the frequency analyses that were performed, the cumulative mass is nearly 100 % for frequencies up to 30 Hz and thereby the chosen time increment is considered sufficient. In addition, the time history signal of the earthquake is sampled with Δt = 0.01 s and thereby the highest reproducible frequency in the sample is 50 Hz.
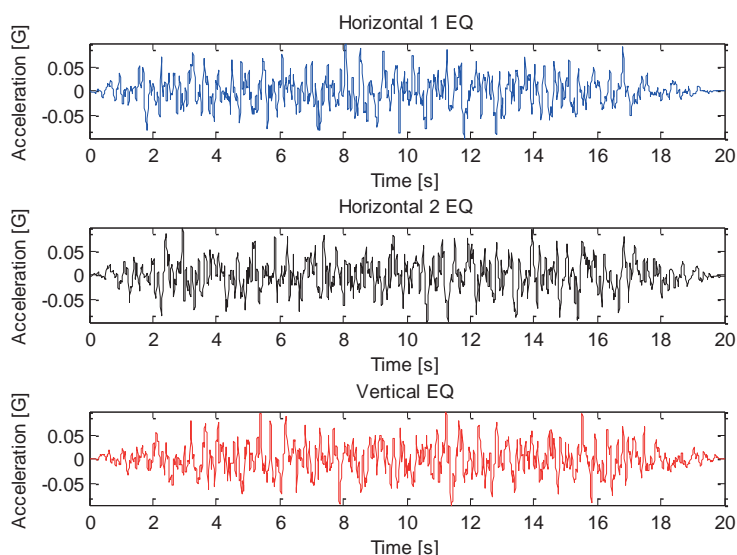
Figure 2: Transient time history signals of the ground accelerations.

In the static analysis, all nodes on the bottom surface of the foundation were constrained for all translations, i.e. in x-, y- and z-direction. In the seismic analysis, these boundary conditions are replaced, where all nodes on the bottom surface were assigned prescribed ground accelerations according to Figure 2. The sides of the foundation have not been assigned boundary conditions in neither the static nor the dynamic analysis. The reason for this is that

these surfaces will be defined with infinite elements in the model with acoustic elements. It is not possible to define prescribed conditions in the form of accelerations, velocities or displacements on nodes that are part of infinite elements if the infinite elements are to function as quiet boundaries. One approach to overcome this would for instance be to calculate corresponding stresses from the induced accelerations. However, considering the large geometry of the rock, it is likely that seismic wave incoherence would influence the results. It is therefore unlikely to assume that the ground vibrations would be identical on all sides. In addition, the rock is defined with zero mass, and therefore it will not produce mass inertia forces. Hence, the approximation adopted here, where the boundary is applied only to the bottom nodes, is considered to be valid for this case.

Material properties and damping

All material properties have been defined by [1]. Rayleigh damping have also been used in all presented analyses. The damping ratio for concrete has been assumed equal to 4 % according to Regulatory Guide 1.61, [3]. The damping of the water is usually assumed to be 0.5 %; this has been judged to be negligible and therefore not included in the analyses.

The lower frequency of the Rayleigh damping have been defined corresponding to the frequency where 5 % of the cumulative effective mass is active, which in this case is $f_1 = 1.27$ Hz. This ensures minimal underestimation of response in the low frequency range according to [4] and [5]. The upper frequency have been defined corresponding to the frequency where 80 % of the cumulative effective mass is active, which in this case is $f_2 = 9.76$ Hz. The corresponding damping values ξ_1 and ξ_2 have been calculated so that the minimum damping in the interval $f_1 - f_2$ is 1 % less than the target damping value, i.e. $\xi_{min} = 3$ %. Based on this approach, the obtained Rayleigh damping coefficients are $\alpha = 0.66314$ and $\beta = 0.0013503$ with the corresponding curve illustrated in Figure 3. The average damping in the interval $f_1 - f_2$ is 3.6 %, i.e. slightly lower than the target value of 4 % and thereby conservative.
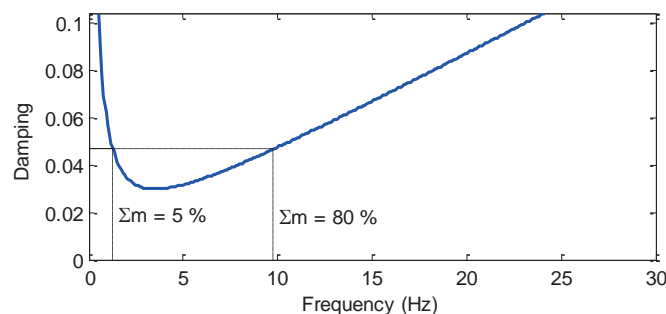
Figure 3: Rayleigh damping curve ($\alpha = 0.66314$ and $\beta = 0.0013503$)

The Rayleigh damping coefficients have been defined in the material definition for concrete but also for the rock. Since the rock have zero density, only the stiffness proportional part of the Rayleigh damping ($\beta = 0.0013503$) will be active. The Rayleigh damping curve has been verified against a modal analysis with uniform damping of 4 %, where the Rayleigh damping gave slightly conservative result.

Model 1: Westergaard added mass approach

According to Westergaard [6], the hydrodynamic forces exerted on a dam due to earthquake ground motions are equivalent to inertia forces of a volume of water attached to the dam moving back and forth with the dam while the rest of the reservoir water remains inactive. The influence of the reservoir on a 2D rigid monolith with vertical upstream face is included by introducing the impulsive mass of the water and thereby, altering the dynamic properties of

the structure. Kuo [7], further developed the method to also account for the curvature of an arch dam, this have however not been considered in this paper. The reason for this is that the simplified added mass model is only used, here, for comparison with the more advanced model with acoustic elements. Therefore, the results from this simplified model are just considered as a rough estimate of the induced stresses etc. A MatLab script have been developed to calculate the tributary surface area for each node on the upstream surface, and based on this the nodal mass has been calculated according to [6]. The calculated nodal masses are illustrated in Figure 4, where the colors in the figure represent the added weight (in kg) for each node on the upstream surface of the arch dam.
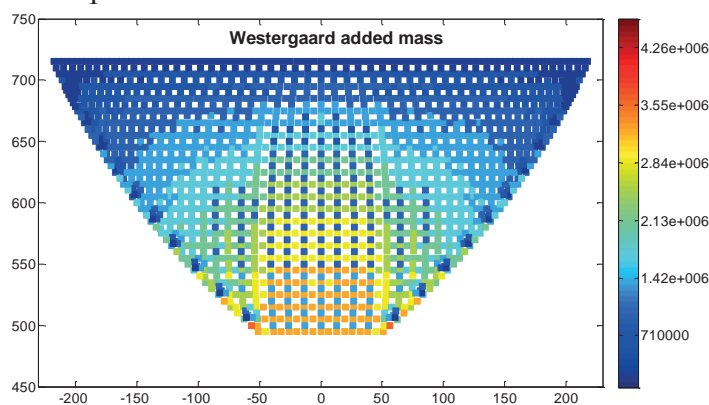
Figure 4: Nodal masses based on Westergaard added masses

Model 2: Acoustic and infinite elements

In the more advanced model, the water has been included by means of 2640 second order acoustic elements. These elements are based on an acoustic formulation with the fluid wave velocity, i.e. the variation in pressure, as the independent variable. These elements do not include any terms for body forces and therefore, the hydrostatic pressure needs to be included as a pressure load on the structure, as previously shown in Figure 1 b). The finite element mesh of the acoustic elements is stationary at all nodes except at the boundaries of the fluid domain, i.e. the fluid-structure interface. For boundaries adjacent to a structural domain, the nodes of the acoustic medium can be prescribed to follow the nodes of the structural domain, giving a pressure change in the acoustic medium. A pressure boundary which prescribes zero acoustic pressure on the free surface has been defined, due to the lack of displacement DOF. This gives no actual displacement of the free surface but is correct in the sense of wave propagation in the medium. In order to account for an infinite long reservoir, 264 additional infinite acoustic elements are defined on the upstream side of the reservoir. In order to prevent reflecting waves on the model edges, 510 infinite elements have been defined for the surfaces on the foundation rock as illustrated in Figure 1 a). The infinite elements provide quiet boundaries and are based on Lysmer and Kuhlemeyer [8] for dynamic response. The damping constants for longitudinal and shear waves are calculated as

$$d_p = \rho \cdot c_p = \sqrt{\rho(\lambda + 2G)} \tag{1}$$

$$d_s = \rho \cdot c_s = \sqrt{\rho \cdot G} \tag{2}$$

where, $\lambda = \dfrac{E \cdot v}{(1+v)(1-2v)}$, $G = \dfrac{E}{2(1+v)}$ and E is the elastic modulus, v is poisons ratio and c_p and c_s are the longitudinal and shear wave speed.

The infinite rock elements were defined with the same properties as rock (see [1]), with the addition of a defined density of 2600 kg/m³, required for the damping. The bottom surface

was defined without infinite elements, due to the fact that the seismic ground motion was applied in the base. The length of the infinite rock elements are 1000 m, i.e. chosen as the total length of the original foundation. The infinite elements are active in static analyses, by providing horizontal stiffness to the foundation.

Eigenfrequencies and modes

The 10 first mode shapes obtained from the acoustic model are illustrated in Figure 5.
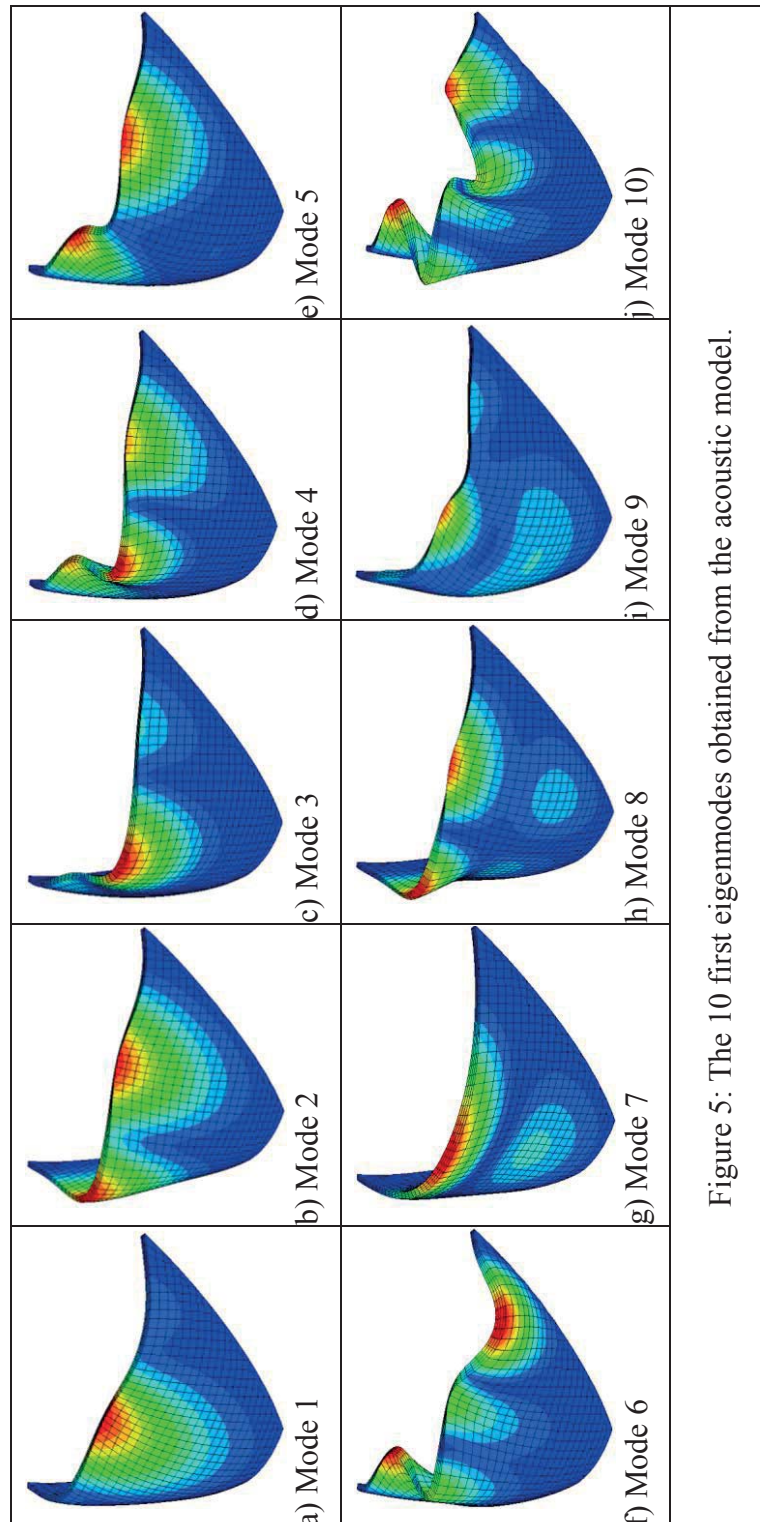
Figure 5: The 10 first eigenmodes obtained from the acoustic model.

In some cases, the acoustic model gives two closely spaced frequencies with the same mode shape. In Table 1, these are therefore presented together as one mode. In addition, some modes in the acoustic model are mainly relevant to the water, and hence these are not presented here. It can however be mentioned that the first mode corresponding to the water is about 0.7 Hz. The frequencies for each mode is also presented from the Westergaard added mass approach and the original model without water for comparison in Table 1.

Table 1: Calculated eigenfrequencies for the ten first modes.

Mode	Frequency (Hz)			
	Acoustic elements		Added mass	W.o. water
1	1.5114		1.3730	2.0002
2	1.5431		1.3291	1.9012
3	1.9056	1.9850		
4	2.2255	2.3534	2.054	2.8785
5	2.4254	2.4665		
6	2.9626	2.9997	2.5633	3.5491
7	3.0084	3.1169	2.5782	3.5998
8	3.2818	3.3150	2.8773	4.1744
9	3.5886			
10	3.7748		3.2224	4.4779

As seen in the table, the acoustic model gives frequencies that are in-between the case without water and the case with Westergaard added mass. Notable is also that the first and second mode have change place in the acoustic model compared to the others models.

Stresses

Stresses are presented for three sections, Left section (-45°), Main section (0°) and Right section (+45°) from the center of the arch, as defined by [1]. The following stresses are presented; maximum and minimum principal stresses, hoop stresses and vertical stresses. For each of these stresses, the max and min envelope for each node on the upstream (US) or downstream (DS) surface are presented. This means that the presented stresses are not occurring at the same time; instead these are the maximum or minimum stresses that occur for the whole time period for each node on the upstream or downstream side of each of the studied sections. As seen in Figure 6 there is quite similar results between the simplified Westergaard added mass method and the method with acoustic and infinite elements. The minimum principal and hoop stresses show, generally, better resemblance between the two models than the max principal and vertical stresses. The largest difference between the models often occurs at the nodes in the base of the arch dam, which may be due to poor discretization. Generally, the Westergaard added mass gives higher maximum principal stresses at the base on the upstream side than the acoustic model, while underestimating the min principal stresses at the base on the downstream side. Both models show high tensile stresses near the base of the arch dam that would result in cracks. It can from this comparison not be drawn any conclusion that the simplified Westergaard added mass approach would be more conservative than the method with acoustic and infinite elements. The analyses also show that, despite the

symmetric shape of the arch dam, there is a difference between the results at the left and right section, as seen in Figure 7.
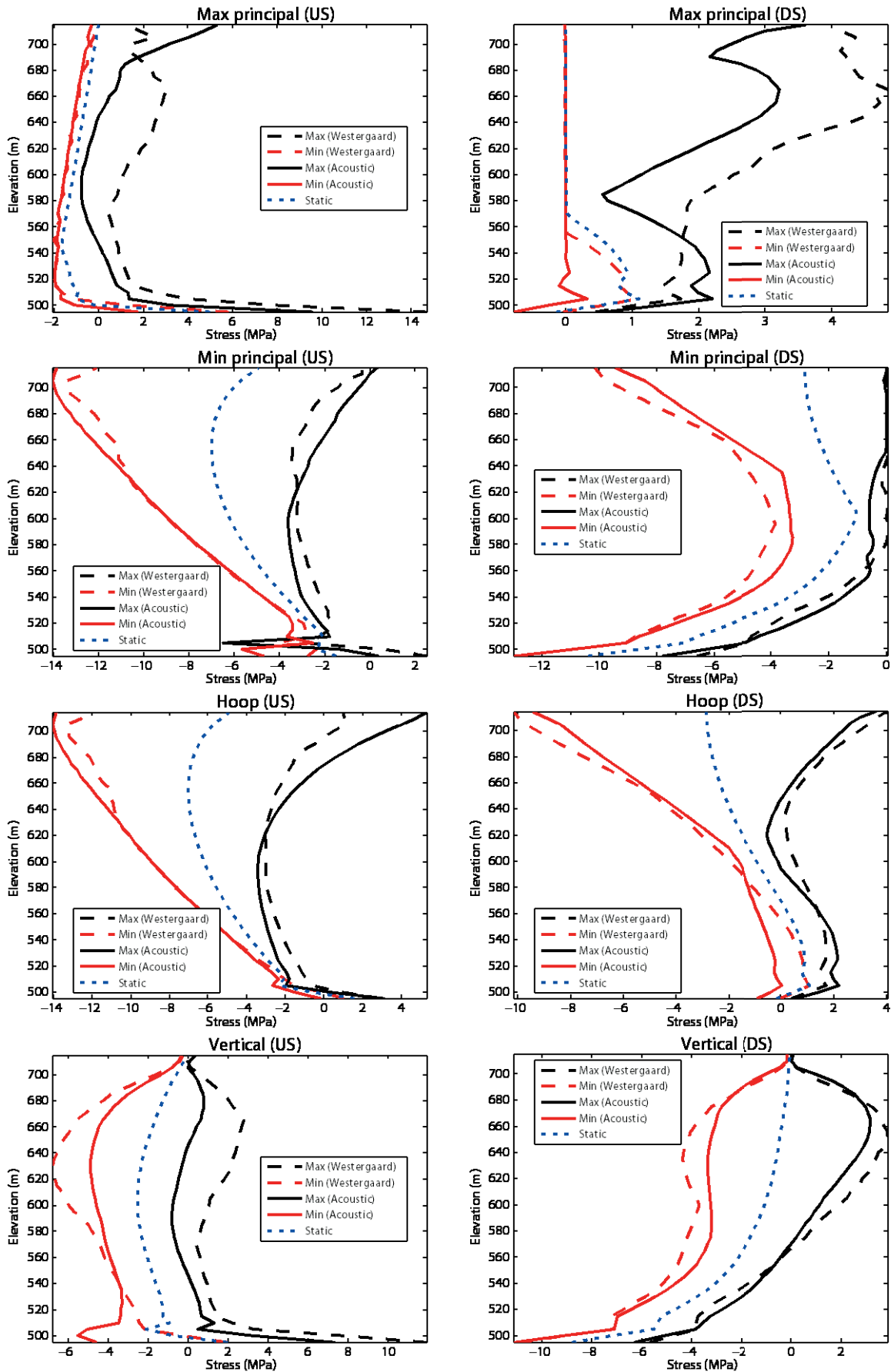
Figure 6 Stresses in the main section (0°) according to the model with acoustic elements and the simplified Westergaard model, on US and DS surface respectively.
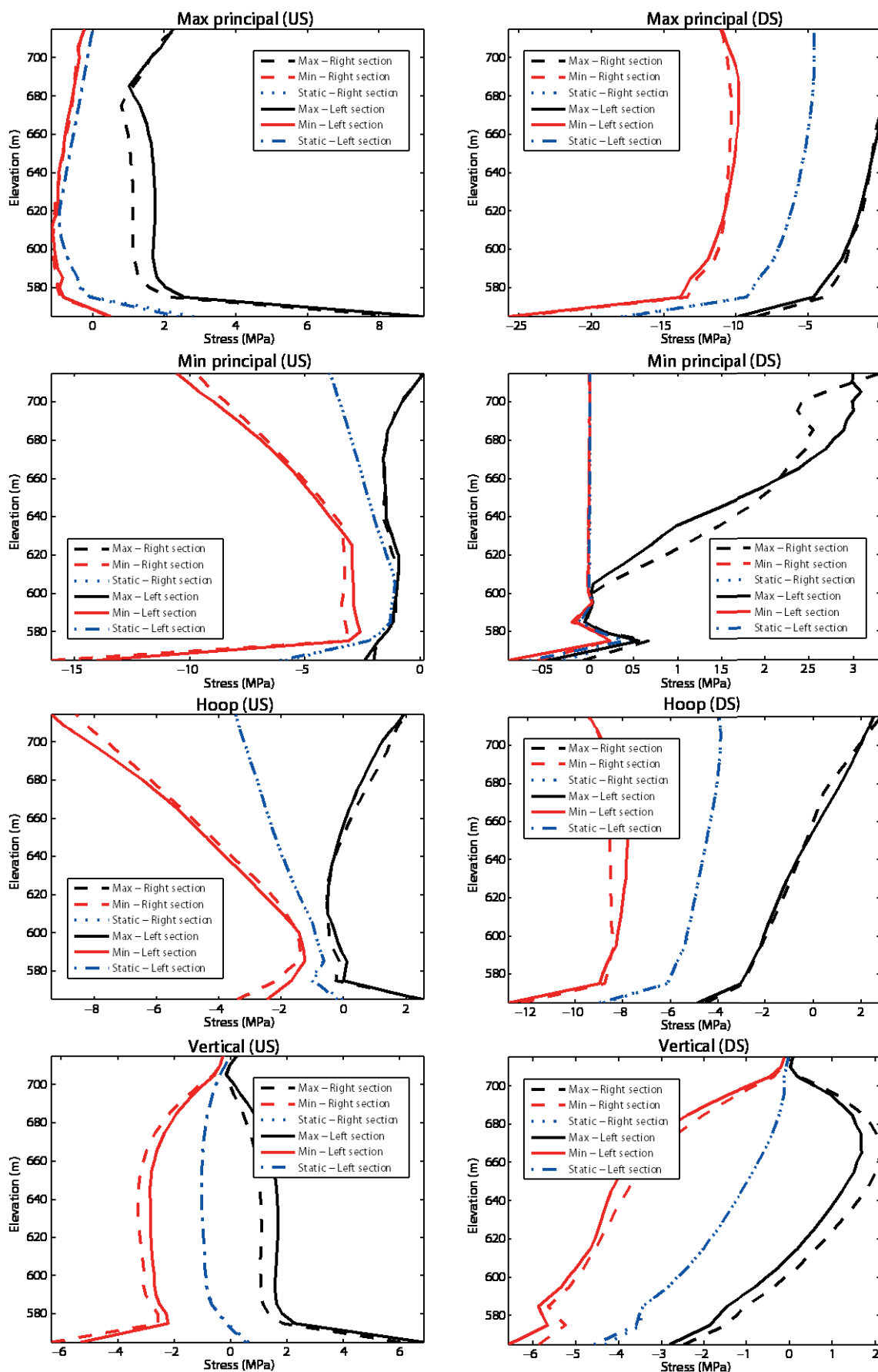
Figure 7: Stresses in the left (-45°) and right section (+45°) according to the model with acoustic elements on US and DS surface respectively.

Displacements

The max and min envelope of the relative radial displacements are presented in Figure 8 for the Main section (0°). In figure, the relative displacement presented i.e. the rigid body displacement due to the earthquake has been removed. In the figure, a comparison between the acoustic model and the simplified Westergaard model is shown. The models give similar results, but the acoustic model gives larger deflections.
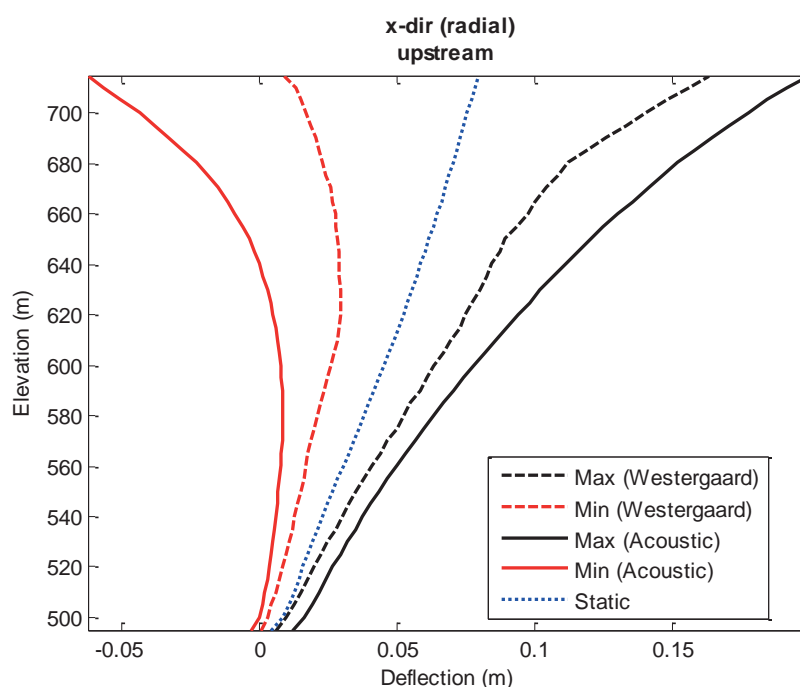
Figure 8: Displacements in the main section (0°) on US surface.

Discussion

A concrete arch dam have been analyzed during seismic loading with a model based on acoustic elements to describe the water and infinite elements to describe quiet boundaries to prevent wave reflection. The results from this model have also been compared to a simplified model based on Westergaards added mass approach. The simplified model is only used for comparison and should therefore be considered as a rough estimate of the induced stresses and displacements. The performed analyses have showed that there are several factors that have been assumed in this study that influence the results, such as

- Rayleigh damping – the choice of damping ratio for the different materials and especially the choice of corresponding frequencies influence the results.
- Seismic excitation – in these analyses, only the bottom of the foundation is subjected to the prescribed seismic excitation. Effects such as seismic wave incoherence have not been considered.
- Infinite boundaries – in the analyses infinite boundaries have defined for both the foundation but also for the reservoir.

The results from the two models are quite similar, where the minimum principal and hoop stresses generally are more similar between the two models than the maximum principal and

vertical stresses. The largest difference between the models often occurs at the nodes in the base of the arch dam, which may be due to poor discretization of the mesh at these points. Generally, the Westergaard added mass gives higher maximum principal stresses at the base on the upstream side than the acoustic model, while often underestimating the min principal stresses at the base on the downstream side. Both models show high tensile stresses near the base of the arch dam that would result in cracks. The analyses also show that, despite the symmetric shape of the arch dam, there is a difference between the results at the left and right section.

Acknowledgements

References

[1] ICOLD, 2013. 12th International Benchmark Workshop on Numerical Analysis of Dams. Theme A – Fluid Structure Interaction. Arch Dam – Reservoir at Seismic loading. Graz University of Technology.

[2] Westergaard, H. M. (1933). Water Pressures on Dams During Earthquakes. Transactions, American Society of Civil Engineers, Vol 98.

[3] US NRC (2007). Damping values for seismic design of nuclear power plants. Regulatory Guide 1.61. U.S. Nuclear Regulatory Commission.

[4] ASCE 4-98, 1998, "Seismic Analysis of Safety-Related Nuclear Structures and Commentary," American Society of Civil Engineers, Reston, Virginia.

[5] ASCE/SEI 43-05, 2005, "Seismic Design Criteria for Structures, Systems, and Components in Nuclear Facilities," American Society of Civil Engineers, Reston, Virginia.

[6] EM1110-6051 (2003). Time-History Dynamic Analysis of Concrete Hydraulic Structures. US Army Corps of Engineers.

[7] Kuo, J.S.-H. (1982). Fluid-structure Interactions: Addedd Mass Computations for Incompressible Fluid. Report No. UCB/EERC-82/09. Earthquake Engineering Research Center, University of California, Berkeley.

[8] Lysmer, J., and R. L. Kuhlemeyer, "Finite Dynamic Model for Infinite Media," Journal of the Engineering Mechanics Division of the ASCE, pp. 859–877, August 1969.

Fluid Structure Interaction
Arch Dam – Reservoir at Seismic loading
A solution using FEnas

M. Brusin[1], Dr. J. Brommundt[1] and H. Stahl[1]

[1] AF-Consult Switzerland Ltd., Täfernstrasse 26, CH-5405 Baden, SWITZERLAND

E-mail: marko.brusin@afconsult.com

Abstract

This paper represents a contribution to the ICOLD – 12th International Benchmark Workshop on Numerical Analysis of Dams, THEME A - Fluid Structure Interaction Arch Dam – Reservoir at Seismic loading. The formulated problem, modeling of a 220 m high and 430 m wide arch dam under static and seismic loads, was addressed by the finite element code FEnas. FEnas is a Swiss code originally developed at the Imperial College London. The interaction between the dam and the water in the reservoir was implemented using the added mass technique in the general form following Westergaard.

The simulations performed included a comparative analysis of two meshes with different spatial discretization. The computed results show that the impact of the discretization is rather small. Moreover, the results of the analyses have been compared to typical deformations observed at Swiss dams and similar studies on existing dams. All results here are in good agreement with preceding studies of this kind.

Introduction

Problem Definition

The problem to be analyzed and solved here is exhaustively described in the problem description provided by the workshop organizers [1], who are referenced as the "formulator" in the following. The stresses and deformations of a dam interacting with the water in its completely filled reservoir under earthquake load shall be simulated. As the title of the benchmark workshops says, this interaction is the focus of this study. Consequently, typical further challenges in studies of this type are handled in a pragmatic way, e.g. all simulations assume linear elastic material behavior. The earthquake is represented by three correlated time series of acceleration in the three dimensions, lasting 20 seconds in total. Two FE meshes are provided, one in coarse and one in fine resolution.

Finite Element Code FEnas

The finite element analysis of the dam was performed using FEnas ECCON IPP/ Version 2.9.3 2012/08/24. FEnas which was initially developed at the Imperial College London and was continuously enhanced and integrated with a graphical user interface by Walder & Trueb Engineering AG, Switzerland [2]. FEnas is capable of solving a wide range of static and dynamic load problems including consideration of thermal impact. The dimension of the problems solvable in FEnas is constrained by aspects of computation only. Nonlinearity in terms of material behavior and geometry can be considered. The typical field of application of FEnas is in design of buildings and concrete structures, including tunnels and dams. The FEnas element library includes all element types necessary for this type of analyses. However, acoustic or fluid elements are not included and cannot be modeled.

Modelling Concept and Implementation

General Assumptions and Approach

The software package FEnas allows to analyze the problem of interaction of fluids and structures under seismic impact using the added mass technique. This technique is considered to be a conservative approach and gives satisfactory results in engineering practice [3]. The mass of water which oscillates along with the structure is added as a discrete mass at all element nodes of the upstream face of the arch dam as described below.

All analyses were carried out for the two meshes provided by the formulator, i.e. a coarse and a fine mesh. For each mesh the following three calculations were performed:

- Linear static analysis for the self-weight load and hydrostatic pressure load.
- Calculation of eigenvectors of oscillation for the first 10 tones, including the added mass of water.
- Linear dynamic analysis by using direct time integration, also including the added mass of water.

For further analysis of the results a superposition of the results of static and dynamic analyses was performed as described below.

All approaches to the modeling, loads, boundary conditions, and material parameters are identical for the simulations with the two meshes. Considering this, if not stated otherwise, the following discussions refer to the fine mesh; references to the coarse mesh are explicitly marked.

Mesh Properties

The mesh was delivered by the formulator of the benchmark competition. Two adaptations were performed:

4. The discretization of the terrain of the coarse mesh did not coincide with the discretisation of the dam at their mutual interface. One line of elements had to be corrected to create a consistently meshed interface.
5. The discretization of the terrain of the fine mesh required the same adaptation. Moreover, the discretisation of the terrain was not adapted to the refined discretisation of the dam. Therefore, the topmost layer of elements of the terrain mesh was refined to gain a consistent discretisation of dam and terrain at their interface.

We consider the impact of these adaptations as minor. Their big advantage is that no code internal treatment and definition of the interfaces with different discretisation is needed but the meshes can be used as such. Due to the selected approach with the added mass, the developed finite element mesh for the reservoir provided by the formulator was not taken into account. The table below provides information about the mesh parameters. Figures of the mesh discretization are given further below.

Table 1: Mesh parameters of the adapted meshes

Total number of	Coarse mesh		Fine mesh	
	Dam	Terrain	Dam	Terrain
nodes	2083	11608	13733	15062
elements	356	2340	2736	3120
Hexahedron-quadratic elements with 20 nodes	312	2340	2736	2700
wedge-quadratic elements with 15 nodes	44	0	0	420

Material Parameters and Boundary Conditions

The formulator provided the following linear elastic isotropic material characteristics.

Table 2: Material parameters

Parameter	Dam	Rock Mass (Terrain)
Density	2400 kg/m^3	massless
Poisson – ratio	0.167	0.2
Young's – modulus	27000 MPa	25000 MPa

Considering that the outer limits of the modeled terrain are sufficiently far away from the dam, the boundary conditions at the outer surface and the bottom of the terrain were determined as springs with large stiffness that practically prevents any movement in all three directions (quasi fixed bearing).

Modeling approach for added mass technique
The mass and its distribution are relevant when calculating the natural frequencies of a structure as well for the dynamic analysis during the earthquake. The specific mass is calculated from density, and is in FEnas automatically taken into account in a physical manner.

In order to take into account the interaction of fluids and structure, it is necessary to add a mass of water which oscillates together with the dam. Water joined to the body dam is added to the points of the upstream face as an additional concentrated mass according to Westergaard's approach in its generalized form [3, 4]. Westergaard showed that the hydrodynamic pressures exerted on the face of the dam due to the earthquake ground motion is equivalent to the inertia forces of a body of water attached to the dam and moving back and forth with the dam while the rest of reservoir water remains inactive. He suggested a parabolic shape for this body of water with a base width equal to 7/8 of the height. In the generalized Westergaard method [3, 4] normal hydrodynamic pressure P_n at any point on the curved surface of the dam is proportional to the total normal acceleration shown in figure below, i.e.:

$$P_n^i = \alpha_i \cdot \ddot{a}_{ni} \tag{1}$$

$$\alpha_i = \frac{7}{8} \cdot \rho_w \cdot \sqrt{H_i \cdot (H_i - Z_i)} \tag{2}$$
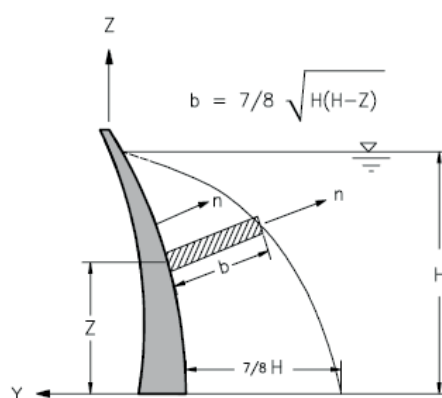
Figure 1: Westergaard hydrodynamic pressure [3]

Where:
  $\ddot{a}_{ni}$ - Total normal acceleration at point i
  α_i - Westergaard pressure coefficient at point i

ρ_w - Mass density of water

H_i - Depth of water at vertical section that includes point i

Z_i - Height of point i above the base of the dam

The normal pressure P_n at each point is then converted to an equivalent normal hydrodynamic force by multiplying by the tributary area associated with that point. This procedure is semi-automated in FEnas, the user has to define the surface load according to Westergaard, while the conversion from surface pressure to added mass at nodes is done automatically by the program. Since the Westergaard coefficient depends on the depth of water in front of the upstream face, which varies with dam side, the value H is taken in accordance with the colors on the next figure, one average value of H correspond for each color.
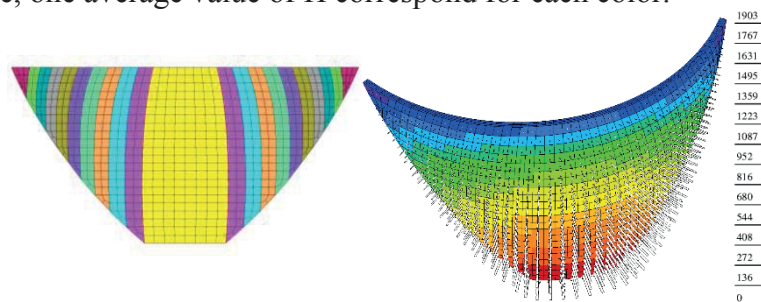
Figure 2: Westergaard added masses technique in FEnas (left: zones of similar H, right, hydrodynamic forces as vectors, colours show magnitude of force in kN/m^2)

Modelling Approach for Self-Weight and Hydrostatic Load

Deadweight or self-weight refer to the same load case. Application of this load case generally mimics the construction schedule. Here, a pragmatic two step modeling approach is implemented. Superposition of the two steps represents deadweight. In the first step, every second cantilever is modeled massless with a very low Young's modulus, whereas all other cantilevers are modeled by their correct properties (cf. Table 2). In the second step, this procedure is repeated exchanging the material parameters between the two sets of cantilevers. For the further analysis, the joints are considered as grouted and the entire construction retains hydrostatic pressure as arch dam.

Hydrostatic load has been defined as surface load perpendicular to the surface of all elements at the upstream surface. The magnitude of the surface load depends on the water level with respect to the vertical position of the element.

Modelling Approach for Determining the Eigenfrequencies

The formulator required calculation of the first 10 eigenfrequencies of the structure; this includes the interaction with the reservoir, i.e. the eigenfrequencies of the dam together with the added mass of water are to be calculated.

The lowest natural frequencies are determined by resolving the characteristic value or eigenvalue problem. Here, only iterative methods can be used to solve eigenvalues problems. FEnas uses the "subspace iteration method". The modes of oscillation are estimated for a number of start vectors (the subspace) and then iteration is used for continuous improvements. The minimum number of start vector required is equal to the number of requested eigenvalues; the maximum number is equal to the number of degrees of freedom of the entire FE structure.

Modelling Approach for Transient Seismic Loads
Linear dynamic analysis was performed using direct time integration (time history analysis). As method for integration of the dynamic equations of motion we have used the Newmark method. The accelerograms given by the formulator were used as such and are plotted in the following figure.
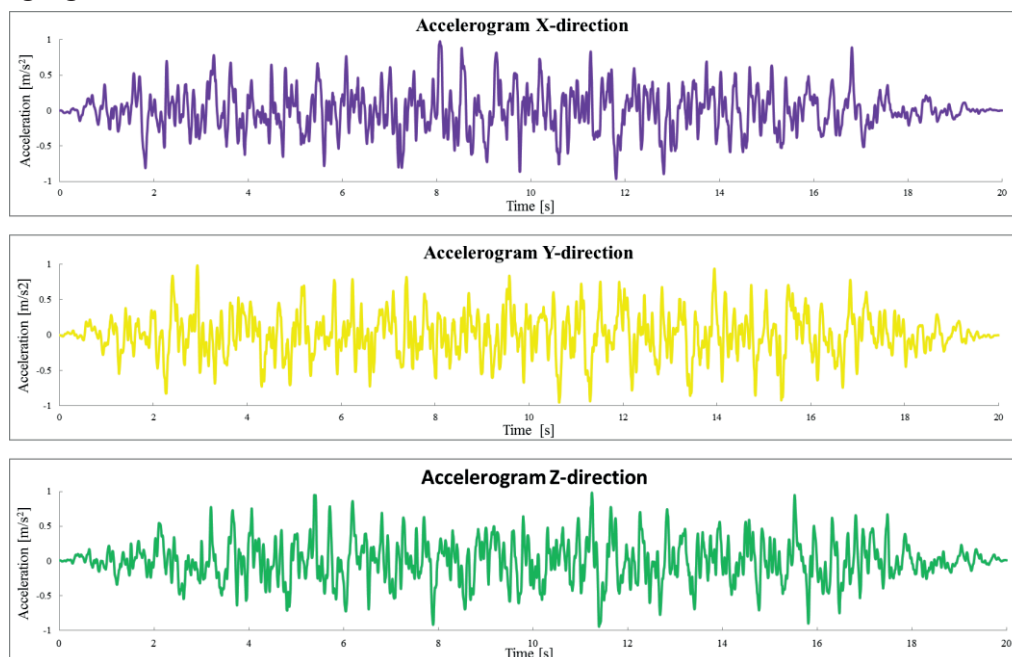
Figure 3: Accelerograms in x, y, z direction

The acceleration values are given on the interval of 0.01 s. All performed simulation used time steps with the same duration. With a total of 2000 time steps of 0.01 s, the total duration of the earthquake is 20 s.

The dynamic analysis is taking into account the Rayleigh damping effect. Raleigh dumping is based on assumption that damping is proportional to the stiffness and mass matrix of the structure. Here, a damping of 5% for the first two eigenfrequencies was considered.

Results

Eigenfrequencies

Table 3: Eigenfrequencies

Mode No.	Coarse mesh		Fine mesh	
	Frequency [Hz]	Period [s]	Frequency [Hz]	Period [s]
1	1.25	0.8000	1.26	0.7937
2	1.34	0.7463	1.32	0.7576
3	2.05	0.4878	2.01	0.4975
4	2.33	0.4292	2.36	0.4237
5	2.47	0.4049	2.50	0.4000
6	3.01	0.3322	3.00	0.3333
7	3.15	0.3175	3.17	0.3155
8	3.66	0.2732	3.65	0.2740
9	3.70	0.2703	3.70	0.2703

| 10 | 3.88 | 0.2577 | 3.88 | 0.2577 |

Mode Shape
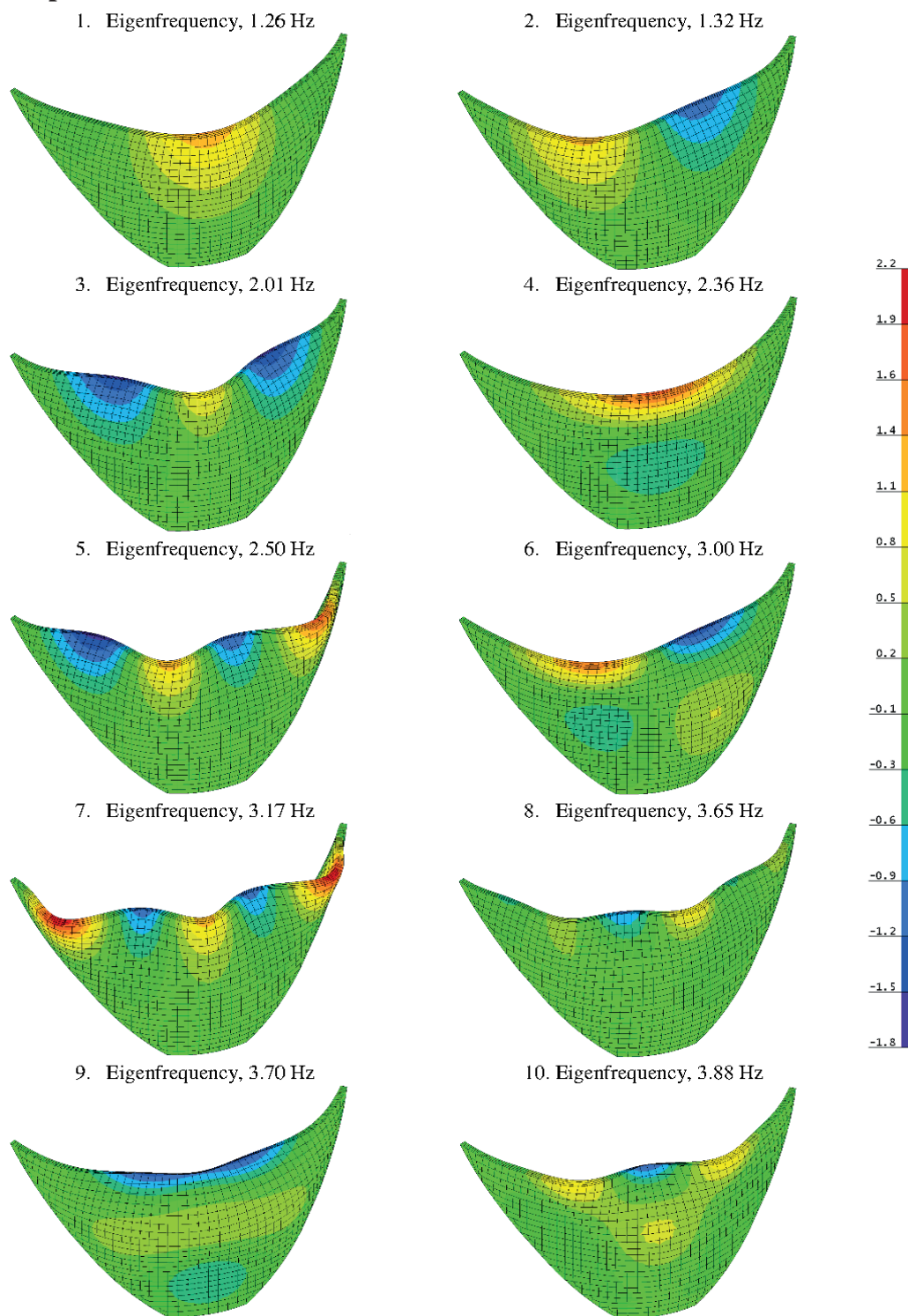
Figure 4: Radial deformation [mm] with mode shapes of the eigenfrequencies exaggerated by a factor of 17000

Stress Analysis

All evaluations of results of stresses were done for vertical stresses, hoop stresses, and where considered useful for principal stresses σ_1 and σ_3. Note that the vertical stresses shown are not

vertical with respect to a global coordinate system but vertical with respect to the element coordinate system. This means that the stresses shown are parallel to the element and dam surface.

Stresses due to Static loads
Stresses of static loads are presented separately for the load of self-weight and for the combination of self-weight and hydrostatic pressure load. They are presented for the upstream and downstream surface allowing checking if the model results are plausible.
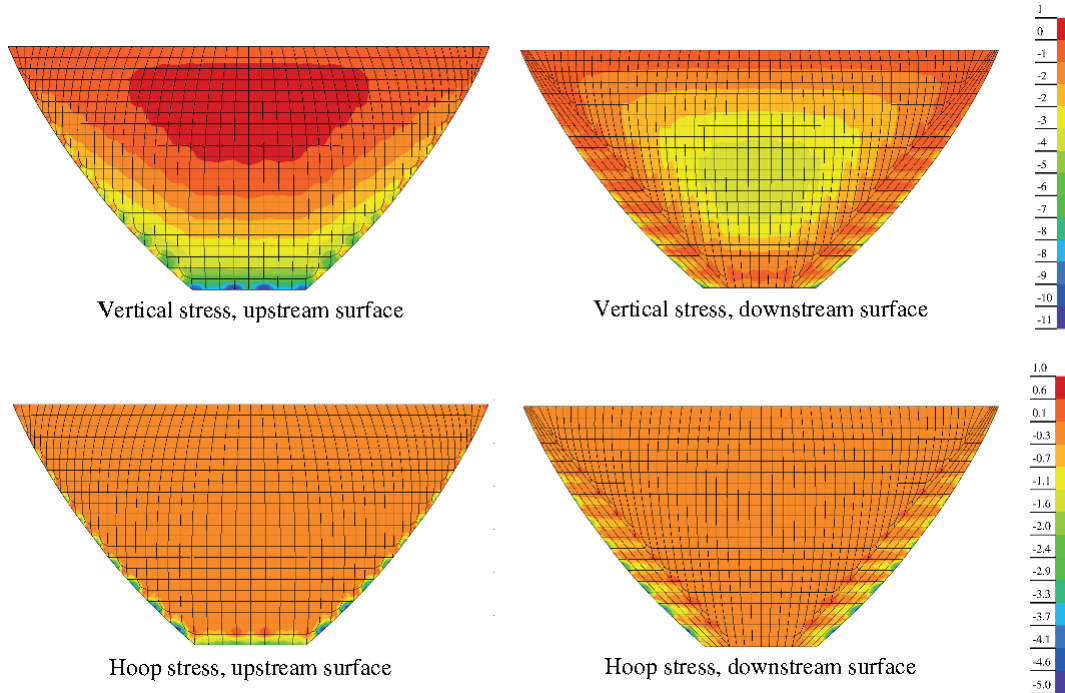
Figure 5: Vertical and hoop stresses [MPa] due to self-weight
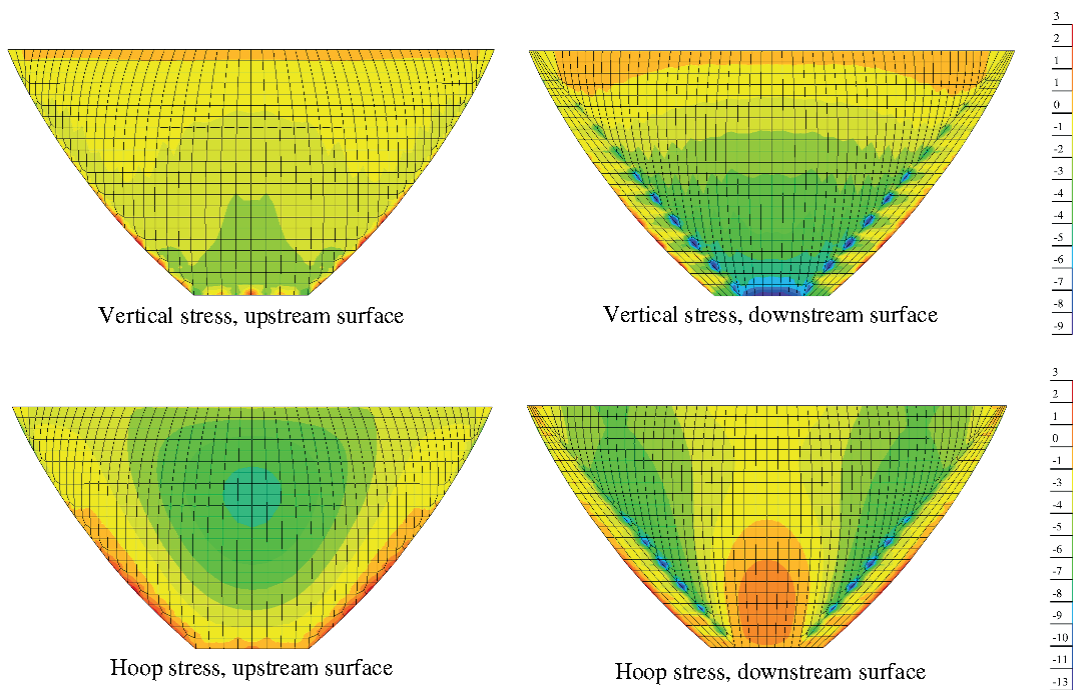
Figure 6: Vertical and hoop stresses [MPa] due to self-weight and hydrostatic pressure

Seismic stress-analysis depending on the time

Monitoring was performed for the vertical and hoop stresses for selected elements on the upstream and downstream face of the dam. There were selected three elements of both surfaces in three different heights at main cross section defined by the formulator, which is considered later (cf. Figure 10). On the figures below you can see the position of the elements at which stresses are monitored. Each of the figures shown below includes minimum (MIN) and maximum (MAX) stress observed at the selected elements (each of the selected elements includes 20 nodes). Note that these are the stress due to seismic loading only, self-weight and water load are not directly considered, water to a certain extend as the seismic loading affects the Westergaard masses as well.
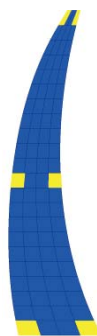
Figure 7: Monitored elements on main cross section
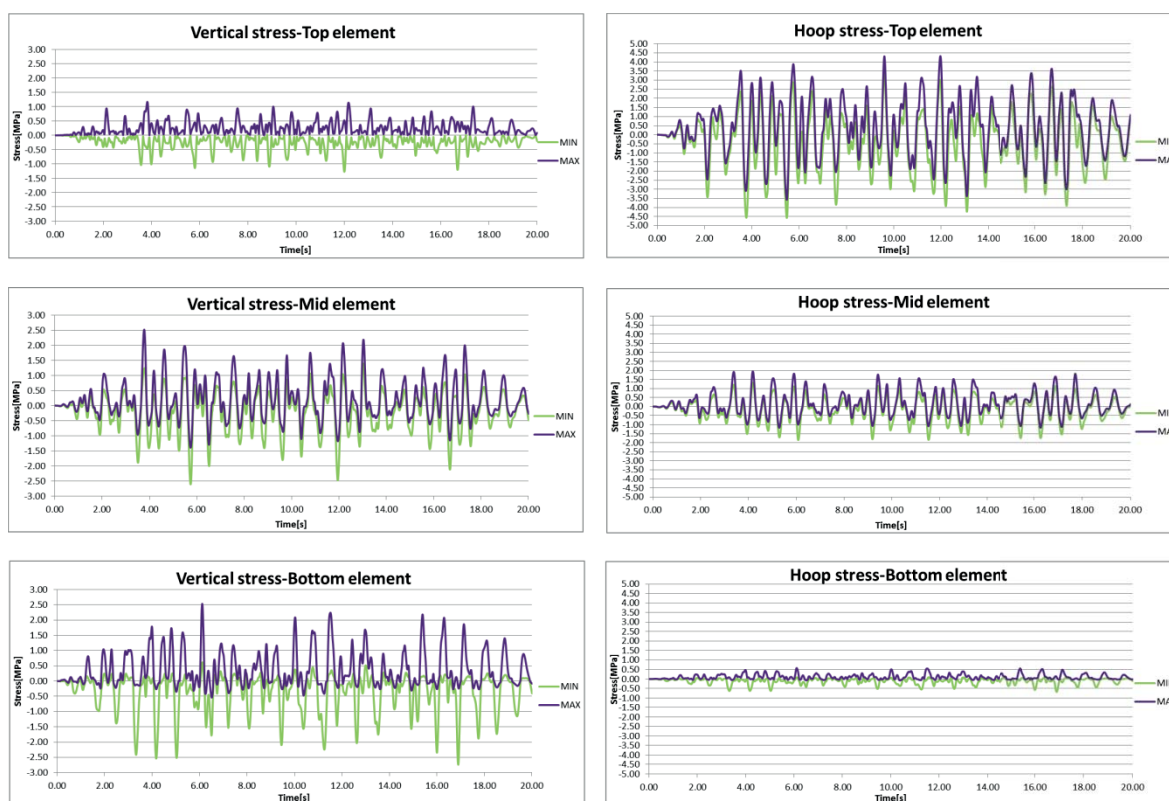
Figure 8: Time series of stresses observed at monitored elements on upstream surface
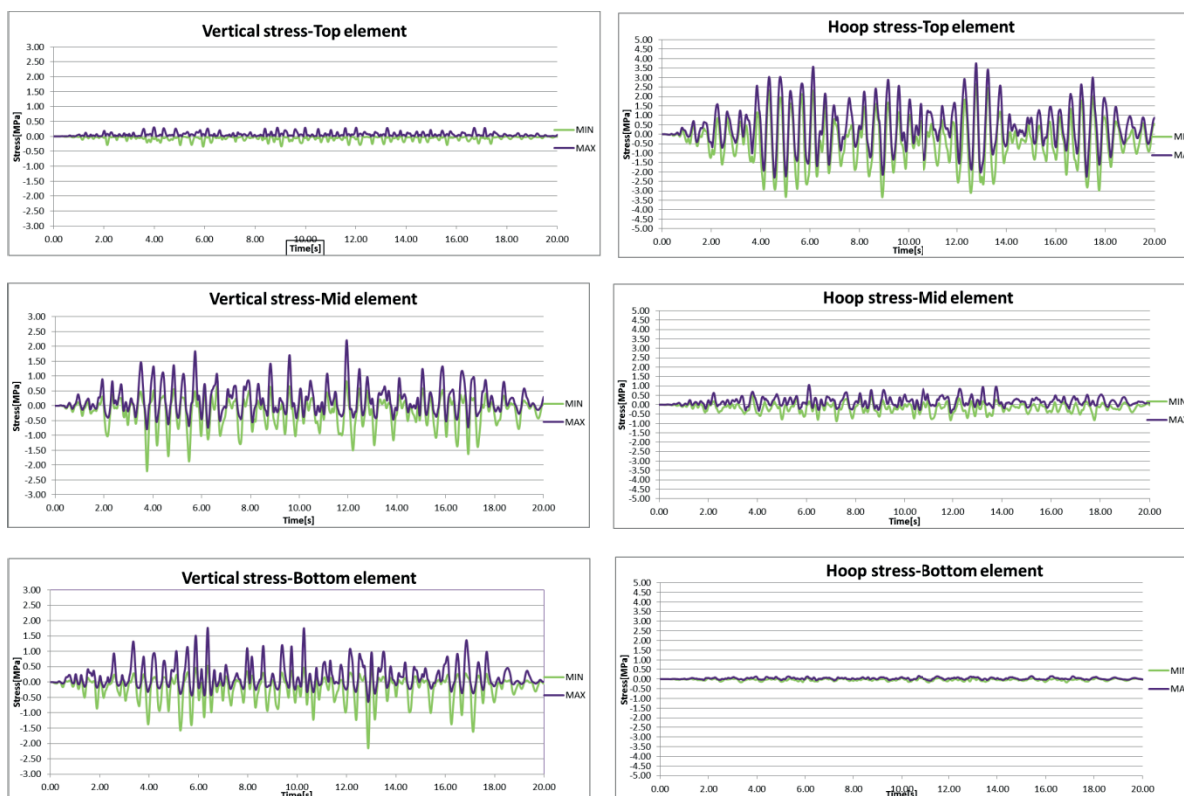
Figure 9: Time series of stresses observed at monitored elements on downstream surface

Evaluation of the stresses for three different cross sections

For three cross-sections, one in the center and two at each side halfway between the center and the right respectively left end of the dam, stresses over dam height are shown for the upstream and downstream surface. The three examined cross-sections are marked on the figure below.
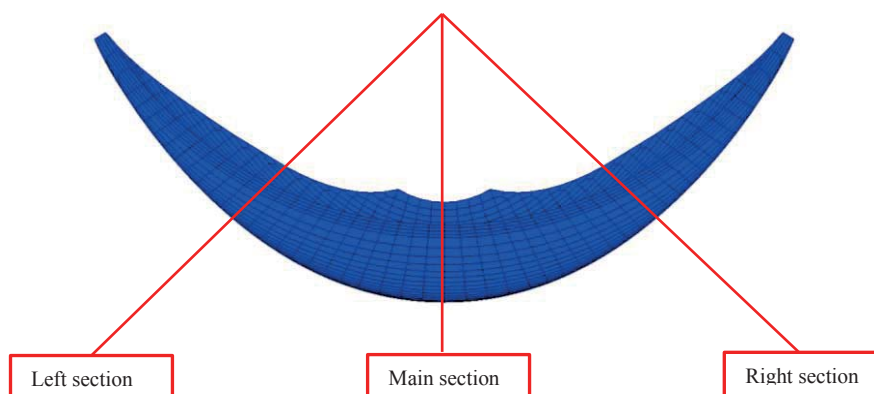
Figure 10: Layout of analyzed cross sections

The following loads respectively load combinations are plotted:

- Self-weight load - [SW]
- Self-weight + hydrostatic pressure load – Normal operating conditions – [NOC]
- Maximum of self-weight + hydrostatic pressure + seismic load – [MAX]
- Minimum of self-weight + hydrostatic pressure + seismic load – [MIN]

It should be noted that the last two evaluations, maximum and minimum, represent envelopes of stresses, i.e. this state of stress is artificial, because the maximum / minimum do not occur at all nodes at the same time.
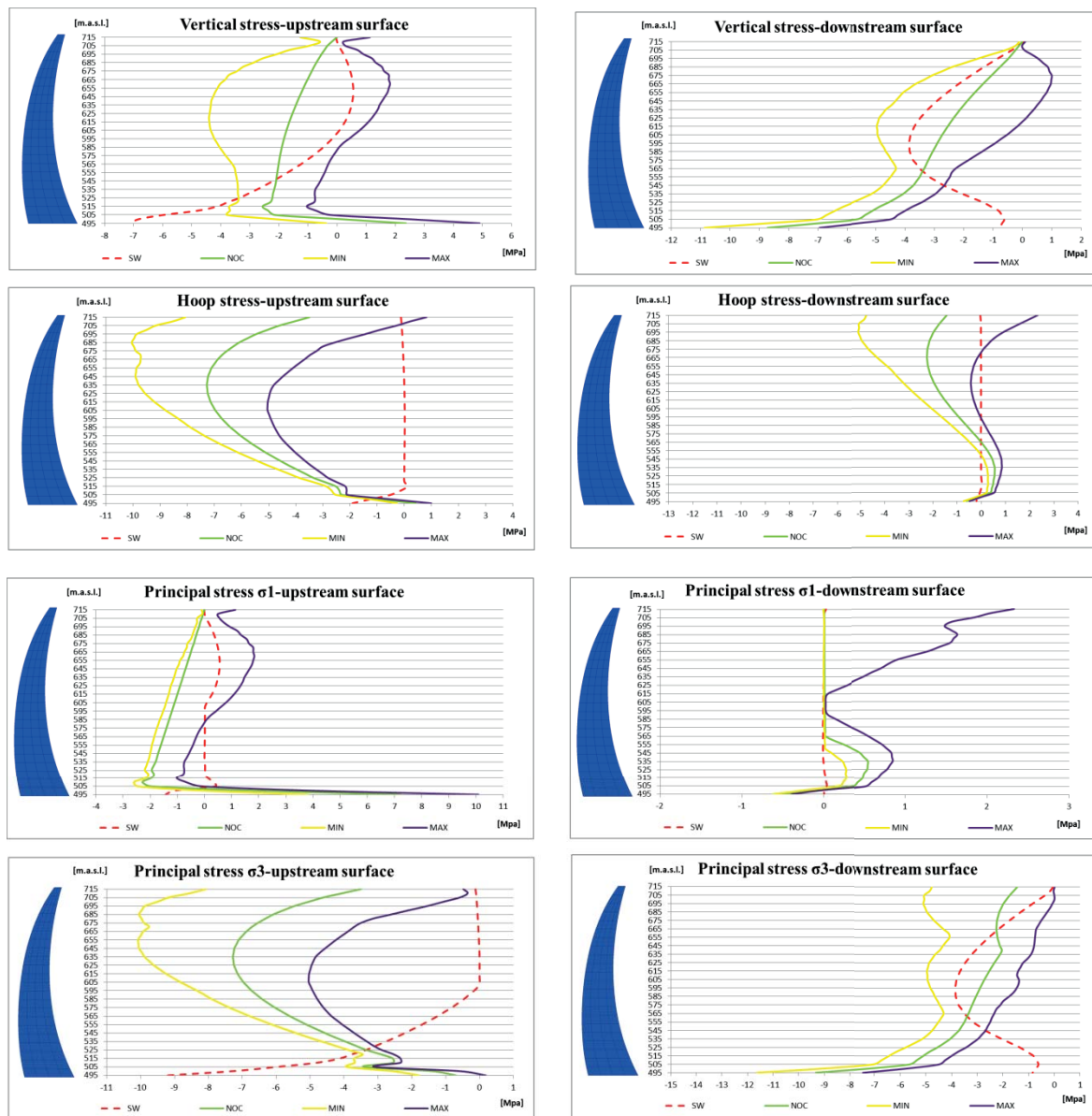
Figure 11: Stresses for main cross section
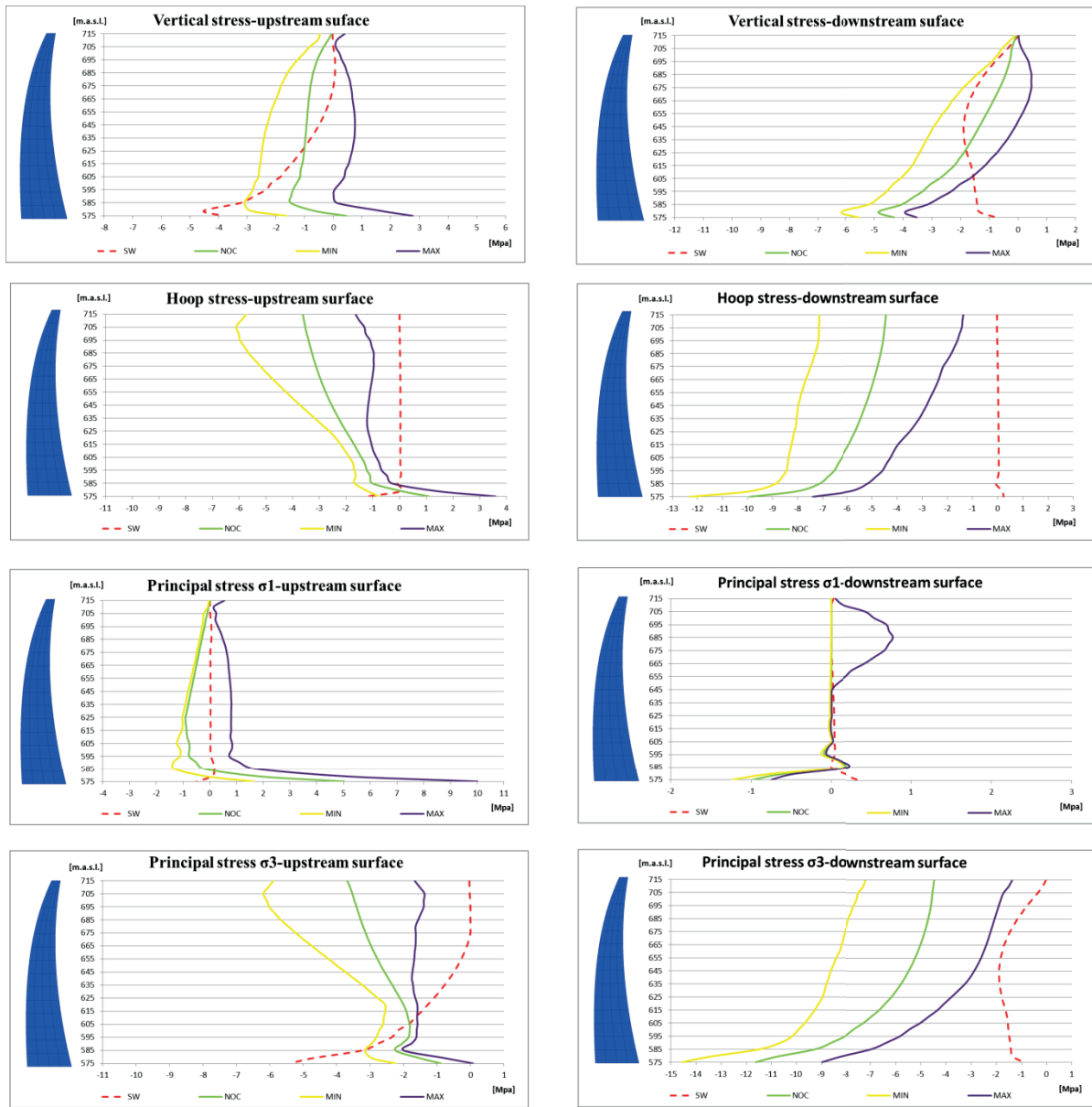
Figure 12: Stresses for left cross section
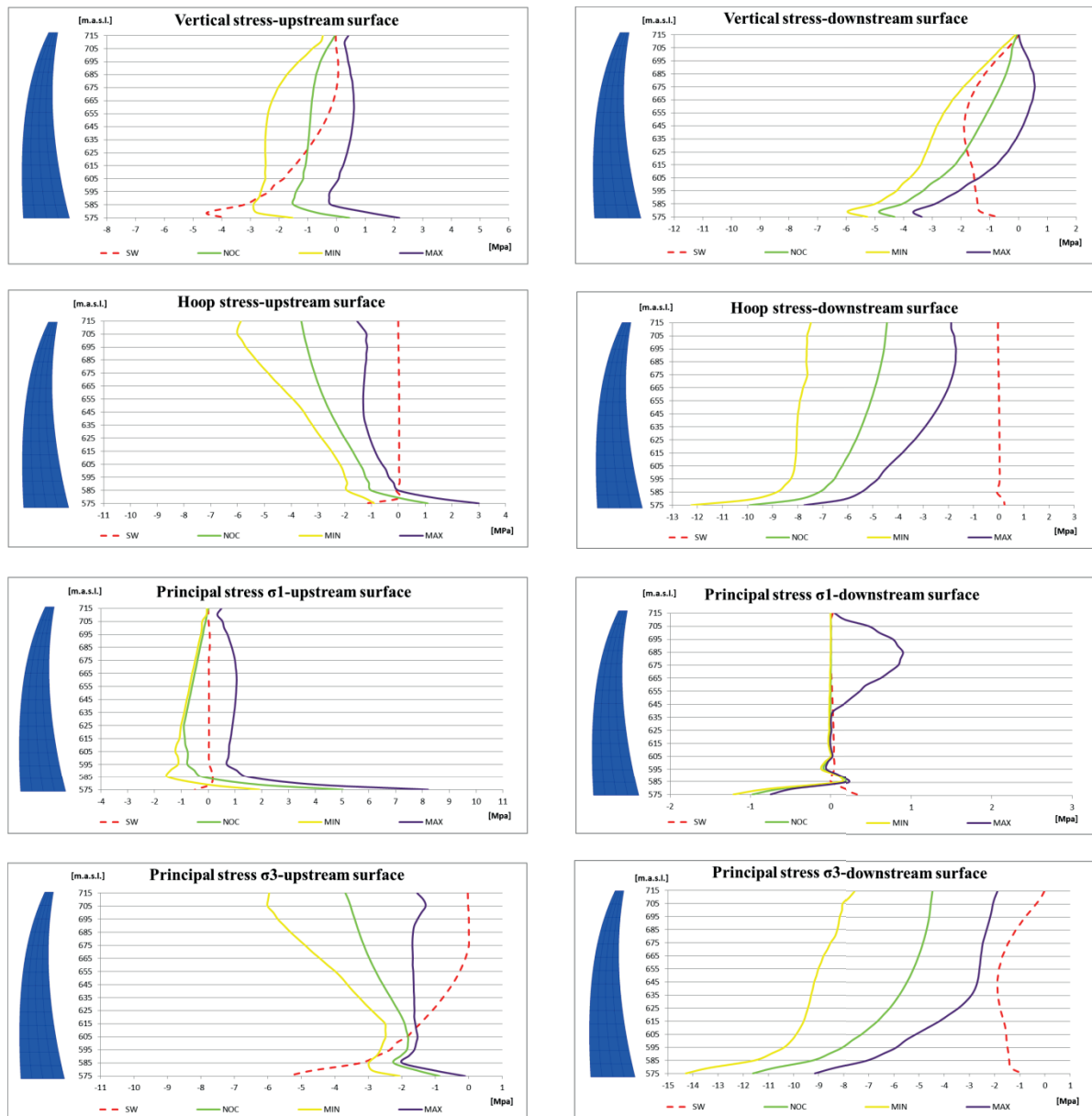
Figure 13: Stresses for right cross section

Radial Deformation

The evaluation of results of radial deformation was done considering the following sequences:
- Radial deformation due to the static loads
- Seismic radial deformation-analysis depending on the time
- Radial deformation analysis for three cross-section (cf. above)

Radial deformation of the static loads

Radial deformations of the static loads are presented separately for the load of self-weight and for the combination of self-weight and hydrostatic pressure load.
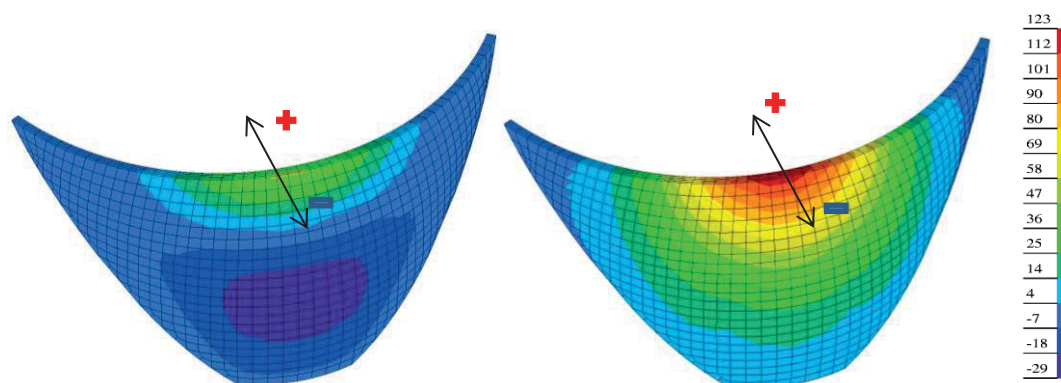
Figure 14: Radial deformation [mm] – self-weight (left), self-weight + hydrostatic pressure (right)

Seismic radial deformation-analysis depending on the time

Monitoring was performed for the radial deformation for selected nodes on the upstream face of the dam. There were selected three nodes of upstream surfaces in three different heights at the three cross section defined by the formulator (see Figure 10). On the figures below you can see the position of the nodes at which radial deformation are monitored. Note that these are the radial deformations due to seismic loading only, self-weight and water load are not directly considered, water to a certain extend as the seismic loading affects the Westergaard masses as well.
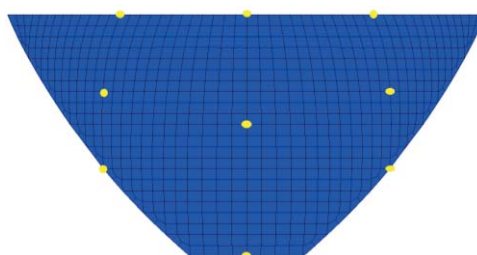
Figure 15: Monitored nodes on upstream surface
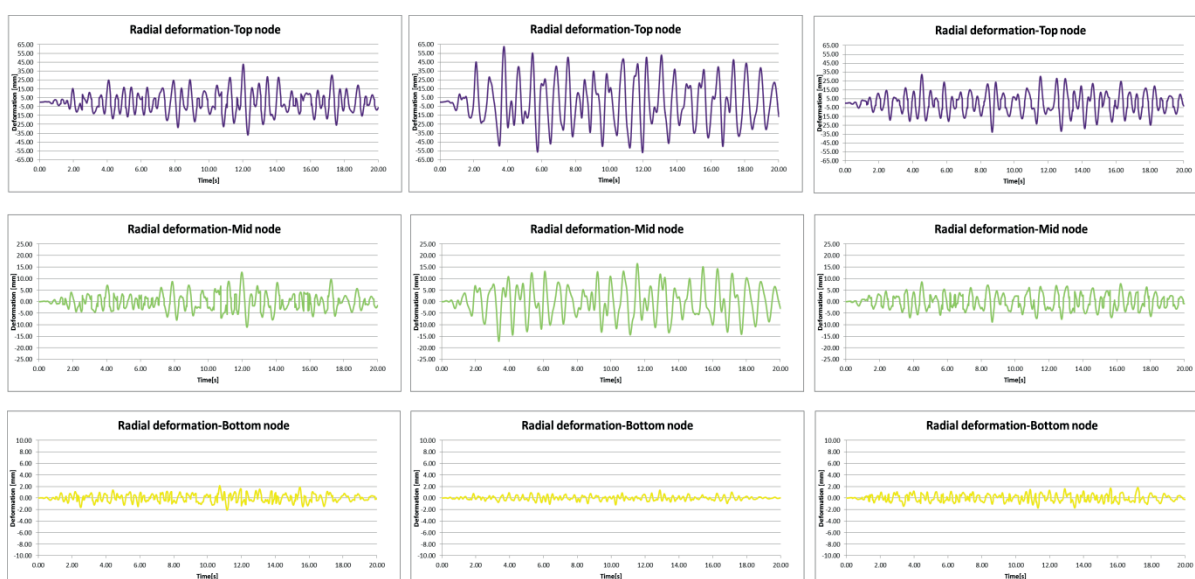
Figure 16: Radial deformation for left, main and right cross section respectively

161

Radial deformation at the three cross sections

For the three cross-sections the radial deformations over height are plotted. Evaluation of the radial deformation is given for the following loads respectively combination of loads:

- Self-weight load - [SW]
- hydrostatic pressure load – Normal operating conditions – [NOC]
- Maximum of hydrostatic pressure + seismic load – [MAX]
- Minimum of hydrostatic pressure + seismic load – [MIN]

These combinations mimic the observations of a pendulum.
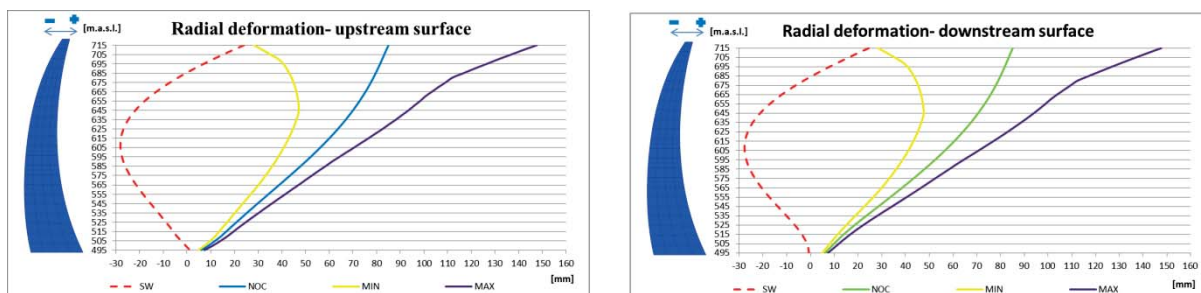
Figure 17: Radial deformation – main cross section
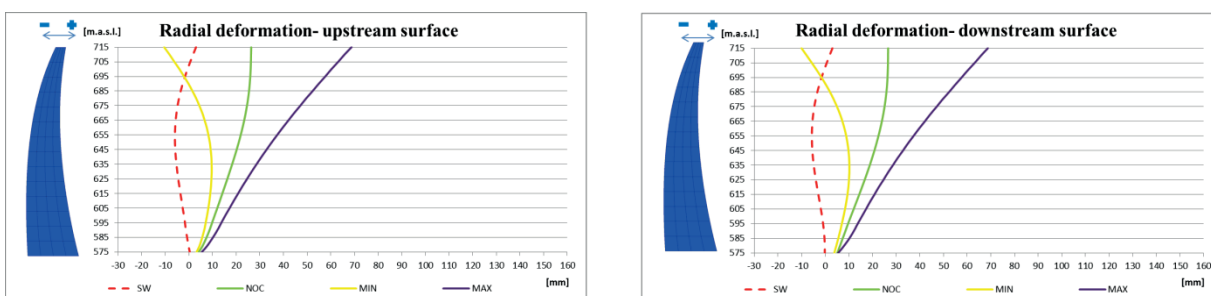
Figure 18: Radial deformation – left cross section
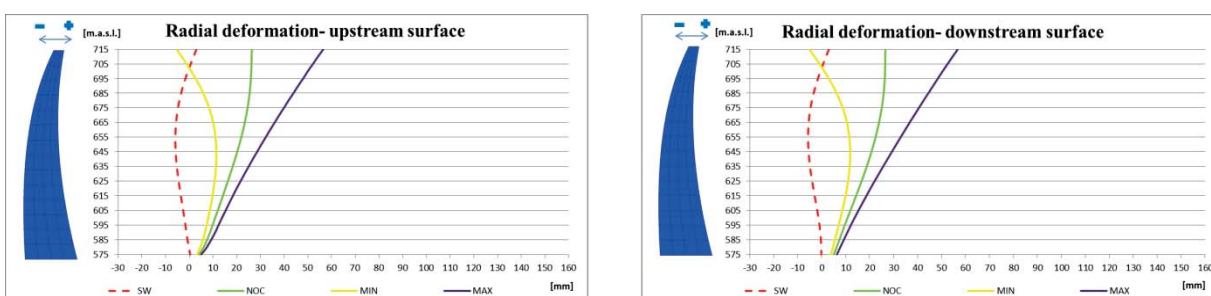
Figure 19: Radial deformation – right cross section

Discussion and Summary

Stress-strain analysis of arch dam during seismic activity including reservoir-structure interaction using added masses technique according to generalized Westergaard approach is presented. Interaction of an arch dam with the impounded water leads to an increase in the dam vibration periods. The fact that water moves with the dam increases the total mass that is in motion. This added mass increases the natural periods of the dam, which in turn affects on the effective earthquake inertia forces. The Westergaard method usually gives the largest

added-mass values, which is evident by its increasing the vibration periods the most. However, this does not automatically give the largest stresses, because response of the dam also depends on the characteristics of the earthquake ground motion. Although Westergaard approach is widespread in practice, for different variants of quasi-static and dynamic analysis of seismic effects, the above-mentioned facts lead to the conclusion that the results must be taken with caution.

After comparison of two different sizes of spatial discretization of meshes we can conclude, that the coarser mesh also gives satisfactory results which can be used in engineering practice. In fact, the differences are small. Whereas the performed simulations with linear material behavior are not very costly in terms of computation time and required computer power for both meshes, the coarser mesh could be very useful as soon as more complex processes, e.g. non-linear material behavior, are to be considered.

Maximum earthquake stresses are located in the central upper portion of the dam as well along the dam-foundation contact zone. Maximum radial deformation occurs in the crest, and decreasing towards lateral sides, as well as towards fixed end.

The vertical stresses observed at the upstream surface show some artefacts for the load cases with the earthquake as they are supposed to be zero at the top of the dam like it is observed for self-weight and self-weight with hydrostatic pressure. These non-zero values are considered to be artefacts. The same artefact in a much smaller magnitude is seen at the top of the downstream surface.

Stress time histories curves shows several significant tensile stress cycles that can lead to open the contraction joints, especially in crown zone, while on the time histories of radial deformation in addition to timing of deformation could be noted as dominant periods of the first few natural frequencies.

The results that are shown have been compared to typical deformations observed at Swiss dams. The overall behavior of the dam here is in good agreement with what AF has seen in reality. The comparison of the results of the earthquake simulations with previous studies of this type performed at AF was positive.

We can conclude that the added mass technique in combination with the direct dynamic analysis relatively quickly and easy produce results useful in engineering practice.

Acknowledgements

References

[1] Graz University of Technology, Institute of Hydraulic Engineering and Water Resources Management, 12th International Benchmark Workshop on Numerical Analysis of Dams, 2.-4. OCTOBER, 2013, GRAZ – AUSTRIA, THEME A - Fluid Structure Interaction Arch Dam – Reservoir at Seismic loading. Download from http://portal.tugraz.at/portal/page/portal/Files/i2130/Icold_bmws2013/Theme_A/Files_and_Information_Theme_A.zip, 23.07.2013

[2] FENAS, Walder + Trüeb Engineering AG. (2013). Walder + Trüeb Engineering AG. http://www.waldertrueb.ch/index.php?id=23&L=2%3Fcomply, 23.07.2013

[3] Ghanaat, Y. (1993). Theoretical Manual for Analysis of Arch Dams. US Army Corps of Engineers. http://www.dtic.mil/dtic/tr/fulltext/u2/a269682.pdf, 24.07.2013

[4] Kuo, J. (1982). Fluid-structure interactions: Added mass computations for incompressible fluid. Earthquake Engineering Research Center. Berkeley: University of California.

Fluid Structure Interaction
Arch Dam-Reservoir at Seismic Loading

S. Shahriari[1]

[1] Institute of Hydraulic Engineering and Water Resources Management, Stremayrgasse 10/2, A-8010 Graz, AUSTRIA

E-mail: shervin.shahriari@student.tugraz.at

Abstract

In the present paper, a direct time domain procedure is used for dynamic linear analysis of the coupled arch dam-reservoir-foundation system. The hydrodynamic force on the upstream face of the dam is modeled by added mass method and compressible fluid elements for comparison. The concrete and massless foundation rock was assumed to be linear elastic. Connection between dam and foundation is modeled by coupling all DOF of the corresponding nodes. Also, viscous damping was applied to the materials by using Rayleigh-Damping. Numerical results showed that the different modeling techniques of the interaction lead to different response of the system and stress distribution in the dam's body. Modeling the interaction by added mass method, increases the period of the system as well as overestimating or underestimating the stresses compare to the model with fluid elements.

Conclusion

The following conclusions are drawn based on the numerical experiments conducted herein:

- Choosing appropriate damping parameters is a very important step in the dynamic analysis of the dam-water-foundation system. Underestimating the system's damping by choosing higher than 7th angular frequency as the second frequency for calculation of Rayleigh-Damping parameters can lead to overestimating the stresses in the model.

- Modal responses of the dam-water-foundation system are calculated using the finite element software, ANSYS. The results showed that the eigenfrequencies from the model with added mass approach were lower than those calculated from the model which utilized acoustic element to model the reservoir.

- Direct time integration procedure is used for dynamic analysis of the system and deformations and stresses are calculated for static and dynamic load cases. Maximum deformation due to static loading was 7.4 cm at the crest level followed by the maximum deformation of 13.6 cm after dynamic analysis. The tensions in arch dams are not desirable; therefore, the tension stresses were studied. Evaluation of hoop stresses indicated that there is no significant tension developed in the main section with maximum value of 0.6 MPa. Furthermore, the maximum tension stress value in the U/S face of the right and left sections is higher than the main section(S=3.6 MPa). Vertical stresses evaluation showed that the maximum tension was occurred at the base of the U/S face of the main section and found to be 6.69 MPa. Also, the maximum compression stress is developed (S=12.5 MPa) at 180 m from the foundation level of the U/S face of the main section.

The Seismic behaviour of an Arch Dam-Reservoir-Foundation System

A. Frigerio[1] and G. Mazzà[2]

[1] Ricerca sul Sistema Energetico – RSE S.p.A., via R. Rubattino 54, Milan, ITALY

E-mail: antonella.frigerio@rse-web.it

Abstract

The paper summarizes the main features and the related results of the linear static, modal and seismic analyses carried out on the concrete arch dam proposed as Theme A of the 12th ICOLD International Benchmark Workshop.

The analyses have been performed by means of the COMSOL Multiphysics software, making reference to the coarse finite elements mesh provided by the Formulators, but some slightly changes.

In the modal and dynamic analysis, the water-dam-foundation interaction has been taken into account. The impounded water has been modeled by means of acoustic finite elements, assuming appropriate boundary conditions to simulate the wave reflecting conditions between the fluid and the foundation, as well as the fluid and the upstream face of the dam, and the non-reflecting condition at the end of the reservoir channel.

Results have been provided according to the requests of the Formulators in terms of radial displacements, hoop and vertical stresses on three vertical sections of the dam.

Introduction

Seismic analyses have been proposed and discussed during some of the first Benchmark Workshops organized by the Committee on Computational Aspects of Analysis and Design of Dams [1,2]. Hence, it appears appropriate the proposal of the present seismic analysis of a large arch dam, [3], in order to verify the possible improvements both on the modeling and on the computational aspects.

In the present paper, all the analyses have been carried out with COMSOL Multiphysics, a software that allows modeling and simulating any physics-based system. In particular, the COMSOL Acoustic, [4], and Structural Mechanics Modules, [5], have been used.

In the following paragraphs the geometrical and physical model will be described and the results will be provided according to the requests of the Formulators.

Geometrical and physical model

The coarse Finite Element mesh provided by the Formulators, [3], has been slightly modified in order to have an exact geometrical match at the interface between the nodes of the fluid and those of the foundation rock.

The reservoir and the foundation domains have been extended upstream to avoid possible numerical influences of the non–reflecting water surface at the end of the reservoir on the dynamic response of the dam under seismic loading conditions.

Finally, the finite elements of the central vertical sections of the dam have been refined to discretize with a more regular grid the whole mesh of the dam (Figure 1).

The displacement field of each finite element of the numerical model has been discretized with quadratic shape functions.
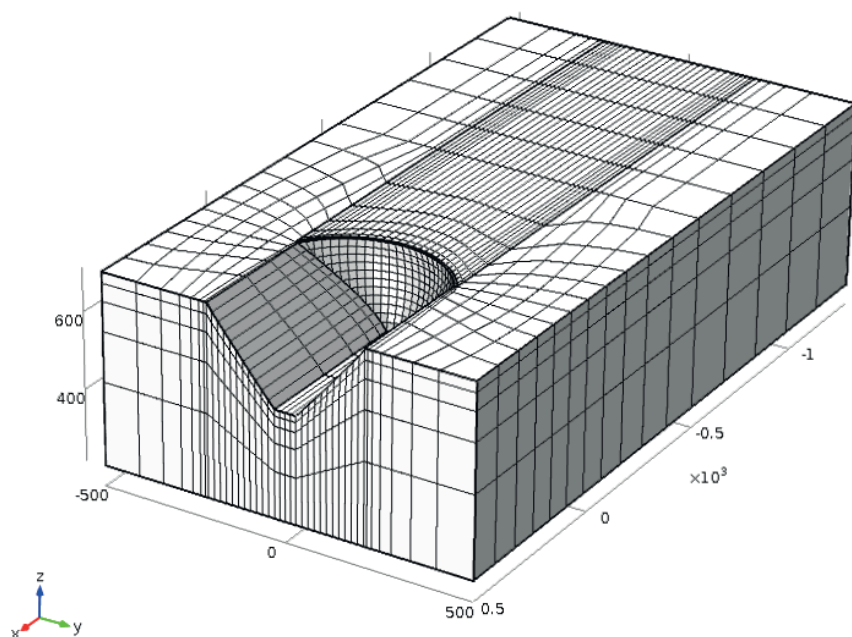
Figure 1: The coarse mesh used to study the dam-reservoir-foundation system

Material properties
Linear elastic constitutive models have been assigned to the dam and the foundation rock. The physical-mechanical properties are summarized in Table 1.

Table 1: Concrete and rock properties

Domain	Material	Density [kg/m³]	Poisson ratio	Young modulus [MPa]
Dam	Concrete	2400	0.167	27000
Foundation	Rock	0	0.200	25000

The Rayleight damping model has been taken into account to define the dam behavior during seismic loading conditions. Assuming a 5% structural damping ratio, the mass and stiffness damping parameters of the Rayleight formulation are as follows:

$$\alpha = 0.94; \beta = 2.65\text{E-}03$$

The reservoir has been discretized by means of acoustic finite elements whose properties are reported in Table 2.

Table 2: Water properties

Domain	Material	Density [kg/m³]	Speed of sound in water [m/s]	Bulk modulus [MPa]
Reservoir	Water	1000	1500	2200

Loading and boundary conditions
According to the formulation of the Theme A, the following loadings sequence has been considered:

- Dead loads
- Hydrostatic water pressure with the maximum water level equal to the dam crest height (i.e. 715 m a.s.l.)
- Seismic loads, provided by the Formulators in terms of accelerations along the three Cartesian directions.

Different boundary conditions have been used for the foundation domain depending on the type of the analysis performed. In case of static and modal analyses, symmetric conditions have been applied to the lateral rock walls whereas fixed constraints have been assigned to the basement rock. In seismic analysis, the accelerations - or the equivalent related displacement varying in time - have been applied to the lateral and bottom surfaces of the foundation.

In modal and seismic analyses, the fluid domain has been modeled by means of acoustic elements, assigning the following boundary conditions:

- Dam-reservoir interface (refer to the COMSOL "node" *acoustic-structure boundary*, [4]):
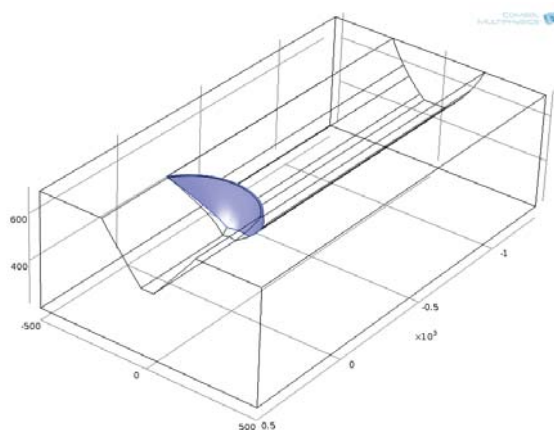
$$-n \cdot \left(-\frac{1}{\rho}(\nabla p - q_d) \right) = -n \cdot u_{tt} \qquad (1)$$

$$\sigma \cdot n = p\, n \qquad (2)$$

where n is the normal to the interface, ρ the water density, p the fluid "acoustic" pressure, q_d the dipole source (equal to zero in the present case), u_{tt} the acceleration field of the structural domain at the fluid interface and σ the stresses tensor.

- Foundation-reservoir interface (refer to the COMSOL "node" *impedance*, [4]):
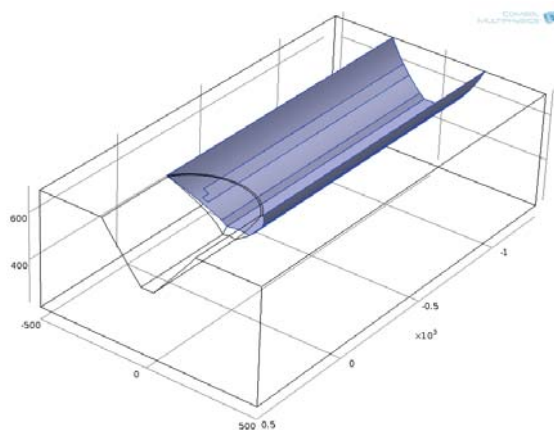
$$-n \cdot \left(-\frac{1}{\rho}(\nabla p - q_d) \right) = \frac{1}{Z_i}\frac{\partial p}{\partial t} \qquad (3)$$

where n is the normal to the reservoir-foundation interface, ρ the water density, p the fluid "acoustic" pressure, q_d the dipole source (equal to zero in the present case), Z_i the acoustic input impedance assumed equal to:

$$Z_i = \rho/q \tag{4}$$

being q a damping coefficient that characterizes the effects of absorption of the hydrodynamic pressure waves at the boundary, according to the following equation [6]:

$$q = \frac{1}{c} \frac{1-\alpha}{1+\alpha} \tag{5}$$

α is the wave reflection coefficient that accounts for the behavior of the absorption of hydrodynamic pressure waves at the boundary, whereas c is the speed of sound in water. According to some literature case studies, α has been considered equal to 0.75, [7].

- Upstream-reservoir surface (refer to the COMSOL "node" *plane wave radiation*, [4]):
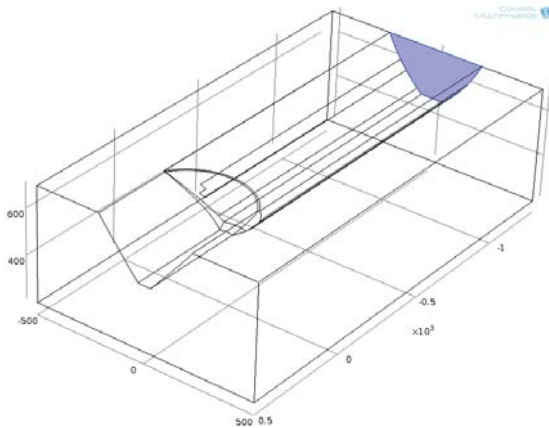
$$-n \cdot \left(-\frac{1}{\rho}(\nabla p - q_d) \right) + \frac{1}{\rho}\left(\frac{1}{c}\frac{\partial p}{\partial t} \right) = Q_i \tag{6}$$

where n is the normal to the reservoir-foundation interface, ρ the water density, p the fluid "acoustic" pressure, q_d the dipole source (equal to zero in the present case), c is the speed of sound in water and Q_i the monopole source (equal to zero in the present case).

- Free surface (refer to the COMSOL "node" *sound soft boundary*, [4]):
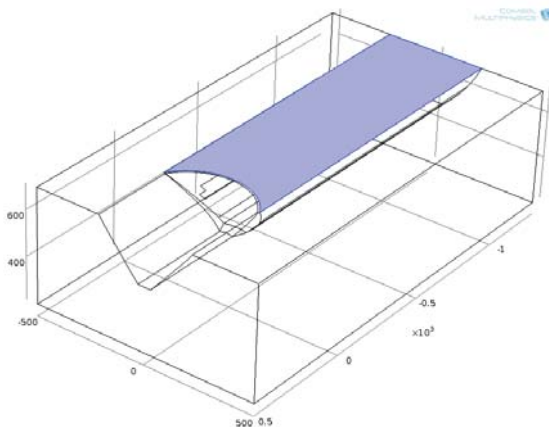
$$p = 0 \tag{7}$$

Numerical analyses

In the following paragraphs the main features of each numerical analysis will be provided, specifying the assumed hypotheses.

Static analysis

A linear static analysis has been carried out in order to apply the dead load and the hydrostatic water pressure, thus the water domain has not been included in the geometrical model.
The applied boundary conditions are reported in the previous paragraph.

Modal analysis

The first 10 eigenfrequencies of the dam have been computed taking into account the dam-reservoir interaction.
The applied boundary conditions are reported in the previous paragraph.

Seismic analysis

Seismic analyses in time domain are generally carried out considering a massless foundation and applying a spatially-uniform ground motion directly at the basement rock.
In the present paper, at first an ordinary differential equations problem has been solved, making reference to the foundation domain only, in order to compute the displacements associated to the earthquake motions (Figure 2). In the subsequent dynamic analysis, these displacements have been applied to the bottom and lateral rock walls to calculate the dynamic response of the dam-reservoir-foundation system.
This procedure has been chosen because it allows computing easily the relative displacements of the system; anyway, as an alternative, the same results could be attained applying directly the accelerations to the foundation boundaries.
The boundary conditions taken into account during the seismic analysis are reported in the previous paragraph.
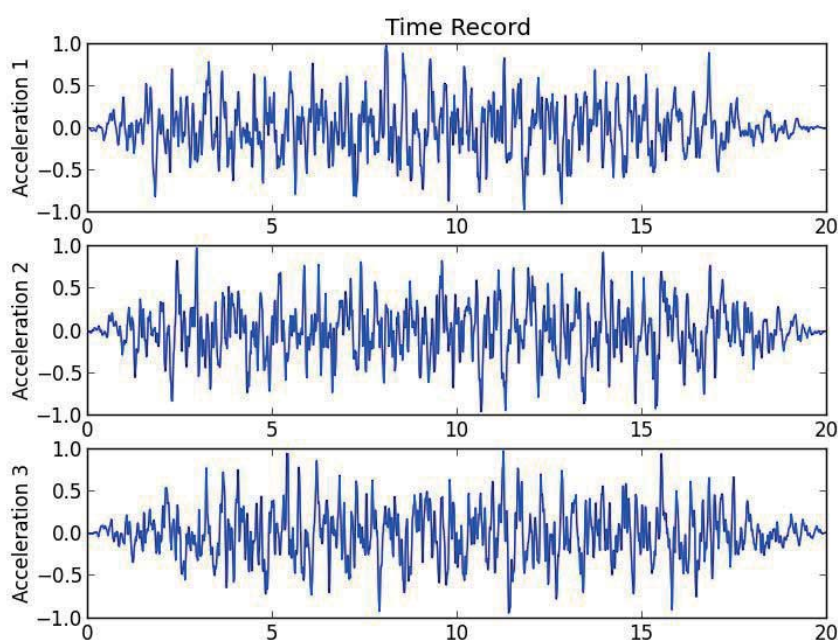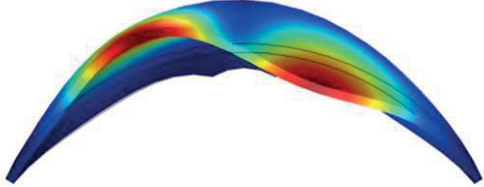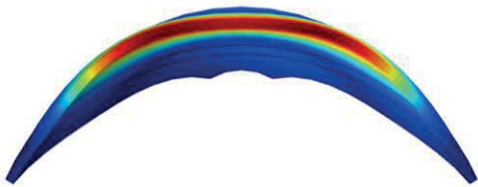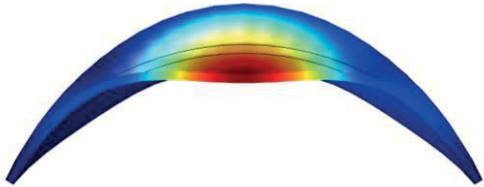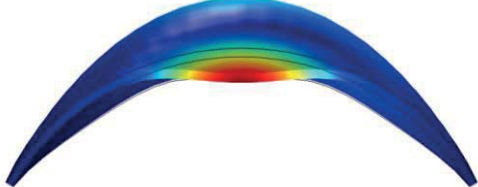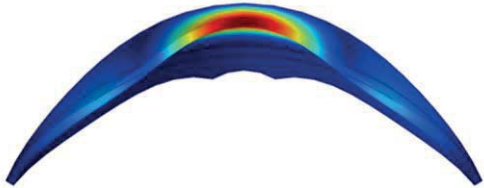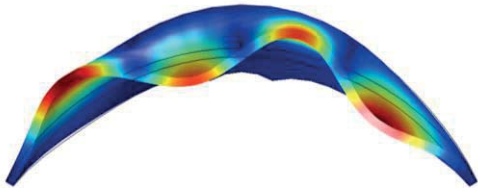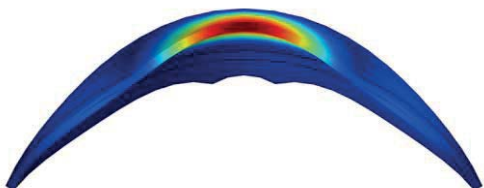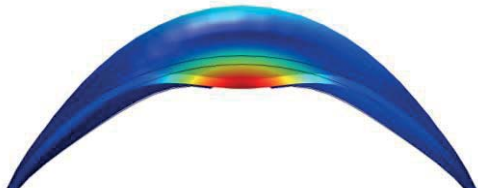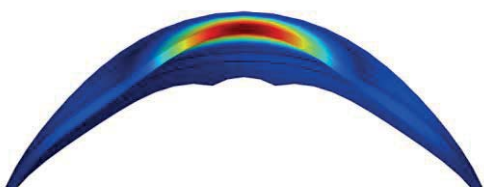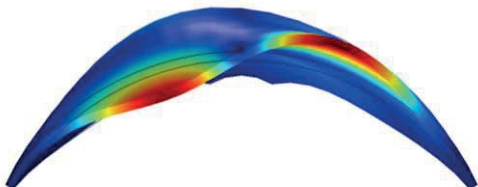
Figure 2: Acceleration time history ($a_{max} \sim 0.1g$)

Results

With reference to the results of modal analysis, the first 10 eigenfrequencies and the related modal shapes are reported in Table 3.

Table 3: Eigenfrequencies and modal shapes

1	1.54247 [Hz]	6	2.51800 [Hz]
2	1.55194 [Hz]	7	2.83905 [Hz]
3	2.09799 [Hz]	8	2.96151 [Hz]
4	2.22299 [Hz]	9	3.19079 [Hz]
5	2.33002 [Hz]	10	3.37707 [Hz]

According to the requests specified by the Formulators, the results of the static and seismic analyses are provided in terms of radial displacements [m], hoop and vertical stresses [MPa] on the upstream and downstream faces of three vertical sections of the dam.

Table 4: Upstream face – Central section (US-C) – Radial displacements, hoop and vertical stresses
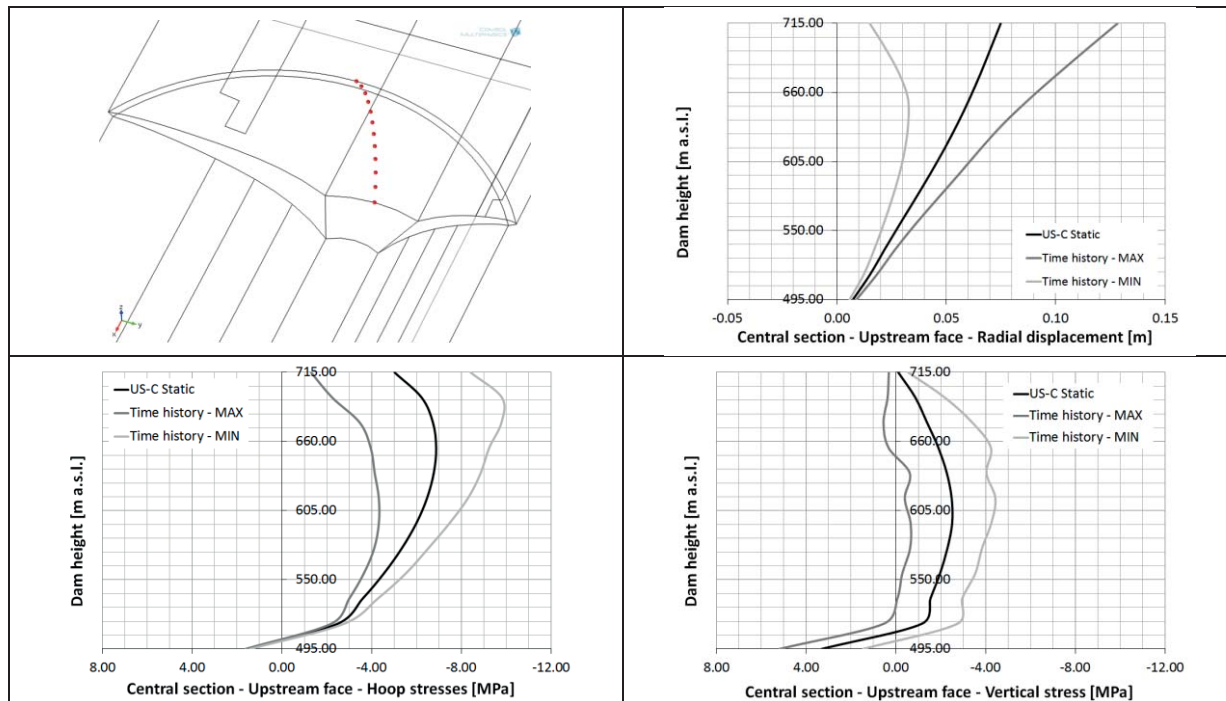
Table 5: Downstream face – Central section (DS-C) – Radial displacements, hoop and vertical stresses
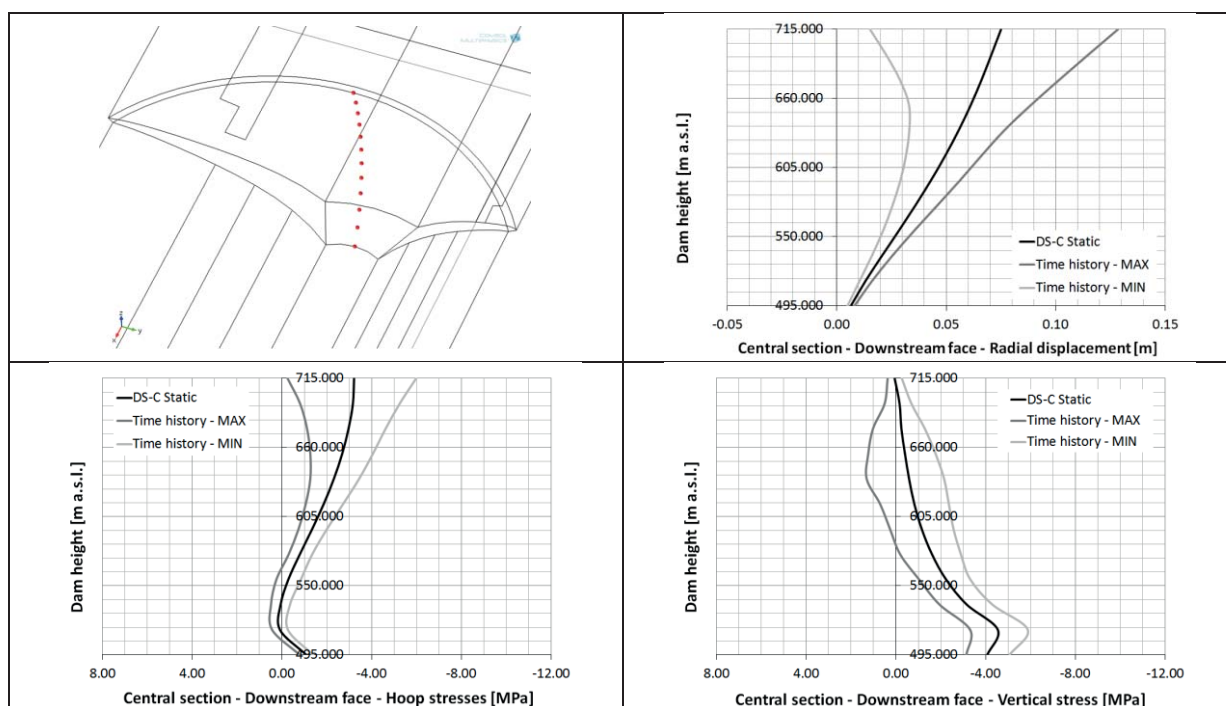
Table 6: Upstream face – Right section (US-R) – Radial displacements, hoop and vertical stresses
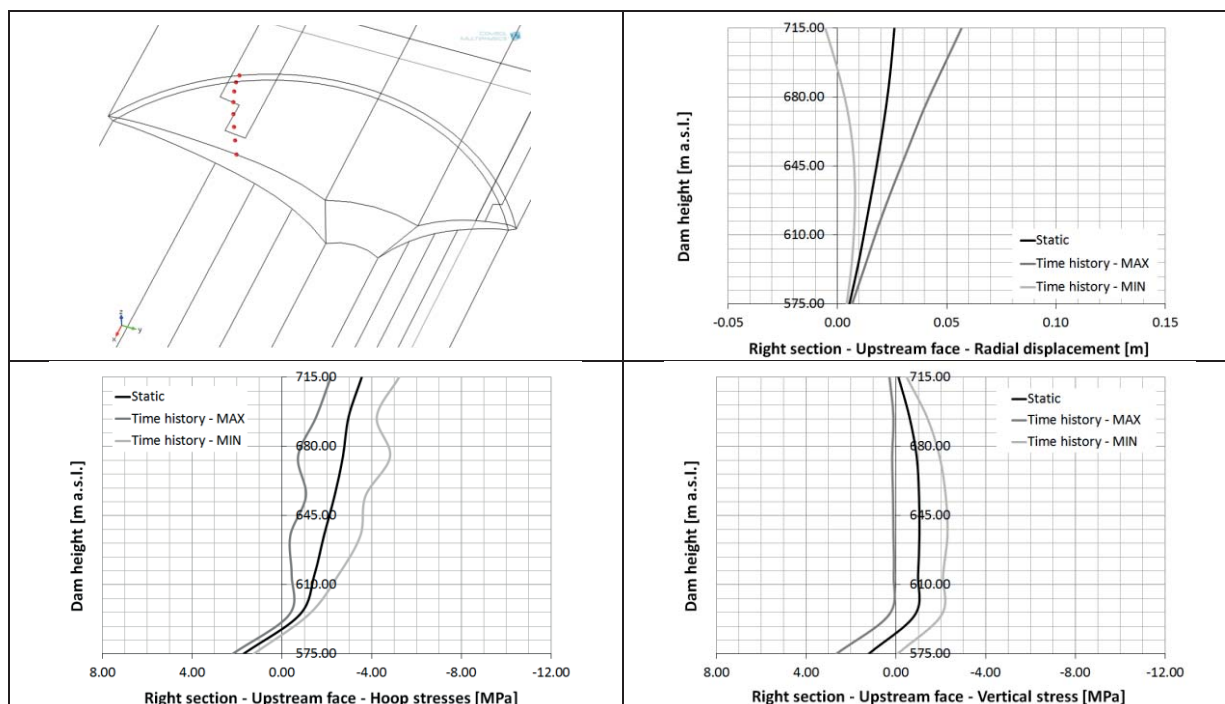
Table 7: Downstream face – Right section (DS-R) – Radial displacements, hoop and vertical stresses
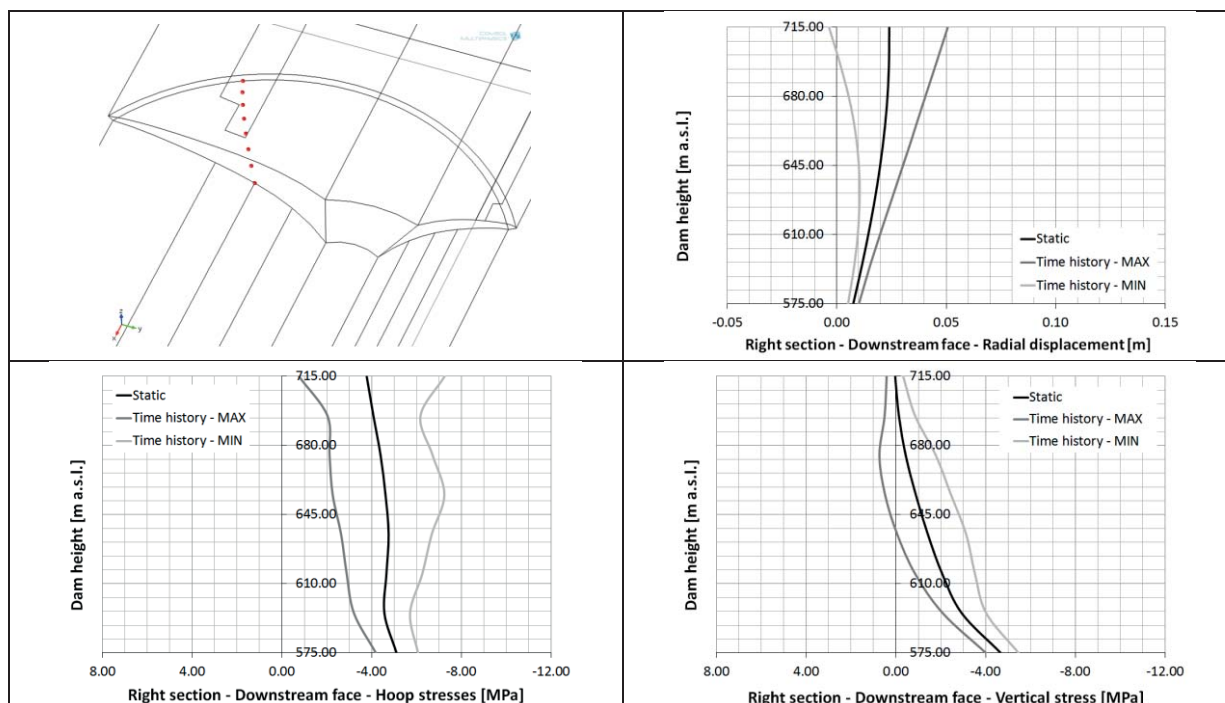
Table 8: Upstream face – Left section (US-L) – Radial displacements, hoop and vertical stresses
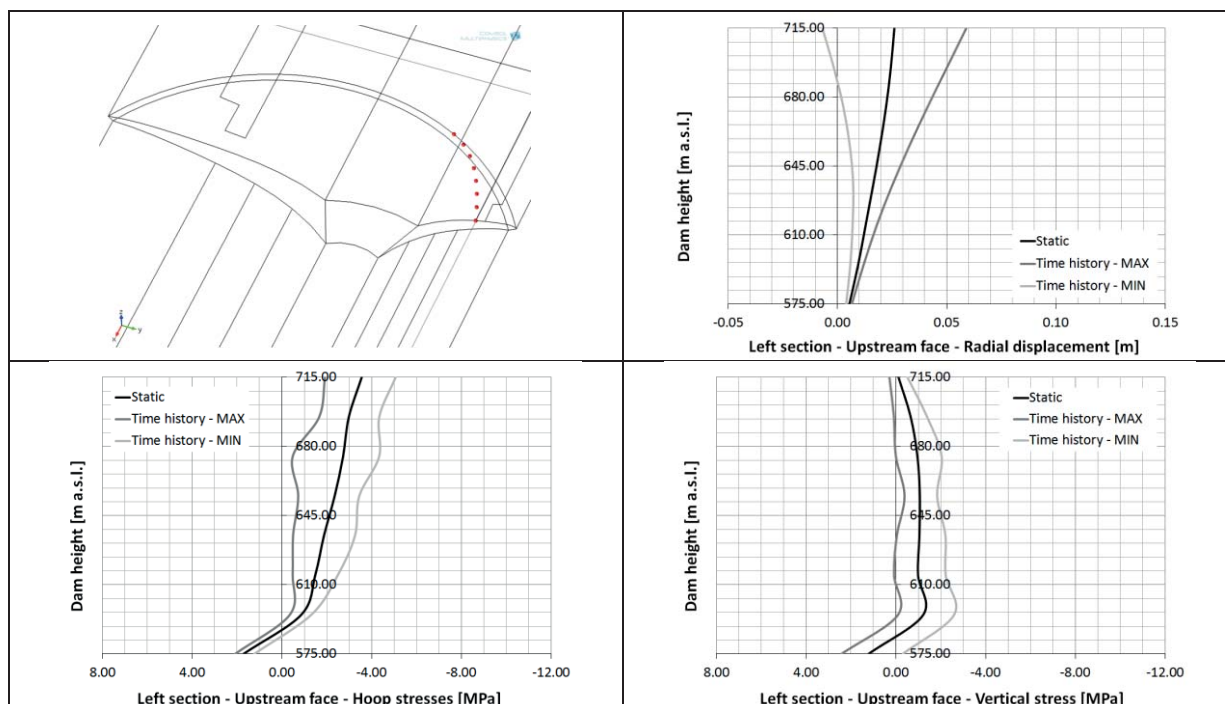
Table 9: Downstream face – Left section (DS-L) – Radial displacements, hoop and vertical stresses
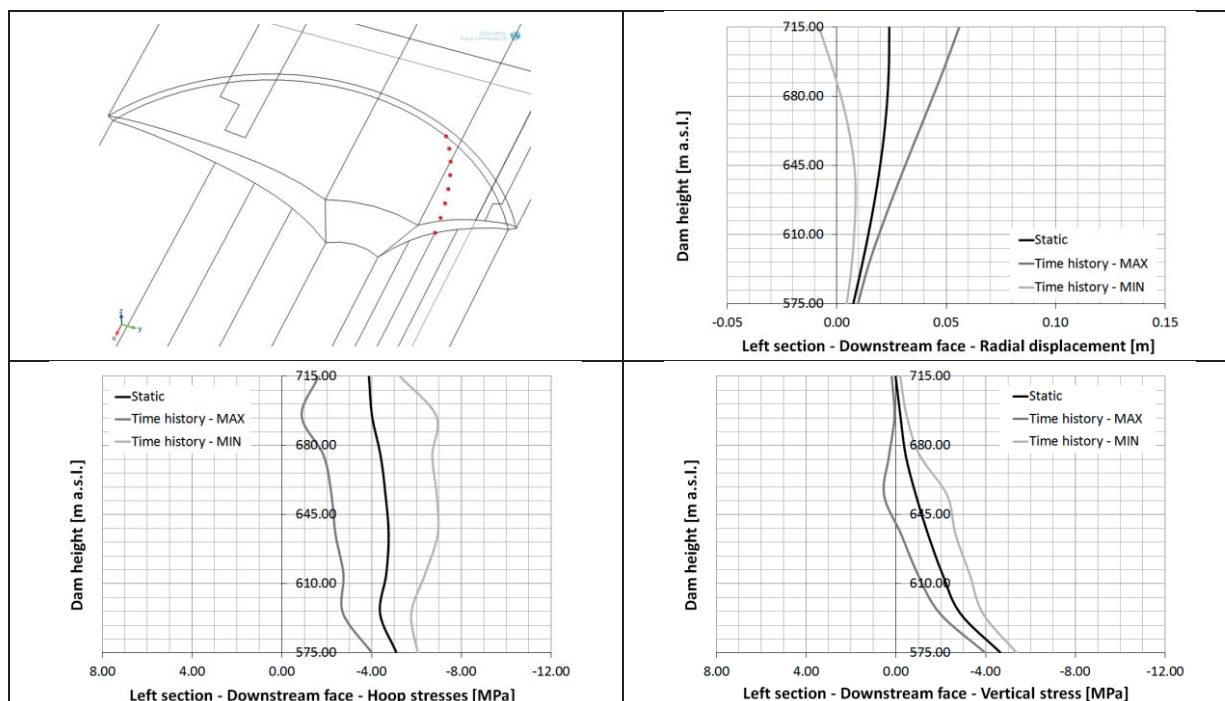
Conclusion

The paper presents the dynamic response of the dam-reservoir-foundation system according to the basic requests of the Formulators. Only the coarse mesh has been considered as some preliminary analyses have demonstrated that, compared to a high computational effort, results showed only slight differences.

A second aspect to be emphasized refers to the boundary conditions assumed for the fluid domain at the rock interface: if a fully reflecting condition is assumed, the stresses computed on the dam are considerably higher than those attained in the case discussed in this paper where a partial absorption conditions has been assumed. This means that experimental investigations should be undertaken in order to define more realistic boundary conditions.

A suggestion for the Formulators, in the synthesis phase, refers to the opportunity to make some comparisons between the main outcomes of Theme A and those of the previous Benchmark Workshops, cited above.

Acknowledgements

References

[1] Theme A − Seismic analysis of the Talvacchia dam. (1992). 2nd ICOLD International Benchmark Workshop on Numerical Analysis of Dams. Committee on Computational Aspects of Dam Analysis and Design. Bergamo, Italy.

[2] Theme A1 − Earthquake of an arch dam including the nonlinear effects of contraction joint opening. (1996). 4th ICOLD International Benchmark Workshop on Numerical Analysis of Dams. Committee on Computational Aspects of Dam Analysis and Design. Madrid, Spain.

[3] Zenz G., Goldgruber M. (2013). Theme A formulation. Fluid Structure Interaction. Arch Dam − Reservoir at Seismic loading. 12th ICOLD Benchmark Workshop on Numerical Analysis of Dams, Graz, Austria.

[4] COMSOL Multiphysics. (2013). Acoustic Module − User's Guide. Version 4.3b

[5] COMSOL Multiphysics. (2013). Structural Mechanics Module − User's Guide. Version 4.3b

[6] Ka-Lun Fok, Anil K. Chopra. (1986). Earthquake analysis of arch dams including dam-water interaction, reservoir boundary absorption and foundation flexibility. Earthquake engineering and structural dynamics, Vol.1, pp 155-184.

[7] Ghanaat Y., Redpath B.B. (1995). Measurement of reservoir-bottom reflection coefficient at seven concrete dam sites. QUEST Structure Report No. QS95-01.

12th International Benchmark Workshop on Numerical Analysis of Dams

Theme A: Fluid Structure Interaction Arch Dam – Reservoir at Seismic Loading

A. Diallo[1] and E. Robbe[1],

[1] EDF-CIH, 15 Avenue Lac du Bourget Savoie Technolac, 73370 Le Bourget du Lac, FRANCE

E-mail: abdoul-salam.diallo@edf.fr, emmanuel.robbe@edf.fr

Abstract

Dynamic response of arch dams to earthquake ground motion is significantly affected by the interaction between the dam and the impounded water. There are several approaches to take into account this dynamic dam-water interaction. The purpose of this benchmark is to compare different modelling techniques with different levels of precision and therefore with different computing efforts. This paper presents the results of the 3 approaches investigated and the fundamental hypotheses adopted for each them. The first approach is a generalized Westergaard added mass, the second approach is an incompressible finite-element added mass and the third approach is based on a sub structuring method where the fluid is compressible. All investigations are carried out for an artificially generated symmetrical arch dam and simplified loading and boundary conditions. In general, Westergaard added mass yields higher compressive and tensile stresses, as well as higher radial displacement. The sub structuring approach, where the compressibility of the water and the impedance of the foundation are taken into account, yields lower stresses.

Introduction

The objective of this paper is to present the seismic analysis of a 220 m high double curvature arch dam undertaken as part of the 12th benchmark study. The results of the analysis are presented for the 3 approaches used to take into account dam-water interaction in accordance with the general assumptions made by the benchmark organizing committee. The analyses of the results focus on the impact of the hydrodynamic approach used on the computed stresses and displacements of the dam.

The following approaches are presented:
- Generalized Westergaard added mass
- Incompressible finite element added mass
- Sub structuring method where water compressibility is taken into account.

For each approach, the fundamental hypotheses are presented and the physical justification is given.

Description of arch dam analysis - modelling methods

The analyses were performed with *Code_Aster*. A computer program developed by EDF; it offers a full range of multiphysical analysis and modelling methods.

Materiel parameters

Because a modal superposition method is used for the three approaches, the Rayleigh damping cannot be used, rather, a value of modal damping is specified for each mode. This value is fixed at 5% which is the value usually considered in real projects.

The mass density of rock is not specified by the benchmark organizing committee because the traditional method assumes that the foundation is massless, however the sub structuring method investigated takes into account the impedance matrix of the foundation rock. It is therefore necessary to specify the mass density of rock; a value of 2400 kg/m3 is considered for the rock in this analysis.

The other material properties are considered in accordance with the general assumptions made by the benchmark organizing committee. Although in practice the dynamic modulus of elasticity is usually considered 25 percent greater than static modulus of elasticity, in this analysis the supplied static values are respected.

Static analysis

The application of the dead load should consider the manner in which the dam was constructed. Arch dams are often constructed as independent cantilever blocks separated by vertical joints. Since these joints are not capable of transferring dead load horizontally until they are grouted, dead loads should be applied to individual cantilever to simulate this condition. This may be accomplished by performing dead load analysis in two steps. First, dead loads are applied to even cantilevers (Set-1) and the stresses are extracted. In second analysis, the dead loads are applied to odd cantilevers (Set-2) separately and the stresses are extracted. The addition of the stresses obtained from the two steps is considered as the initial stress state of the dam and the displacement of the dam due to the dead load is not considered. Water loads due to the hydrostatic pressures of the normal water level are external forces acting on the u/s face of the dam. The hydrostatic pressures are applied to the monolithic arch structure after the construction joints are grouted.

Dynamic modelling

The methods used in this analysis are based on the modal superposition method. The modal analyses performed for the empty dam show that 90 percent of the mass of the dam is excited by a frequency range between 1.93 and 10 Hz. The maximum of the seismic is also in the same range (1-10 Hz).A significant amplification can therefore be expected.

The different approaches used to take into account the fluid-structure interaction are:

a) Generalized Westergaard Added-mass

The added-mass representation of dam-water interaction during earthquake ground shaking was first introduced by Westergaard [1]. In his analysis of a rigid 2D gravity dam with a vertical upstream face, Westergaard showed that the hydrodynamic pressures exerted on the face of the dam due to the earthquake ground motion is equivalent to the inertia forces of a body of water attached to the dam and moving back and forth with the dam while the rest of reservoir water remains inactive.

A general form of the Westergaard added-mass concept which accounts for the 3D geometry [2] can be applied to the earthquake analysis of arch dams.

The general formulation is based on the same parabolic pressure distribution with depth used by Westergaard, except that it makes use of the fact that the normal hydrodynamic pressure P_n at any point on the curved surface of the dam is proportional to the total normal acceleration,$\ddot{u}_n^t$:

$$P_n = \alpha \ddot{u}_n^t \tag{1}$$

$$\alpha = \frac{7}{8}\rho_w\sqrt{H(H-Z)} \qquad\qquad\qquad (2)$$

ρ_w: Density of water;
α: Westergaard pressure coefficient;
H: Water depth;
Z: Level of the point on the curved surface of the dam.
The normal pressure P_n at each point is then converted to an equivalent normal hydrodynamic force by multiplying by the tributary area associated with that point.

b) Incompressible Finite-Element Added Mass – Potential Approach

The added-mass representation of the impounded water can be obtained more accurately by a finite-element solution of the pressure wave equation, which fully accounts for the complex geometry of the dam and the reservoir. The impounded water represented by the wave equation is discretized using a finite element mesh of incompressible liquid elements. The solution is obtained by numerical procedures with the following boundary conditions:

$$\Delta P(x,y,z,t) = 0 \qquad\qquad\qquad (3)$$

- The hydrodynamic pressures at the water – free surface are assumed to be zero, that is, the effects of surface waves are neglected.
- The reservoir bottom and sides, as well as a vertical plane at the upstream end of the reservoir model, are assumed to be rigid. For rigid boundaries the normal pressure gradients or the total normal accelerations are zero.
- The normal pressure gradients at the dam-water interface are proportional to the total normal accelerations of the fluid.

The computed pressures for the nodal points on the upstream face of the dam are then converted into equivalent nodal forces, from which an added-mass matrix representing the inertial effects of the incompressible water is obtained.

c) Compressible Water with Absorptive Reservoir Boundary- Substructuring Method

The substructuring method consists of dividing the complete system into three substructures: the structure, the water, and the foundation, each of which can be partially analysed independently of the others. The structure is represented by a 3D finite element, which permits modelling of a general geometry and linear elastic material properties. The water domain and the foundation region are represented by boundary elements.

The added mass representation of the impounded water described above ignores the effect of water compressibility and reservoir boundary absorption. However, the water compressibility and reservoir boundary absorption can significantly affect the hydrodynamic pressure and hence response of arch dams to earthquakes [3].

Interaction of the dam with the foundation rock leads to an increase in vibration periods, primarily due to the flexibility of the foundation rock. Dam-foundation interaction also decreases the dam response if damping arising from material damping in the foundation rock and radiation damping associated with wave propagation away from the dam are considered in the analysis.

Procedures for earthquake response analysis of arch dams including dam-water interaction, water compressibility, reservoir boundary effects and dam-foundation interaction are developed by EDF [4]. In this procedure, the radiative damping and the hysteretic damping of the foundation are also considered. To represent the infinity domain, Green's functions are used in the fluid domain and in the foundation domain.

In the fluid domain, the Helmholtz equation is discretized using boundary elements.

$$\Delta p \ + \frac{\omega^2}{c_w^2} p = 0 \tag{4}$$

The solution is obtained by numerical procedures with the following boundary conditions:

- The hydrodynamic pressures at the water – free surface are assumed to be zero, that is, the effects of surface waves are neglected.

- The normal pressure gradients at the dam-water interface are proportional to the total normal accelerations of the fluid.

- The normal pressure gradients at the foundation-water interface (reservoir boundary) are proportional to the total normal accelerations of the fluid.

- The hydrodynamic pressure wave impinging on the reservoir boundary is partly reflected into the water, and partly refracted (absorbed) into the boundary materials. The partial absorption at the reservoir boundary is approximately represented by a reflection coefficient known as "α", which is the ratio of reflected to incident wave amplitude.

In the foundation domain, the Navier equation is also discretized using boundary elements. To take into account the infinity domain, Green functions are used.

$$div\ \sigma_f + f_f = \rho_f \frac{\partial^2 u}{\partial t^2} \tag{5}$$

The solution is obtained by numerical procedures with the following assumptions:

- The rock foundation is assumed homogeneous, isotropic and linear elastic.

- A value of 5% is considered for the modal damping.

Results and comparison of the different approaches

Modal Analysis
The interaction of an arch dam with the impounded water leads to a decrease in the dam vibration frequencies. This is because the dam cannot move without displacing the water in contact with it. The fact that water moves with the dam increases the total mass that is in motion. This added mass decreases the natural frequencies of the dam, which in turn affects the response spectrum ordinate and hence the effective earthquake inertia forces. The flexibility of the foundation rock also decreases vibration frequencies of the dam.
Table 1 gives the fundamental modes obtained by the 3 approaches investigated in this analysis. The results show that the Westergaard method gives the largest added-mass value, as evidenced by its decreasing the fundamental frequency the most. However, this does not automatically means that Westergaard approach gives the largest stresses, because the response of the dam also depends on the characteristics of the earthquake ground motion.

Table 1: fundamental period of the dam

	Empty reservoir	Full reservoir		
		Westergaard	Incompressible fluid elements	Compressible fluid element with 50% wave absorption
Fundamental frequency	1.93 Hz	1.29 Hz	1.57 Hz	1.49 Hz

Stresses and displacement

Under static loads, the maximum radial displacement reaches 8.32 cm at the top of the central cantilever. This displacement is only due to hydrostatic pressure acting on the u/s face of the dam.

The relatively symmetrical deformation of the arch dam leads to the compression of the lower portion of the d/s face of the dam and to tractions in the abutments on the u/s face of the dam. The maximum static principal stress (compression) reaches 9.32 MPa at lower portion in the abutments on the d/s face of the dam. The minimum static principal stress (tensile) also reaches 4.40 MPa at the lower portion of the u/s of the dam. This tensile stress (4.40 MPa) could lead to the opening of a joint at the contact between dam and the foundation rock. However the contraction joint opening/closing is not modelled.

Figures 1 and 2 give the principal stress contours under static loads.
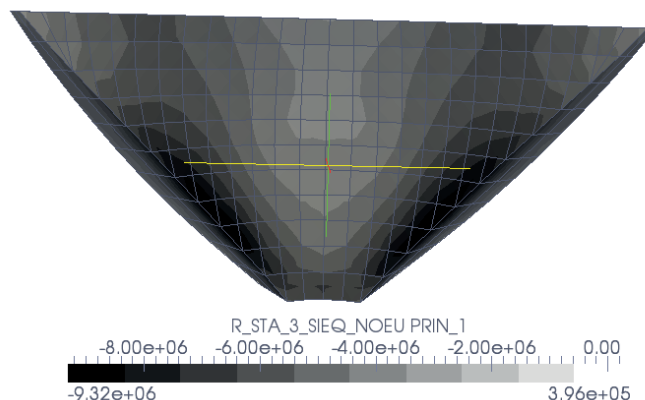
Figure 1: Principal stresses (compression) under static loads
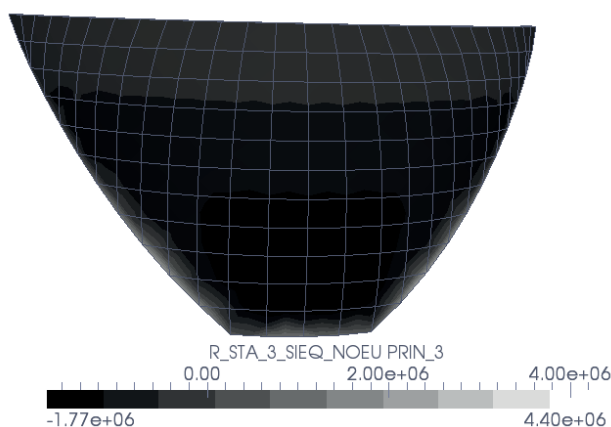
Figure 2: Principal stresses (tensile) under static loads

During the ground motion, the maximum displacement of dynamic vibrations is about 6 cm with the respect to the initial displaced shape of the dam.

The maximum displacements represented in fig 3 show that the Westergaard method yields higher radial displacements at the crest of the dam. The substructuring method where we take

into account the radiative damping and hysteric damping in the foundation as well wave absorption at the reservoir boundary, yields lower displacements (20% of reduction).
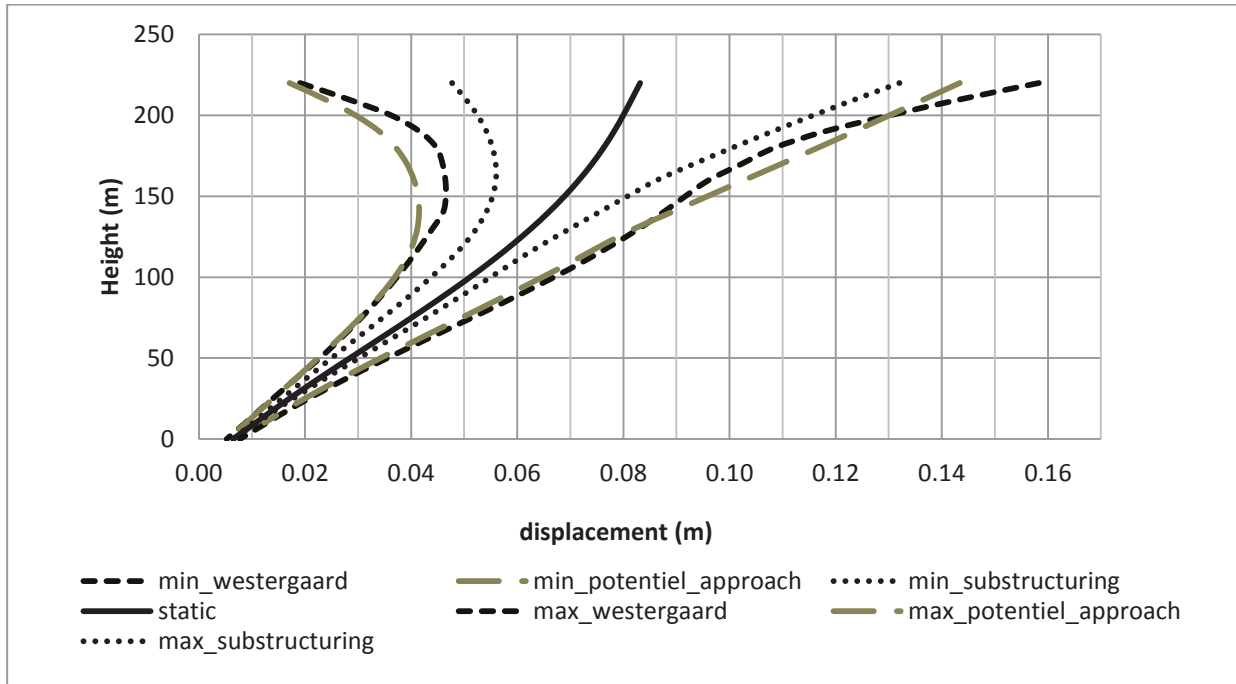
Figure 3: Maximum displacement of the central cantilever at the d/s face of the dam

In general, the Westergaard method yields higher compressive and tensile stresses. Indeed, the seismic tensile vertical stresses at the u/s face of the main cantilever vary from 2.4 MPa for the Westergaard method to 0.2 MPa for the substructuring method at a point at ¾ of the dam height (cf fig4).
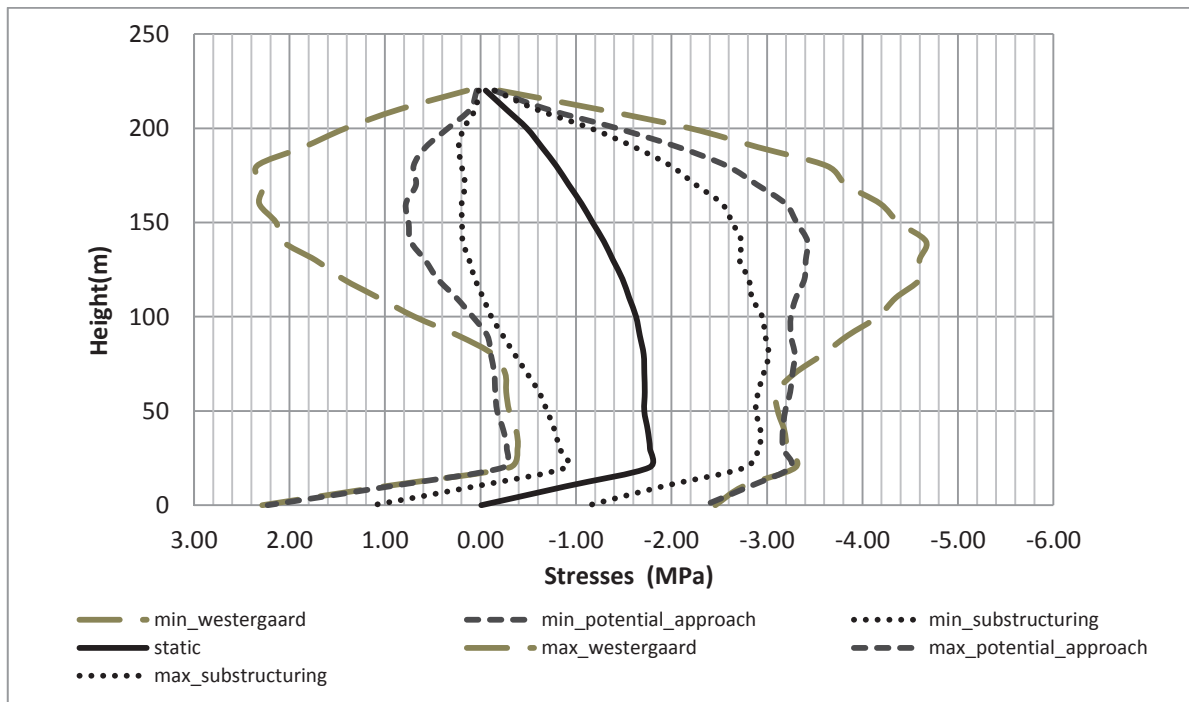
Figure 4: Vertical stresses at u/s face during the ground motion

Figure 5 gives maximum hoop stresses at the d/s face of the central cantilever during the earthquake. It shows a tensile stress varying from 1.6 MPa for Sub structuring method to 2.2 MPa for Westergaard and potential approach at the top part of the cantilever; this could lead to the opening of vertical joints.
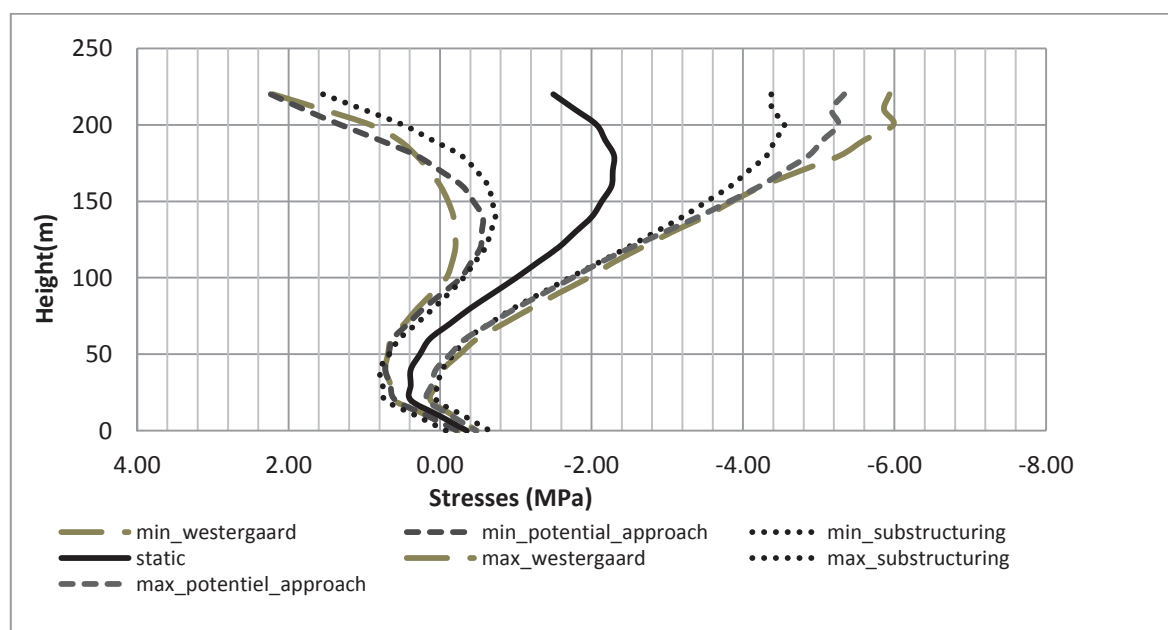
Figure 5: Hoop stresses at d/s face during the ground motion

In general, the ground motion increases the maximum principal stress observed at the lower portion of the abutments on the d/s face of the dam as well the minimum principal stress observed at the lower portion of u/s face of the dam.

Thus, the maximum compressive stresses during the ground motion varying from 11.26 MPa for sub structuring method to 12.77 MPa for added mass approach on the d/s face of dam (cf fig6 right_section). At ¾ dam height on the u/s face, the maximum compressive stresses also varying slightly, from 9.82 MPa for sub- structuring approach to 10.45 MPa (cf fig 6 main_section).
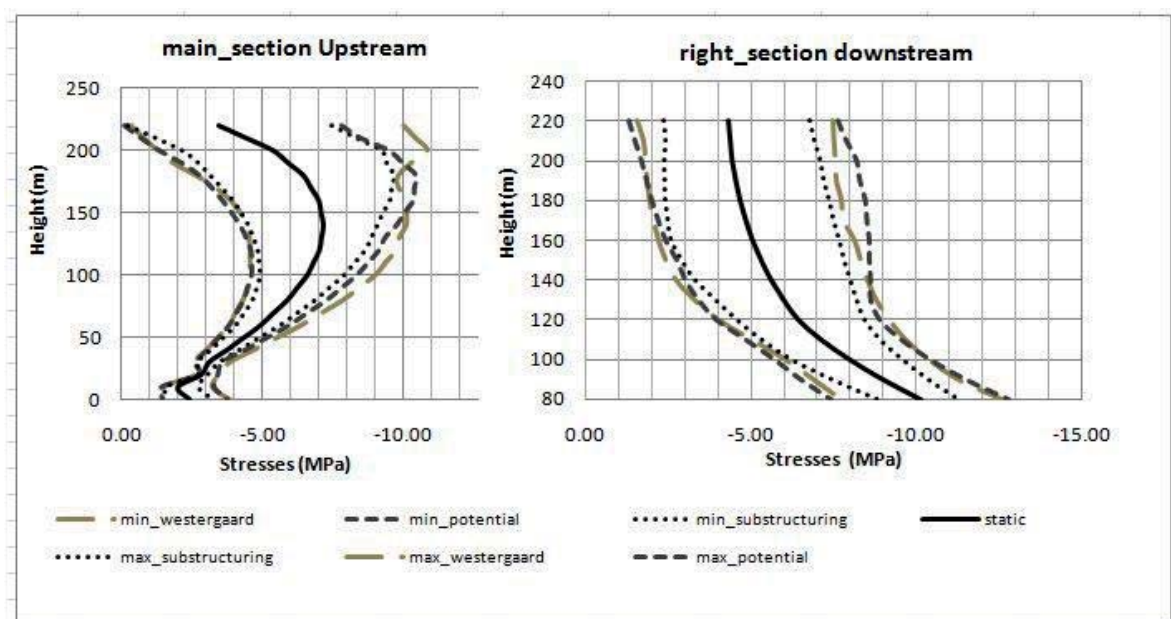
Figure 6: Maximum principal stresses at u/s face of central cantilever and d/s face of right section

In figure 7, we notice that the substructuring method increases slightly the tensile stress at the contact between dam and the foundation (2.84 MPa under static loads and 3.14 MPa during earthquake). However this amplification is very significant with added-mass methods, thus with Westergaard added mass, the tensile stress reaches 5.96 MPa during the earthquake and with the potential approach it is about 5.24 MPa. These tensile stresses could lead to the opening of the contact between the dam and the foundation.
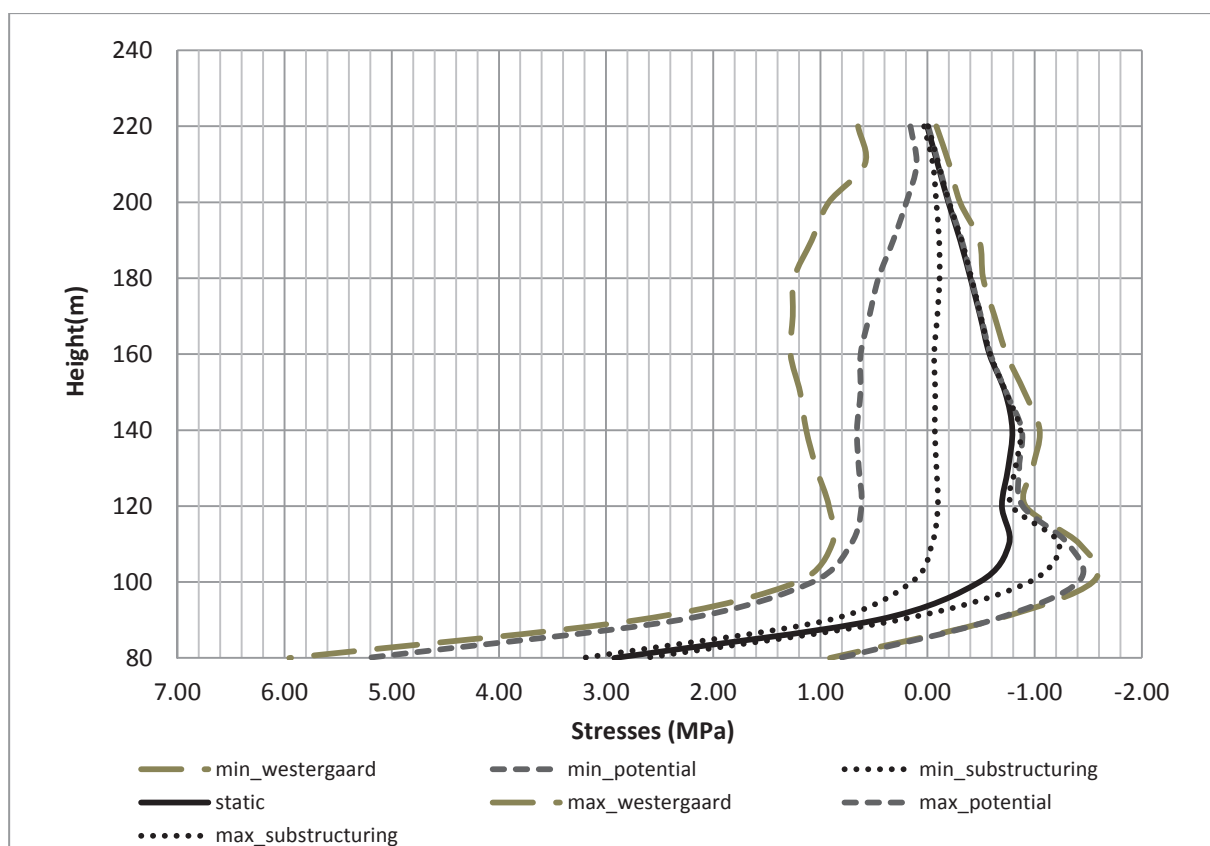
Figure 7: Minimum principal stresses (tension) at the u/s face of right section

Influence of reservoir boundary absorption

A hydrodynamic pressure wave impinging on the reservoir boundary is partly reflected into the water, and partly refracted (absorbed) into the boundary materials. If the reservoir boundary materials are relatively soft, an important fraction of the reservoir water energy can be absorbed, leading to a major reduction in the dynamic response of the dam. Therefore, the values of the absorption ratio for the design and safety evaluation of dams subjected to earthquake loading should be measured or selected conservatively.

The purpose of this section is to show the effect of this absorption on the dynamic response of the dam by studying 3 cases of absorption (0%, 50% and 100% absorption).

As expected, wave absorption at the reservoir boundary reduces significantly the dynamic response of the dam. Figure 8 gives the radial spectrum at the crest of the dam and for fundamental frequency (f1=1.49 Hz), we observe that the correspondent pseudo acceleration varies from 1.93g (total absorption) to 4.14 g (without absorption).
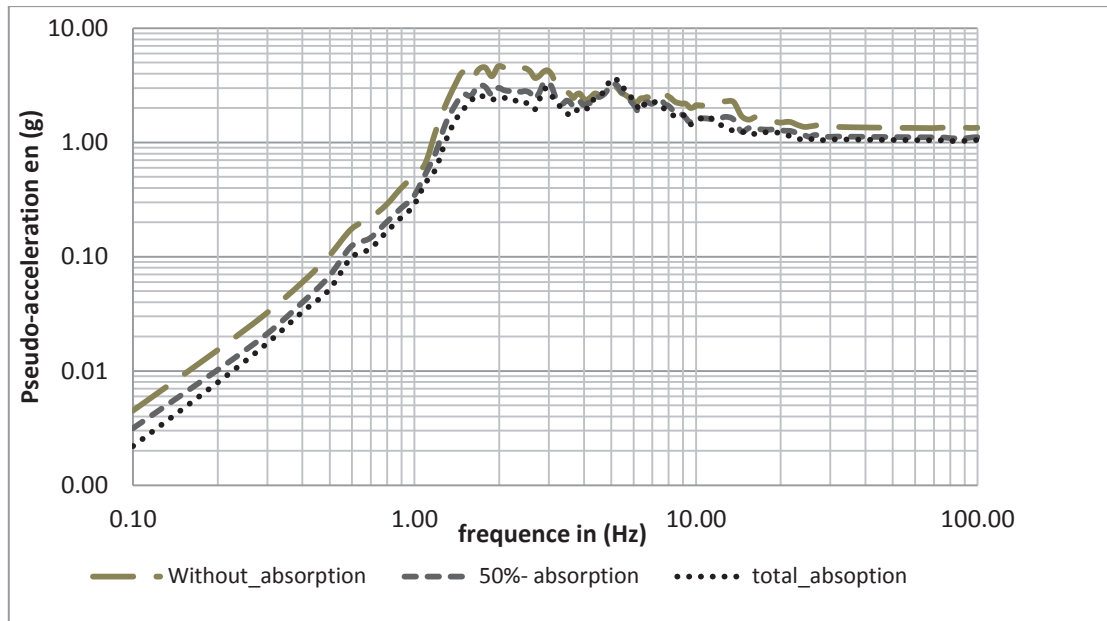
Figure 8: radial spectrum at the crest of the dam for 3 cases of absorption

Reservoir boundary absorption also decreases compressive and tensile stresses (cf fig 9), as well as the radial displacement (cf fig 10). In figure 9, we observe that the maximum stress varies from 8.95 MPa *(total absorption)* to 11.26 MPa (without absorption) at ¾ dam height on the u/s face of the main section.

Figure 10 gives the radial displacement of the central cantilever for 3 cases of absorption and we can observe that the crest displacement varies from 11.4 cm (total absorption) to 15.9 cm (without absorption).
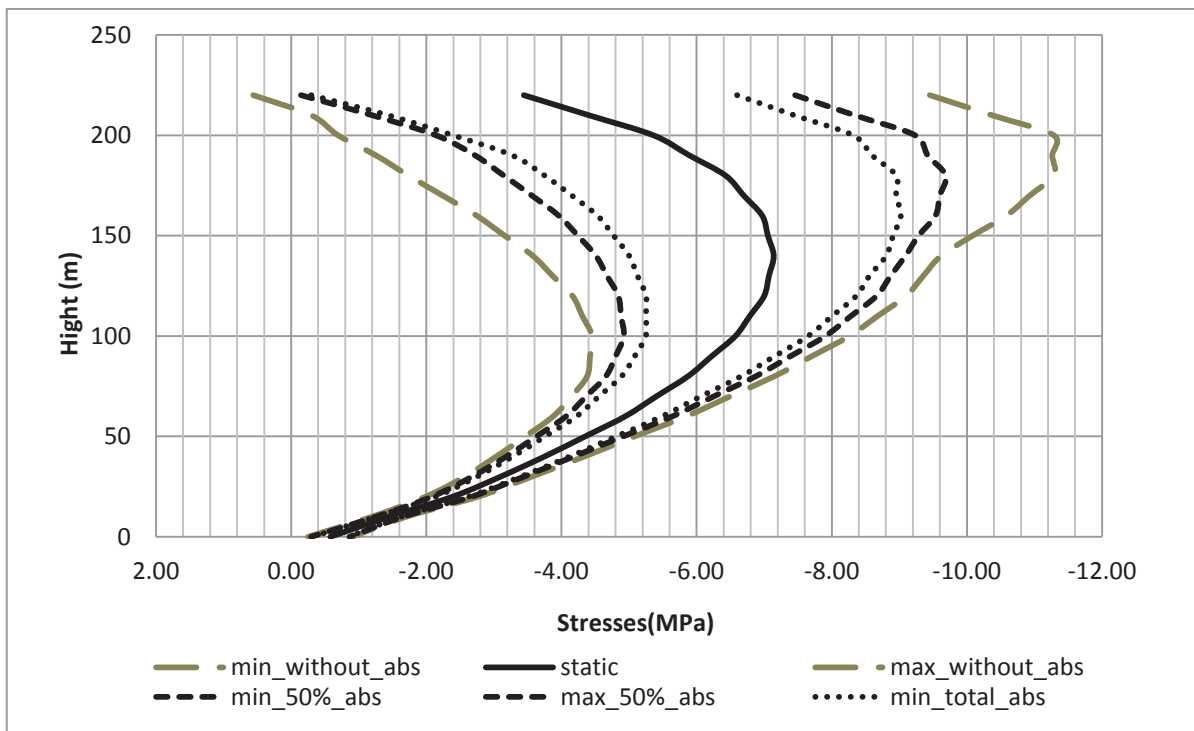
Figure 9**:** Hoop stress of the central cantilever for 3 cases of absorption
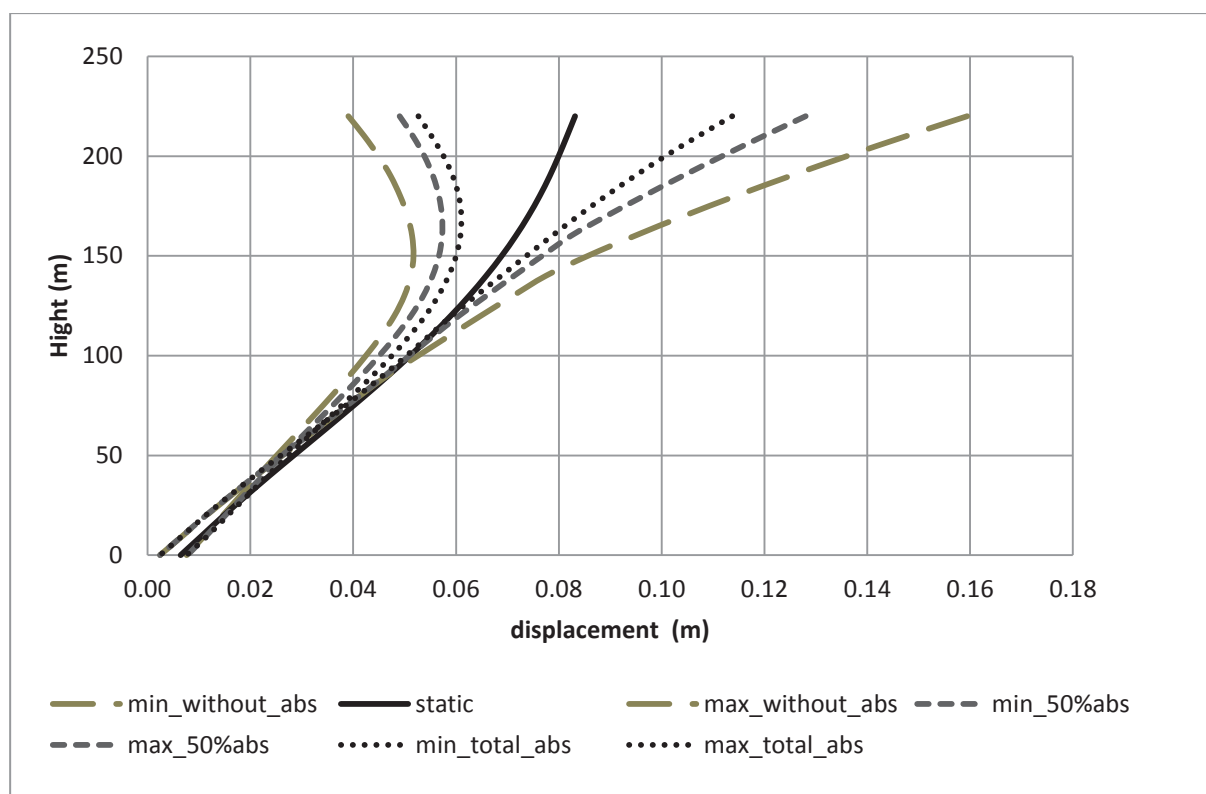
Figure 10: Radial displacement of central cantilever for 3 cases of absorption

Conclusion

The different approaches to hydrodynamic effect modelling investigated in the present study lead to similar behaviour regarding the structural response of the example arch dam. In general, the Westergaard approach yields higher compressive and tensile stresses, as well as higher radial displacements. The substructuring method where wave absorption is taken into account at the reservoir boundary decreases significantly the dynamic response of the dam due to the increased damping of the coupled system.

Acknowledgements

References

[1] Westergaard, H.M (1933), "*Water pressure on dam during earthquakes*", transactions American Society of Civil engineers, Vol 98.
[2] Kuo, 1982 "*Fluid structure interactions: Added Mass Computations for incompressible fluid*". Report No. UCB/EERC-82/09, University of California Earthquake Engineering Research Center, Berkeley.
[3] Fok and Choppra 1985 " *Earthquake Analysis and Response of Concrete Dams*" Report No UCB/EERC-85/07, University of California Earthquake Engineering Research Center, Berkeley
[4] www.code_aster.org

THEME B

Theme B
Long Term Behaviour of a Rockfill Dam

Formulators:

Camilo Marulanda, Ph.D., & Joan Manuel Larrahondo, Ph.D.

INGETEC

Cra 6 No. 30A-30 Bogotá, Colombia

marulanda@ingetec.com.co & larrahondo@ingetec.com.co

Introduction

Overview: Long Term Rockfill Behhaviour
It is widely accepted that rockfill in dam shells exhibit time-dependent, creep-like behaviour ([1]-[3]). Early work by Terzaghi (1960) [2] proposed that such behaviour was due to breakage of rock particles at highly-stressed contacts. Once broken, the rockfill particles would rearrange to attain more stable configurations, thus inducing displacements.

Interestingly, most of the experimental evidence available to date still suggests that the main cause of the time-dependent rockfill behaviour is particle breakage and crushing, phenomena enhanced by the presence of water [2]. Furthermore, a number of constitutive models have been proposed to describe such time dependence, including logarithmic, hyperbolic, and visco-elastic relationships between long-term strain and time [1].

Earth-core rockfill dams (ECRD) typically show dramatic deformations upon reservoir first filling [1]. Time-dependent deformation depends on water content of rock particles, such that yield is highest in saturated rock particles, while tends to fade for very dry materials [2].

Since the work by McDowell and Bolton (1998) [2], successive deformation stages are recognized in rockfill-type granular materials subjected to compression stresses as the confining stress is increased. At low stresses, deformation is due to particle rearrangement. From a micromechanical point of view, rockfill deforms mainly because of interparticle sliding and rotation [1]. As the confining stress increases, the granular skeleton becomes gradually blocked, and particle breakage and crushing are triggered. Such mechanism is called "clastic yielding". Finally, for very high stresses the strain vs. log stress plots have upward-directed concavity. This is attributed to the comminution limit of small particles.

The time-dependent deformation of rockfill can thus be explained by progressive breakage and crushing of stressed particles [1]. Particle breakage takes place as subcritical propagation of preexisting microcracks within loaded rock particles. The velocity of crack propagation is a function of the local stress intensity factor and the prevailing relative humidity. Particle breakage combines with complex localised crushing at interparticle contacts to boost rockfill deformation [1].

Not a large number of databases are available that comprise 25 years or more of instrumentation data from a rockfill dam. The problem proposed in this document consists in reproducing the development of displacements and stresses of a real-case dam during construction, reservoir impoundment, and operation.

Benchmark Example: Alberto Lleras Dam (Guavio Hydroelectric Project), Colombia

Dam Description

The case history that is being proposed as benchmark example for the Theme B of the 12th Workshop on Numerical Analysis of Dams is that of the Alberto Lleras Dam, part of the Guavio Hydroelectric Project in Colombia.

The Guavio Hydroelectric Project is located in the Cundinamarca region of central Colombia, some 120 km northeast from Bogotá. The project spans between the towns of Ubalá, where the dam is located, and Mambita, where the underground powerhouse is located [4]. The project harnesses the hydropower potential of the lower Guavio River (1100 m nominal head) and comprises the following components designed by INGETEC ([4]-[6]):

- The Alberto Lleras Dam: a 245-m high, clay-core rockfill dam, the highest of its kind in South America [3]. The total dam volume is about 17 x 106 m3 which impounds a 14-km long, 950 x 106 m3 reservoir.
- A 34-m high, 4500 m3/s capacity, ogee-type spillway controlled by radial gates and two 600-m long tunnels
- A 13.3-km long, 8 m diameter power tunnel and a 505-m high pressure shaft
- A 234-m long, 17-m wide, 35-m high underground powerhose located 560 m below ground. The total installed generating capacity of the Guavio project is 1600 MW, currently delivered by eight Pelton turbines.
- A 1160-m long diversion tunnel as well as two other tunnels, 2330 m and 2190 m long, respectively, that divert the Batatas and Chivor Rivers into the Guavio reservoir
- A 5.2-km long, 8-m diameter tailrace tunnel to return the Guavio river water back to its main course

The Guavio project was built between 1979 and 1995 [2] and first filling took place in February 1992. The average flow of the river at the dam site is 62 m³/s. Figure 1 presents an aerial view of the Guavio Project and the Alberto Lleras Dam.

Available instrumentation data span from 1987 through 2013. Specifically, measurements include data from:

- 78 level survey points on the dam crest and faces
- 8 Vertical Movement Recorders (RMV)
- 24 Pneumatic Settlement Sensors (SNA)
- 40 pressure cells (CP)
- 26 pneumatic piezometers (PZ)

Figure 1: General view of the Guavio Hydroelectric Project and the Alberto Lleras Dam [4]

The objective for the participants of Theme B is to reproduce, via a numerical model, the displacements observed on the maximum cross section of the Alberto Lleras Dam.

The minimum requirements that shall be incorporated in their numerical model are a three-dimensional model using the provided simplified topography and the use of the known dam zoning and the construction sequence.

Geology Overview

The greater Guavio project area comprises Palaeozoic rocks overlain by Mesozoic rocks [5]. The dam site is underlain by Palaeozoic quartzite, argillite, and limestone. At the dam site, the river features a 600-m deep, narrow canyon. The upper half of the canyon at the dam site (left abutment) exhibits Cretaceous rocks.

The Palaeozoic formations strike diagonally with respect to the river canyon and dip upstream. Most of these rocks below 30 m of depth are fresh, hard, and depict low permeability [5]. The limestone shows frequent karstic features (caverns) which were tackled via an extensive grouting programme.

No geological faults exist at the dam foundation area [5]. The steep slopes of the canyon rendered some relief joints parallel to the river flow. No particular treatment was necessary for these joints.

Input Data

All detailed input data information is provided in this manuscript's attachments. A description of each database follows.

Dam Geometry

Attachment 1 contains all drawings related to dam location geometry. Specifically, the following data files are provided:

- Maximum longitudinal section and description of dam zones (as-built; Oct. 1989; DWG and PDF files)
- Plan view and topography (as built; 50-m elevation contours; Nov. 1989; DWG and PDF files)
- Dam zoning description table (XLS file), including placed volumes and as-built compaction specifications

Construction Sequence

Construction of the dam started on June 1983 with foundation excavation work [7]. Fill placement operations initiated on September 1984 and ran through August 1989.

In general, during the six rainy months of the year (May-October) rockfill was placed and compacted in the outer portions of the shell. During the remaining six drier months (November-April), fill placement was concentrated in the central portion of the dam, namely the core and confining rockfill [7].

Attachment 2 contains all drawings and data related to construction sequence. The following data files are provided:

- Construction sequence plan (maximum longitudinal section; as-built; Nov. 1989)
- Fill placement sequence summary table (XLS file)

Material Properties

The outer portions of the shell rockfill comprised weathered fragments of quartzite, argillite, and limestone [7]. On the other hand, the inner part of the dam below the core consisted in sound, fresh, and clean rockfill.

The dam core consists mainly in shale fragments in a silty clay matrix [7] obtained from a nearby quarry named San Pedro. The core material features medium plasticity and fines content >30%.

Attachment 3 contains all drawings and data related to material characterization. Specifically, the following data files are provided:

- DWG, PDF, and XLS files containing rockfill properties varying with dam depth
- DWG, PDF, and XLS files containing earth-core properties varying with dam depth
- One XLS file containing as-built grain size distribution bands for each dam zone
- One XLS file containing compressibility curves (pre-construction) for the earth core and shell rockfill materials

For illustration purposes, material parameter data that were employed during the geotechnical design of the dam are provided next:

- Earth core and shell rockfill compressibility: an experimental programme was undertaken prior to construction to obtain design compressibility parameters from both the earth core material and the rockfill.

  30-cm thick samples of dam-core material were subjected to one-dimensional consolidation tests in a 30-cm diameter oedometer. The earth-core materials featured maximum grain size of 6.5 cm and natural water content during testing. Samples were reconstituted via compaction of five layers using a 30-lb hammer falling freely from a height of 24 in. Between 160 and 200 blows per layer were applied.

  The rockfill material compressibility was also studied using the same large oedometer as that of the core materials. However, rockfill samples were tested dry and using the same grain size distribution as that of the construction specification (with maximum grain size of 6.5 cm). Samples were reconstituted by compaction of four layers with a vibrating table during 1.5 min each layer. During the loading process, the samples were intentionally inundated at the 16 kg/cm2 loading step.

  The following table presents the experimental programme initial conditions and results in terms of compressibility coefficient. Attachment 3 also contains the compressibility curves obtained from these tests.

Results	Water content of the < # 4 sieve fraction (%)	Dry density (Ton/m^3)	a_v (10^{-3}cm^2/kg)
Max	28	1.84	4.7
Ave	24	1.77	3.6
Min	21	1.71	2.6
Max	-	2.25	2.1
Ave	-	2.17	1.6
Min	-	2.03	0.8

- Plasticity of the earth core material (measured values during the dam geotechnical design phase)

Liquid limit (%)	39
Plastic limit (%)	26
Plasticity index (%)	13

Instrumentation data

During construction and particularly after reaching 2/3 of the dam height, large displacements took place within the dam core [7]. As a result, most of the cable of the pneumatic and electric instruments was destroyed. Overall, about 50% of the original instruments installed were lost due to construction operations.

Available instrumentation data for this workshop span from 1987 through 2013. Attachment 4 contains all drawings and data related to instrumentation data. Specifically, the following files are provided:

- Five folders with XLS data files
- Two layouts of installed instrumentation (as-builts; plan view and maximum longitudinal section; DWG and PDF; July 1990)

A brief description of available instrumentation data follows.

Movements

- Surface movements: Data from a total of 63 level survey instruments, labelled 13 through 75 are provided. Survey elevation data span from 1989 through 2013.

- Vertical Movement Recorders (RMV) or "crossarm gages": nine folders are provided containing monthly RMV data, spanning from 1989 through 1995. Additionally, for the 1996-2008 period, a XLS file is provided with data collected in eight of the nine available RMVs.

  RMV instruments or crossarm gages consist of a series of telescopic pipe sections with alternate sections anchored to the embankment fill by horizontal channel crossarms located at certain depth intervals, typically 3 m ([8] See Figure 2). The crossarms ensure that the coupled pipes move together as compression of the fill progresses. Measuring points are located at the lower end of each inner pipe; depths to such measuring points are usually sounded by a probe with spring-loaded sensing pawls, lowered on a steel tape. To produce a measurement, the probe is lowered just below a given inner pipe and then raised until the paws latch against the lower end.

- Pneumatic Settlement Sensors (SNA): two folders; instruments 28-41 with monthly data from 1987 to 1996; instruments 49-58 with monthly data from 1988 to 1995.
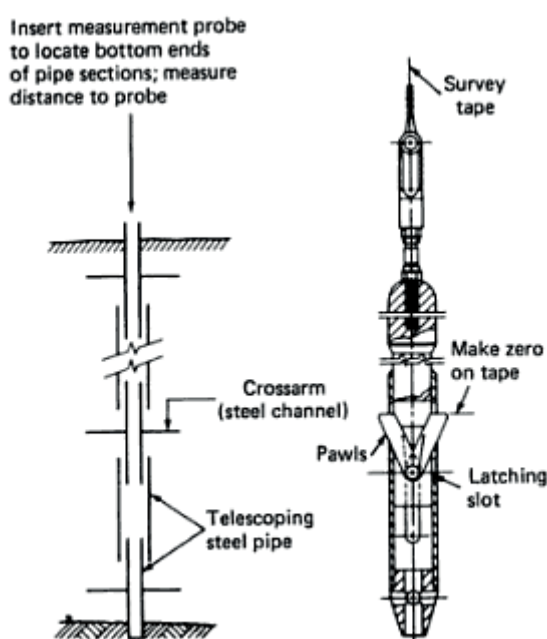
Figure 2: RMV (crossarm gage) schematic [8]. Left: telescopic pipe array. Right: measurement probe

Pressure Cells (CP)

Three folders are provided. All total pressure cell data is reported in kg/cm^2. Monthly data are provided as follows:

- CP 1-24: data from 1986 to 1998; CP 1, 3, 5, 6, and 7 are at 1405 masl elevation; CP 8 through 24 are at 1463 masl elevation
- CP 28-37: 1987 to 1998 at 1523 masl elevation

- CP 41-46: data from 1988 to 1997 at 1589 masl elevation

Pneumatic Piezometers (PZ)
- One XLS file is provided that contains data collected from the dam foundation piezometers (PZ 82, 83, and 84). Data were collected monthly spanning from 1988 through 2004.
- 15 XLS data files are provided with data collected from the dam core piezometers (PZ 45 through 49) at 1523 masl elevation. Data were collected monthly spanning from 1987 through 2001.

Requested Results

All workshop participants are kindly requested to provide a paper, 15 pages maximum, in which all assumptions are clearly stated, particularly regarding initial and boundary conditions.

To facilitate results rating, the participants must also submit their key results under a prescribed format whereby an Excel file under the name **ThB_ResXXXX.xls** shall be created (XXXX represents a name or acronym of the participant's organisation).

Fill Displacements
Displacement contours for three longitudinal sections and one cross section along the dam crest shall be presented. Results at the end of construction, at the condition prior to impoundment, and after reservoir impoundment shall be included.

Stresses within the Dam
Calculated principal and vertical stresses obtained from the analysis on five locations within the fill are requested. The results shall be presented both at the end of construction and after partial and full impoundment.

Creep and Arching Effects
A discussion supported with simulation results is requested regarding long-term displacement behaviour including possible arching effects within the dam body.

Groundwater Flow
The participants are requested to submit the resulting groundwater flow net under 1620 masl reservoir level water level conditions.

Acknowledgements
The formulators are grateful to EMGESA Colombia for allowing the use of the instrumentation data for this workshop

References

[1] Oldecop, L. A. and Alonso, E. E. (2007). Theoretical Investigation of the Time-Dependent Behaviour of Rockfill. Géotechnique, V. 57, No. 3, pp. 289–301

[2] Oldecop, L. A. and Alonso, E. E. (2001). A Model for Rockill Compressibility. Géotechnique, V. 51, No. 2, pp. 127-139

[3] Justo, J. L., Durand, P. y Justo, E. (2003). Un Modelo Tridimensional para el Estudio de la Fluencia en Presas de Materiales Sueltos. Rev. Int. Mét. Num. Cálc. Dis. Ing. V. 19, No. 3, pp. 313-330 (in Spanish)

[4] INGETEC S.A. (2013). Hydropower Projects – Guavio
http://www.ingetec.com.co/experiencia-ingles/textos-proyectos-ingles/proyecto-hidroelectricos-ingles/guavio-ingles.htm (Accessed 2013)

[5] Marulanda, A. and Amaya, F. (1989). The Design and Construction of Colombia's Guavio Dam. Water Power and Dam Construction, December 1989. pp. 41-60

[6] INGETEC S.A. (2013). Hydroelectric Developments. http://www.ingetec.com.co/brochures-ingles/BROCHURE-HIDROELECTRICAS-INGLES.pdf (Accessed 2013)

[7] Amaya, F. and Marulanda, A. (1993). Behavior of Guavio Dam during Construction and First Filling. Proceedings of the International Symposium on High Earth-Rockfill Dams. ICOLD-CSHEE. Beijing, China.

[8] Dunnicliff, J. (1988). Geotechnical Instrumentation for Monitoring and Performance. John Wiley & Sons. 577 p.

PAPERS

THEME B

Solution to Theme B
Long Term Behaviour of a Rockfill Dam

F. Ezbakhe[1], I. Escuder-Bueno[1]

[1] Universidad Politécnica de Valencia, Spain

E-mail: iescuder@hma.upv.es

Preface

The authors acknowledge that the solution herein presented is very simplified and should not be taken as a professional reference by any means.

However, with the purpose of enabling the formulator to estimate the order of magnitude of the lack of accuracy and/or physical inconsistencies by using methods as simplified and empirical as those herein presented, the paper may be of certain interest.

Introduction

Theme B of the 12th Benchmark Workshop on Numerical Analysis of Dams (ICOLD) consists in the evaluation of the long term behavior of a rockfill dam, analyzing the case of the Alberto Lleras Dam, part of the Guavio Hydroelectric Project in Colombia.

The objective is to reproduce, via a numerical model, the behavior of the dam during the construction, impoundment and exploitation, providing the evolution of displacements and stresses within the dam as results.

For the solution presented in this paper, the problem has been solved by FLAC3D (Itasca), a finite differences program developed by Itasca Consulting Group, Minnesota. This software uses the finite differences method to analyze the mechanical behavior of a continuous medium in 3D until it reaches an equilibrium state.

Figure 1: View of the Alberto Lleras Dam

Statement of the problem

Alberto Lleras Dam is a clay-core rockfill dam which main features are given in the next table:

Table 1: Main features of the Alberto Lleras Dam

Height	245m
Width	950m
Dam volume	7hm3
Reservoir volume	950hm3

Construction of the dam lasted five years, from September 1984 to August 1989. In general, during the six rainy months of the year (May-October) rockfill was placed and compacted in the outer portions of the shell. During the remaining six drier months (November-April), fill placement was concentrated in the central portion of the dam. The impoundment started on February 1992 and run through September 1992.

The dam consists in three rockfill zones, with similar mechanical parameters but different granulometric composition. It includes also two transition zones and a clay core, featuring a medium plasticity clay matrix.
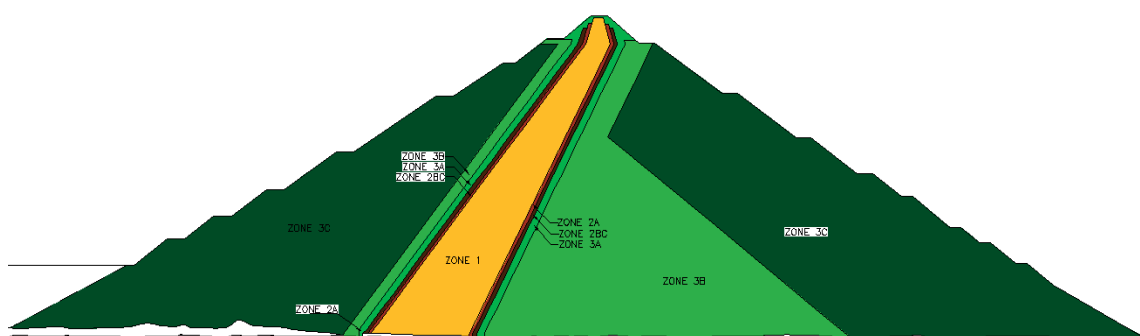
Figure 2: View of the Alberto Lleras Dam

The dam site is underlain by quartzite, argilite and limestone, with no geological faults. The formations strike diagonally with respect to the river canyon and are fresh, hard and depict low permeability.

Features of the implemented model

Geometrical model

From a simplification of the real topography and geometry of the problem, a 3D geometrical model of the dam was implemented, formed by 7286 nodes and 5800 solid elements. Next figures show the FLAC 3D geometrical model of the dam.

Figure 3: FLAC 3D geometrical model

Mechanical model

The mechanical model selected for the solution herein presented is linear-elastic. This model was chosen for its simplicity and wide applicability solving soil and rock mechanics problems.

In this model, strain increments generate stress increments according to the linear and reversible law of Hooke:
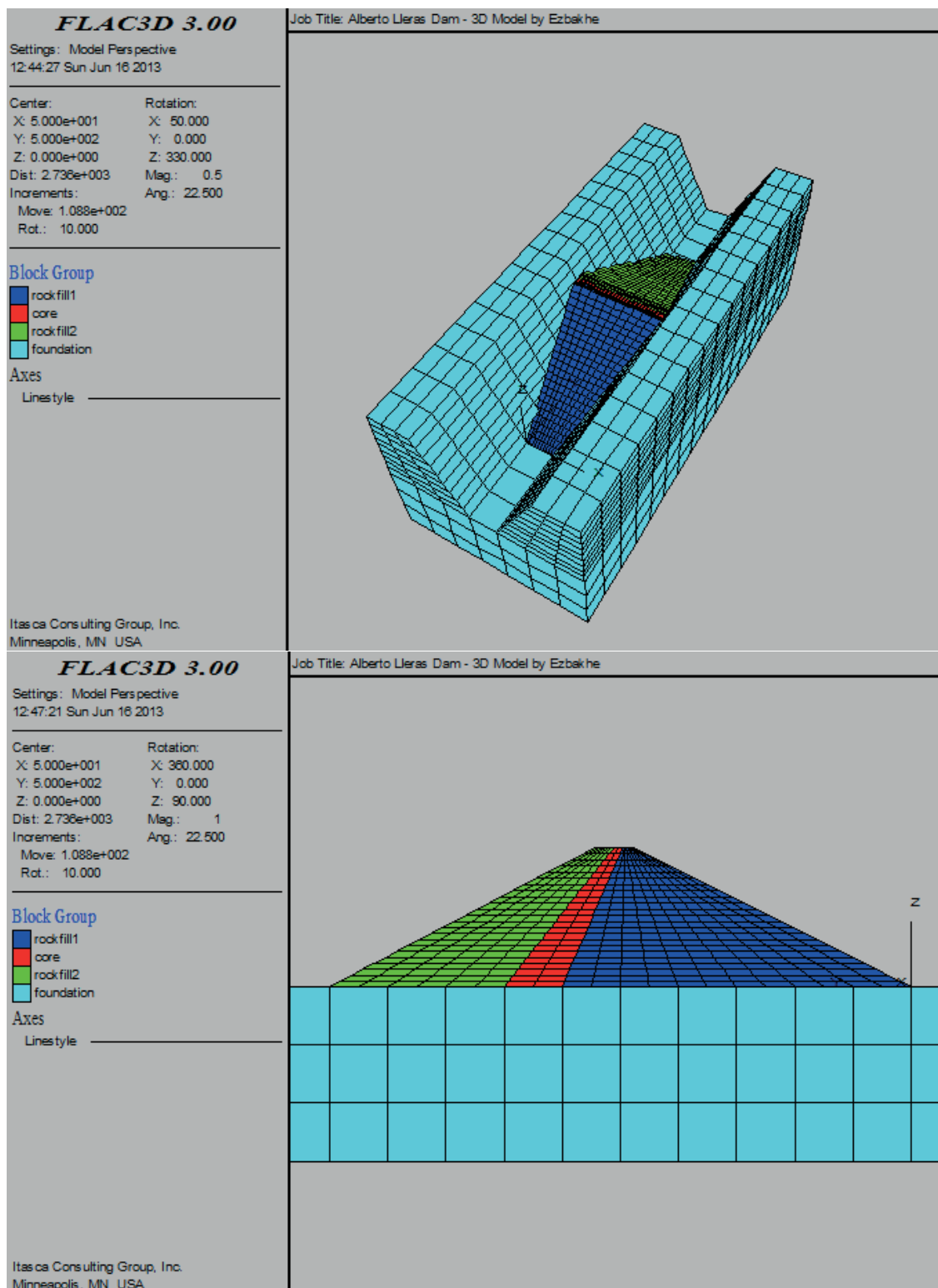
$$\Delta\sigma_{ij} = 2G\Delta\epsilon_{ij} + \alpha_2\Delta\epsilon_{kk}\,\delta_{ij} \tag{1}$$

where the Einstein summation convention applies, δ_ij is the Kroenecker delta symbol, and α_2 is a material constant related to the bulk modulus, K, and shear modulus, G, as:

$$\alpha_2 = K - \frac{2}{3}G \tag{2}$$

New stress values are then obtained from the relation:

$$\sigma_{ij}^{N} = \sigma_{ij} + \Delta\sigma_{ij} \tag{3}$$

Next table provides the values that have been adopted for the mechanical model:

Table 2: Mechanical parameters

	Density (kg/m3)	Bulk modulus (Pa)	Shear modulus (Pa)
Core	2010	7.5·106	5.4·106
Rockfill	2750	8.5·107	4.7·107
Foundation	2500	4·1010	3·1010

The boundary conditions applied are:
- – Plane x=-300 (lateral surface). Movements constrained on the x-axis
- – Plane x=400 (lateral surface). Movements constrained on the x-axis
- – Plane y=-300 (front surface). Movements constrained on the y-axis
- – Plane y=1300 (back surface). Movements constrained on the y-axis
- – Plane z=-300 (underside). Movements constrained on all axis

Constructive behaviour

The construction process may affect the stress state, particularly if excess pore pressures develop in the soils and do not dissipate completely during the construction stages. In addition, staged modeling of the embankment lift construction also provides a better representation of the stresses in the embankment.

In this case, due to the difficulty involved in modeling the actual construction sequence, it has been simplified considering that it takes place in uniform layers of 10m high. Thus, the numerical process is to activate each layer, assigning materials and properties, and calculating the model to reach equilibrium.

Post-constructive behaviour

In Geotechnical Engineering, time-dependent settlement is associated to the process of consolidation. This behavior would be therefore determined by the rate at which water is able to flow through the ground pores under a certain hydraulic gradient.

Boughton (1970) found that this settlement also occurred during the construction process. For calculation purposes, Boughton got a good fit for the form of post-construction deformations

by applying the entire weight of the structure at once. Then, adopting a scale factor, he got a good fit for the magnitude of the deformations.

In this case, the scale factor used is 1.05 for dry behavior (from the completion of construction to the start of filling) and 1.11 for the behavior of the wet rockfill (with filled reservoir).

Results

Settlements

Settlements of the dam body are obtained at three different times:
- August 1989 completed the construction of the dam
- January 1992 immediately before the first filling
- September 1992 1630 masl reservoir

Settlements are also obtained in nine point of the dam:

Table 3: Settlements in the dam

|	aug-89		jan-92		sep-92	
	Settlement (m)	Elevation (masl)	Settlement (m)	Elevation (masl)	Settlement (m)	Elevation (masl)
M-30	0.00	1641.081	0.810	1640.271	0.971	1640.110
M-36	0.00	1641.020	0.875	1640.145	1.043	1639.977
M-48	0.00	1641.751	0.363	1641.388	0.470	1641.281
M-53	0.00	1640.420	0.290	1640.130	0.368	1640.052
M-64	1.54	1604.027	1.974	1603.594	2.070	1603.498
M-66	1.60	1570.985	1.827	1570.758	2.032	1570.553
M-72	1.46	1515.672	1.617	1515.513	1.715	1515.415
SNA-30	3.60	1517.435	4.037	1516.995	4.593	1516.439
SNA-38	3.42	1518.242	3.872	1517.790	3.991	1517.671
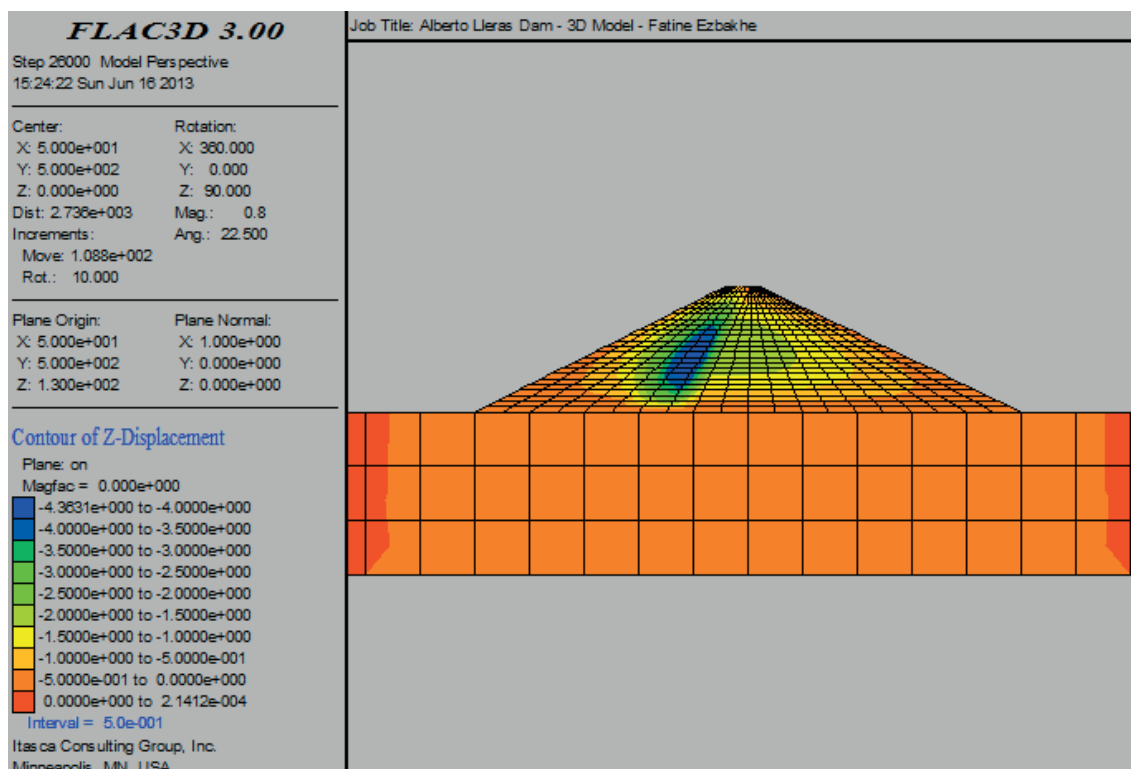
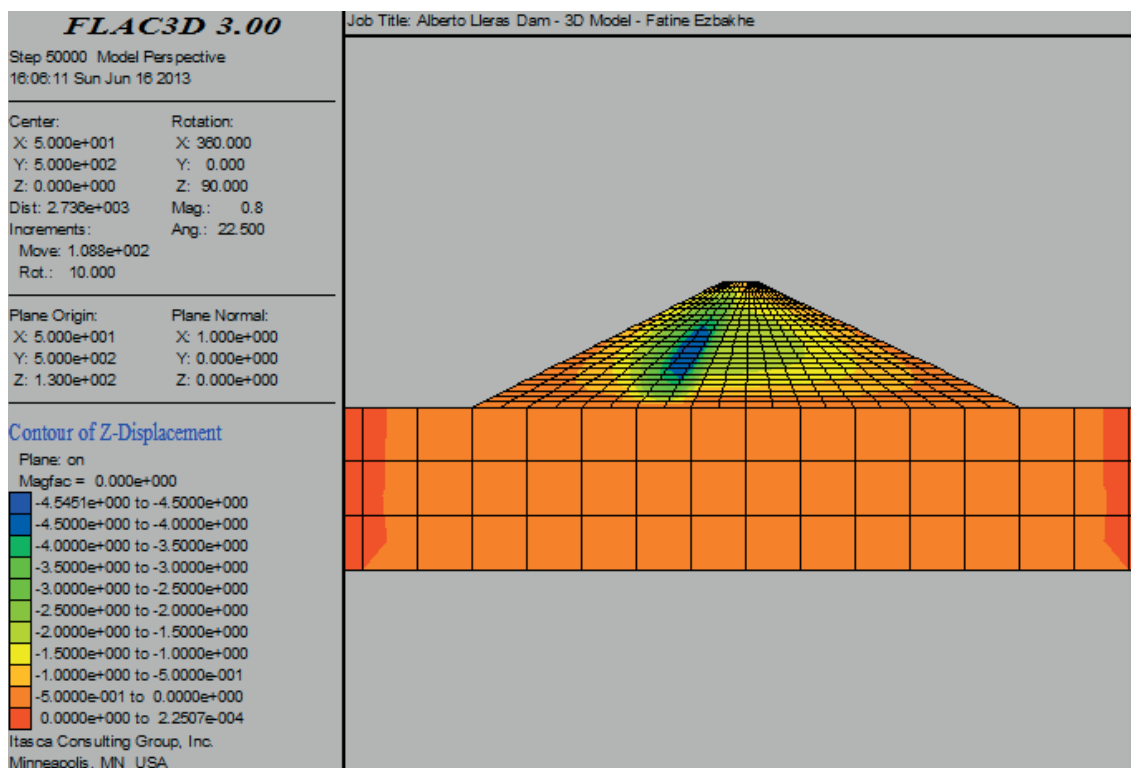Figure 4: Settlements in August 1989
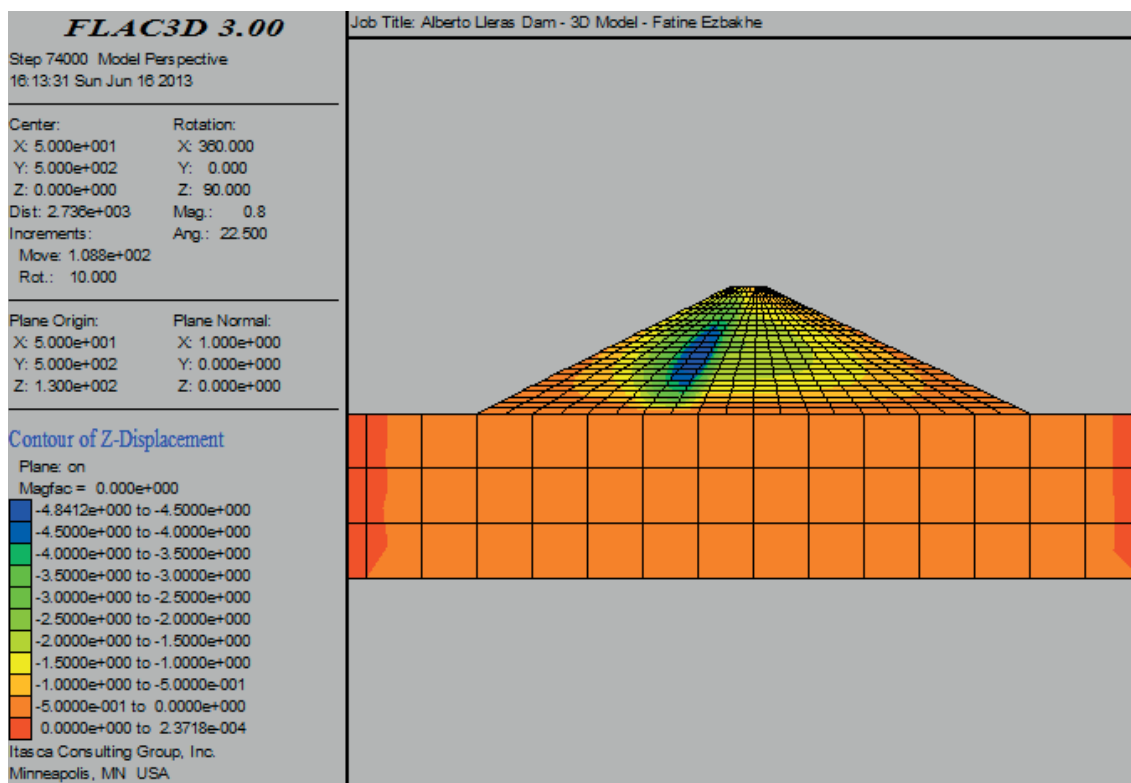

Figure 5: Settlements in January 1992

Figure 6: Settlements in September 1992

Stresses

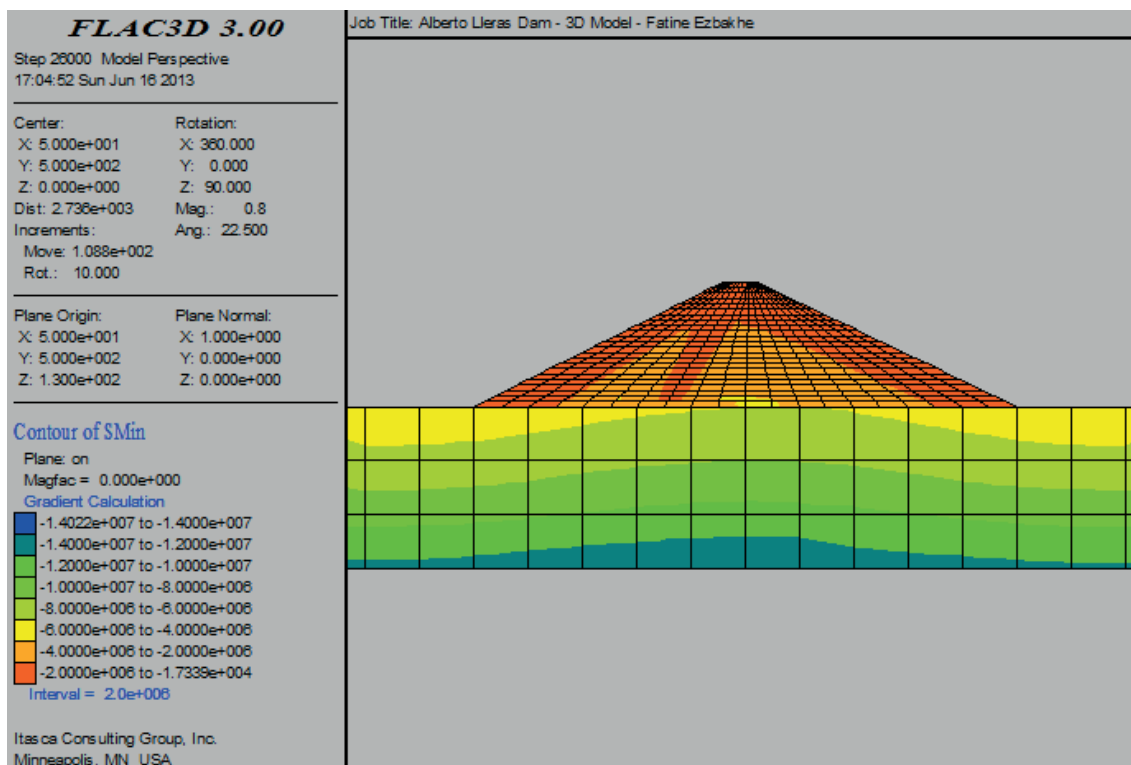Next figure represents the stresses of the dam after dam construction:

Figure 7: Principal stresses in August 1989

Principal stresses (s1) and vertical stresses (sv) are also obteined in five different points:

Table 4: Stresses in the dam

ID	@ EOC		Reservoir at EL 1575		Reservoir at EL 1630	
	s_1 [Kpa]	s_v [Kpa]	s_1 [Kpa]	s_v [Kpa]	s_1 [Kpa]	s_v [Kpa]
CP-11	1594.3	1556.5	1619.1	1599.9	1752.3	1725.6
CP-6	1345.2	1281.2	3015.2	1964.7	3237.5	2482.1
CP-19	1909.4	1554.0	2240.3	1914.9	2806.5	2019.0
CP-22	2871.0	1459.6	2884.9	1947.6	2916.8	1992.0
CP-3	2769.7	2653.6	3438.1	2949.6	3475.0	2969.2

Conclusion

In order to study the long dam's long term behavior, a linear elastic analysis has been realized. This means that a linear analysis is performed for each time step and when the equilibrium is reached the calculus moves to next instant of time.

The implemented model considers the dam body as a structure without interfaces and permits the evolution of the displacements and stresses over time.

The simulation of this evolution can resembles to some extent to the data collected by auscultation, with a margin of error due to the different simplifications made in the model.

References

[1] Escuder, I. *"Estudio del comportamiento tenso-deformacional de pedraplenes inundables mediante simulaciones numéricas formuladas en diferencias finitas y calibradas con lecturas de instrumentación"*. Doctoral Thesis

[2] Itasca Consulting Group, Inc., "Fast Lagrangian Analysis of Continua in 3 Dimensions version 3.1: Theory and Background, Optional features", Minneapolis, Minnesota, 2006

[3] ICOLD, "Guidelines for use of numerical models in dam engineering", Bulletin 155